

國立交通大學
材料科學與工程學系
博士論文

智慧型磁性水膠及奈米微球
於藥物控制釋放之研究

Study on Intelligent Magnetic Hydrogel and Nanosphere
for Drug Controlled Release

研究生：劉定宇
指導教授：陳三元 博士

中華民國九十七年七月

智慧型磁性水膠及奈米微球於藥物控制釋放之研究

Study on Intelligent Magnetic Hydrogel and Nanosphere for Drug
Controlled Release

研究生：劉定宇

Student：Ting-Yu Liu

指導教授：陳三元

Advisor：San-Yuan Chen

國立交通大學
材料科學與工程系
博士論文

A Thesis

Submitted to Department of Materials Science and Engineering

College of Engineering

National Chiao Tung University

In partial Fulfillment of the Requirements

For the Degree of

Doctor of Philosophy

in

Materials Science and Engineering

July 2008

Hsinchu, Taiwan, Republic of China

中華民國九十七年七月

智慧型磁性水膠及奈米微球於藥物控制釋放之研究

研究生：劉定宇

指導教授：陳三元

國立交通大學材料科學與工程系

摘要

在控制藥物釋放的系統中-特別是在外力場刺激下以及可標定式(targeting)作用之智慧型藥物釋放系統-在全球已經引起各學界與業界人士的注意。為了能夠有效地控制藥物釋放的行為，我們已經發展出能夠藉由外加磁場作為驅動力來控制藥物釋放的一系列磁敏感性水膠材料，利用磁場作為驅動力的好處在於磁力是一種超距力(非接觸力)，在生醫材料的應用上比較能夠被操控，因此能夠替代傳統的酸鹼敏感性或熱敏感性的水膠材料。

此論文第一部份，主要著重於直流電(DC)磁場對於ferrogel之控制藥物釋放，當磁場啟動時，ferrogel裡的奈米磁性粒子會聚集形成“pearl-chain”結構，因此造成ferrogel體積及孔洞的縮小及關閉情形，藥物因此較難通過，我們稱為“close” configuration (關閉效應)，並且在磁場關閉的瞬間會有噴出效應(bursting)的產生，因此在這部分的工作，主要是針對不同無機(氧化鐵)/有機(高分子)比例之ferroge對於磁敏感性、關閉效應及噴出效應之探討，並找出影響這些效應的關鍵因素，包括氧化鐵顆粒大小、孔隙度、磁化強度(magnetization)，高分子交聯度等，找出最佳製作ferroge之條件，進而達到最佳化的磁敏感效應。

而在第二部分中，主要著重在於ferrogel在交流電(AC)磁場下之控制藥物釋放情形。此機制與DC磁場下大不相同，主要是奈米磁性粉體在快速翻轉下造成ferrogel的結構被撐開，或是在溫度敏感型高分子下，奈米磁性粉體快速翻轉所造成之溫度上升(局部放熱效應)，溫度敏感型高

分子因此收縮所造成之pumping效應，將藥物噴出(bursting)，因此，我們將結合熱敏感以及磁敏感性兩種特性的材料加以製備成核(磁性材料)-殼(溫度敏感性水膠，Pluronic®)結構的奈米磁性粒子(藥物載體)，並且觀察其奈米粒子在交流電(AC)磁場下(局部加熱效應)之藥物投遞狀況及殺死細胞之情形。首先，利用TEM、XRD、拉曼光譜、XPS來觀察溫度敏感型磁性奈米粒子的表面特性及結構。然後再使用動態光散射(DLS)來量測此藥物載體隨溫度改變之粒徑大小及臨界溫度轉換點(CMT)。當溫度因為局部加熱而升高時，Pluronic®會由原本親水性的結構轉變成疏水性的結構，因此造成整個材料的收縮，而載體中的藥物便能夠藉此收縮作用而被擠壓出來，最後並達到控制釋放藥物之效果，並藉由局部加熱及所釋放之抗癌藥物來殺死腫瘤細胞。最後，此磁性奈米粒子之細胞毒性及免疫反應(生物相容性測試)也將被探討，以確保可以實際應用於人體。

由於磁性奈米粒子(水膠)還能利用MRI來作為細胞追蹤的標的，或是在磁性奈米粒子表面接枝特定抗體，使此特殊架接的奈米粒子可以與特定細胞之抗原結合，以達到標定式之藥物釋放。除此之外，磁性奈米粒子具備可回收性又能夠有效分離特定的細胞，因此此功能性磁性奈米粒子(水膠)將可以被預期廣泛應用於生物醫學材料上。

關鍵詞：氧化鐵、磁性水膠、磁敏感性、溫度敏感性、藥物控制釋放

Study on Intelligent Magnetic Hydrogel and Nanosphere for Drug Controlled Release

Student : Ting-Yu Liu

Advisor : San-Yuan Chen

Department of Materials Science and Engineering
National Chiao Tung University

Abstract

Controlled drug release has been received greatest attention worldwide, especially stimuli-responsive- or targeted-drug-delivery systems. In order to accelerate the response of an adaptive gel to stimuli, the use of magnetic field sensitive gels as a new type of actuator has been developed in our preliminary study by direct current (DC) magnetic fields. Magnetic-sensitive polymer is superior to that traditional stimulus response polymer, such as pH or thermal sensitive polymer, because magnetic stimulation is an action-at-distance force (non-contact force) which is easier to adapting to biomedical devices. The magneto-elastic properties of ferrogels could be applicable to a variety of fields as a new driving mechanism.

The first part in this paper is focused on the direct current (DC) magnetic field to control drug release on the ferrogel. The “closure” configuration, which means the pore size of ferrogel would decrease to obstruct the drug to pass through, would take place with the pearl-chain structure formation while DC magnetic field was applied. However, the accumulated drug was spurt (bursting effect) to the environment instantly when the magnetic fields instantly switched “off”. Some factors of the ferrogel would be investigated, ex. ratio of inorganic (iron oxide) and organic (polymer), the size of iron oxide nanoparticles, porosity, magnetization, and crosslinking degree to achieve the optimum magnetic-sensitive behavior.

To increase the degree of stimuli-responsive in magnetic fields, core (magnet)-shell (Pluronic®)-typed magnetic nanoparticles (drug-carriers), which combined the thermal and magnetic sensitive properties; therefore,

dual-functional drug-carriers would be developed by in-situ co-precipitation process. Furthermore, drug-delivery rate at on-off operation of AC magnetic fields (hyperthermia effects) and the conditions of killing-tumor cells also would be observed. Some characterizations would be investigated using transmission electron microscope (TEM), X-ray diffraction (XRD), Raman spectrometry, X-ray photoelectron spectroscopy (XPS), and vibrating sample magnetometer (VSM). The critical micellization temperature (CMT) or lower critical solution temperatures (LCST) would be measured by dynamic light scattering (DLS) or a differential scanning calorimeter (DSC). When the arising temperature of drug-carriers is higher than CMT, the drugs can be burst from the drug-carriers by the volume compressed.

In order to *in vivo* test in the future, some biocompatibility test, including cytotoxicity would be evaluated. In addition, the magnetic nanoparticles still provides some advantages, such as using magnetic resonance image (MRI) techniques for cell-tracking and grafted probe-proteins (such as biotin or antibody) onto magnetic nanoparticles for “target” drug delivery, as well as the magnetic materials could be “recycle” used and separating cells by magnet catching. Therefore, the magnetic drug-carriers (ferrogel) are able to be triggered by thermal and magnetic changes, and especially put emphasis on “target” drug-delivery and the conditions of killing tumor-cells, as well as cell-tracking by MRI, or others detecting technique also would be anticipated.

Keywords: Iron oxide, ferrogel, magnetic sensitive behavior, thermal sensitive behavior, drug controlled release

Acknowledgments

First of all, I am deeply appreciative to my supervisor Prof. Dr. San-Yuan Chen for his all-out supports, useful discussions and kindness advices during my study period. Prof. Dr. San-Yuan Chen is not only a benevolent supervisor but also a very erudite philosopher. I have benefited much from his philosophy of life. I also sincerely thank Prof. Dr. Dean-Mo Liu of for his fruitful discussions and warmhearted help in my paper writing work. Moreover, I am grateful to Prof. Dr. I-Wei Chen for giving me an opportunity to study in the University of Pennsylvania (UPENN, USA) as a visiting student. I really learn a lot from your advising. Also, I thank Prof. Dr. Ging-Ho Hsiue, Dr. Kung-Hwa Wej, Dr. Tai-Horng Young and Dr. Ming-Chien Yang attend ing my thesis defence as referees and give me many valuable suggestions.

My works have largely been a collaborative effort. Therefore, I would like to thank my colleagues: Shang-Hsiu, Kun-Ho, Chi-Sheng, Yen-Yu, and Hung-Chou in the National Chiao Tung University. Finally, I want to thank my family (especially my wife-Li-Ying and my baby-Ivy) and friends for their selfless supports and encouragement during my study period.

Ting-Yu Liu at summer, 2008

Contents

中文摘要	I
Abstract	III
Acknowledgments	V
Contents	VI
Figure Captions	XVII
Table Captions	XVII
Chapter 1 Introduction	1
Chapter 2 Literature Review and Theory	8
2.1 Hydrogels in Biomedicine	8
2.1.1 Biological Hydrogels	8
2.1.2 Synthetic Hydrogels	9
2.1.3 Responsive Hydrogel Systems	11
2.2 Fabrication of the hydrogel for drug carriers	13
2.2.1 Lyophilization (freeze-drying) process	13
2.2.2 Freezing and thawing process	15
2.2.3 Double emulsion Technique	15
2.3 Polymeric Hydrogel for modulated drug release	17
2.3.1 Electric field (pH sensitive) Stimulus	18
2.3.2 Light Stimulus	19
2.3.3 Mechanical Signal stimulus	21
2.3.4 Temperature stimulus	22
2.3.5 Magnetic fields stimulus	24
2.4 Ferrogel	26
2.4.1 Synthesis of magnetic iron oxide nanoparticles	27
2.4.2 Hysteresis	28
2.5 Magnetic composites for biomedical applications	30
2.5.1 Inductive Heating	34
2.5.2 Controlled drug release via magnetic field stimulus	35
Chapter 3 Experiment Methods	40
3.1 Flowchart of Experiment Process	40

3.2 Drug delivery test	41
3.3 Drug diffusion test	43
3.4 Characteristics Analysis	44
3.5 Methylthiazol tetrazolium (MTT) assay	46
Chapter 4 Biodegradable Ferrogel (Gelatin)	48
4.1 Introduction	48
4.2 Gelatin Ferrogel.....	51
4.2.1 Fabrication of gelatin ferrogel.....	51
4.2.2 Characterzation of gelatin ferrogel	51
4.3 Gelatin Ferrosponges.....	56
4.3.1 Fabrication of ferrosponges.....	56
4.3.2 Characterization of magnetic-sensitive ferrosponges	57
4.3.3 Crystalline phase identification of Ferrosponges	58
4.3.4 Magnetic property of Ferrosponges	60
4.3.5 Nanostructural analysis of Ferrosponges.....	61
4.3.6 Drug release behaviors of ferrosponges	62
4.3.7 Magnetically controlled drug release of ferrosponges	64
4.3.8 Magnetic-sensitive behavior of ferrosponges.....	67
Chapter 5 Non-Biodegradable Ferrogel (PVA): Effect of particle size and switching duration time	71
5.1 Introduction	71
5.2 Ferrogel preparation.....	72
5.3 Phisycal crosslinking (freezing and thawing process) of ferrogel	73
5.4 Characterization of magnetic-sensitive ferrogels.....	74
5.5 Effects of switching duration time (SDT).....	77
5.6 Effects of Fe ₃ O ₄ particle size	80
5.7 Mechanism of magnetic-sensitive drug release behavior	81
5.8 Particle size effect in the AC magnetic field (HFMF)	83
Chapter 6 Non-Biodegradable Ferrogel (PVA): Effect of Fe₃O₄ and PVA.....	85
6.1 Introduction	85
6.2 Ferrogel preparation.....	87
6.3 Role of iron oxide content.....	88

6.4 Effects of space restriction	92
6.5 Effects of magnetization	96
6.6 Role of PVA content	98
6.7 Melting temperature (T_m) of PVA ferrogel	102
6.8 Other applications (Arrangement nanoparticles in the ferrogel)	102
Chapter 7 Thermo-sensitive Ferrofluids	105
7.1. Introduction	105
7.2 Fabrication of thermo-sensitive ferrofluids.....	105
7.3 Characterization of thermo-sensitive ferrofluids	106
Chapter 8 Thermal and Magnetic Nano Ferrospheres	110
8.1 Introduction	110
8.2 Fabrication of Pluronic® F127 ferrosphere.....	114
8.3 Morphology and Characterization of F127-MNPs.....	115
8.5 Drug delivery test by HFMF	120
8.6 Cytotoxicity test.....	124
Chapter 9 Thermal and Magenetic Nano Ferrocapsules	126
9.1 Introduction	126
9.2 Fabrication of Pluronic® ferrocapsules.....	127
9.2.1 Synthesis of Activated PEO-PPO-PEO Polymers (F127 and F68) ..	127
9.2.2 Fabrication of Activated PEO-PPO-PEO Nanocapsules	128
9.2.3 Fabrication of Double-layer Cross-linked Pluronic®/Gelatin Nanocapsules	128
9.2.4 Encapsulated Drug and Iron Oxide Nanoparticles into Nanocapsules	131
9.3 Structure of NPC-Activated F127 and F68	132
9.4 Size of Nanocapsules.....	133
9.5 Cross-linked Nanocapsules	135
9.6 Nano Ferrocapsules Formation	137
9.7 Thermo sensitive behavior	140
9.8 Drug release behavior	141
9.8.1 Nanocapsules	141
9.8.2 Nano ferrocapsules.....	146
9.9 Overall Discussion.....	147

9.9.1 Pluronic/Gelatin Cross-linking @Nanocapsules.....	147
9.9.2 Pluronic®/Gelatin Nano Ferrocapsules	150
9.9.3 Thermo sensitive behavior	150
9.9.4 Drug release behavior	151
Chapter 10 Application.....	154
10.1 Fluorescence dye release in the ferrocapsules	154
Chapter 11 Conclusion.....	159
11.1 Biodegradable Ferrogel (Gelatin)	159
11.2 Non-Biodegradable Ferrogel (PVA)	159
11.3 Thermal sensitive Ferrogel (Pluronic®)	159
References	165
Appendix 1: Magntic Variables and Units	173
Appendix 2: (News) Smart magnetic hydrogels for drug release	175
Appendix 3: Controlled Pulsatile Drug Release from a Ferrogel	176
by a High-Frequency Magnetic Field.....	176
Appendix 4: Magnetic Nanoparticles as recycling anticoagulants	179
Curriculum Vitae	186
Publications	187



Figure Captions

Fig. 1.1 Diagram of dual-functional (thermo/magnetic) drug-carriers test.....	6
Fig. 2.1 Chemical structure of gelatin (triple helix structure).....	9
Fig. 2.2 Chemical structure of genipin	9
Fig. 2.3 Representative chemical structures of synthetic neutral polymers	11
Fig. 2.4 (a) Thermal sensitive behavior of Pluronic® gel; (b) Polymer structures of Pluronic®, Pluronic® R, Tetronic® and Tetronic®	12
Fig. 2.5 Schematic representation of the freeze drying process and morphology of structure of scaffolds by SEM	13
Fig. 2.6 Different degrees of orientation during freeze drying. From left to right: -196°C, -80°C, and -20°C	14
Fig. 2.7 Schematic illustration of gel formation by freezing and thawing	15
Fig. 2.8 Scheme showing the formation of phospholipids vesicle from double emulsion technique ($W_1/O/W_2$ droplet).....	16
Fig. 2.9 Various delivery and release mechanisms of hydrogels	18
Fig. 2.10 Diagram of drug controlled release of chitosan by electric stimulus	19
Fig. 2.11 Synthetic scheme of novel shell cross-linked gold-Pluronic micelles exhibiting a thermosensitive swelling/shrinking behavior	20
Fig. 2.12 (a) A representative nanoshell-composite hydrogel in the fully swollen and collapsed states; (b) Deswelling ratio of hydrogels in periods when a diode laser was turned off (A) or on at 2.6Wcm^{-2} (B)	20
Fig. 2.13 Schematic description of anticipated drug release from polymeric matrices under mechanical signaling: (a) Expected release behavior of drug that does not strongly interact with the matrix; (b) Proposed release behavior of drug that interacts with the matrix. (solid circle: free drug; open circle: bound drug)	21
Fig. 2.14 Diagram of deformation (a) and stress relaxation (b) of alginate gels under mechanical loading in vitro, which involves 5 cycles of compression for 2 min followed by relaxation for 8 min.....	22
Fig. 2.15 (a) Schematic illustration of on–off release from a squeezing hydrogel device for drug delivery; (b) Interactions between PIPAAm-PBMA micelles and cells modulated by temperature control	23
Fig. 2.16 Thermally reversible Pluronic®/heparin nanocapsules exhibiting 1000-fold volume transition	24

Fig. 2.17 (a) Snapshots from the motion of a magnetic-field-sensitive polymer gel, and the rule behind the gel indicates the amplitude of the oscillation, which is more than 4 cm; (b) Snapshots from the motion of a magnetic gel, and the rule behind the gel indicates the amplitude of the oscillation, which is about 3 cm	26
Fig. 2.18 Scheme showing the reaction mechanism of magnetite particle formation from an aqueous mixture of ferrous and ferric chloride by addition of a base.....	28
Fig. 2.19 Full-loop hysteresis curve. M_s is the saturation magnetization, M_r is the magnetization remanence (at $H=0$), and H_c is the coercivity	29
Fig. 2.20 Relationship of the particle size and hysteresis coercivity (H_c)	30
Fig. 2.21 Magnetic composites for biomedical applications: (a) Cell targeting, (b) Cell labelling, (c) MRI, (d) Local Drug delivery, (e) Hyperthermia (inductive heating).....	33
Fig. 2.22 Heating ability of each ferrite increased with an increase of the areas of hysteresis loops and the frequency of alternating magnetic field	34
Fig. 2.23 Diagram of (a)&(b) the equipment of the alternating magnetic field for killing tumor cells in the mice (c) without (d) with heating nano-magnetic-particles.....	35
Fig. 2.24 Application of the technique of ferrogel and hyperthermia	38
Fig. 2.25 Drug bursting delivery with the temperature increase and the volume compressing of polymer gel: Volume compressing of ferrosphere to form channel to induce the drug pass through	39
Fig. 3.1 Equipment of high frequency magnetic field	42
Fig. 3.2 Diaphragm cell for measuring the permeability coefficient.....	44
Fig. 4.1 Schematic drawing of drug release from the magnetic-sensitive ferrosponges with and without applying external magnetic field	50
Fig. 4.2 (a) OM photos of the gelatin gels with different cross-linked densities and (b) UV spectroscopy analysis of different cross-linked gelatin hydrogels.....	52
Fig. 4.3 (a) SEM observation of Fe_3O_4 nanoparticles distributed in gelatin hydrogels and (b) sensitive swelling rate of the ferrogels dependent on switching MF.	53
Fig. 4.4 Mechanism of “close” configuration of the ferrogels due to the aggregation of Fe_3O_4 nanoparticles under “on” MF causes the porosity of the ferrogels to decrease.	54
Fig. 4.5 (a) Drugs release rate profiles of the Ge0.003 ferrogels in MF switching	

“on” or “off” mode (b) hysteresis loop analysis of the magnetic hydrogels using VSM.	55
Fig. 4.6 Sensitive drugs release properties of the ferrogels dependent on switching “on-off” mode for a given MF.	55
Fig. 4.7 SEM images of the ferrosponges for 5wt% (a) and 15wt% (b) gelatin concentrations.	58
Fig. 4.8 (a) XRD and (b) Raman spectra of the ferrosponges.	59
Fig. 4.9 Vibrating sample magnetometry measurements for the ferrosponges with various contents of iron oxide nanoparticles.	60
Fig. 4.10 SEM images of iron oxide nanoparticles structure of the sponges obtained by thermally removing gelatin matrix for the ferrosponges with (a) original 5G-5F and (b) 15G-5F compositions, and (c) associated with the pore size distribution of the ferrosponges treated with and without magnetic field.	62
Fig. 4.11 Drug release profiles of 5G series of the ferrosponges.	64
Fig. 4.12 Drug release profiles with and without applying magnetic field (“MF on” and “MF off”, respectively.) for 5G-5F ferrosponge.	65
Fig. 4.13 A plot of $\ln(M_t/M_\infty)$ versus $\ln(t)$ of (a) 5G-5F, (b) 5G-1F and (c) 5G-3F showed a two-step relationship for calculating the values of k and n , and the corresponding schematic drawing of the shrinkage of the mesopores in the ferrosponges (d) while a magnetic field was applying.	67
Fig. 4.14 Comparison of the magnetic-sensitive behaviors of the ferrosponges for both 5G and 15G series compositions.	68
Fig. 4.15 Inorganic/organic ratios of ferrosponges related to the magnetic sensitive behaviors (%) and saturation magnetization (M_s).	69
Fig. 4.16 Relative drug release rates of the ferrosponges under repeated on-off MF operations, showing a fast degradation in the release rate with less MNP concentration, but much improved release behavior with respect to cyclic operation when MNP is increased and seems to be optimized in 5G-5F composition, i.e., indicating an improved anti-fatigue property.	70
Fig. 5.1 DSC analysis of PVA physical crosslinking by freezing and thawing cycles: (a) cooling curve; (b) heat flow and temperature change with different cycles.	74
Fig. 5.2 (a) Cross-sectional SEM image of magnetic particles disperse in PVA hydrogels and OM photos of PVA5-LM17 ferrogels; (b) Swelling ratio and swelling rate of PVA5-LM17 ferrogel in the magnetic fields switching	

“on”-“off” mode.	75
Fig. 5.3 Rapid permeation properties and “close” configuration of the ferrogels dependent on (a) different switching duration time (SDT) and (b) various particle size of Fe_3O_4 of the ferrogels in the continuous switching “on-off” mode for a given magnetic fields; the drug permeation amount on switching “on-off” mode, and corresponding differential curve are shown in each figure in order to show the maximum drug bursting.....	79
Fig. 5.4 Hysteresis loop analysis of the ferrogels incorporated with various particle sizes of Fe_3O_4	81
Fig. 5.5 Mechanism of “close” configuration of the ferrogels due to the aggregation of Fe_3O_4 nanoparticles under “on” magnetic fields causes the porosity of the ferrogels to decrease.	82
Fig. 5.6 Comparison of hyperthermia effect and drug release behavior in the various particle size of ferrogel	84
Fig. 6.1 Diagram of the mechanism of “closure” configuration of ferrogels.....	86
Fig. 6.2 Pearl-chain structure was developed with the magnetic field	86
Fig. 6.3 SEM image of pearl-chain structure.....	87
Fig. 6.4 (a) Both permeability coefficient (P) and partition coefficient (H) of ferrogels in “on” or “off” mode of a given magnetic field; (b) Diffusion coefficient (D) of ferrogels in “on” or “off” mode of a given magnetic field.; (c) Magnetic-sensitive behaviors of ferrogels with different Fe_3O_4 concentration; Region A: Region of Increasing “Sensitivity”; Region B: Saturation Region; Region C: Region of Decreasing “Sensitivity”	91
Fig. 6.5 (a) Models of the unit cell ($600nm^2$) of PVA-based ferrogels which Fe_3O_4 particles distributed; (b) SEM cross-section image of PVA10-MP34 ferrogel. (c) Schematic drawing of the relationship of surface-to-surface distance between two neighboring particles (d) and available free volume (V_{free}).....	93
Fig. 6.6 Comparison of (a) porosity (%), volume fraction of Fe_3O_4 particles ($V_f(Fe_3O_4)$) and magnetization (Ms); (b) both available free volume (V_{free}) and interaction energy (E_{int}) of ferrogels dependence of various Fe_3O_4 concentrations.....	95
Fig. 6.7 Hysteresis loop analysis of the ferrogels incorporated with various Fe_3O_4 additions measured by VSM.	97
Fig. 6.8 Permeability coefficient of various PVA addition in “on” or “off” mode of a	

given magnetic field with (a) 17% Fe ₃ O ₄ contents and (b) 34% Fe ₃ O ₄ contents; (c) Comparison of magnetic sensitive behaviors between 17% and 34% Fe ₃ O ₄ contents.....	100
Fig. 6.9 Correlation of both available free volume (V_{free}) and interaction energy (E_{int}) in the ferrogels between 17% Fe ₃ O ₄ and 34% Fe ₃ O ₄ contents.....	101
Fig. 6.10 Comparison of melting temperature (T_m) in the pure PVA10, PVA10-MP17 and PVA10-MP34 ferrogel by DSC.....	102
Fig. 6.11 Schematic representation of the experimental set-up for ferrogel preparation under uniform magnetic field: (a) & (a1) drug diffusion direction is vertical to the arrangement of iron oxide nanoparticle; (b) & (b1) drug diffusion direction is parallel to the the arrangement of iron oxide nanoparticle.....	103
Fig. 6.12 Drug diffusion behavior in the various ferrogel; random, vertical and parallel means the arrangement of iron oxide nanoparticle is random, vertical and parallel to the drug diffusion direction, respectively.....	104
Fig. 7.1 (a) TEM photo of core-shell NMPs; (b)XRD pattern of core-shell NMPs.; (c) Magnetization curve of core-shell NMPs using VSM.	106
Fig. 7.2 DSC heating and cooling scans of pure F127-fluids and F127-ferrofluids..	107
Fig. 7.3 Series image of thermo response behavior of ferrofluids: (a)&(b) liquid state (ferrofluids); (c)&(d) gel state (ferrogel).....	108
Fig. 8.1 Diagram showing the proposed synthesis process of F127-MNPs: (a1) F127/iron salts nanosphere formation by sonication; (a2) F127-MNPs formation after adding ammonia solution to pH=10; Proposed mechanism for drug encapsulation and delivery process of F127-MNPs by HFMF: (b1) Drug diffuses into the nanospheres at lower temperature (4°C, swelling state); (b2) Slight volume shrinkage and drug encapsulated in the nanospheres after slight heating to 15°C; (b3) Sharp volume shrinkage with accelerative drug release under HFMF treatment.	113
Fig. 8.2 TEM image of the morphology of (a) Pure F127 nanospheres; (b) Distribution of F127-MNPs; (b1) TEM image of F127-MNPs nanospheres (iron oxide nanoparticles were encapsulated in the F127 nanospheres); (b2) High resolution TEM image showing crystalline condition of iron oxide in the F127 nanosphere; (c) Diffraction pattern of F127-MNPs.	116
Fig. 8.3 Characterization analysis of F127 and F127-MNP nanospheres: (a) X-ray diffraction, (b) Raman spectra, and (c) XPS spectra.....	118
Fig. 8.4 Hydrophilic/Hydrophobic test of F127-MNPs with various temperatures:	

Solid circle curve indicates CMT test by PL (left axis), whereas particle size test by DLS (right axis) is indicated by open circle curve.....	120
Fig. 8.5 (a) Inductive heating experiments under HFMF treatment; solid circle curve and open circle curve indicate F127-MNPs and F127 nanospheres, respectively; temperature increased to 62°C for the F127-MNPs under HFMF treatment for 60 min, but, for F127 nanospheres, it reached only 30°C; (b) Drug delivery test of F127-MNPs. Solid circle curve indicates that the samples were first incubated at 15°C (water bath) for 50 min and then exposed to HFMF (magnetic-thermal effect). Open circle curve indicates that, after incubated at 15°C for 50 min, the samples were incubated at 35°C in a water bath (thermal effect, without HFMF), but open triangle means the samples have been incubated at 15°C in a water bath (50 + 30 min).....	122
Fig. 8.6 BET analysis on pore size change and TEM images of F127-MNPs with and without HFMF. One sample is without HFMF treatment (left side), and the other one is “after” the magnetic filed treatment (right side) in the TEM images.	123
Fig. 8.7 Comparison of SMCs proliferation on the F127-MNPs loading drug (DOX) with and without HFMF by MTT assay. The star means they display insignificant difference, while the double star means that they display significant difference. (n=5).....	124
Fig. 8.8 Proliferation of smooth muscle cell for 72 hr incubation in the F127-MNPs (a) without drug in the absence of HFMF; (b) with drug in the absence of HFMF; (c) with drug in the presence of HFMF.	125
Fig. 9.1 ¹ H NMR spectra of activated Pluronic® (a) F128 and (b) F68 by NPC.....	133
Fig. 9.2 Relationship of particle size and content of Pluronic® (a) F127-NPC; (b) F68-NPC) in the single emulsion, double emulsion, and W1-in-oil process.	134
Fig. 9.3 Relationship of particle size distribution and gelatin concentration measured by DLS.	135
Fig. 9.4 TEM images of formation of activated Pluronic® F68 nanocapsules: Pluronic® particle is self-assembly to the geometry of sphere structure (a) without washing and (b) after washing; (c) nanosphere was crosslinked by gelatin and EDC.....	137
Fig. 9.5 Crystallization change with the Pluronic® concentration increase measured by XRD.....	138
Fig. 9.6 TEM images of (a) 1g/ml, (b) 0.5g/ml and (c) 0.3g/ml of Pluronic®	

F68-NPC nano ferrocapsules; (a1) 1g/ml, (b1) 0.5g/ml and (c1) 0.3g/ml of iron carbonyl nanoparticles loading in the nanocapsules; (a2) 1g/ml, (b2) 0.5g/ml and (c2) 0.3g/ml of TEM diffraction pattern of ferrocapsules; (a3) Skin layer in the ferrocapsule; (d) ferrocapsules have been disintegrated after HFMF treatment.....	139
Fig. 9.7 CMT measurement and particle size change with temperature change by DLS.....	141
Fig. 9.8 (a) Drug delivery behavior of nanocapsules and ferrocapsule under thermal and HFMF modulation; (b) calculation of the parameters of drug delivery (n, k and D_e)	144
Fig. 9.9 (a) Diagram of comparison of particle size change in the activated Pluronic® F127 and F68 nanocapsules; TEM images of F68-NPC (b) multiple core under dilute concentration (c) single core under high concentration; (d) F127-NPC single core nanocapsules.....	149
Fig. 10.1 Fluorescence dye release behavior from the ferrocapsules: (a) without HFMF and UV light; (b) without HFMF and with UV light; (c) with HFMF without UV light; (d) with HFMF and UV light.....	155
Fig. 10.2 Scheme of the coating process and chemical reaction of F127-NPC ferrofluids loading F68-NPC ferrocapsules on the Si substrate.....	157
Fig. 10.3 Fluorescence dye release behavior from the Si substrate coating with ferrogel (a) without HFMF and UV light ; (b) without HFMF and with UV light ; (c) with HFMF without UV light ; (d)with HFMF and UV light.....	158

Table Captions

Table 2.1 Critical diameter of single-domain (D_s) and super paramagnetic (D_{sp}) in the magnetic materials	29
Table 2.2 Magnetic composites for biomedical applications	31
Table 2.3 Sustained zero-order release under DC magnetic field.....	36
Table 2.4 Pulsatile release under AC (oscillating) magnetic field.....	37
Table 4.1 Cumulative drugs release of the ferrogels in “on” or “off” mode of a given magnetic field at 120 min.	53
Table 4.2 Reagents used for the synthesis of ferrosponges	57
Table 4.3 k and n values of ferrosponges under the modes of magnetic on (MF on) and off (MF off).	66
Table 5.1 Permeability coefficient of the ferrogels in “on” or “off” mode of a given magnetic field.....	76
Table 6.1 Average permeability coefficient (P) of the ferrogels at a given magnetic field.....	88
Table 9.1 Characterization of F127 and F68-series micelles in the content of 1g/ml Pluronic®	136
Table 9.2 Calculation of the parameters of drug delivery (n, k and D_e) in the Pure 68, F68-Ge, F68-EDC and F68-EDC-IO	145

Chapter 1

Introduction

Controlled drug release has received greatest attention worldwide since the past few decades because it revolutionizes the use of a given active drug with a therapeutically smarter, more effective, and more patient-wide compliant manner to treat diseases [Qiu, 2001; Miyata, 2002; Weissleder, 1995]. With the advancement and understanding of materials technology up-to-date, a number of methods have been successfully proposed to integrate an active drug molecule and a host materials, which in the past where a physical blend between drug (powder) and a polymeric binder is prepared for administration, with a delicate consideration of how the host matrix can be designed to regulate the release of drug in a controllable manner. Preparation of a drug delivery system is highly challenging with respect to the nature of drug to be incorporated, the physical, chemical, and biological property of host matrix, the profile of release, and ultimate bioavailability for the drug to target the sites of disease. In tradition, a polymeric host can be designed with a property suitable to properly anchor either physically or chemically with a given drug molecules, wherein the drug molecules are physically encapsulated into the host, and a subsequently release of the drug can be achieved via diffusion of drug, degradation of the host, and a combination thereof after the drug delivery system is administrated into patient's body.

At present there are several adaptive (smart, intelligent) materials that can actuate or alter their properties in response to a changing environment. Among them mechanical actuators has been the subject of much investigation in recent years [Deng, 2003; Kim, 2002; Fernandes, 2003; Xulu, 2003; Zrínyi, 2000 & 1998]. They undergo a controllable change of shape due to some physical effects and can convert energy (electrical, thermal, chemical) directly to mechanical energy. This can be used to do work against load. Certain polymer gels represent one class of actuators that have the unique ability to change elastic and swelling properties in a reversible manner. These wet and soft materials offer lifelike capabilities for the future direction of technological development. Volume phase transition in response to infinitesimal change of external stimuli like pH, temperature, solvent composition, electric field, and

light has been observed in various gels. Their application in devices such as actuators, sensors, separators artificial muscles, and controlled delivery systems has been suggested and are in progress.

Attempts at developing stimuli-responsive gels for technological purposes are complicated by the fact that structural changes, like shape and swelling degree changes that occur, are kinetically restricted by the collective diffusion of chains and the friction between the polymer network and the swelling agent. This disadvantage often hinders the effort of designing optimal gels for different applications. In order to accelerate the response of an adaptive gel to stimuli, the use of magnetic field sensitive gels as a new type of actuator has been developed. Furthermore, this magnetic-sensitive polymer is even superior to that traditional stimuli response polymer, such as pH or thermal sensitive polymer, because magnetic stimulation is an action-at-distance force (non-contact force) which is easier to adapting to biomedical devices. The magneto-elastic properties of ferrogels could be applicable to a variety of fields as a new driving mechanism.

For the purpose to control release by magnetic field, this thesis was mainly categorized two parts: Chapter 4, 5 and 6 focus on the controlled release by direct current (DC) magnetic fields and the material is gelatin (biodegradable polymer) in the Chapter 4; PVA (non-biodegradable polymer) in the Chapter 5 and 6. The mechanism in the DC magnetic fields controlled is the “closure” configuration with the pearl-chain structure formation while the field was applied. However, the accumulated drug was spurt to the environment instantly when the magnetic fields instantly switched “off”. Another part (Chapter 7, 8, 9 and 10) emphasized on controlled release by alternating current (AC) magnetic field and the material is belong to thermal sensitive polymer (Pluronic® F127 and F68). The mechanism in the AC magnetic fields controlled is the “bursting” effect, which is subjecting to a rapid conformational change as the magnetic phase being heated rapidly in the presence of high frequency magnetic field (HFMF) and a subsequent heat transfer to the shell, causing the considerable elastic volume shrinkage, resulting in a burst release of a model drug.

Briftly, Chapter 4 describes the magnetic hydrogels were successfully fabricated by mixing gelatin hydrogels and Fe_3O_4 nanoparticles (ca. 40-60 nm) through

chemically-cross-linked process using genipin (GP). The cross-sectional SEM observation demonstrates that the Fe_3O_4 nanoparticles were fairly uniformly distributed in gelatin hydrogels. Moreover, the in vitro release data reveal that it is able to control drug release profile of the resulting hydrogels by switching “on” or “off” mode of a given magnetic field. While applying magnetic fields to the magnetic hydrogels the release rate of vitamin B_{12} of the hydrogels decreased considerably, comparing to those while switching off the field, suggesting a “closure” configuration of the hydrogels as a result of the aggregation of Fe_3O_4 nanoparticles. Based on this mechanism, a smart magnetic hydrogels can be potentially developed as drug delivery system and also used for the application of biomedical devices.

Besides, in order to increase the drug loading (%), magnetic sponge-like hydrogels (ferrosponges) were fabricated by using an in-situ synthesis of magnetic nanoparticles (MNPs) in the presence of various concentrations of gelatin. The resulting ferrosponges show an interconnected nanopore structure which serves as a reservoir to accommodate therapeutic drugs and the nanoporous networks demonstrate magnetic sensitive behavior under the application of a given magnetic field. The ferrosponges showed high swelling ratios, together with excellent elasticity and hydrophilicity, allow them to respond rapidly to an external magnetic stimulation for fast and repeatable swelling-deswelling (or expansion-contractile) operations. The ferrosponges with lower gelatin concentration exhibited good performance on magnetification. Furthermore, drug release from the ferrosponges is relatively magnetic-sensitive and is dominated by its magnetism and associated interaction between the magnetic nanoparticle and the gelatin matrix under an external magnetic field. Higher MNPs concentration in the ferrosponges exhibited higher degree of magnetic sensitive which is due to stronger interparticle forces. By taking these peculiar magnetic sensitive behaviors of the ferrosponges, a novel drug delivery system can be designed for practical clinical uses.

Chapter 5 illustrates an intelligent magnetic hydrogel (ferro-gel) was fabricated by mixing polyvinyl alcohol (PVA) hydrogels and Fe_3O_4 magnetic particles through freezing-thawing cycle. While the external direct current magnetic field was applied to the ferro-gel, the drug was accumulated around the ferro-gel, but the accumulated

drug was spurt to the environment instantly when the magnetic fields instantly switched “off”. Furthermore, rapid to slow drug release can be tunable while the magnetic field was switched from “off” to “on” mode. The drug release behavior from the ferrogel is strongly dominated by the particle size of Fe_3O_4 under a given magnetic field. The best “magnetic-sensitive effects” are observed for the ferrogels with larger Fe_3O_4 particle due to its stronger saturation magnetization and smaller coercive force. Furthermore, the amount of drug release can be controlled by fine-tuning of the switching duration time (SDT) through an externally controllable on-off operation in a given magnetic field. It was demonstrated that the highest burst drug amounts and best “closure” configuration of the ferrogel were observed for the SDT of 10 min and 5 min, respectively. By taking these peculiar magnetic-sensitive characteristics of the novel ferrogels currently synthesized, it is highly expected to have a controllable or programmable drug release profile that can be designed for practical clinical needs.

To be continued, in Chapter 6, the influence of the constituting components, i.e., Fe_3O_4 and PVA, on the magnetic-sensitive behavior of the ferrogels was systematically investigated in terms of permeability coefficient (P), partition coefficient (H), space restriction and magnetization. The results show that, the P value in these ferrogels decreases and displays a magnetic sensitivity when it is subjected to magnetic field (MF), which is correlated with the change of H value. In addition, it was found that although the factor of space restriction or magnetization exerts opposite effect on resulting magnetic sensitive behavior, the superior magnetic-sensitive behavior was observed for the ferrogels with an optimal composition of 17-34% Fe_3O_4 and 10-12.5% PVA, and can be well correlated with theoretical calculation from the critical parameters of available free volume (V_{free}) per nanoparticle and magnetization. A map of magnetic sensitive behavior was constructed, where a region with relatively stable and highly stimuli-responsive behavior in terms of the concentration of Fe_3O_4 was observed, however, below or above the “saturation” region (17-34% Fe_3O_4), a reduction in the magnetic sensitive behavior was detected. The resulting ferrogels can be engineered with a precise control of the opening and closure of pore configuration, which allows a burst release or no-release action of therapeutically active agent to be controlled externally and magnetically. This suggests this type of ferrogel can be

considered as a class of novel magnetically-tunable drug delivery system.

In Chapter 7, thermal-sensitive ferrofluids (F127-ferrofluids) consisting of core-shell-type magnetic nanoparticles dispersed in Pluronic F127-containing aqueous solution were prepared. The core (magnet)-shell (Pluronic F127) nanoparticles were synthesized by in-situ co-precipitation process, which were characterized using transmission electron microscope, X-ray diffraction and vibrating sample magnetometer. The F127-ferrofluids gelled above the lower critical solution temperatures (LCST) of approximately 23-28°C which was higher than that of pure Pluronic F127-fluids (21-25°C). The increase in the LCST of the F127-ferrofluids may be attributed as a result of a physical interaction between the F127 molecules and the core-shell magnetic nanoparticles.

Chapter 8 demonstrated Novel dual-functional nanospheres composed of magnetic iron oxide nanoparticles embedded in a thermo-sensitive Pluronic® F127 (F127) matrix were successfully synthesized by an in-situ co-precipitation process. The nanospheres were characterized by X-ray diffraction, transmission electron microscopy, X-ray photoelectron spectroscopy and Raman spectroscopy. Experimental observations indicated that the F127 was subjected to a rapid structural change when the magnetic phase caused rapid heating after a short exposure to a high-frequency magnetic field (HFMF). During the field duration, considerable volume shrinkage of the nanospheres, 2.3-fold diameter reduction, was detected. This has been translated to an instantaneous release of a drug, Doxorubicin (DOX), when the DOX was encapsulated within the nanospheres. Such a rapidly responsive release of the DOX from the nanospheres was due to an intimate contact between the nanomagnet and F127, where an effective thermal and mechanical transfer between core and shell phases was efficiently taking place in the presence of the magnetic field.

In summary, the dual-functional drug-carriers is able to be triggered by thermal and magnetic changes, and especially put emphasis on “target” drug-delivery by grafting target protein and killing tumor-cells by inductive heating and drug delivery, as

well as cell-tracking by MRI, or others detecting technique also would be evaluated, shown in Fig. 1.1

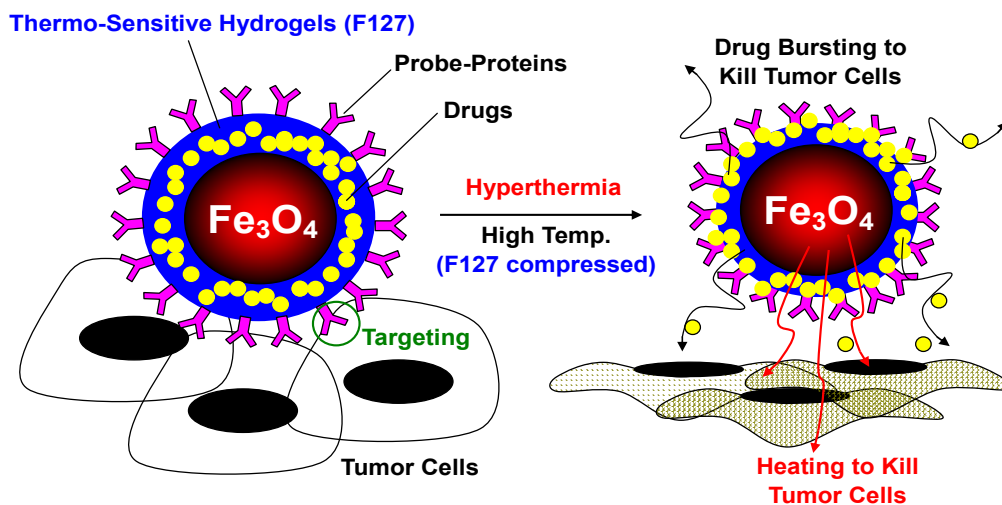
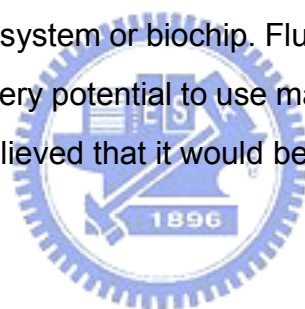


Fig. 1.1 Diagram of dual-functional (thermo/magnetic) drug-carriers test

In addition, Chapter 9 describes Magnetic nanocomposites (iron oxide) accompanying temperature responsive hydrogels (activated Pluronic® F127 and F68) used to fabricate the drug carrier (nanocapsules) for remote controlled drug delivery have been successfully synthesized by double emulsion and in-situ precipitation process. The relationship of the nanocapsules particle size and activated Pluronic® concentration would be investigated by dynamic light scattering. The change of thermo response behavior of Pluronic®, ex. critical micellization temperature (CMT) modified by activated and cross-linked and the effect between the formation of iron oxide nanoparticles (combination of Fe_3O_4 and iron carbonyl phase crystal) and Pluronic® content would be characterized in this paper. The results show that the particle size of Pluronic® nanocapsules reduces with Pluronic® concentration increase, and it displays the saturated concentration at the 0.1g/ml Pluronic® addition. CMT of nanocapsules would left shift about 4°C after 4-Nitrophenyl chloroformate (NPC) activating, right shift 1°C to after partially cross-linking by gelatin, but almost no obvious change after fully cross-linking by EDC and encapsulating iron oxide nanoparticles. In addition, high frequency magnetic field (HFMF) was used to trigger

the drug release from the nano ferrocapsules. Experimental observations indicated that Pluronic® shell is subjecting to a rapid conformational change as the magnetic nanoparticles being heated rapidly in the presence of HFMF and a subsequent heat transfer to the shell, causing considerable elastic volume shrinkage, resulting in a squeezing release of a model drug (vitamin B₁₂). The synthesized Pluronic® F68 nano ferrocapsules exhibited a 2.6-fold diameter reduction from 20°C to 45°C, and drug burst release in the HFMF (5-mins operation, ca. 45°C) exhibited 20 times higher than that in the incubation at 45°C water bath (natural release). The rapidly responsive release from the dual-functional nanocapsules is due to intimate contacts between the magnetic nanoparticles core and Pluronic® shell, where an effective thermal and mechanical transfer between core and shell phases was efficiently taking place.

In Chapter 10, the simple trial to combine ferrofluids (Chapter 7) and ferrocapsules (Chapter 9) and then coat on the Si substrate to develop an intelligent magnetic/thermal drug release system or biochip. Fluorescence dye was released just in the presence of HFMF. It is very potential to use magnetic force as a driving force to control drug release and we believed that it would be exploited in the future decade.



Chapter 2

Literature Review and Theory

2.1 Hydrogels in Biomedicine

Hydrogels that exhibit both liquid-like and solid-like behavior have a variety of functional properties, such as swelling, mechanical, permeation, surface and optical properties [Qiu, 2001]. Such properties have provided many potential applications of hydrogels in fields such as drug controlled release and biotechnology. In addition, hydrogels are the center of research emphasis in nanotechnology because of their perceived “intelligence”. They can be used as thin films, scaffolds, or nanoparticles in a wide range of biomedical and biological applications. Some recent developments in engineering uncrosslinked and crosslinked hydrogel (e.g., (1) natural, (2) synthetic polymers and (3) responsive hydrogel) [Peppas, 2006] for these applications were briefly introduced in this section.

2.1.1 Biological Hydrogels

In general, hydrogels from natural sources can be derived from polymers such as gelatin (or collagen), hyaluronic acid (HA), fibrin, alginate, agarose, and chitosan [Peppas, 2006; Lee, 2001]. Depending on their origin and composition, various natural polymers have specific utilities and properties. Many natural polymers, such as collagen, hyaluronic acid, and fibrin, are derived from various components of the mammalian extracellular matrix. Gelatin (or collagen) is the main protein of the mammalian extracellular matrix, while HA is a polysaccharide that is found in nearly all animal tissues. Alternatively, alginate and agarose are polysaccharides that are derived from marine algae sources. The advantages of natural polymers include low toxicity and biocompatibility. Gelatin (or collagen), a protein, triple helix structure (Fig. 2.1) and other mammalian-derived protein-based polymers are effective matrices for cellular growth because they contain many cell-signaling domains present in the in vivo extracellular matrix. Gelatin (or collagen) gels can be created through natural means without chemical modifications. However, in many cases these gels are mechanically weak.

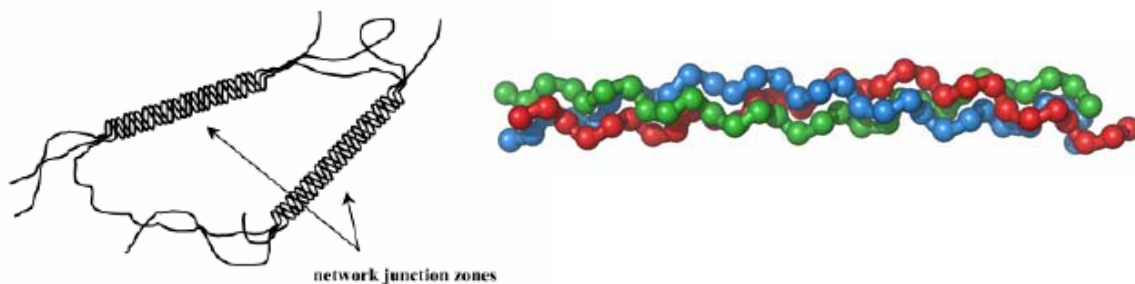


Fig. 2.1 Chemical structure of gelatin (triple helix structure) [Crescenzi, 2002; Wikipedia]

To synthesize gels with enhanced mechanical properties, various methods have been developed such as chemical crosslinking [Lee, 2001&2003], crosslinking with UV or temperature, [Lee, 2001; Schoof, 2001] or mixing with other polymeric agents [Lee, 2001; Chen, 2000]. Among of them, genipin (Fig.2.2), the active compound found in the gardenia fruit extract, which is used in traditional Chinese medicine to relieve the symptoms of type 2 diabetes, is an excellent natural cross-linker for proteins, collagen, gelatin, and chitosan cross-linking. It has a low acute toxicity, with LD₅₀ i.v. 382 mg/kg in mice, therefore, much less toxic than glutaraldehyde and many other commonly used synthetic cross-linking reagents. It is also used for pharmaceutical purposes, such as choleric action for liver diseases control.

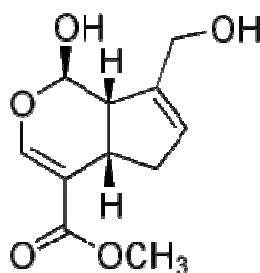


Fig. 2.2 Chemical structure of genipin [Extracted from wikipedia]

2.1.2 Synthetic Hydrogels

Polymer networks can be synthesized using various chemical methods (e.g., photo- and thermal-initiated polymerization) and physical methods (e.g. freezing-thawing methods). The polymer engineer can design and synthesize polymer networks with molecular-scale control over structure such as crosslinking density and

with tailored properties, such as biodegradation, mechanical strength, and chemical and biological response to stimuli [Peppas, 2006; Lee, 2001]. Neutral synthetic polymers can be generated from derivatives of poly(hydroxyethyl methacrylate) (PHEMA), poly-(ethylene glycol) (PEG), and poly(vinyl alcohol) (PVA) (Fig. 2.3). PVA hydrogels are one of the most widely studied and used materials for biomedical applications [Hassan, 2000]. PVA hydrogels are stable and elastic gels that can be formed by the physically crosslinked (repeated freezing and thawing process) or chemically crosslinked [Nuttelman, 2001]. PVA must be crosslinked in order to be useful for a wide variety of applications, specifically in the areas of medicine and pharmaceutical sciences. Some of the common crosslinking agents (chemical crosslinking) that have been used for PVA hydrogel preparation include glutaraldehyde, acetaldehyde, formaldehyde, and other monoaldehydes. When these crosslinking agents are used in the presence of sulfuric acid, acetic acid, or methanol, acetal bridges form between the pendent hydroxyl groups of the PVA chains. As with any crosslinking agent, however, residual amounts are present in the ensuing PVA gel. It becomes extremely undesirable to perform the time-consuming extraction procedures in order to remove this residue. If the residue is not removed, the gel is unacceptable for biomedical or pharmaceutical applications because, if it were placed directly in the body, the release of this toxic residue would have obvious undesirable effects. However, the physically crosslinked versions (freezing and thawing process) of PVA hydrogels are biodegradable, and thus can be used for various biomedical applications [Martens, 2003; Wan, 2002; Mandal, 2002; Shaheen, 2002]. This method has advantages over the use of chemical crosslinking agents as they do not leave behind toxic, elutable agents. In addition, photocrosslinkable PVA hydrogels have been synthesized that facilitate cell adhesion in tissue-engineering applications.

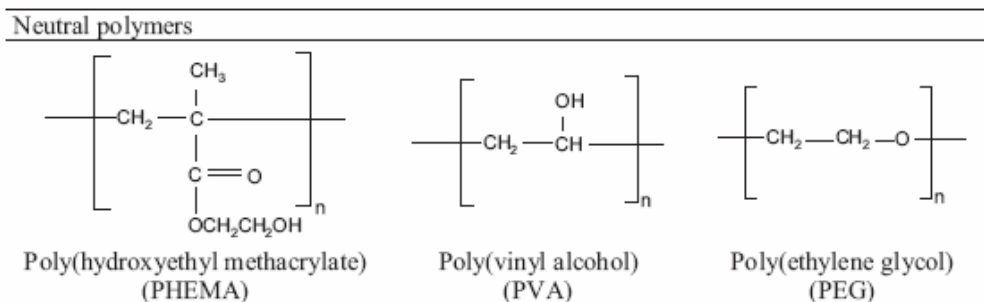


Fig. 2.3 Representative chemical structures of synthetic neutral polymers
[Peppas, 2006]

2.1.3 Responsive Hydrogel Systems

By tailoring their molecular structure, polymer networks can be created that interact with their environment in a preprogrammed and intelligent manner. Environmentally responsive hydrogels have been synthesized that are capable of sensing and responding to changes to external stimuli, such as changes to pH and temperature. Temperature-responsive hydrogels are one of the most widely studied responsive hydrogel systems. These systems, which are mostly based on poly(N-isopropylacrylamide) (PNIPAAm) and its derivatives, undergo a reversible volume phase transition with a change in the temperature of the environmental conditions. This type of behavior is related to polymer phase separation as the temperature is raised to a critical value known as the lower critical solution temperature (LCST). Networks showing a lower critical miscibility temperature tend to shrink or collapse as the temperature is increased above the LCST, and the gels swell upon lowering the temperature below the LCST. For example, PNIPAAm exhibits a LCST around 33°C. PNIPAAm and other thermosensitive hydrogels have been studied for variety of applications, including drug delivery and tissue engineering [Jeong, 2002; Sershen, 2003].

Another major polymer is tri-block copolymers composed of poly (ethylene oxide)-poly (propylene oxide)-poly (ethylene oxide) (PEO-PPO-PEO) are a kind of temperature-sensitive polymers, and they also demonstrate reversible solution transition behaviors in aqueous solution [Bromberg, 2003 & 2004; Csetneki, 2006]. It is nontoxic, non-immunogenic, and approved by the US Food and Drug

Administration (FDA) for various clinical uses. Because of the nontoxic (little residual toxicity was found in the PNIPAAm) and their LCST (or called critical micellization temperature, CMT) phenomenon at around the body temperature, they have been used widely in the development of controlled drug delivery systems based on the sol-gel phase conversion at the body temperature. The mechanism of the temperature change for Pluronic® was described in Fig. 2.4-(a).

In addition, a large number of PEO-PPO block copolymers are commercially available under the name of Pluronic® (or Poloxamers®) and Tetronics® [Qiu, 2001]. Their structures are shown in Fig. 2.4-(b)

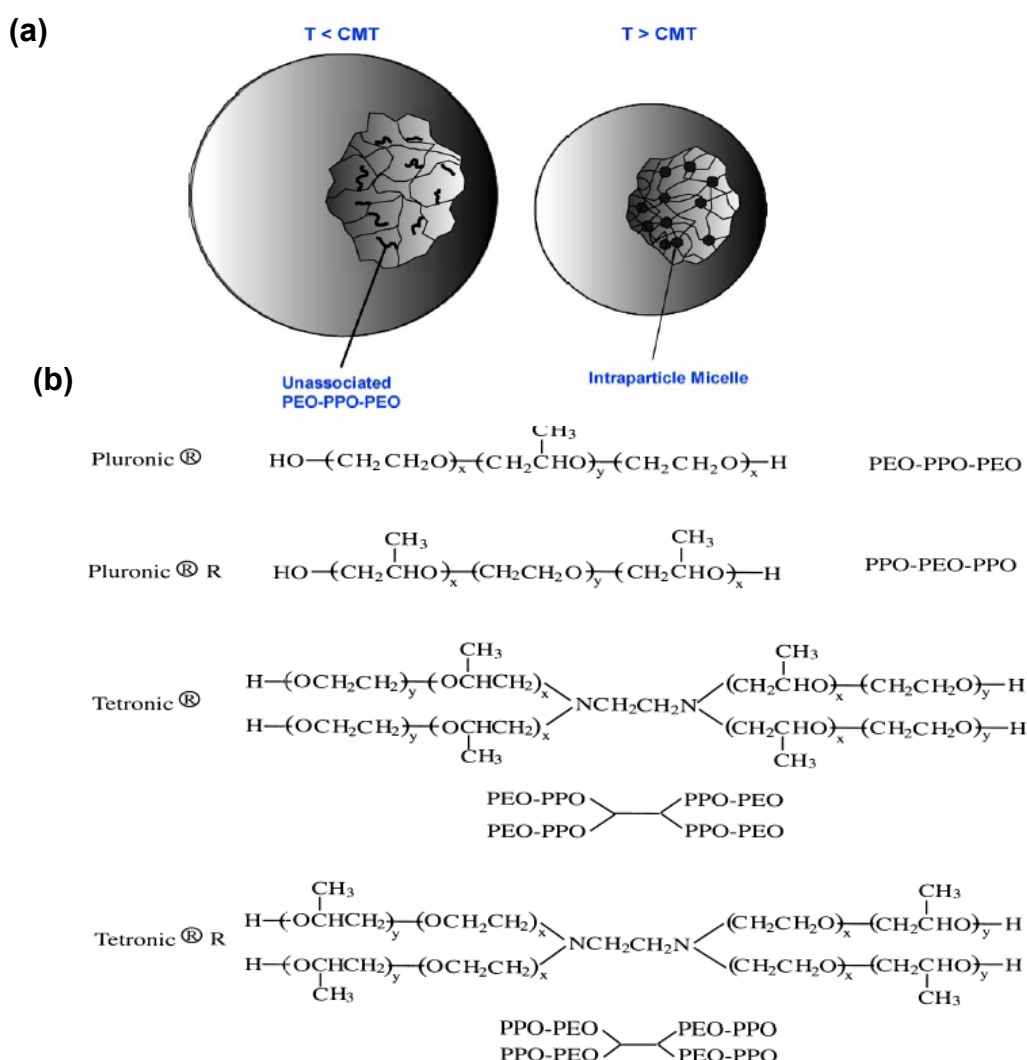


Fig. 2.4 (a) Thermal sensitive behavior of Pluronic® gel; (b) Polymer structures of Pluronic®, Pluronic® R, Tetronic® and Tetronic® R [Bromberg, *Int. J. Pharm.*, 2004; Qiu, 2001]

2.2 Fabrication of the hydrogel for drug carriers

A number of different techniques are available to prepare the hydrogel for drug carriers, such as free-radical polymerization, chemical crosslinking, phase inversion, lyophilization (freeze-drying) process, freezing and thawing process, and emulsion techniques. In particular, (1) lyophilization (freeze-drying) process, (2) freezing and thawing process and (3) emulsion techniques were used in this study and would be introduced detail in this section.

2.2.1 Lyophilization (freeze-drying) process

In the lyophilization (or freeze drying) process, materials are frozen prior to the sublimation of the ice in a freeze drying apparatus. The growing ice crystals during freezing create the pores inside a three-dimensional sample and the subsequent sublimation of the crystals leaves a three-dimensional porous scaffold (see Fig. 2.5).

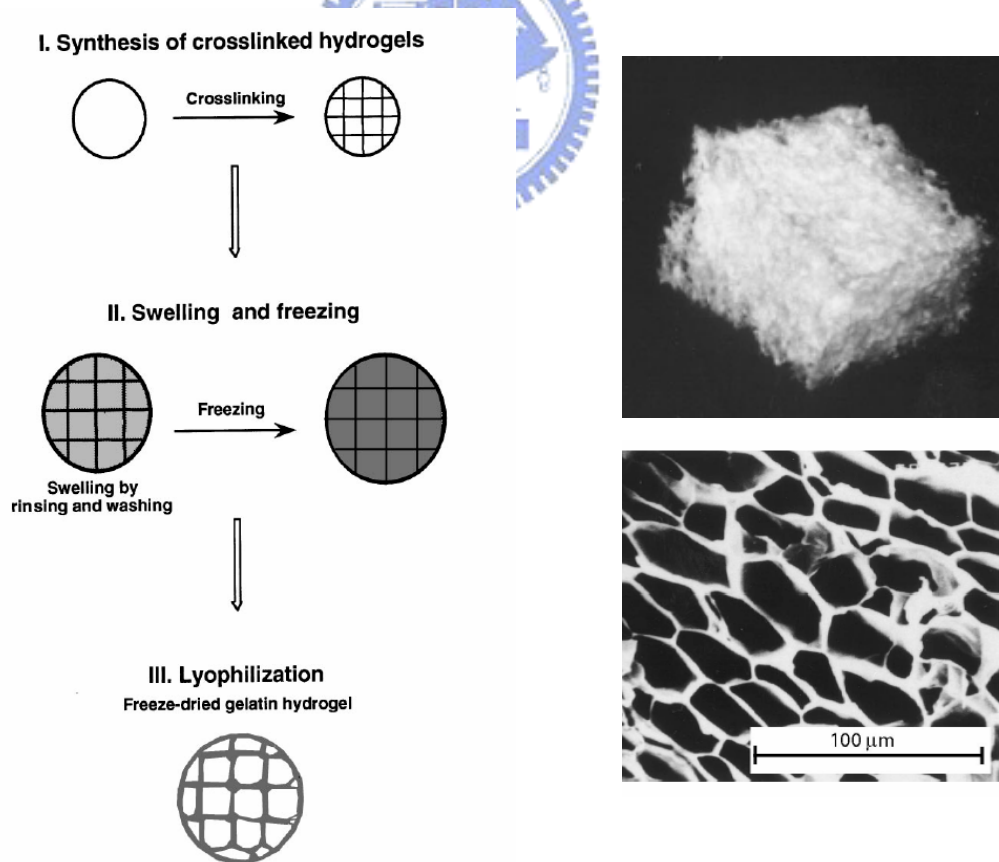


Fig. 2.5 Schematic representation of the freeze drying process and morphology of structure of scaffolds by SEM [Kang, 1999]

Kang et al. were able to influence the pore size of three-dimensional freeze dried gelatin samples by adjusting the temperature of freezing prior to the lyophilization process. They found that as the freezing temperature was lowered, the compactness of the freeze dried samples increased. At -20°C the pore size of the samples was around $250\text{-}300\ \mu\text{m}$ and the wall thickness was thin, which resulted in a weak and brittle scaffold. As the freezing temperature was lowered to -80°C and -196°C a scaffold was created with smaller pore size ($45\text{-}50\ \mu\text{m}$) and thicker walls. This resulted in a more elastic material. The difference in pore size and inner structure of the hydrogels reflects the differences in heat transfer rates during the freezing process of the hydrogel [Kang, 1999]. It is possible that at a higher freezing temperature, the number of nuclei of ice crystallization initially formed is smaller than that at a lower freezing temperature, leading to an increased final size of ice crystals. Since the larger ice crystals push to expand the hydrogel chains to a greater extent, the pore size of hydrogels will be increased, while the structure undergoes destruction. Rapid cooling causes formation of many nuclei of ice crystals, resulting in the formation of smaller-sized pores. In the final stage, frozen materials are dried by sublimation of ice crystals under vacuum at a temperature below freezing. It is possible to influence the orientation of the pores by subjecting the samples to a temperature gradient. According to Kang et al. this gradient can only be created during fast cooling methods, for example liquid nitrogen and -80°C . The lower the freezing temperature, the more oriented the pore structure will be [Kang, 1999] (see Fig. 2.6).

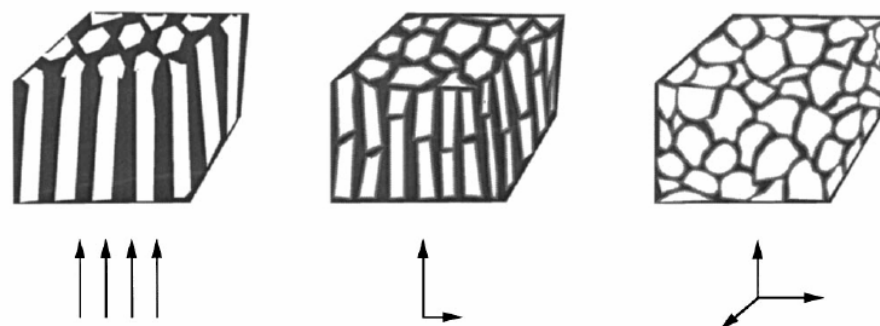


Fig. 2.6 Different degrees of orientation during freeze drying. From left to right: -196°C , -80°C , and -20°C [Kang, 1999]

2.2.2 Freezing and thawing process [Hatakeyema, 2005]

As shown in schematic illustration (Fig. 2.7), the molecular motion of PVA segments in the solution (Fig. 2.7-(a)) ceases when water freezes. With decreasing temperature, size of ice increases (Fig. 2.7-(b)) and the hydroxyl groups of PVA molecules participate in hydrogen bonding. Loose crosslinking networks are formed in the first freezing and thawing cycles (Fig. 2.7-(c)). In the network, the polymer chains are restricted to limited regions because of the presence of permanent elastic constraints and the segment exhibits limited thermal fluctuation around fixed average positions. On this account, the number of crosslinking points increases and molecular chains aggregate with increasing freezing and thawing cycles. The cell walls of PVA hydrogels become thicker with increasing freezing and thawing cycles.

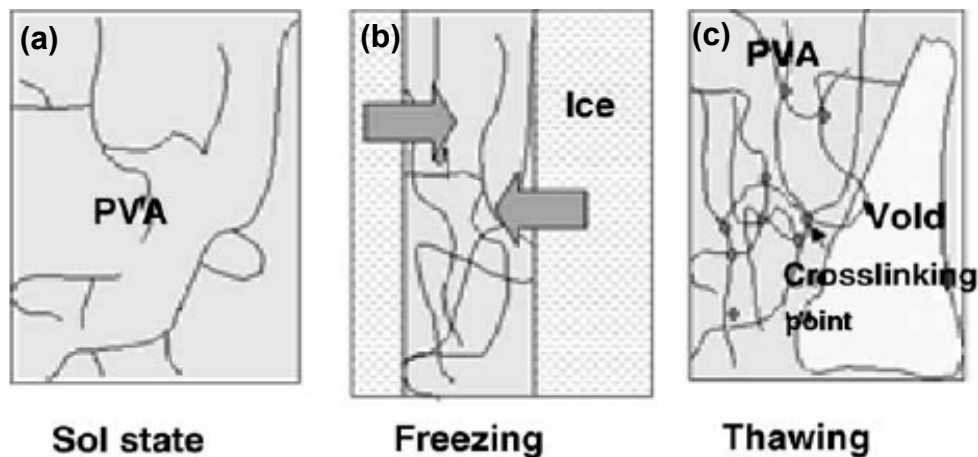


Fig. 2.7 Schematic illustration of gel formation by freezing and thawing
[Hatakeyema, 2005]

2.2.3 Double emulsion Technique

[extracted by <http://www.research.ucla.edu/tech/ucla07-574.htm> (UCLA)]

Simple emulsions are dispersions of droplets of one liquid phase in another immiscible liquid phase. The most common are oil-in-water (O/W) or water-in-oil (W/O) emulsions that typically have microscale diameters. Double emulsions are more complex emulsions that consist of droplets within droplets, such as water-in-oil-in-water ($W_1/O/W_2$). The two primary means of creating double emulsions

are structured microfluidic methods and sequential emulsification. Microfluidic methods are capable of producing highly uniform W/O/W emulsions, but it is a low-throughput process. A W/O/W double emulsion (see Fig. 2.8) created by sequential emulsification must be size-fractionated to achieve uniform monodisperse droplets, but fractionation is also a low-throughput process. Most double emulsions rely on two surfactants for stability, not a single surfactant that can stabilize both inner and outer droplets. Little existing double emulsification methods have so far been successful in creating nanoscale double emulsions in which both the inner and outer droplets are both sub-100 nm just using a single type of surfactant.

However, the invention utilizes novel amphiphilic diblock copolypeptides (such as Pluronic®, PEO-PPO-PEO) that function as surfactants to stabilize stable double emulsions that can be formed using a variety of mixing methods using a single interfacial agent that is not biased against complex droplet topologies. An additional innovation is that both the inner aqueous droplets and outer oil droplets can be formed with diameters as small as tens of nanometers.

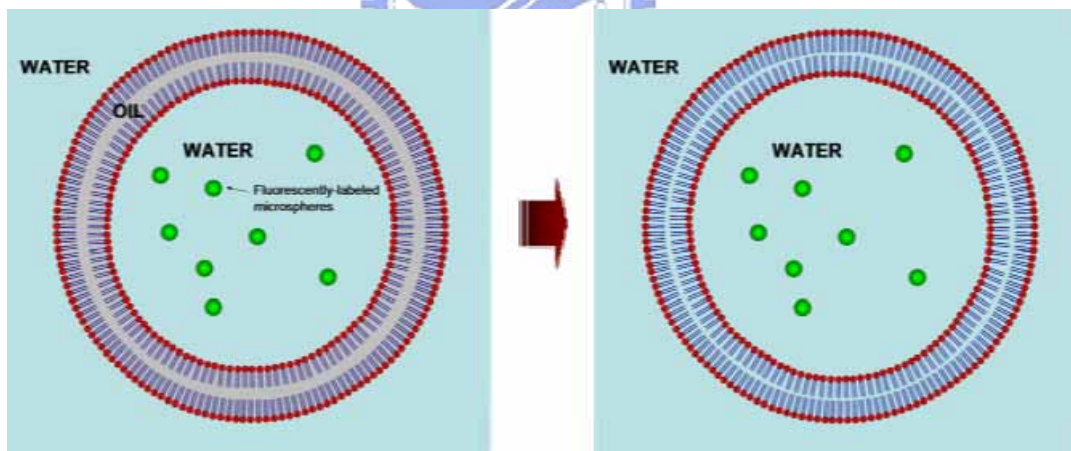


Fig. 2.8 Scheme showing the formation of phospholipids vesicle from double emulsion technique ($W_1/O/W_2$ droplet) [Extracted by <http://www.seas.harvard.edu/weitzlab/liposomes>]

Amphiphilic diblock copolypeptides stabilized double emulsions provide both microscale and nanoscale drug delivery vehicles that can package both water-soluble and oil-soluble drugs or other cargo. Dual delivery of hydrophobic and hydrophilic

cargo will have applications in pharmaceuticals, cosmetics, and personal care products.

The advantage of double emulsion is (1) control of inner and outer droplet sizes from the microscale down to tens of nanometers; (2) tunable block lengths and compositions of the diblock copolypeptides to alter emulsion properties; (3) the inner liquid droplet (e.g. water) can contain water soluble cargo: DNA, RNA, oligonucleotides, peptides, proteins, salts, viruses, vitamins, serums, molecular motors, drug molecules, cells, vesicles, nanoparticles, fullerenes, carbon nanotubes, sugars, quantum dots, metal nanoparticles, magnetic nanoparticles, fluorescent dyes, etc.; (4) The outer droplet (e.g. oil) can contain hydrophobic cargo: fats, lipids, waxes, oils, fragrances, cholesterol, steroids, drug molecules, polymers, polypeptides, micelles, quantum dots, nanoparticles, carbon nanotubes, fullerenes, etc. A variety of oils can be used, including oils that are biologically compatible.

2.3 Polymeric Hydrogel for modulated drug release

Hydrogels have been widely applied as intelligent carriers in controlled drug-delivery systems [Peppas, 2000, 2004 & 2006]. Researchers have engineered their physical and chemical properties at the molecular level to optimize their properties, such as permeability (e.g., sustained-release applications), enviro-responsive nature (e.g., pulsatile-release applications), surface functionality (e.g., PEG coatings for stealth release), biodegradability (e.g., bioresorbable applications), and surface biorecognition sites (e.g., targeted release and bioadhesion applications), for controlled drug-delivery applications (Fig. 2.9). Control of hydrogel swelling properties can be used as a method to trigger drug release [Peppas, 2004]. One example of how the change in the swelling properties of hydrogels can be used in drug delivery is a PVA and PEG system [Stringer, 1996]. By controlling the polymer chain length, polymer composition, and initiation concentration and other factors, it is possible to control the density and degree of network crosslinking.

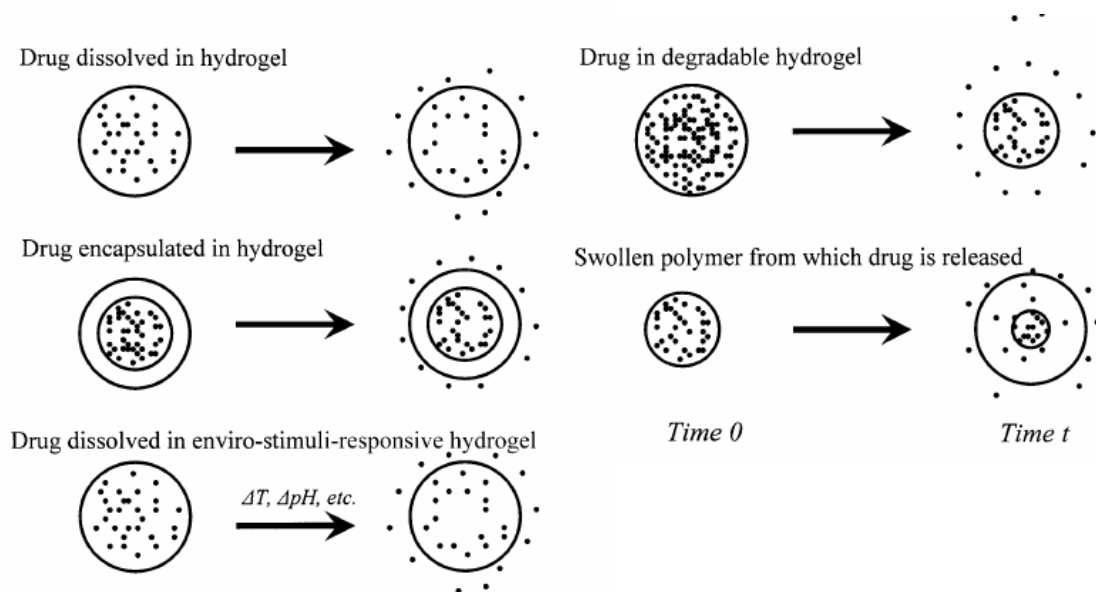


Fig. 2.9 Various delivery and release mechanisms of hydrogels [Peppas, 2006]

In addition, five kind techniques of stimulated drug release were illustrated, which are not self-regulating, but instead require externally generated environmental changes to initiate drug delivery. These can include (1) electric fields, (2) light, (3) mechanical forces, (4) temperature, and (5) magnetic fields, which might be coupled to biosensors to obtain systems that automatically initiate drug release in response to the measured physiological demand.

2.3.1 Electric field (pH sensitive) Stimulus

Electric current is a signal that can be used to trigger drug delivery. One way to accomplish this is to fabricate a pH-sensitive polymer (ex. chitosan) and use the presence or absence of an electric current to change the local pH, initiating erosion of the polymer matrix [Sershen, 2002]. Amino-polysaccharide chitosan that undergoes pH-dependent hydrogel formation was illustrated [Fernandes, 2003]. At low pH (pH < 6), chitosan is protonated and soluble. When the pH is raised above about 6.3, the amino groups become deprotonated and this polysaccharide can form an insoluble hydrogel network. The high localized pH is generated electrochemically at the cathode surface due to the hydrogen evolution reaction. The rate of this electrochemical reaction is proportional to the current density and can be adjusted by the applied voltage. As indicated in Fig. 2.10, proton consumption at the cathode surface is partially compensated for by proton generation from the dissociation of

water. A pH gradient can be generated adjacent to the cathode surface, depending on the relative rates of hydroxyl ion generation and hydroxyl ion diffusion from the interfacial region. The generation of a pH gradient at the cathode surface can cause the structure change of chitosan gel, which displays insoluble condition at left side (cathode side), but soluble condition at right side. The drug can be controlled-release at the right side by pH gradient.

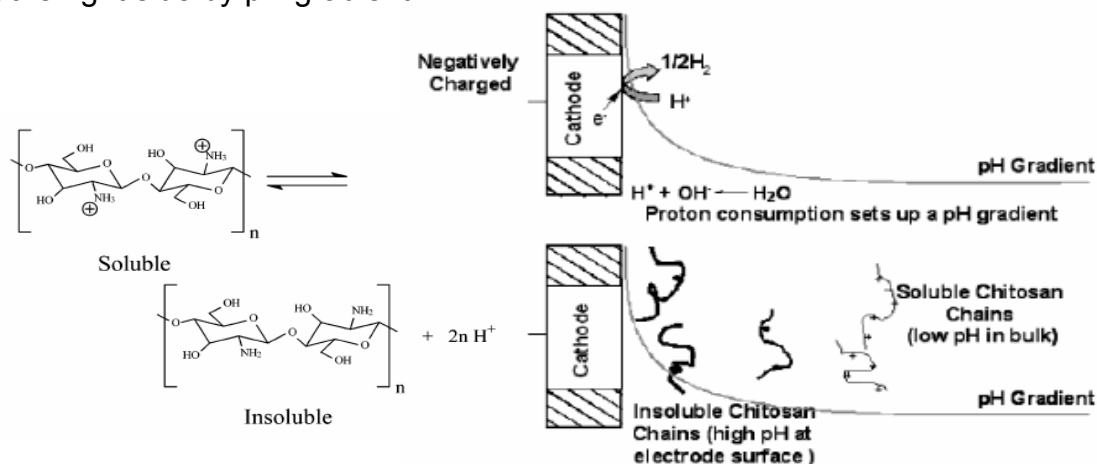


Fig. 2.10 Diagram of drug controlled release of chitosan by electric stimulus
[Fernandes, 2003]

2.3.2 Light Stimulus

The interaction between light and a material can also be used to modulate drug delivery. This can be accomplished by combining a material that absorbs light at a desired wavelength and a material that uses energy from the absorbed light to modulate drug delivery [Sershen, 2002]. Near-infrared light has been used to modulate the release of various proteins from a composite material fabricated from gold nanoshells and thermal-sensitive polymer (poly (NIPAAm-co-AAm) or Pluronic®) [Bae, 2006], as show in Fig. 2.11. Gold nanoshells are a new class of optically active nanoparticles that consist of a thin layer of gold surrounding a dielectric core [Sershen, 2001]. Varying the shell thickness, core diameter, and the total nanoparticle diameter allows the optical properties of the nanoshells to be tuned over the visible and near IR spectrum. Since the core and shell sizes can be easily manipulated, the optical extinction profiles of the nanoshells can be modified to optimally adsorb light emitted from various lasers.

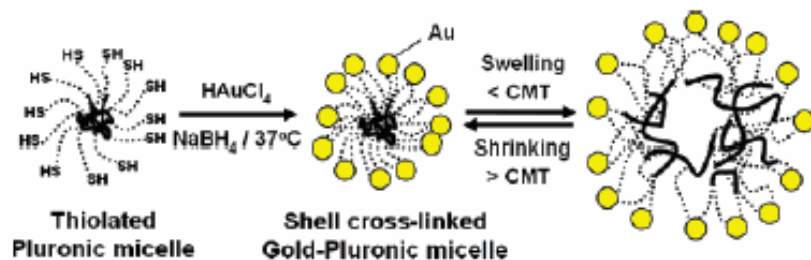


Fig. 2.11 Synthetic scheme of novel shell cross-linked gold-Pluronic micelles exhibiting a thermosensitive swelling/shrinking behavior [Bae, 2006]

For the purpose of initiating a temperature change with light; light at wavelengths between 800 and 1200 nm is transmitted through tissue with relatively little attenuation, absorbed by the nanoparticles, and converted to heat. Significantly enhanced drug release from composite hydrogels has been achieved in response to irradiation by light at 1064 nm. Embedding the nanoshells in the NIPAAm-co-AAm hydrogel formed composite materials that possessed the adsorption spectrum of the nanoshells and the phase transition characteristics of NIPAAm-co-AAm copolymer with an LCST of 40°C. When exposed to near-infrared light, the nanoshells absorb the light and convert it to heat, raising the temperature of the composite hydrogel above its LCST. This in turn initiates the thermoresponsive collapse of the hydrogel, resulting in an increased rate of release of soluble drug held within the polymer matrix. Figure 2.12 illustrated the collapse of the composite hydrogels and the deswelling behavior in response to near-infrared irradiation.

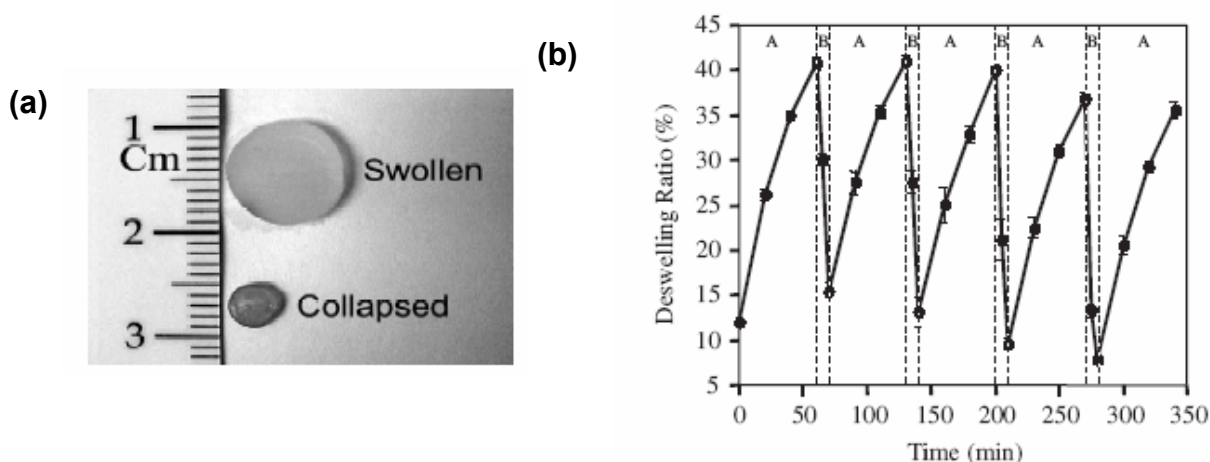


Fig. 2.12 (a) A representative nanoshell-composite hydrogel in the fully swollen and collapsed states; (b) Deswelling ratio of hydrogels in periods when a diode laser was (A) turned off or (B) on at 2.6 Wcm⁻² [Sershen, 2001]

2.3.3 Mechanical Signal stimulus

Drug delivery can also be initiated by the mechanical stimulation of an implant. Two different types of model systems can be considered in the design of controlled drug-delivery devices [Sershen, 2002], which respond to mechanical signals depending on the interaction of the drug with the polymer [Lee, 2001]. One model system is filled with drug molecules that do not bind or interact with matrices (i.e., free drug). The release of these free drug molecules could be enhanced by simple mechanical signals due to the increased pressure within the matrix, which leads to an exodus and depletion of drug at each incident (Fig. 2.13-(a)). However, mechanical signaling does not significantly contribute to the release behavior of free drug molecules from many hydrogel systems as the rapid depletion enables the fast release of free drug even during the relaxation time period (i.e., no mechanical signals). The other possible model system is composed of both free and bound drug molecules, which interact with the polymer matrix through ionic or secondary forces. When these types of systems are subjected to repeated mechanical signals, free drug molecules can be released in response to the increased pressure. The free drug can be subsequently replenished during re-laxation by dissociation of previously bound drug. This allows the systems to respond to repeated cycles of mechanical signaling (Fig. 2.13-(b)).

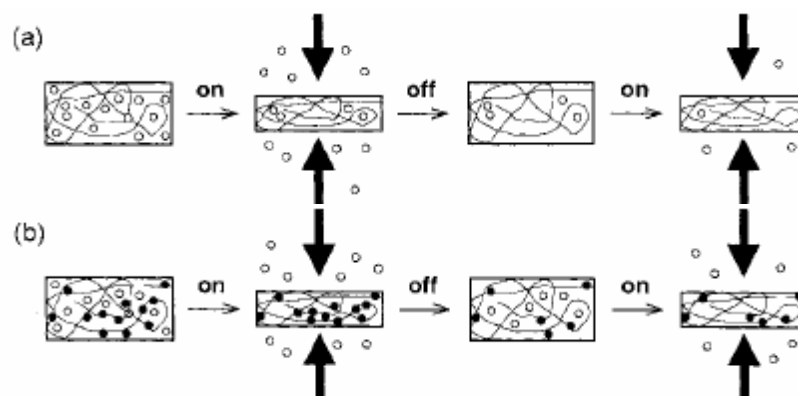


Fig. 2.13 Schematic description of anticipated drug release from polymeric matrices under mechanical signaling: (a) Expected release behavior of drug that does not strongly interact with the matrix; (b) Proposed release behavior of drug that interacts with the matrix. (solid circle: free drug; open circle: bound drug) [Lee, 2001]

It also was demonstrated that model drug (e.g., growth-factor) release from polymer matrices (e.g., alginate gels) could be significantly influenced by the mechanical stimulation, and this approach was proven to be useful for regeneration of blood vessels in animal models, as shown in Fig. 2.14.

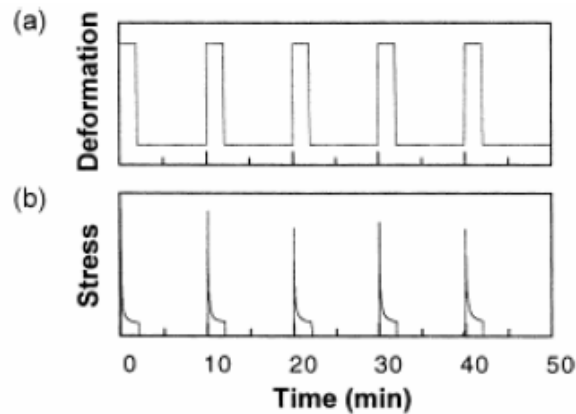


Fig. 2.14 Diagram of deformation (a) and stress relaxation (b) of alginate gels under mechanical loading in vitro, which involves 5 cycles of compression for 2 min followed by relaxation for 8 min [Lee, 2001]

2.3.4 Temperature stimulus

Thermally-responsive hydrogels and membranes have been extensively evaluated as platforms for the pulsatile delivery of drugs. One of the characteristics of temperature reponse hydrogels is the presence of LCST or CMT, a temperature at which a hydrogel made of the material will undergo a phase change. In solution, this temperature would correspond to the transition of the uncrosslinked polymer from an extended coil to globule [Seršen, 2002]. The driving force for this phase change is based on interactions between the polymer and the water surrounding the polymer. When the temperature of the hydrogel is held below its LCST, the most thermodynamically stable configuration for the free (non-bulk) water molecules is to remain clustered around the hydrophobic polymer. When the temperature is increased over the LCST, the collapse of hydrogel is initiated by the movement of the previously clustered water from around polymer into bulk solution. This movement is prompted by a gain in the entropy of the water as the system adjusts to the increased temperature [Tanaka, 1998 &1999; Sasaki, 1997]. Once the water molecules are removed from the polymer, it collapses on itself in order to reduce the exposure of the

hydrophobic domains to the bulk water.

Thermally sensitive materials can be fabricated to exhibit positive thermally controlled drug delivery. block copolymers of (poly(N-isopropylacrylamide-bbutylmethacrylate)(PIPAAm-PBMA)) is an example of such a material. The micelle inner core formed by self-aggregates of PBMA segments successfully loaded with a drug (adriamycin), and the outer shell of PIPAAm chains played a role of stabilization and initiation of micellar thermo-response. Polymeric micelles incorporated with adriamycin showed a dramatic thermo-responsive on/ off switching behavior for both drug release and in vitro cytotoxicity according to the temperature responsive structural changes of a micellar shell structure. Upon collapse, the hydrogel will expel soluble drug held within the polymer matrix. At temperature below the LCST of the copolymer, the release rate is governe by the diffusion of the model drug out of the hydrogel, as show in Fig. 2.15-(a)&(b)

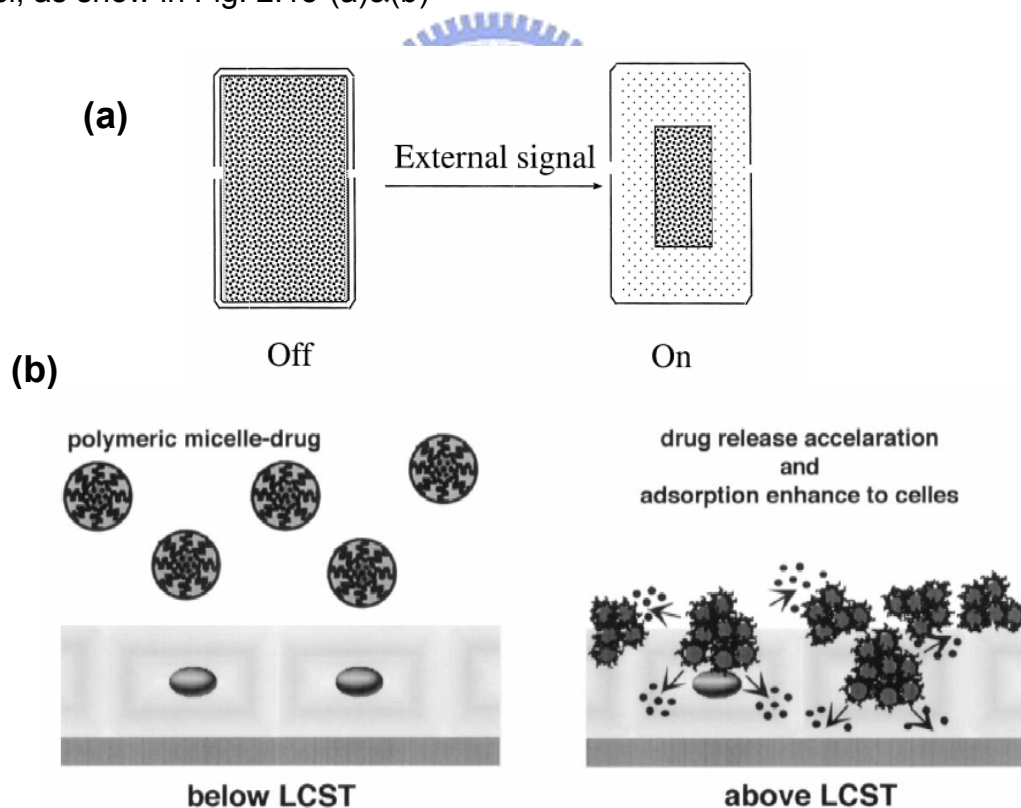


Fig. 2.15 (a) Schematic illustration of on–off release from a squeezing hydrogel device for drug delivery; (b) Interactions between PIPAAm-PBMA micelles and cells modulated by temperature control [Gutowska, 1997; Chung, 1999]

In addition, Choi et al. [Choi, 2006] reported Pluronic®/heparin nanocapsules fabricated by single emulsion technology, as shown in Fig. 2.16. They exhibited the violent volume change (1000-fold volume transition) while the temperature from 25°C to 37°C (336 nm at 25°C to 32 nm at 37°C), implying excellent thermal sensitive behavior. The drug can be squeezed-out with the violent volume change while the increased temperature. Thus, the micelle structure (or nanocapsules) of Pluronic® series polymer (F127 or F68) would be used in this paper.

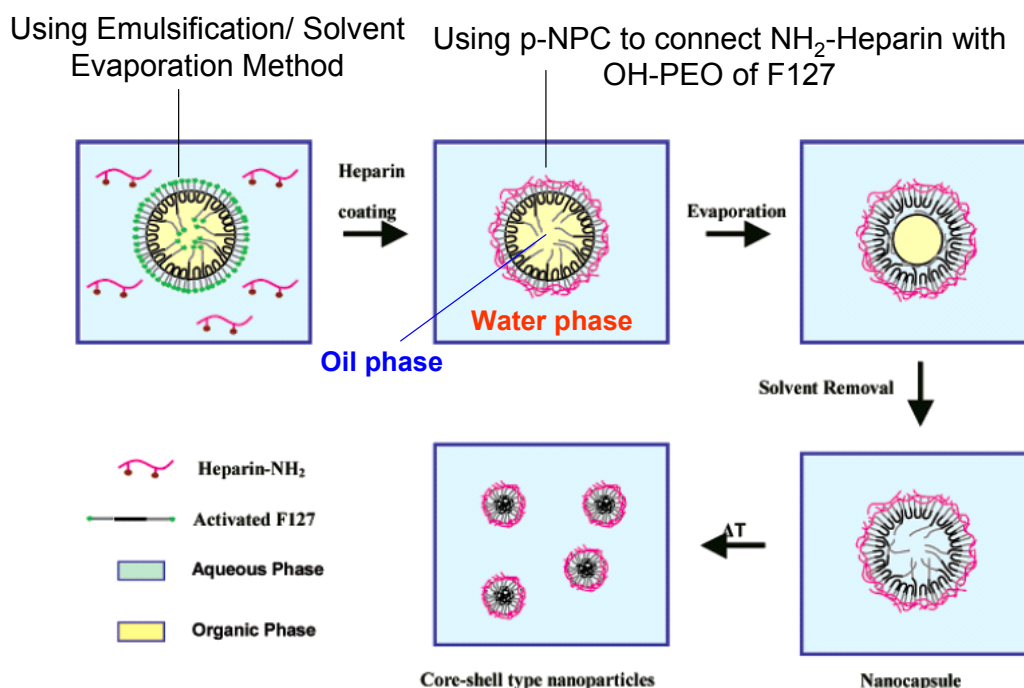


Fig. 2.16 Thermally reversible Pluronic®/heparin nanocapsules exhibiting 1000-fold volume transition [Choi, 2006]

2.3.5 Magnetic fields stimulus

The use of an oscillating magnetic field to modulate the rate of drug delivery from a magnetic polymer matrix (mini- or micro-size) was one of the first methodologies investigated to achieve an externally controlled drug delivery system [Hsieh, 1981] for 25 years ago (1981-1988). In these studies, Hsieh et al. and Saslawski et al. [Saslawski, 1988] embedded magnetic steel beads in an EVAc copolymer and polyethylenimine/alginate matrix that was loaded with bovine serum albumin and insulin as a model drug, respectively. They demonstrated increased

rates of drug release in the presence of an oscillating magnetic field ranging from 0.5-1000 gauss [Edelman, 1985]. The rate of release could be modulated by altering the position, orientation, and magnetic strength of the embedded materials, as well as by changing the amplitude and frequency of the magnetic field [Kost, 1985]. During exposure to the magnetic field, the beads oscillate within the matrix, alternatively creating compressive and tensile forces. This in turn acts as a pump to push an increased amount of the drug molecule out of the matrix.

However, few reports were found on the study on the magnetic hydrogel (or called ferrogel) for drug delivery in the later 15 years (1989-2004). Until 2005, Chen et al. [Chen, *Macromol. Symp.*, 2005] reported a PVP ferrogel which exhibited passive drug (Bleomycin A5 Hydrochloride, BLM) release that could be exploited to enhance therapeutic efficacy to kill the tumor cell (VX2 squamous cell carcinoma) in the auricles of the rabbits. Also, Lu et al. [Lu, 2005] illustrated that an external alternating magnetic field of 100-300 Hz and 1200 Oe were applied to rotate the embedded Co@Au polyelectrolyte (PSS/PAH) microcapsules (diameter: 5 μm), which subsequently disturbed and distorted the capsule wall and drastically increased its permeability to macromolecules like FITC-labeled dextran.

Among them, magnetic fields stimulus provide more interesting opportunities since they can be effectively activated in a controllable manner through a non-contact stimulus, through a non-contact stimulus, as compared with other type of stimulus. Although near-infrared light stimulus also displayed the similar inductive heating ability from gold nanoparticles, the manipulation and heating ability in the magnetic nanoparticles were superior to those of the gold nanoparticles. Many researchers (including us) were interested in this topic, and thus paid attention to investigate about the behavior of ferrogel in the drug controlled release. Detail introduction about the characteristics of the ferrogel for the drug delivery using magnetic fields would be illustrated in the next section.

2.4 Ferrogel

Magnetic field sensitive gels, or as we call them "ferrogels", are typical representatives of smart materials [Xulu, 2003; Zrínyi, 2000 & 1998]. In a ferrogel finely distributed colloidal particles having superparamagnetic behavior are incorporated into the swollen network. These particles couple the shape of the gel to the external magnetic field. Shape distortion occurs instantaneously and disappears abruptly when the external field is removed. A discontinuous elongation and contraction in response to infinitesimal change in external magnetic field has been observed. Many kinds of such gels have been developed and studied with regard to their applications to several biomedical and industrial fields such as controlled drug delivery systems and muscle-like soft linear actuators. Saslawski et al [Saslawski, 1988] reported the gelatin microsphere that was cross-linked by polyethylenimine for the pulsed delivery of insulin by oscillating magnetic field. The release rate of insulin from the alginate sphere with strontium ferrite microparticles (1 μm) dispersed can be much enhanced compared with that in the absence of magnetic field. Zrínyi et al. [Zrínyi, 1998] reported that the magnetically-sensitive hydrogels can undergo quick, controllable changes in shape by introducing magnetic particles into the chemically cross-linked PVA that can be used as a new type of actuator to mimic muscular contraction, as shown in Fig. 2.17.

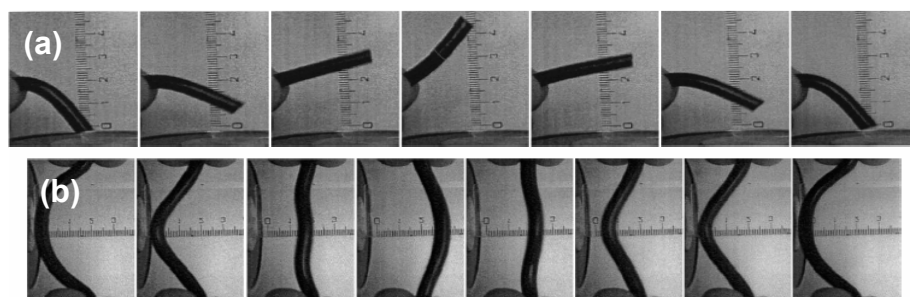


Fig. 2.17 (a) Snapshots from the motion of a magnetic-field-sensitive polymer gel, and the rule behind the gel indicates the amplitude of the oscillation, which is more than 4 cm; (b) Snapshots from the motion of a magnetic gel, and the rule behind the gel indicates the amplitude of the oscillation, which is about 3 cm [Zrínyi, 1998]

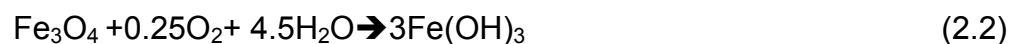
2.4.1 Synthesis of magnetic iron oxide nanoparticles

It has long been of scientific and technological challenge to synthesize the magnetic nanoparticles of customized size and shape. Physical methods such as gas phase deposition and electron beam lithography are elaborate procedures that suffer from the inability to control the size of particles [Gupta, 2005] in the nanometer size range. The wet chemical routes to magnetic nanoparticles are simpler, more tractable and more efficient with appreciable control over size, composition and sometimes even the shape of the nanoparticles. Iron oxides (either Fe_3O_4 or $\gamma\text{-Fe}_2\text{O}_3$) can be synthesized through the co-precipitation of Fe^{2+} and Fe^{3+} aqueous salt solutions by addition of a base [Gupta, 2005]. The control of size, shape and composition of nanoparticles depends on the type of salts used (e.g. chlorides, sulphates, nitrates, perchlorates, etc.), Fe^{2+} and Fe^{3+} ratio, pH and ionic strength of the media [33,34].

Conventionally, magnetite is prepared by adding a base to an aqueous mixture of Fe^{2+} and Fe^{3+} chloride at a 1:2 molar ratio. The precipitated magnetite is black in color. The chemical reaction of Fe_3O_4 precipitation is given in Fig. 2.18. The overall reaction may be written as follows [Gupta, 2005]:



According to the thermodynamics of this reaction, a complete precipitation of Fe_3O_4 should be expected between pH 9 and 14, while maintaining a molar ratio of $\text{Fe}^{3+}:\text{Fe}^{2+}$ is 2:1 under a non-oxidizing oxygenfree environment. Otherwise, Fe_3O_4 might also be oxidized as reaction (2.2)



This would critically affect the physical and chemical properties of the nanosized magnetic particles. In order to prevent them from possible oxidation in air as well as from agglomeration, Fe_3O_4 nanoparticles produced by reaction (2.1) are usually coated with organic or inorganic molecules during the precipitation process.

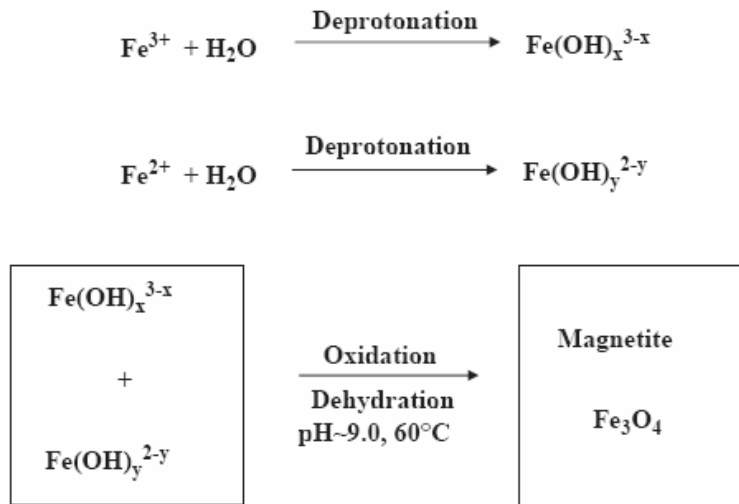


Fig. 2.18 Scheme showing the reaction mechanism of magnetite particle formation from an aqueous mixture of ferrous and ferric chloride by addition of a base [Gupta, 2005]

2.4.2 Hysteresis

When a ferromagnetic material is magnetized by an increasing applied field and then the field is decreased, the magnetization does not follow the initial magnetization curve obtained during the increase. The irreversibility is called hysteresis. An example of a full or major (i.e., M is taken to near M_s) hysteresis curve (or loop) is given in Fig. 2.19. At extremely high applied fields, the magnetization approaches the saturation magnetization, M_s . Then if the field is decreased to zero, the M versus H curve does not follow the initial curve but instead lags behind until, when $H=0$ again, a remanent magnetization remains, the remanence M_r . If the field is now applied in the reverse direction (a negative field), M is forced to zero at a field magnitude called the hysteresis coercivity, H_c . Increasing this negative field still further forces the magnetization to saturation in the negative direction. Symmetric behavior of this hysteresis curve is obtained as H is varied widely between large positive and negative values. One could say that hysteresis is due to internal friction. Hence the area inside the loop is the magnetic energy that is dissipated while circling the loop.

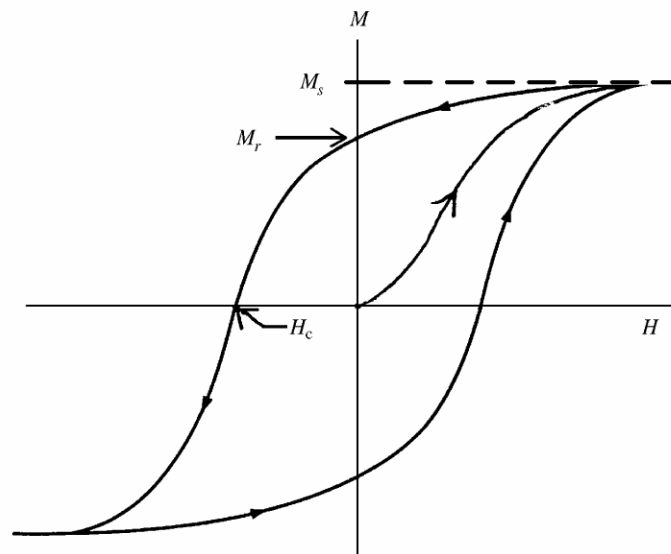


Fig. 2.19 Full-loop hysteresis curve. M_s is the saturation magnetization, M_r is the magnetization remanence (at $H=0$), and H_c is the coercivity [Klabunde, 2001]

Table 2.1 Critical diameter of single-domain (D_s) and super paramagnetic (D_{sp}) in the magnetic materials [Klabunde, 2001]

Material	D_s (nm)	D_{sp} (nm)
Fe	14	1.5
Co	70	2.5
Ni	55	
Fe_3O_4	128	5
γ - Fe_2O_3	166	

In addition, the “closure” effects of ferrogel in the DC magnetic fields and the “bursting” effect of ferrogel in the AC magnetic fields were dependent on the particle size of magnetic nanoparticles, which means the saturation magnetization (M_s) hysteresis coercivity (H_c) were very important factor in the ferrogel. As Fe_3O_4 for example, it exhibited the superparamagnetic behavior (H_c is near to zero) while the particle size is lower than the 5 nm. Moreover, H_c arrive the maximum while the particle size is 128 nm (the critical point of single domain and multi domain of iron particles). H_c displayed the saturation while the particle size is higher than 200nm, as shown in Table 2.1 and Fig. 2.20.

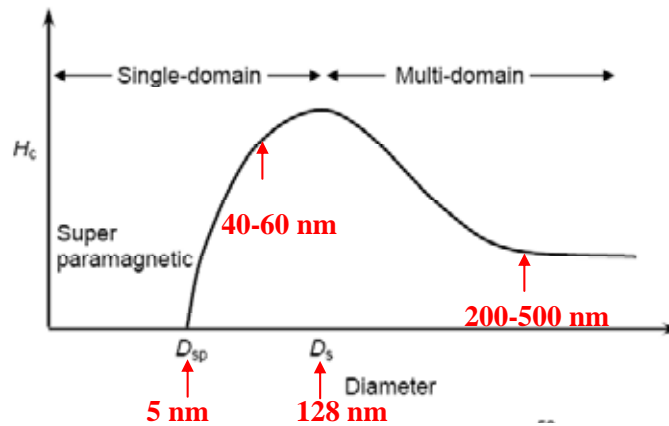


Fig. 2.20 Relationship of the particle size and hysteresis coercivity (H_c) [Klabunde, 2001]

In addition, M_s would increase with the particle size increased. Therefore, the better “clouser” effect in the DC magnetic fields would be observed in the higher M_s and lower H_c , but the rapider “bursting” effect (inductive heating effect) in the DC magnetic fields would be found in the higher H_c , implying the faster heating conducting.

2.5 Magnetic composites for biomedical applications

Magnetic composites (or ferrogel) offer a high potential for several biomedical applications [Gupta, 2005], such as:

- (I) Cell therapy, labelling, targeting and separating/purifying cell populations (Fig. 2.21 (a)&(b));
- (II) Magnetic resonance imaging (MRI) (Fig. 2.21-(c));
- (III) Shape memory for artificial muscle (Fig. 2.17);
- (III) Hyperthermia (inductive heating) (Fig. 2.21-(e));
- (VI) Drug delivery by external magnetic field stimulus (Fig, 2.21-(d));

Related literatures were listed below (Table 2.2):

Table 2.2 Magnetic composites for biomedical applications

Materials	Model Drug	Application	Ref.
<u>Cell therapy, labelling, targeting and separating/purifying cell populations</u>			
Chitosan	No drug	Affinity purification of enzymes	An, 2003
Mesoporous silica nanorods (MSNs)	Fluorescein	The drug could be encapsulated and released from the magnet-MSN delivery system by using cell-produced antioxidants (e.g.dihydrolipoic acid) as triggers in the presence of an external magnetic field.	Giri, 2005
PECA or PCL	Cisplatin /Gemcitabine	Sufficient magnetic susceptibility for targeted delivery and Sustained release behavior	Yang, 2006
PNIPAAm	No drug	For controlling protein (HSA) adsorption and desorption	Elaissari, 2001
Fluorescent chitosan/CdTe QDs	Cefradine (hydrophilic antibiotic)	Magnetic targeting, fluorescent imaging and stimulus-responsive drug release (pH-sensitive) properties into one drug delivery system	Li, 2007
FITC-labeled magnetic PNIPAM	Doxorubicin	Thermal-sensitive drug release; Magnetic drug targeting and tissue labeling	Deng, 2005
PLLA	Tamoxifen	Good potential as a carrier for the targeted release of tamoxifen to kill MCF-7 breast cancer (without MF)	Hu, 2006
Porous magnetic hollow silica nanosphere	Ibuprofen	High potential applications in controlled and target releasing (without MF)	Zhou, 2007
O-carboxylmet hylated chitosan (O-CMC)	MTX	Derivatized with a peptide sequence from the HIV-tat protein to improve the translocational property and cellar uptake of the nanoparticles; Magnetic targeting carrier to kill U-937 tumor cells.	Zhao, 2005
Oleic acid (OA)-Pluronic-	Doxorubicin	Sustained delivery of anticancer agents; Magnetic targeting and/or imaging.	Jain, 2005
CdTe/ PAH-PSS	No drug	Microcapsules addressable by a magnetic Field and magnetic imaging.	Gaponik, 2004
Dextran-g-poly (NIPAAm-co-D	No drug	LCST of viable drug-targeting delivery system	Zhang, 2007

MAAm)			
Pluronic®	hydrophilic Eosin Y/ hydrophobic ibuprofen	Controlled drug targeting delivery and Thermo stimulus release (No MF)	Chen, 2007

Magnetic resonance imaging (MRI)

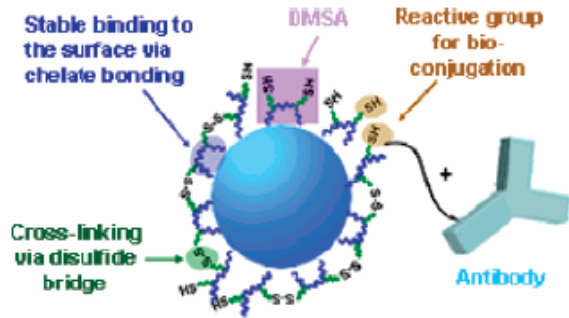
PHDCA/PEI	Doxorubicin	Simultaneous magnetically targeted cancer therapy and diagnosis via MRI	Seo, 2007
PEG	No drug	Optical and MRI multifunctional nanoprobe for targeting Gliomas	Veisoh, 2005
DMSA	No drug	Utilization for cancer diagnosis via MRI	Jun, 2005

Shape memory for artificial muscle

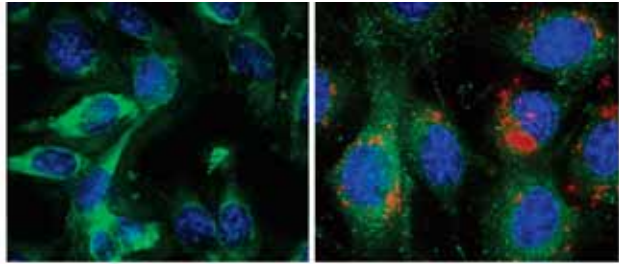
PNIPAAm or PVA	No drug	Gel beads form straight chainlike structures under MF; The particles attract each other when aligned end to end, and repel each other in the side-by-side situation (Pearl-chain structure develops)	Zrínyi, 2000
PVA	No drug	Through freezing–thawing cycles; Viscoelastic properties; Shape transition of magnetic field sensitive polymer gels for artificial muscle	Zrínyi, 1998; Szabó, 1998
TPU	No drug	Shape memory for artificial muscle	Mohr, 2006

For these applications, the particles must have combined properties of high magnetic saturation, biocompatibility and interactive functions at the surface. The surfaces of these particles could be modified through the creation of few atomic layers of organic polymer or inorganic metallic (e.g., gold) or oxide surfaces (e.g. silica or alumina), suitable for further functionalization by the attachment of various bioactive molecules. They are either dispersed through a large volume of a polymeric bead or occur as core in colloidal reagent with a biodegradable shell. As the magnetic particles accumulate, e.g., in tumour tissue, they can play an important role in detection through MRI or electron microscopic imaging to locate and measure binding or as drug carrier for certain anti-cancer drugs. In the present study, it would be focus on (1) inductive heating (Sec. 2.5.1) the intelligent drug delivery by magnetic field stimulus (Sec. 2.5.2).

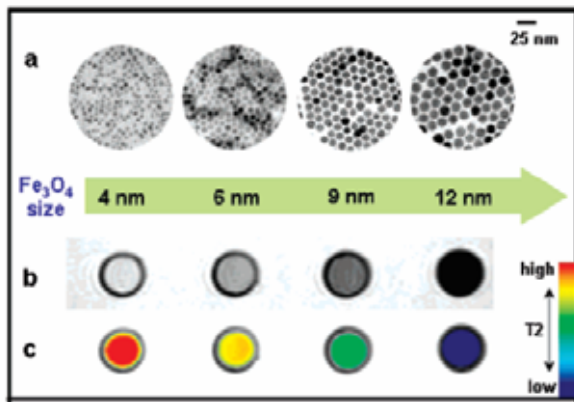
(a)



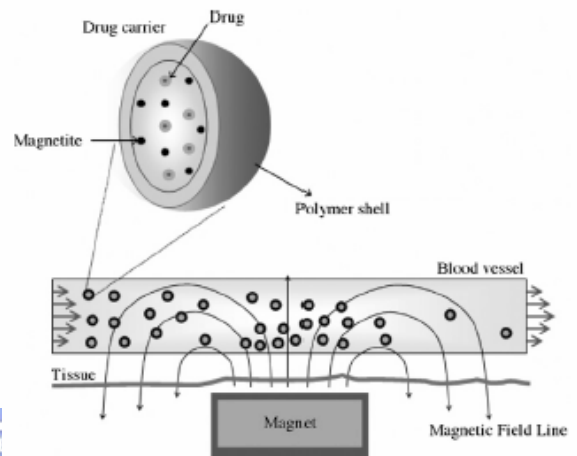
(b)



(c)



(d)



(e)

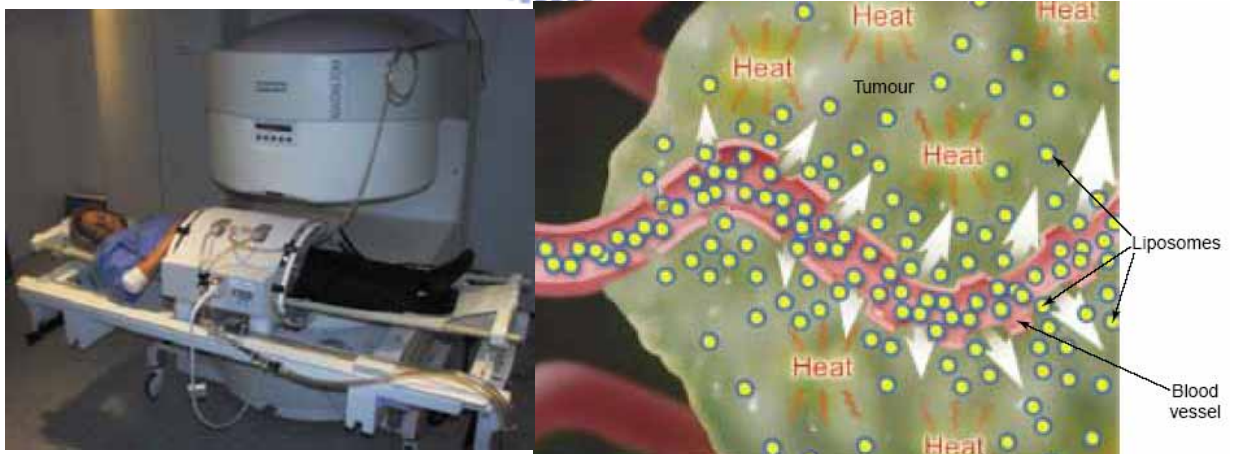


Fig. 2.21 Magnetic composites for biomedical applications: (a) Cell targeting, (b) Cell labelling, (c) MRI, (d) Local Drug delivery, (e) Hyperthermia (inductive heating) [Jun, 2005; Ellenbogen, 2005; Yang, 2006; Habeck, 2001]

2.5.1 Inductive Heating

“Hyperthermia” (inductive heating) in the alternating current (AC) magnetic fields, which the thermal energy from a hysteresis loss of ferrites depends on the type of the remagnetization process, has been the subjects of many studies in recent years. Hyperthermia is usually used for cancer treatment modality that destroys tumors by elevating the temperature of the cancerous tissue to approximately 40-90°C for 10-20 min. The heating ability of each ferrite increased with an increase of the areas of hysteresis loops and the frequency of alternating magnetic field, as shown in Fig.2.22 [Kim, 2005; Park, 2005]

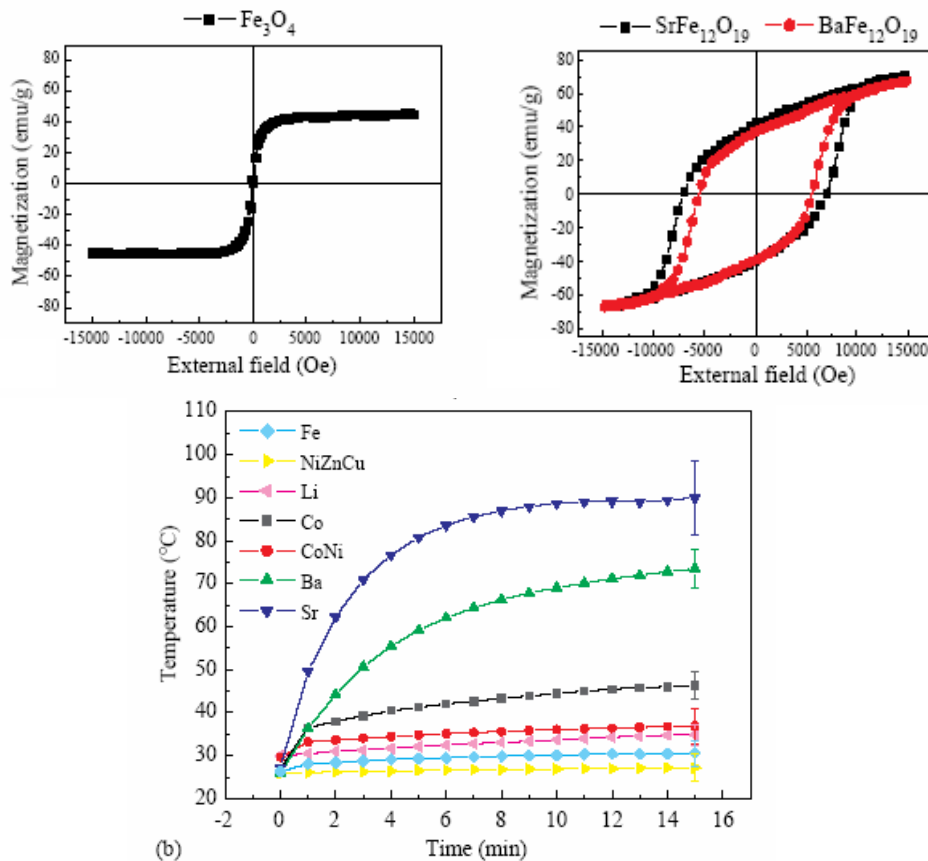


Fig. 2.22 Heating ability of each ferrite increased with an increase of the areas of hysteresis loops and the frequency of alternating magnetic field [Kim, 2005]

It can be divided into three broad categories: whole body hyperthermia, regional hyperthermia and local hyperthermia. Local hyperthermia is often preferred, since the capability of heating only the desired volume (tumor) without affecting the surrounding

tissue is more ideal. The diagram of killing tumor cells by inductive heating of nano-magnetic-particles under alternating magnetic field, as shown in Fig. 2.23

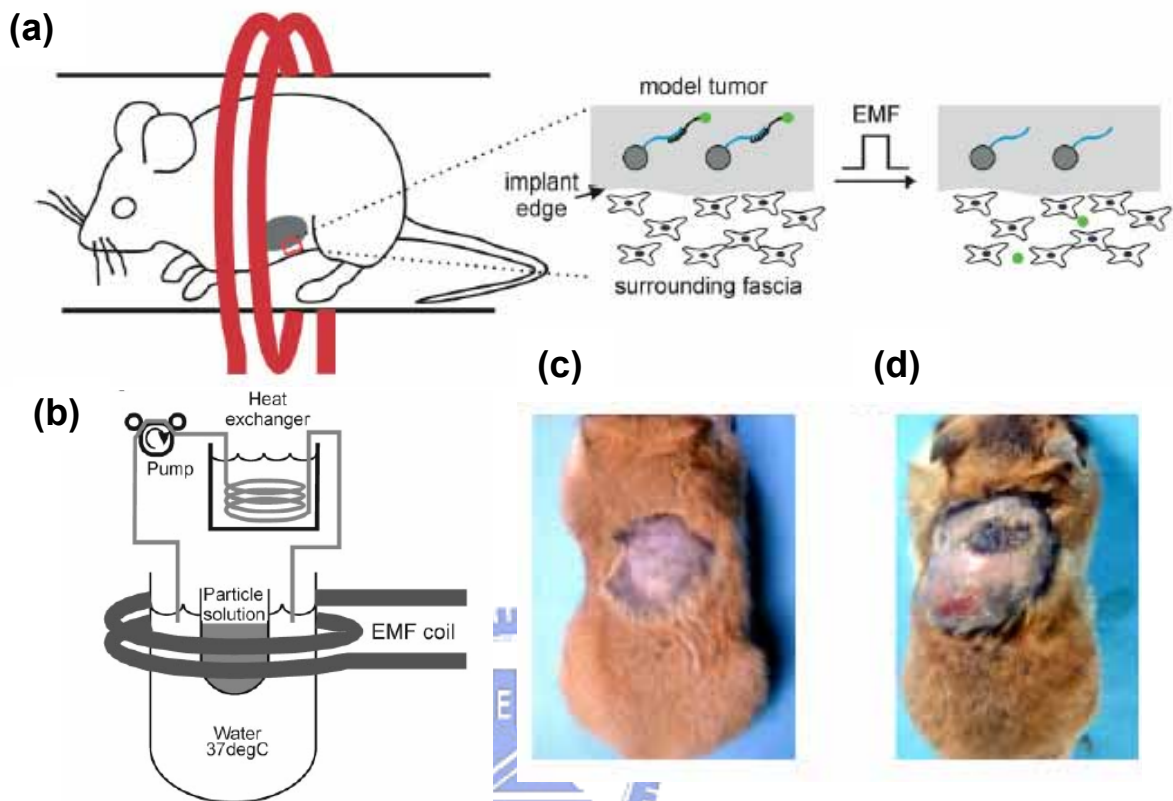


Fig. 2.23 Diagram of (a)&(b) the equipment of the alternating magnetic field for killing tumor cells in the mice (c) without (d) with heating nano-magnetic-particles [Matsuoka, 2004; Derfus, 2007]

2.5.2 Controlled drug release via magnetic field stimulus

The field of controlled drug delivery via magnetic field stimulus would be summarized to two directions ((I) DC magnetic field, and (II) AC magnetic Field). One was achieving sustained zero-order release of a therapeutic agent over a prolonged period of time. This goal has been met by a DC magnetic field stimulus. The particle-particle interactions become dominant in a DC magnetic field. The imposed field induces electric or magnetic dipoles. As a result, mutual particle interactions occur if the particles are so closely spaced that the local field can influence their neighbours. This mutual interaction can be very strong, leading to a significant change in the structure of particle ensembles. The particles attract each other when aligned

end to end, and repel each other in the side-by-side situation. Due to the attractive forces pearl-chain structure development, the field-induced chain formation would slightly shrink the volume of ferrogel to induce the “closure” configuration formation. The “closure” configuration under a DC magnetic field would reduce the rate of drug release, and thus it could achieve the purpose of sustained zero-order release to enhance therapeutic efficacy. Related reports were listed below (Table 2.3):

Table 2.3 Sustained zero-order release under DC magnetic field

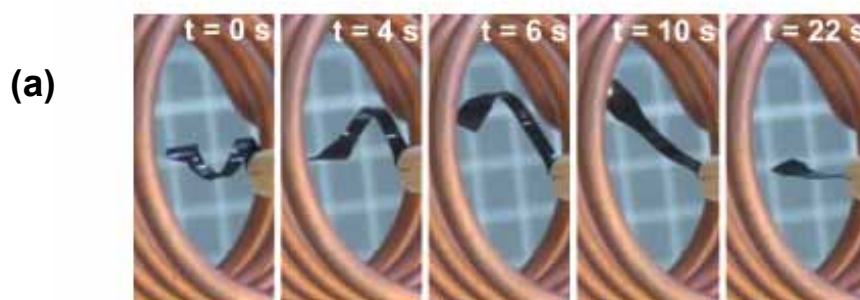
Materials	Model Drug	Application	Ref.
PVP/PVA	Bleomycin A5 hydrochloride (BLM)	Passive drug release that could be exploited to enhance therapeutic efficacy to kill the tumor cell (VX2 squamous cell carcinoma) in the auricles of the rabbits.	Chen, Macromol. Symp., 2005; Ding, 2007; Adriane, 2006
PVA or Scleroglucan (SCL)	Theophylline	Reduced drug delivery could be an advantage, depending on expected drug effect. For example, a slower release will bring a wider delivery time.	Francois, 2007

The second one is the controlled delivery of a therapeutic molecule in a pulsatile or accelerated drug release. This goal has been met by an AC magnetic field stimulus (inductive heating), which accompanied with the responsive hydrogel (e.g., thermosensitive polymer). The behavior of accelerated drug release was caused by not only an inductive heating effect to induce the volume shrinkage, but also pore rupture induced by the violent magnetic vibration of nanoparticles under an AC magnetic field. Therefore, AC magnetic field-induced energy can cause the vibration of iron oxide and enlarge pores increasing the permeability of the hydrogel. In the meantime, the heat energy was conveyed to shrink the hydrogel to pump the drug out. Related reports were listed below (Table 2.4):

Table 2.4 Pulsatile release under AC (oscillating) magnetic field

Materials	Model Drug	Application	Ref.
Collagen	Rhodamine-Labeled Dextran	Accelerative drug release and the self-repair capability of collagen gels following the structural damage caused by AC MF	De Paoli, 2006
PSS/PAH-Co@Au	FITC-labeled dextran.	disturbed and distorted the capsule wall and drastically increased its permeability	Lu, 2005
PS, PMEMA or PCL	p-MOED	Inductive heating and accelerative drug release (Review paper)	Kaiser, 2006; Schmidt, 2007
PNIPAAm	Methylene blue/ Rhodamine B	Inductive heating and De-swelling accompanied by a release of the model drug	Müller-Schulthea, 2006
PNIPAAm	No drug	PNIPAAm layer could absorb the heat induced in the magnetite cores in response to an alternating MF to induce effective aggregation formation or hydrophobic interaction	Wakamatsu, 2006
PCL	No drug	UCST systems; Inductive heating	Schmidt, 2005
Dextran	Fluorescent DNA	(1) Remotely Triggered Release, (2) inductive heating, (3) imaged non-invasively by magnetic resonance imaging	Derfus, 2007
Alginate	Insulin	Accelerative drug release	Saslaeski, 1988
EVAc	BSA	Accelerative drug release	Hsieh, 1981

In particular, combined the system of ferrogel and inductive heating has been reported by R. Mohr and Z. Lu [Mohr, 2006; Lu, 2005]. Noncontact triggering of shape changes in polymers has been realized by incorporating magnetic nanoparticles in shape-memory polymers and inductive heating of these compounds in alternating magnetic fields to increase the permeability of the shell layer, as shown in Fig. 2.24.



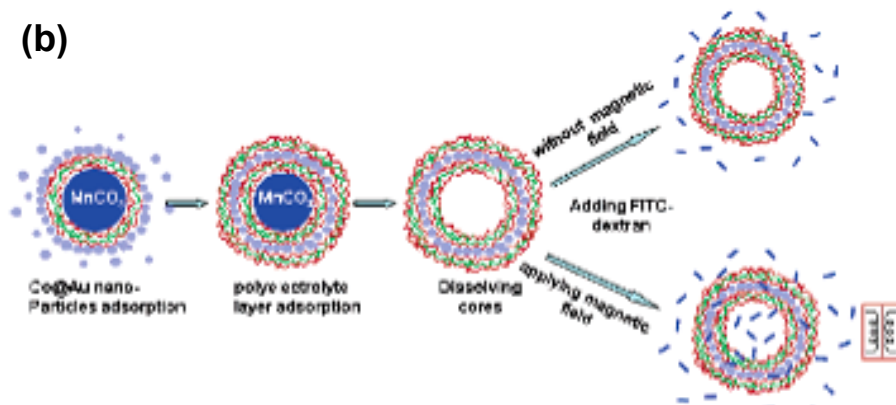


Fig. 2.24 Application of the technique of ferrogel and inductive heating [Mohr, 2006; Lu, 2005].

From our views, this special heating characterization of magnetic materials can be used in the other disease therapeutic systems. In other words, to develop functional nano-sized magnetite particles, a stable dispersion of the magnetic nanoparticles in organic or aqueous media are critically required an effective surface modification with organic compounds or polymers as dispersing agents.

Hybrid materials of macroscopic dimensions that include magnetic nanoparticles in a thermoresponsive polymer matrix are described in two classes of material, either based on shape memory polymers or on thermoresponsive gels [Schmidt, 2007]. The incorporation of magnetic nanoparticles into macroscopic hydrogels leads to magneto-responsive gels called ferrogels. The polymeric matrices serve as highly flexible environment for the particles in the swollen state. Under the influence of an external static magnetic field, the magnetic dipoles become aligned along the magnetic field and an orientation of the gel. Due to enhanced interparticle interactions, a volume contraction can be observed at sufficient field strength. The combination of elasticity and magnetic properties is of great interest for basic research.

Besides, combined magnetic and thermal material to fabricate a thermo-sensitive ferrogel is a promising method for drug delivery. The actuating mechanism of this-type ferrogel is used for the hyperthermia of ferrogel to arise temperature. When the arising temperature of thermosensitive polymers (Pluronic® or PNIPAAm) are higher than CMT or LCST, the drugs can be burst from the ferrogel by the volume compressed (thermoreponse behavior), as illustrated in Fig. 2.25.

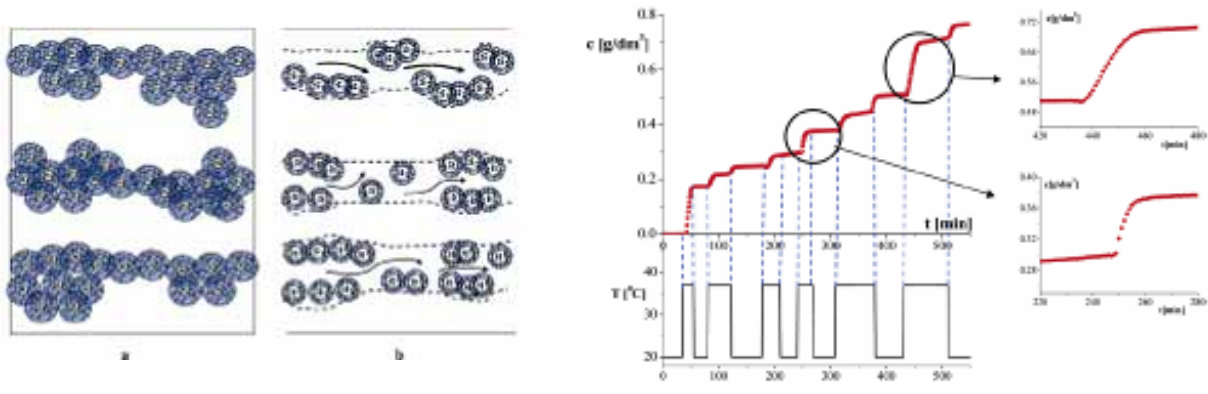


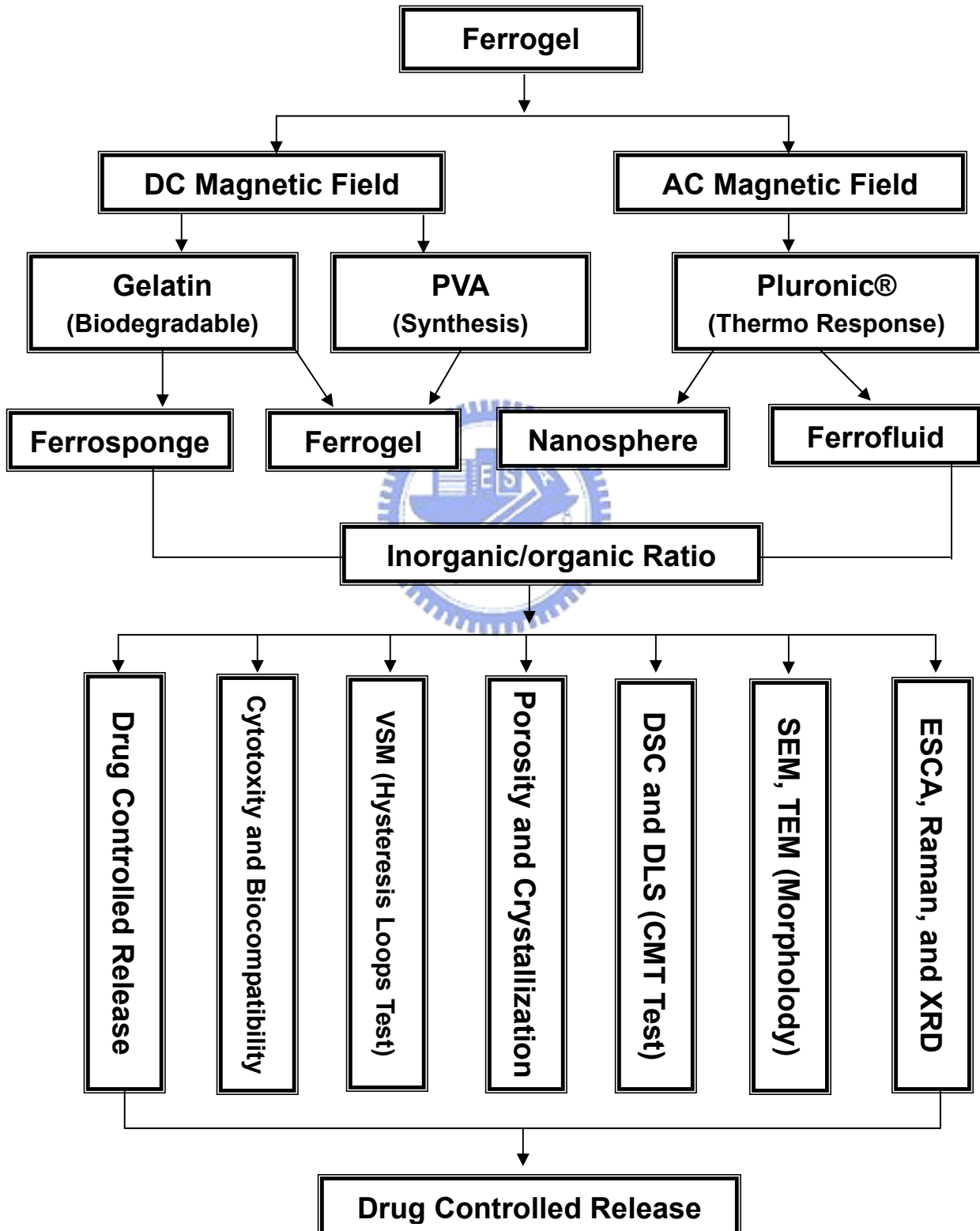
Fig. 2.25 Drug bursting delivery with the temperature increase and the volume compressing of polymer gel: Volume compressing of ferrosphere to form channel to induce the drug pass through [Csetneki, 2006]



Chapter 3

Experiment Methods

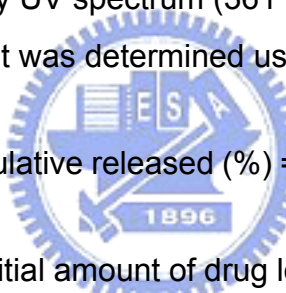
3.1 Flowchart of Experiment Process



3.2 Drug delivery test

In vitro drug release testing was carried out by incubating the drug carriers (ex. ferrogel, ferrosponges, ferrosphere and ferrocapsules) encapsulated model drug in 20 ml of buffer solution at various temperatures (4, 25, 37, 45°C). A direct-current (DC) magnetic field (MF) with 400 Oe was applied to control the drug release profiles from the drug carriers. The release of the drug from the drug carriers was measured at a controlled temperature of 37 ± 0.1 °C in a flow-through cell with 40 ml phosphate buffered solution. The drug release behavior of the drug carriers was characterized with the continuously applied magnetic field. Furthermore, the external magnetic fields switched alternatively between “on” (MF ON) and “off” (MF OFF) mode in a specific period was applied for several cycles.

At specific time intervals, buffer solution were withdrawn, the concentration of drug released was measured by UV spectrum (361 nm for vitamin B₁₂ and 482 nm for DOX). The drug release percent was determined using Eq. (3.1) [Lin, 2005]:


$$\text{Cumulative released (\%)} = \frac{R_t}{L} \times 100\% \quad (3.1)$$

where L and R_t represent the initial amount of drug loaded and the cumulative amount of drug released at time t.

To investigate the diffusion mechanism in the gel, the drug released data were fitted to Eq. (3.2) as follows: [Ritger, 1987; Ahn, 2002]

$$\frac{M_t}{M_\infty} = kt^n \quad (3.2)$$

The cumulative concentration of released the model drug at time t and at the end of the experiment (to approximate the infinite time) was used to calculate M_t/M_∞. M_t is the mass of sirolimus released at time t, M_∞ is the mass released at time infinity, and M_t/M_∞ is the fractional mass of released sirolimus; k is a characteristic constants, and n is a characteristic exponent related to the mode of transport of the penetrant. By taking logarithm on both sides of Eq. (3.2), Eq. (3.3) was used to calculate the diffusion parameters (n and k) for M_t/M_∞ < 0.6.

$$\ln\left(\frac{M_t}{M_\infty}\right) = n \ln t + \ln k \quad (3.3)$$

The effective diffusion coefficient (D_e) for $M_t/M_\infty < 0.6$ [Leach, 2005] was calculated using Eq. (3.4):

$$\frac{M_t}{M_\infty} = 4\left(\frac{D_e t}{\pi d^2}\right)^{1/2} \quad (3.4)$$

where d is the initial diameter or thickness of the drug carriers. Therefore, the fraction of the model drug released should be proportional to the square root of the released time. The cumulative concentration of released model drug at time t and at the end of the experiment (to approximate the infinite time) were used to calculate M_t/M_∞ , which was in turn used to calculate D_e .

In addition, the effect of hyperthermia of the drug carriers in the drug release testing by applying externally a high frequency magnetic field (HFMF) of 50-100 kHz and 15 kW (see Fig. 3.1). The coil of HFMF is 8 loops, and the strength of magnetic field is 2.5k A/m. The similar equipment was also reported by Mohr et al [Mohr, 2006]. Because the HFMF generates heat around the copper coil during operation, it was kept at 25°C through a cooling water bath to prevent thermally-induced interference from environment. 4 ml PBS containing 10 mg the drug carriers were charged in the glass tube and then the glass tube was put into the copper coil. At specific time intervals under HFMF treatment, buffer solution was withdrawn, the concentration of drug released was measured by UV spectrum (8453, Agilent, USA)



Fig. 3.1 Equipment of high frequency magnetic field

3.3 Drug diffusion test

The diffusion coefficients of the solutes were measured under switching MF (magnetic strength of about 400 Oe measured by Gauss meter) in a diffusion diaphragm cell (side-by-side cell) (see Fig. 3.2). The solution in the donor side is 80 ml of isotonic phosphate buffer (PBS) (pH7.4) containing 200 ppm of the model drug (vitamin B₁₂). The receptor compartment, separated by the ferrogel, was filled with 80 ml of PBS solution. The concentration of each compound in the receptor compartment was determined at $\lambda=361$ nm using a UV spectrophotometer. The permeation coefficient (P, cm²/min) was calculated according to the following equation for the diaphragm cell:

$$\ln\left(\frac{C_{do}}{C_d - C_r}\right) = \frac{2[DH]At}{\delta V}, (P = DH) \quad (3.5)$$

where C_{d0} is the initial concentration of the permeant in the donor compartment; C_d and C_r are indicative of the concentrations in the donor side and receptor side, respectively; D is the diffusion coefficient (cm²/min) [Singha, 1999; Yang, 2003; Miyajima, 1999; Liu, 2006]; H is the partition coefficient; A is the effective area of the ferrogel; δ is the thickness of the ferrogel; V are respectively the volumes of solution in the donor and receptor compartment (both are 80 ml). By plotting $\ln[C_{d0}/(C_d - C_r)]$ versus time (t), the permeability coefficient (P) can be calculated from the slope of the line by Eq.(3.5). Each data point was obtained by averaging of at least three measurements.

Moreover, the dry weight (W_{dry}) of drug-free ferrogel was immersed in the release medium until equilibrium state and then the wet weight (W_{wet}) were recorded. Subsequently, the ferrogel was immersed in 10ml of vitamin B12-containing medium. Partition coefficient (H) was determined from the initial (C₀) and equilibrium (C_e) concentrations of vitamin B12-containing mediums by Eq. (3.6) [Miyajima, 1999; Liu, 2006].

$$H = \frac{W_{dry}(C_0 - C_e)}{W_{wet}C_e} \quad (3.6)$$

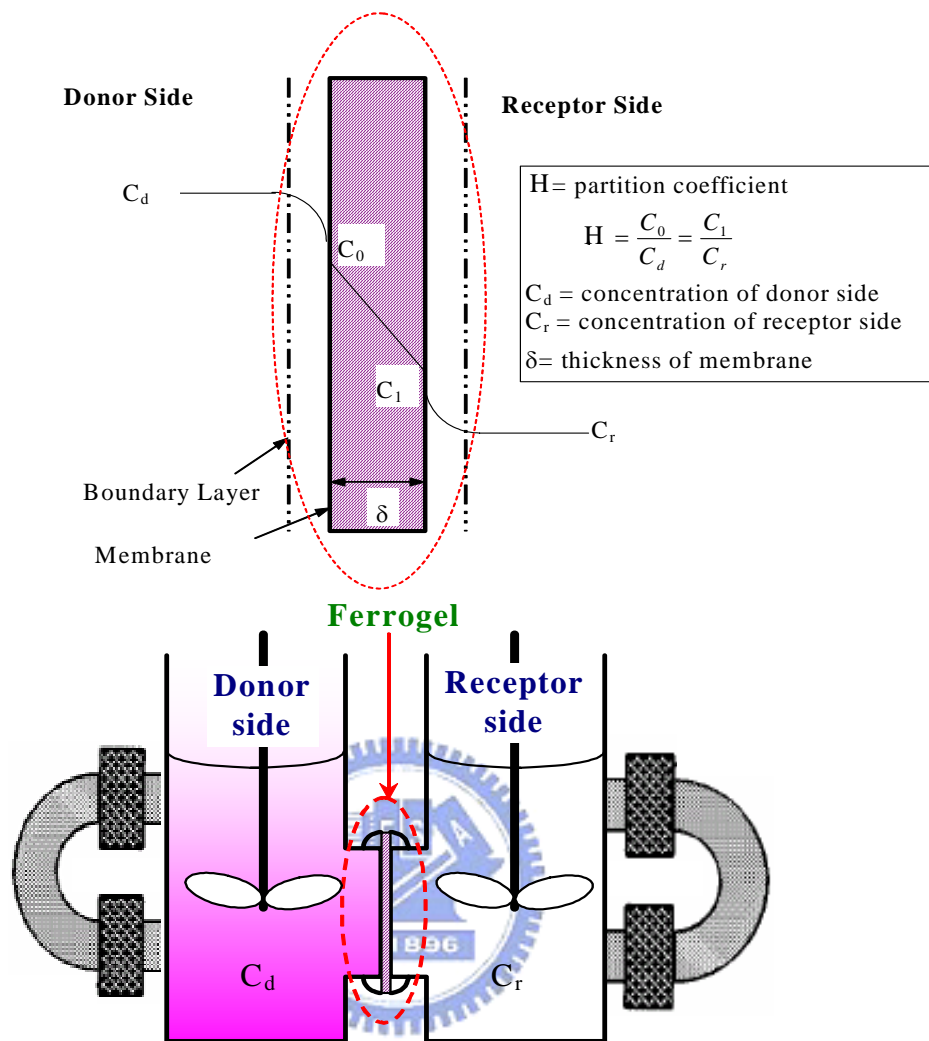


Fig. 3.2 Diaphragm cell for measuring the permeability coefficient

3.4 Characteristics Analysis

The Raman spectra were obtained using a backscattering geometry. The 632 nm of a He-Ne laser was focused through an Olympus microscope with a 100× lens to give a spot size of 1 μm. The spectra was obtained using a 60 seconds acquisition time and averaged over 3 accumulations. X-ray diffractometer (XRD, M18XHF, Mac Science, Tokyo, Japan) was used to identify the crystallographic phase of ferrosponges, at a scanning rate of 6° per min over a range of 2θ from 10° to 70°. Additionally, the magnetization of the ferrogel was measured with a vibrating-sample magnetometer (VSM, Oxford) at 298K and ±6000G applied magnetic field. The structure of ferrogel and morphologies of magnetic nanoparticles were examined

using field emission scanning electron microscopy (FE-SEM, JEOL-6500, Japan) and transmission electron microscope (TEM, JEOL-2010, Japan).

Pyrene loading was studied in order to assess the temperature-dependent aggregation within microgels. A stock solution of 1 mM pyrene in absolute methanol was prepared, from which 2 μ l was added to 3 ml of 100 mg F127-shell MNPs aqueous sample. The sample was then allowed to equilibrate for 24 h at a given temperature, and then excitation and emission spectra were recorded using spectrofluorophotometer (PL). There are five vibrational peaks in the pyrene emission spectra. The ratio of the intensities of the first (373 nm) to the third (384 nm) vibronic peak (I_{372}/I_{385}) in the emission spectra of the monomer pyrene was used to estimate the polarity of the pyrene microenvironment [Bromberg, 1999 & 2003].

BET analysis (Quantachrome, NOVA 2000, USA) was conducted using N₂ gas absorption isotherms at 77K, and the pore size were calculated following the approach by Barrett, Joyner, and Halenda (BJH). The nanospheres were dried by 80°C in vacuum condition for 1 day before BET analysis, afterwards the sample was de-gassed for 150°C and 2 hours following BET analysis [Hu, 2008].

The chemical structure of the activated polymers was characterized by NMR. Proton nuclear magnetic resonance spectroscopy (¹H-NMR) spectra were used to confirm the sites and degrees of substitution. The samples were dissolved in CDCl₃ and the spectra were recorded by NMR spectrometer (Bruker Avance-500) at 500 MHz for proton, equipped with a microprocessor-controlled gradient unit and an inverse-detection multinuclear BBI probe with an actively shielded z-gradient coil. For size characterization of nanocapsules, dynamic light scattering (DLS, zetasizer-3000HS, Malvern, UK) was used. Microscopy was performed using a transmission electron microscope (TEM, JEM-2010, JEOL, Japan) operating at 200 kV to reveal the microstructure of nanocapsules.

In addition, the porosity of the ferrogels was determined by measuring the true density and the bulk density [Yang, 2003]. To measure the true density, a freeze-dried ferrogels were placed in a vacuum oven and the weight of the sample was measured (M). Afterwards, the ferrogels were put into the cell chamber cup of a pycnometer (Micromeritics, 1305) to measure the true volume (V_t). The true density (ρ_t) was then

calculated according to Eq. (3.7). To measure the bulk density, ferrogels were vacuum dried and then the area was measured. The thickness of the ferrogels was measured ten times with a digital gauge meter (Mitutoyo IDF-112) to obtain the bulk volume (V_b). The bulk density (ρ_b) was then calculated according to Eq. (3.8). The porosity (ε) of the ferrogels was calculated according to Eq. (3.9).

$$\rho_t = M/V_t \quad (3.7)$$

$$\rho_b = M/V_b \quad (3.8)$$

$$\varepsilon = V_{bulk} / V_{true} - 1 \quad (3.9)$$

3.5 Methylthiazol tetrazolium (MTT) assay [Chen, *Mat. Sci. Eng. C-Bio. S.*, 2005]

Cell (smooth muscle cell) proliferation was assessed using a methylthiazol tetrazolium (MTT) assay, which measured mitochondrial dehydrogenase activity of viable cells spectrophotometrically. MTT reagent is a pale yellow substrate which produces a dark blue formazan product when it is incubated with viable cells. Smooth muscle cell (SMCs, TG/HA-VSMC smooth muscle cell, human normal aorta smooth muscle cell, BCRC number: 60293) were purchased from FIRDI and grown in culture medium containing 90% F-12K medium with modifications-Ham's F12K medium with 2 mM L-glutamine adjusted to contain 1.5 g/L sodium bicarbonate supplemented with 10 mM HEPES, 10mM TES, 0.05 mg/ml ascorbic acid, 0.01 mg/ml insulin, 0.01 mg/ml transferrin, 10 ng/ml sodium selenite and 0.03mg/ml ECGS and 10% fetal bovine serum. 1 mg of F127-MNPs sterilized by hydrogen peroxide gas plasma system (STERRAD® 50 system, a Johnson & Johnson Company, USA) and then placed into the wells of 6-well culture plates in contact with 2ml of SMCs (2×10^5 cells/ml, 3 to 4 passages) and were incubated in 5% CO₂ at 37°C for 72 hr.

After cell culturing for 72 hr, the viability of SMCs was determined by MTT assay. 0.5 ml MTT (5 mg/ ml PBS solution, Sigma, USA) solution and 2ml serum free

medium was added to each well (6-well culture plates). After 4 hr incubation at 37°C, 2 ml of DMSO (dimethyl sulfoxide) was added to dissolve the formazan crystals. The dissolvable solution was jogged homogeneously about 15 min by the shaker. The optical density of the formazan solution was read on an UV–VIS spectrophotometer at 570 nm. All experiments were repeated five times. Data from the MTT assays were analyzed by means of Student's t-test. A P-value less than 0.05 were considered to be significant.



Chapter 4

Biodegradable Ferrogel (Gelatin)

4.1 Introduction

In recent years, stimuli-responsive polymers, which can be responsive to external stimuli, such as pH, temperature, and electric field, have attracted a great deal of interest due to their potential applications in controlled drug delivery [Zrínyi, 2000]. Gelatin is a widely used polymer in pharmaceutical products [Cortesi, 1998]. Furthermore, it is of special interest in controlled release applications because of their soft tissue biocompatibility, the ease with which the drugs are dispersed in the matrix, and the high degree of control achieved by selecting the physical and chemical properties of the polymer network.

Magnetic materials have been widely used in the field of biotechnology in bio-separation, artificial muscles and drug carriers [Neuberger, 2005; Pankhurst, 2003; Rosengart, 2005]. Some researchers have reported that the drug carriers of magnetic gels applied in targeting [Rotariu, 2005]. However, to our best knowledge, it is less seen to use magnetic fields to control drug release rate. Therefore, the combination of the gelatin and magnetic particles is a potential research to prepare the stimuli-polymer which can be applied in controlled drugs release by magnetic field.

Environmental sensitive hydrogels (smart hydrogels) with controlled drug release have been received great attention in the field of medicine, pharmaceuticals, and biomaterials science. These hydrogels provides advantages over conventional therapeutic dosage forms by having higher delivery efficiency, site-specific delivery, controlled dose, and elimination or reduction of harmful side effects to the patients. By these wide advantages of the hydrogels, a number of researches have been successfully proposed to integrate active drug molecules and host materials, where to manipulate drug release desirably. For example, through conventional bolus injection, drug concentrations at site of therapeutic actions were only a portion of the treatment period in the therapeutic window [Uhrich, 1999]. By contrast, drug delivery from the controlled polymeric systems could maintain drug concentrations within the therapeutic window for prolonged time.

Such smart hydrogels possess such 'sensing' properties which allow to change in swelling behaviors, permeability, and elasticity upon only minute alternations in the environmental conditions. Many physical and chemical stimuli have been applied to induce various responses in response to change in temperature [Zhang, 2004; Eeckman, 2004; Gutowska, 1997; Chiu, 2005; Claude, 2004], pH [Etrych, 2001; Chen, 2004], glucose [Chu, 2004], electric field [Murdan, 2003; Sutani, 2001] and magnetic field [Zrínyi, 2000], for the smart hydrogels [Qiu, 2001] which administer drug release considerably and can be potentially used in extended field. So far, many kinds of magnetic sensitive hydrogels (ferrogels) have been developed and studied with regard to biomedical materials. These hydrogels were usually prepared by introducing magnetic nanoparticles into a polymer matrix, and a macroscopic change in the shapes of the resulting ferrogels in response to external magnetic stimuli can be easily manipulated, which permit these ferrogels to be employed as muscle-like soft linear actuators and drug delivery systems [Mitsumata, 1999; Xulu, 2000; Zrínyi, 1998]. For example, magnetic-field-sensitive gelatin microspheres were reported for pulsed release of insulin via an oscillating magnetic field [Saslawski, 1988; Lu, 2005] and the release rate of insulin in the alginate microspheres with magnetic particles is much faster than that in absence of an external magnetic field. Although magnetic nanoparticles (MNPs) were widely used for magnetic resonance contrast enhancement, tissue repair, immunoassay, hyperthermia, drug targeting and delivery and in cell separation [Gupta, 2005; Neuberger, 2005], to the best of our knowledge, there has been little investigation on drug delivery under a direct current (DC) magnetic field through the use of magnetic nanoparticles in the ferrogels. Drug delivery from the magnetic sensitive ferrogels can be triggered by a non-contact force (an external magnetic field), which is superior to the traditional stimuli response polymers, such as pH or temperature sensitive polymer. By this concept, a Magnetic Targeted Carriers (MTCs) has been designed which could adsorb pharmaceutical agents through application of an externally magnetic field for site-specific targeting and sustained release of drugs [Fricker, 2001]. In addition, according to our previous study, it was demonstrated that a direct current (DC) magnetic field can be used to manipulate the drug release behaviors from a smart magnetic hydrogel [Liu, 2006]

through an on-off switch of a magnetic field.

However, a number of drawbacks still exist to use the magnetic hydrogels for drug delivery systems. For instance, it could not display fast and outstanding magnetic sensitive behaviors to control drug release. Zhang et al. reported that macroporous temperature-sensitive hydrogels exhibited a tremendously faster response to the external temperature changes due to their unique macroporous structures [Zhang, 2004 & 2001]. In addition, pHEMA sponges were developed to achieve rapid and reliable delivery of bioactive substances for long-term implantable drug delivery devices [Dziubla, 2001], and plasmid DNA with a sustained release from polymeric scaffolds was investigated for tissue regeneration [Storrie, 2006]. Therefore, in this work, a magnetic-sensitive sponge hydrogels (ferrosponges) was developed in this study to overcome those above-mentioned problems. The resulting ferrosponge is able to absorb a large amount of water and shows fast recovery property. Furthermore, magnetic sensitive walls of ferrosponges constructed by MNPs can effectively reduce their wall permeability and decrease the drug release via a given magnetic field, as shown in Fig. 4.1. For this purpose, a magnetic sponge hydrogel composed of a biocompatible gelatin and magnetic nanoparticles (MNPs) is investigated in terms of the concentrations of magnetic nanoparticle and gelatin. The drug release behavior from this ferrosponge in response to a magnetic field is investigated.

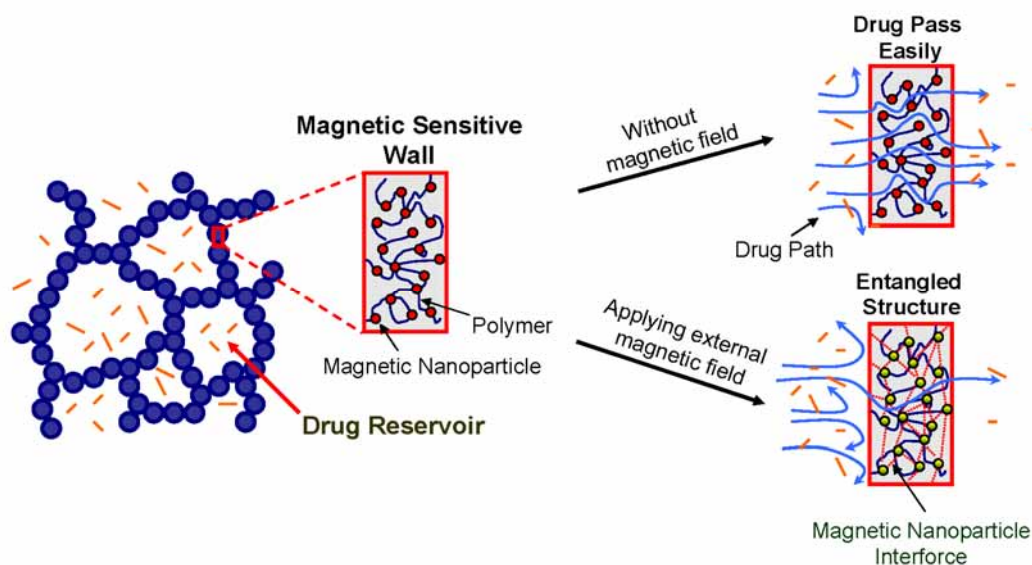


Fig. 4.1 Schematic drawing of drug release from the magnetic-sensitive ferrosponges with and without applying external magnetic field

4.2 Gelatin Ferrogel

4.2.1 Fabrication of gelatin ferrogel

For the preparation of the magnetic hydrogels (or called ferrogel), the gelatin (15 wt %) was first dissolved in deionized water at 45°C to ensure that the gelatin can be fully dissolved. After that, 4 wt% Fe₃O₄ nanoparticles (from Alfa Aesar) including 0.03 wt % drugs (vitamin B₁₂, from Sigma) and genipin (Challenge Bioproducts Co., Ltd., Taiwan) with different weight ratio were added to the above gelatin solution under stirring for 30 min at 40 °C and then incubated in 25 °C for 2 days. The genipin-cross-linked ferrogel were respectively designated as Ge0.06, Ge0.03, Ge0.01 and Ge0.003 by their different cross-link density. For example, Ge0.06 means genipin content is 0.06 wt%.

The swelling rate of the ferrogels was measured as prescribed in our previous study [Yang, 2003] and the switching “on” mode of a given magnetic fields (MF) is about 400 Oe. For drugs release test, the ferrogels containing vitamin B₁₂ were first immersed in 20 ml of phosphate buffer (PBS) (pH7.4) and then UV-visible spectroscopy was used for the characterization of absorbance peaks at 361 nm to determine the vitamin B₁₂ release concentration.

4.2.2 Characterization of gelatin ferrogel

Fig. 4.2-(a) showed the gelatin gels containing vitamin B₁₂ (no Fe₃O₄ particles) were cross-linked by genipin with various weight ratios. After the gelatin/genipin solution was incubated for 2 days, the color of the gels transfers from pink (the color of vitamin B₁₂) to purple (lower cross-linked density) or dark blue (higher cross-linked density). The UV spectrum in Fig. 4.2-(b) also demonstrated the color change. The above results may suggest that the gelatin could react with a variety of the genipin concentration to display different colors and morphologies. The darker the color of the gels, the denser the porosity of the gels, and the porosity or pore size of the gelatin gels would influence the drugs release properties. In addition, it was observed that the Fe₃O₄ nanoparticles were fairly uniformly distributed in gelatin hydrogels as evidenced from the cross-sectional SEM image in Fig. 4.3-(a). Hence, it also proves that the gelatin solution is an excellent dispersing agent for Fe₃O₄ nanoparticles.

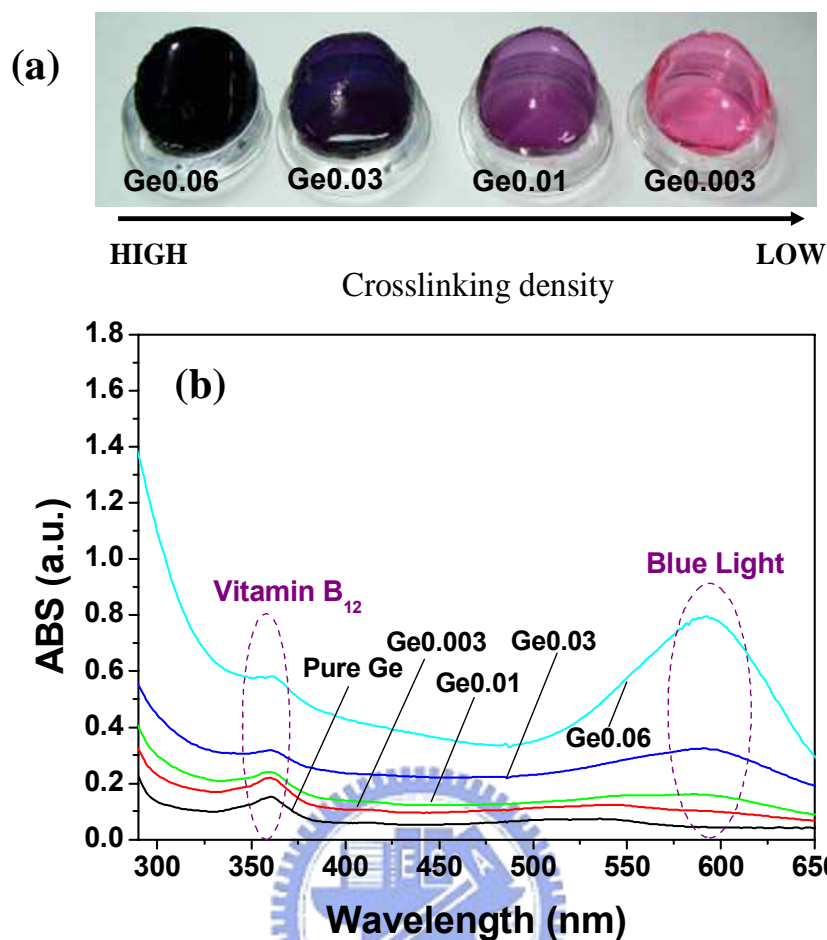


Fig. 4.2 (a) OM photos of the gelatin gels with different cross-linked densities and (b) UV spectroscopy analysis of different cross-linked gelatin hyrogels

The swelling properties of the magnetic hydrogels as a function of switching MF were illustrated in Fig. 4.3-(b). While switching “on” mode of a given MF, it was found that not only swelling rate decreased sharply but also de-swelling in the differential curve. However, it will restore back to original states while switching “off” mode. The sensitive properties may be attributed to the fact that the porosity or the pore size of the ferrogels would decrease in switching “on” mode. The mechanism of the “close” configuration of ferrogels can be further illustrated in Fig. 4.4. While the MF switching in “on” mode, the Fe_3O_4 particles tend to aggregate together and this causes the porosity of the ferrogel to decrease. Therefore, a swelling rate was reduced and a decreased drugs release rate was induced.

Table 4.1 Cumulative drugs release of the ferrogels in “on” or “off” mode of a given magnetic field at 120 min

Ferrogel	Ge0.003	Ge0.01	Ge0.03	Ge0.06
MF OFF	56.5 %	52.2%	49.9%	48.0%
MF ON	47.4 %	45.5%	44.4%	44.1%
OFF- ON	9.1 %	6.7%	5.5%	3.9%

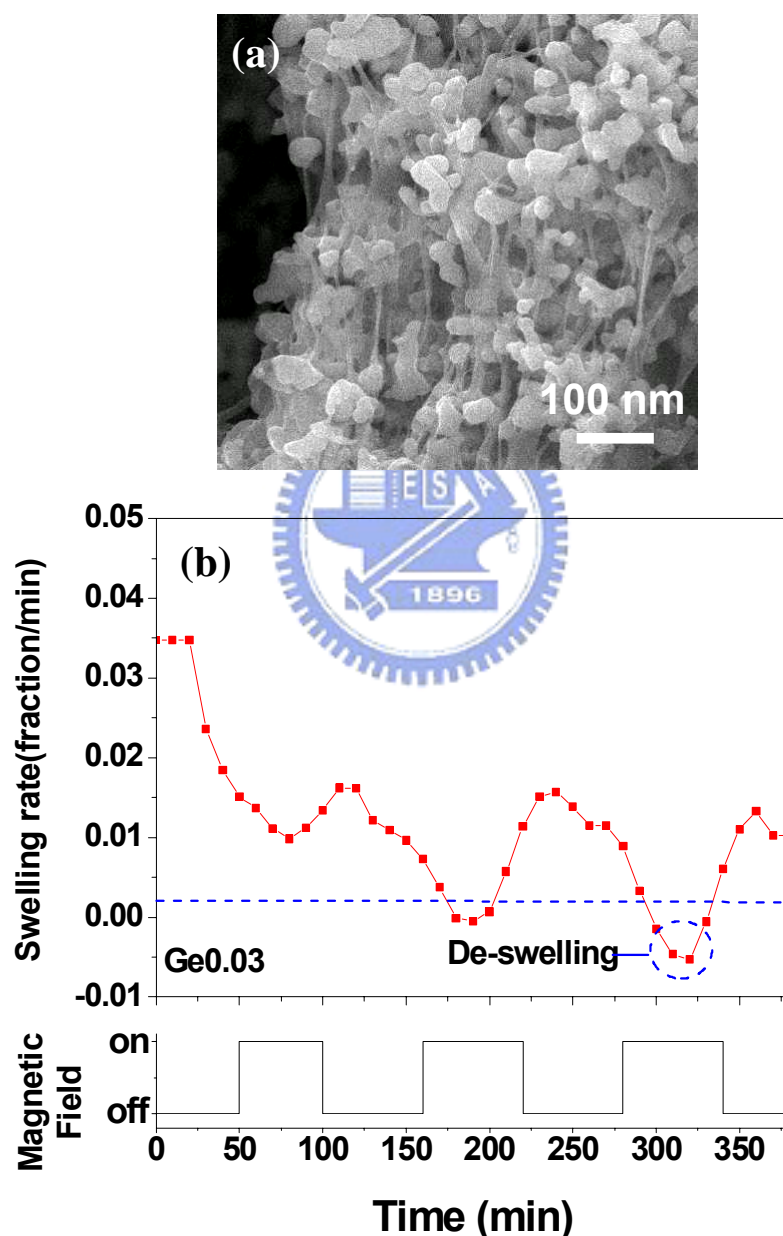


Fig. 4.3 (a) SEM observation of Fe₃O₄ nanoparticles distributed in gelatin hydrogels and (b) sensitive swelling rate of the ferrogels dependent on switching MF

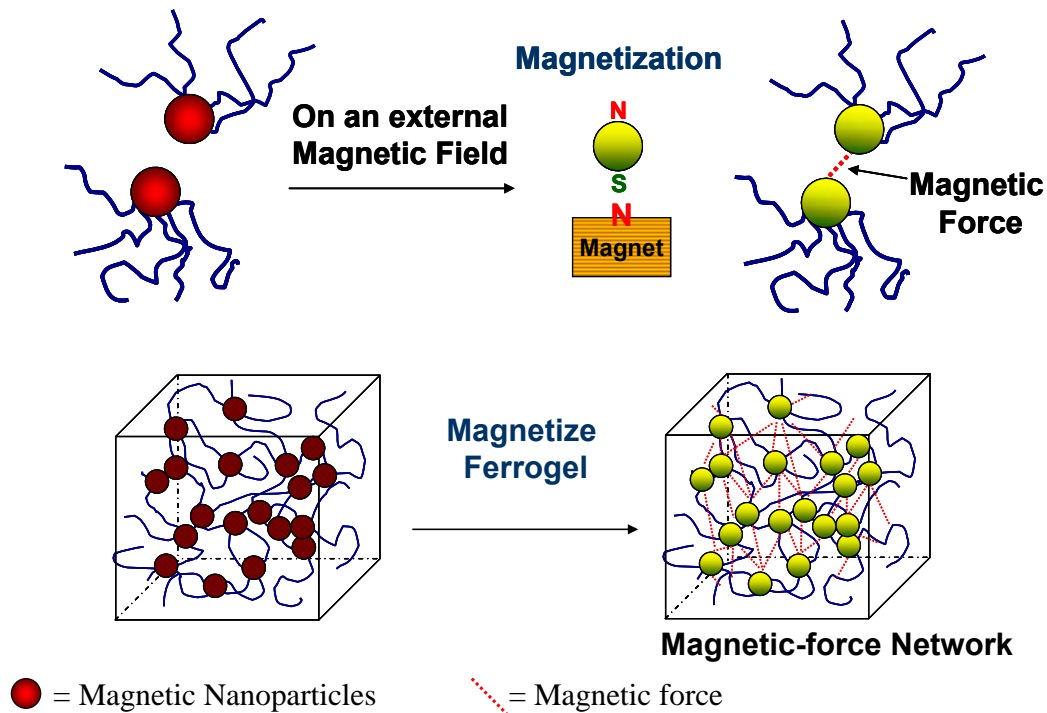


Fig. 4.4 Mechanism of “close” configuration of the ferrogels due to the aggregation of Fe_3O_4 nanoparticles under “on” MF causes the porosity of the ferrogels to decrease (Interparticle magnetic force)

Fig. 4.5-(a) exhibits the “close” configuration of Ge0.003 ferrogel, the drugs release rate decreased in switching “on” mode. Moreover, Table 4.1 shows the vitamin B_{12} release conditions of different cross-linked density ferrogel in MF switching “on” or “off” mode. It was observed that the lower cross-linked density of the ferrogels, the more distinct the magnetic sensitive properties (OFF-ON) (9.1%). The reason is that the ferrogels with a lower cross-linked density display the softer properties which could cause the porosity to be easily modified due to the more free movement of the gelatin hydrogels chains of magnetic nanoparticles. Furthermore, the Ge0.003 ferrogel displays a higher magnetization (M_s) (9.199 emu/g) than the Ge0.03 ferrogels (6.023 emu/g) as measured from the vibrating sample magnetometer (VSM) and shown in Fig.4.5-(b). Based on the above two reasons, it could be demonstrated that the lower cross-linked density ferrogels display more obvious magnetic sensitive properties. Besides, the magnetic sensitive properties of the drugs release could be found in continuous switching “on-off” mode for a given MF, as shown in Fig. 4.6. The differential curve of drugs release rate showed that the drugs release decrease in

switching “on” mode, and restore original states in switching “off” mode. These sensitive characterizations are similar with the swelling rate.

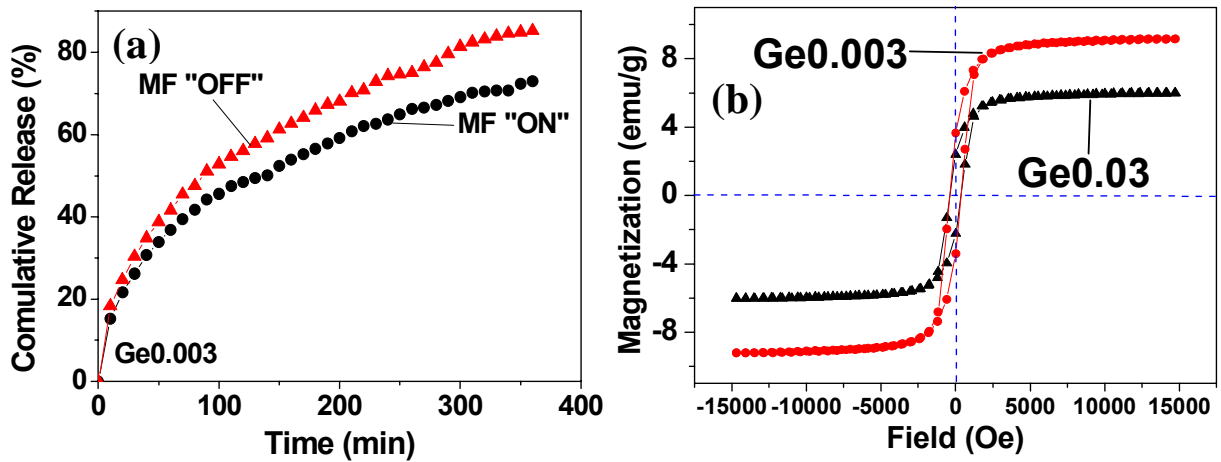


Fig. 4.5 (a) Drugs release rate profiles of the Ge0.003 ferrogels in MF switching “on” or “off” mode (b) hysteresis loop analysis of the magnetic hydrogels using VSM

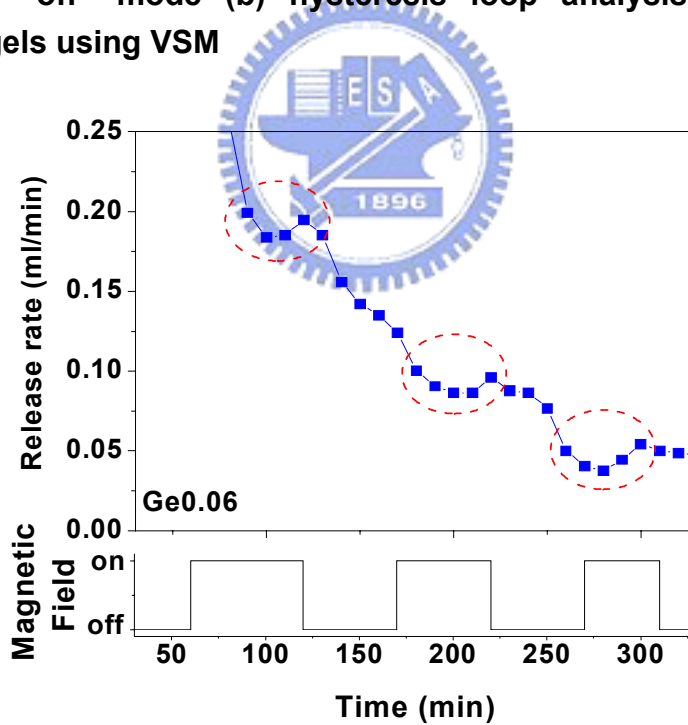


Fig. 4.6 Sensitive drugs release properties of the ferrogels dependent on switching “on-off” mode for a given MF

4.3 Gelatin Ferrosponges

4.3.1 Fabrication of ferrosponges

The commercially available gelatin from bovine skin (type A, ~300 bloom), 1-Ethyl-3-(3-Dimethylaminopropyl) Carbodiimide Hydrochloride (EDC) and model drug vitamin B12 were purchased from Sigma Chemical Co.. Iron (II) chloride (FeCl_2) and Iron (III) Chloride (FeCl_3) were obtained from Fluka and Riedel-deHaen, respectively, and used as received. Ammonia hydroxide (NH_4OH) in the form of 33% water solution was obtained from Riedel-deHaen. Phosphate buffered saline (PBS) was purchased from Ultra Biotechnology Corporation.

Magnetic sponge hydrogels (ferrosponges) were fabricated by in-situ co-precipitation process, and iron oxide nanoparticles were deposited directly in the gelatin hydrogel. Briefly, gelatin was dissolved in the D.I. water for 2 hours at 40°C . After gelatin was fully dissolved in the solution, appropriate amount of FeCl_2 and FeCl_3 was added to the gelatin solution to form the hybrid sols. (The molar ratio of $\text{FeCl}_2/\text{FeCl}_3$ was kept constant at 2:1, and the reagents used for synthesis was showed in Table 4.2) When completely dissolved, the hybrid sols were rapid cooled to 4°C to gel the gelatin which was then immersed in a water solution of NH_4OH to start the iron oxide formation process. Immediately, the gels became black, indicating that the iron oxide nanoparticles have been formed in the system. After the in-situ co-precipitation of iron oxide nanoparticles, the ferrosponge were washed by D.I. water for several times to remove un-reacted NH_4OH solution, and then the ferrosponge were subsequently kept in the freezing baths maintained at -80°C for 1 day and finally lyophilized in a freeze-dryer for 3 days. Finally, the macroporous structures were formed and cured by 1-ethyl-3-[3-(dimethylammino) propyl] carbodiimide (EDC) in the 9:1 acetone: water solution at 4°C .

Table 4.2 Reagents used for the synthesis of ferrosponges

system	Sample	Gelatin (g)	FeCl ₂ (g)	FeCl ₃ (g)	water (mL)	S % ^a	MNPs ^b (wt %)
5G series	5G-1F	5	1	2.7	100	10.1	3.7
	5G-3F	5	3	7.1	100	8.1	6.5
	5G-5F	5	5	13.5	100	6.1	9.4
15G series	15G-1F	15	1	2.7	100	9.4	2.7
	15G-3F	15	3	7.1	100	7.7	5.3
	15G-5F	15	5	13.5	100	6.7	7.1

^aS%: Swelling ratio=(Weight of wet ferrosponge)/(Weight of dried ferrosponge)

^bMNPs (wt%): The weight fraction of magnetic nanoparticles(MNPs) measured by TGA

4.3.2 Characterization of magnetic-sensitive ferrosponges

Magnetic-sensitive ferrosponges composed of gelatin and magnetic nanoparticles (MNPs) were prepared through an in-situ co-precipitation process. The traditional method of preparing iron oxide nanoparticles usually used the chemical co-precipitation of iron salts in the alkaline medium:



However, the iron oxide nanoparticles formed by using this traditional method aggregated easily [Lin, 2005]. To prevent aggregation, the gelatin and iron salts were mixed in advance to become a homogeneous mixture in which iron cation and the carboxylic acid groups of polymer allow to form a homogeneous complex structure in the solution [Lin, 2005]. While the ammonia solution was added, the iron oxide nanoparticles were directly formed in the presence of the gelatin, resulting in a sponge-like structure after lyophilizing. The ferrosponges shown in Fig. 4.7 exhibited a three-dimensional porous structure with macroporous and an anastomosing network of gelatin matrix. The mean pore size shown in Fig. 4.7-(a) for the 5 wt% gelatin matrix of ferrosponges was microscopically measured to be $100 \pm 23 \mu\text{m}$, which was larger than that ($50 \pm 24 \mu\text{m}$) for the 15 wt% gelatin matrix of ferrosponges, Fig. 4.7-(b). It was found that the morphology and pore size of the ferrosponges seemed to be greatly dependent upon the gelatin matrix rather than the amounts of MNPs. The macropores

of the ferrosponges appeared to be well-arranged, which displayed membrane-like wall structure. The magnified image in the Fig. 4.7-(b) showed the surface morphology of the ferrosponge, where a rougher surface than that of traditional sponges was observed in the ferrosponges, which is due to the presence of the MNPs in the ferrosponges.

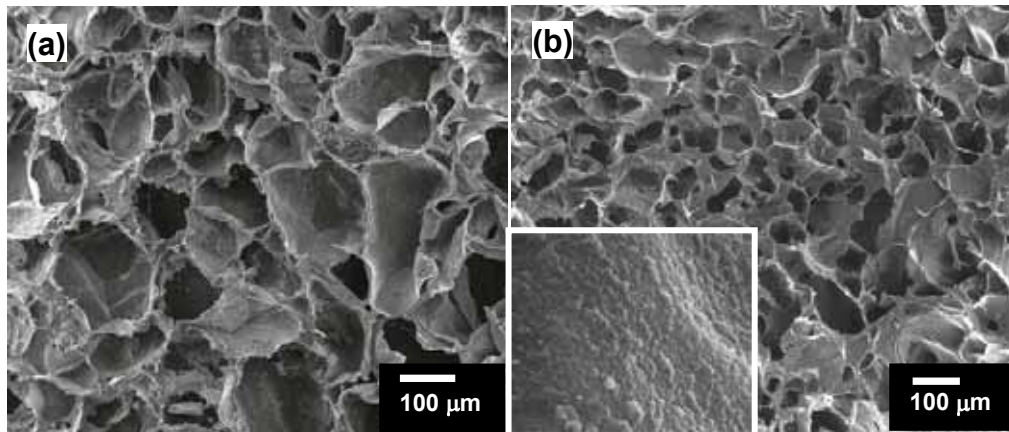


Fig. 4.7 SEM images of the ferrosponges for 5wt% (a) and 15wt% (b) gelatin concentrations

4.3.3 Crystalline phase identification of Ferrosponges

X-ray diffraction (XRD) analysis showed that the crystalline phases of iron oxide in the ferrosponges are γ -Fe₂O₃ (maghemite) or Fe₃O₄ (magnetite), Fig. 3(a). However, it is very difficult to distinguish Fe₃O₄ from γ -Fe₂O₃ because these two phases exhibited similar XRD patterns (according to Fe₃O₄ (JCPDS [85-1436]) and γ -Fe₂O₃ (JCPDS [04-0755])) [Long, 2004]. In addition to the diffraction peaks of iron oxide, one more peak at $2\theta \sim 21^\circ$ was observed and can be identified as the semi-crystalline gelatin. Furthermore, the diffraction data were also used to measure the primary particle size according to Scherrer analysis for diffraction peak widths of (311) peak, wherein the (311) peak is common to both magnetite and maghemite phases. The primary particle size of iron oxide in the ferrosponges was estimated ranging from 8 to 12 nm.

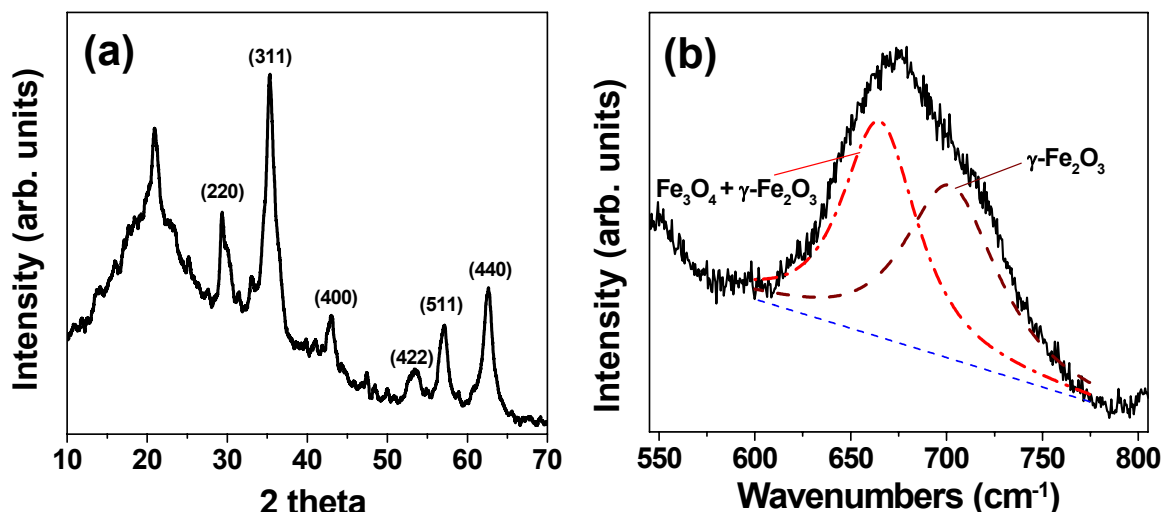


Fig. 4.8 (a) XRD and (b) Raman spectra of the ferrosponges

Raman spectroscopy is potentially more useful than the X-ray diffraction techniques in distinguishing $\gamma\text{-Fe}_2\text{O}_3$ from Fe_3O_4 and was used to track subtle structural differences between the vibration frequencies of $\gamma\text{-Fe}_2\text{O}_3$ and Fe_3O_4 [de Faria, 1997]. Fig. 4.8-(b) shows that, although the iron oxide nanoparticles were surrounded with gelatin, a significant difference between these phases can be recognized from the Raman spectrum. The 665 cm^{-1} band, assigned to the characteristic band of Fe_3O_4 , observed in the Raman spectra displays a symmetrical peak and is attributed to the vibration modes consisting of stretching of oxygen atoms along Fe-O bonds. On the other hand, the characteristic peaks for $\gamma\text{-Fe}_2\text{O}_3$ present at 721 cm^{-1} and a weaker band at 667 cm^{-1} [Long, 2004]. Both evidences support the ferrosponges consisting of $\gamma\text{-Fe}_2\text{O}_3$ and Fe_3O_4 phases.

As the result shown in Table 4.2, the content of iron oxide nanoparticles in the sample 5G-5F could reach 9.4 % measured by TGA. It was observed that the amount of the iron oxide nanoparticles were related to the starting concentration of iron salts. Generally, it was thought that the amount of iron oxide nanoparticles were proportional to the concentration of iron salts, albeit not in a direct proportional correlation, they do exist a linear relationship. This is due to the fact that the inorganic nanoparticles directly formed in the polymer matrix could be hindered by polymer-particle interactions [Lin, 2005; Tannenbaum, 2005]. Therefore, the amount of iron oxide nanoparticles developed in sample 5G-5F was lower by five times than

that in sample 5G-1F.

4.3.4 Magnetic property of Ferrosponges

The magnetic properties of the ferrosponges with various iron oxide contents were studied with VSM at ambient temperature, with the magnetic field sweeping from -6000 to +6000 G. As shown in Fig. 4.9, the magnetization-magnetic field curves for all the ferrosponges show similar shape with negligible hysteresis. This indicates that these ferrosponges exhibit superparamagnetic characteristics but with different saturation magnetization (M_s). The sample 5G-5F displayed the largest M_s of 23.6 emu/g, and it was observed that the M_s decreased with the decrease of iron oxide. The saturation magnetization (M_s) of the ferrosponges was also dependent on the inorganic/organic ratios, as summarized in Table 4.2. However, although the weight fractions of MNPs in the 15G series are slightly lower than those in the 5G series, the inorganic/organic ratios of 15G series are much lower as compared with 5G series. Correspondingly, the M_s for 15G series was lower than that for 5G series. The correlation of the M_s with the magnetic sensitive behaviors of these ferrosponges will be discussed in forthcoming analysis.

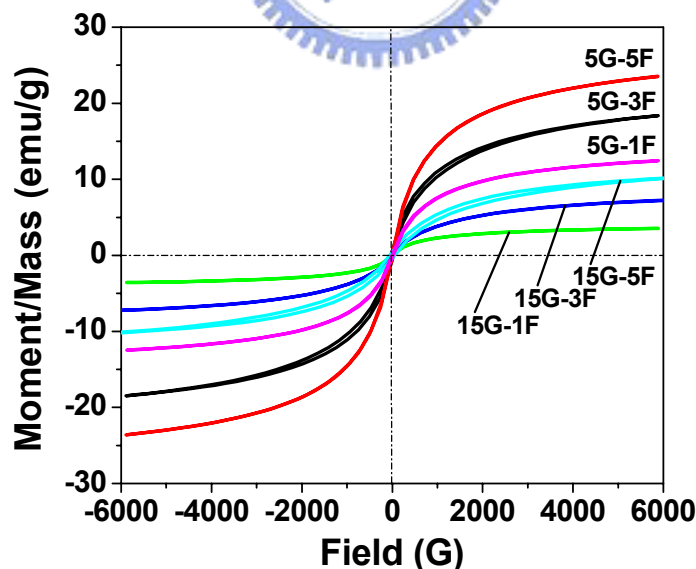


Fig. 4.9 Vibrating sample magnetometry measurements for the ferrosponges with various contents of iron oxide nanoparticles

4.3.5 Nanostructural analysis of Ferrosponges

In order to examine the microstructure and morphology of the resulting nanoparticulate network structure, the gelatin was intentionally removed thermally when a porous structure made of the magnetic nanoparticles remained intact.

The pores in the magnetic solid network structure are characterized as two categories; one with a size ranging from 100-200 nm, as a macroporosity, located between the walls or struts, and the one inside the walls or struts has a size of only a few nanometers, as a mesoporosity. Such a mesoporosity is formed due partly to thermal removal of the gelatin between the nanoparticles, and in part, as an interparticle voids developed upon in-situ synthesis, as shown in Fig. 4.10. In comparison with 5G-5F and 15G-5F, in Fig. 4.10-(a) and 4.10-(b), respectively, sample 5G-5F exhibited looser structure than that of the sample 15G-5F, having a denser structure when the gelatin was completely burned off. However, it seems no considerable difference between the mesoporosity of these two samples. Therefore, it can be concluded that the concentration of gelatin used to synthesize the ferrosponges affects strongly the macroporosity of the sponge but negligibly for mesoporosity development. High resolution SEM images of 5G-5F and 15G-5F were presented in Fig. 4.10-(a) and 4.10-(b), respectively. The iron oxide nanoparticles were clearly observed and exhibited a spherical shape with average particle size about 10 nm, which is relatively closed to the size calculated by Scherr's equation. Such a nanometric scale of the magnetic particles allows the achievement of super-paramagnetization upon magnetic stimulation and this is evidenced in Fig. 4 where little or no hysteresis behavior was detected. The pore size distribution of iron oxide nanoparticles exhibited in Fig. 4.10-(c) demonstrated that there were numerous nanopores within the magnetic nanostructures. The mean pore diameter was 9.1 nm, and the pore size distribution ranged from 3 nm to 30 nm, which may affect the diffusion rate of the B12 molecules. It is also conceivable that a manipulation of these nanopores by a magnetic force can be effectively used for a control release of drug. The sizes of mesopores after treating with magnetic field decreased considerably (Fig. 4.10-(c)) in pore volume and pore size, to an average size of 4.6 nm, indicating a result of re-arrangement of the magnetic nanoparticles to form more compact, rigid

structure. Although the change in the pore size is detected from the magnetic nanoparticle network, this can also be translated as shrinkage in the pore size in the ferrosponge upon applying a magnetic field. The variation of the mesopores in the ferrosponges under magnetic stimulation is able to act as a diffusion regulator for control release of drug molecules.

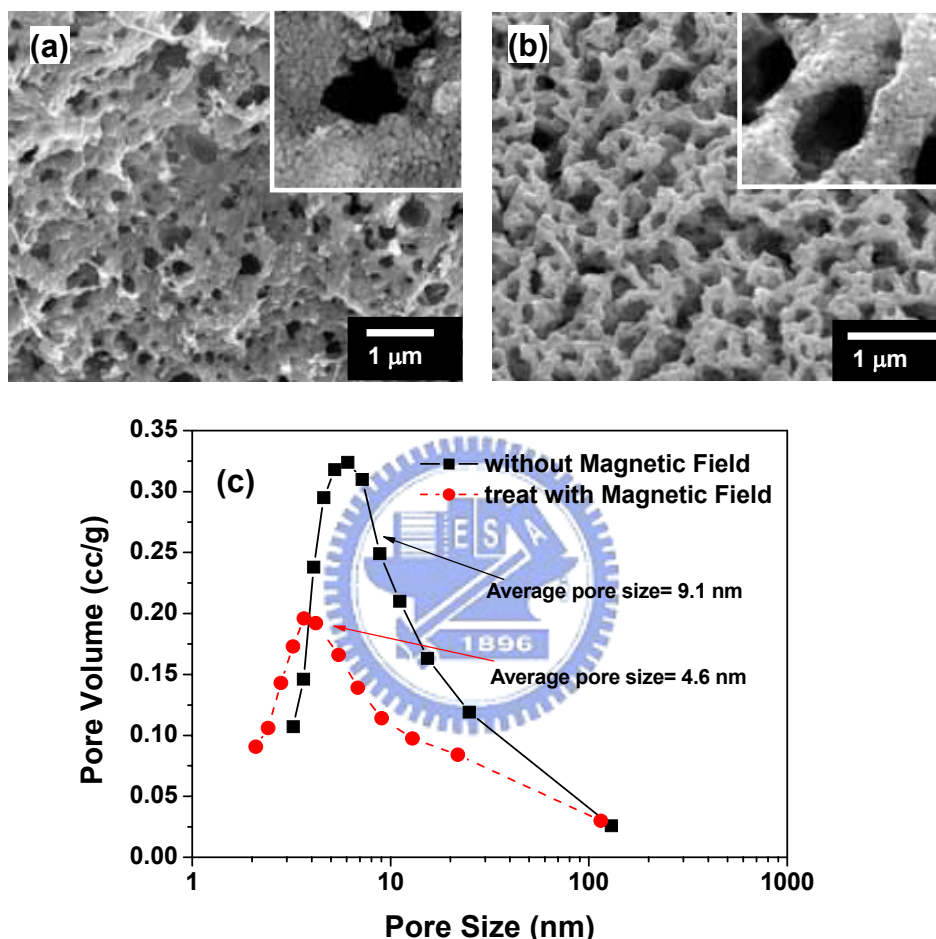


Fig. 4.10 SEM images of iron oxide nanoparticles structure of the sponges obtained by thermally removing gelatin matrix for the ferrosponges with (a) original 5G-5F and (b) 15G-5F compositions, and (c) associated with the pore size distribution of the ferrosponges treated with and without magnetic field

4.3.6 Drug release behaviors of ferrosponges

Therefore, along the line of magnetic manipulation, drug (vitamin B₁₂) release profiles from the ferrosponges were expected and demonstrated in Fig. 6. Initial burst

release was observed from the ferrosponges in the first 60 minutes and the amounts of drug release from the ferrosponges were almost equal for all the ferrosponges. Although the ferrosponges had been washed before the releasing test, the initial burst was believed to result from the outermost layer of the ferrosponges. After the initial burst, the ferrosponges showed different release rates, from 60 to 250 minutes, according to the concentration of the nanoparticles. Typically, pure gelatin sponge showed a faster drug release rate than that of the nanoparticle-containing ferrosponges. According to our previous studies, it demonstrated that a strong interaction exists between iron oxide nanoparticles and polymer side chains in the composite [Liu, 2006]. In addition, Hongbin et al. also reported that the inorganic nanoparticles restricted relaxation behavior in the nanocomposites because of the polymer-nanoparticle interactions [Lu, 2003].

When these strong interactions were developed in the ferrosponges, the drug-release behavior can be affected and restricted via molecular relaxation. The drug molecules released from a nanocomposite can be blocked by the nanoparticles, acting as a physical barrier for drug diffusion. In the meantime, the presence of numerous nanoparticles along the path of drug diffusion gives rise to a considerable increase in the mean free path for drug diffusion. Therefore, the drug released from the ferrosponges showing a lower rate than that from pure gelatin sponges. A near-linear drug release profile was later developed after a time period greater than 250 minutes for all the samples, irrespective of the presence of nanoparticles, suggesting the release of the drug is reaching a state-steady diffusion. Again, the higher concentration of the nanoparticles in the ferrosponges, the lower amount of the drug was released in this linear-kinetic region. This indicates the rate of drug release being considerably retarded by those nanometric physical barriers in the matrix, but the release profiles for all the ferrosponges appeared following a similar (near) zero-order kinetics according to Fig. 4.11.

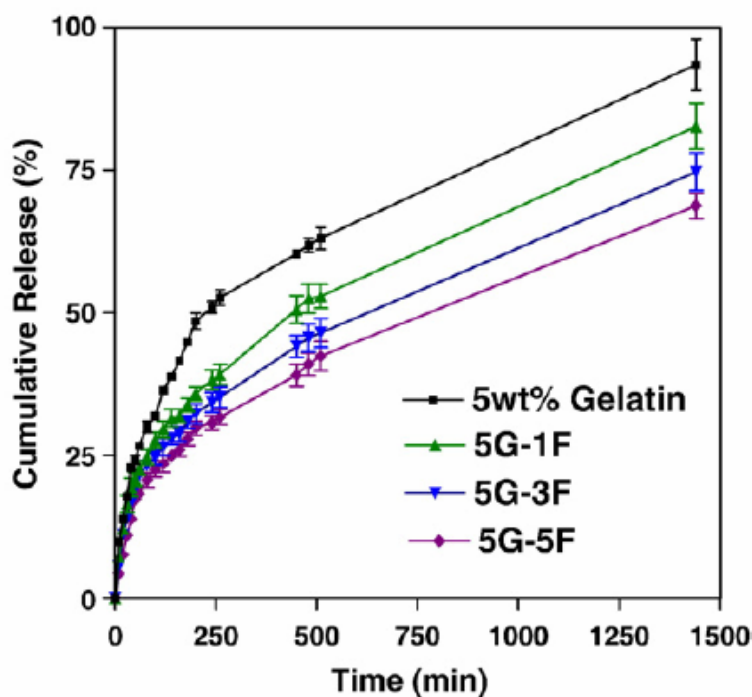


Fig. 4.11 Drug release profiles of 5G series of the ferrosponges

4.3.7 Magnetically controlled drug release of ferrosponges

Fig. 4.12 shows the release profiles of vitamin B12 from the ferrosponges under “on” and “off” operations of an external magnetic field (MF) at 37°C. The amount of drug that released under “on” mode was relatively low; about 25%, compared to that operated under “off” mode, 40%, over a time span of 360 minutes. This finding strongly indicates that the applied magnetic field effectively retarded drug release from the ferrosponge of 5G-5F composition by as large as 60%. More specifically, the drug release profile is considerably changed even from the very beginning of release when the ferrosponge was subjected to a given MF. The release kinetic showed a parabolic profile from the beginning to about 120 minutes, after then, a linear profile of drug release followed till the end of the release test.

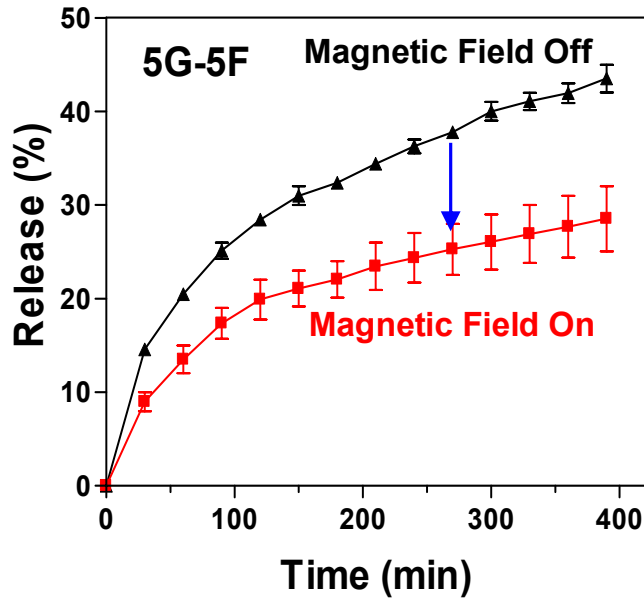


Fig. 4.12 Drug release profiles with and without applying magnetic field (“MF on” and “MF off”, respectively.) for 5G-5F ferrosponge

By taking Eq. 3.2 & 3.3, a kinetic analysis of drug release from the 5G-5F ferrosponge can be obtained, as shown in Fig. 4.13, where a two-stage release kinetics for the ferrosponge is displayed, with and without the presence of the magnetic field. Both exponent constant, n and rate constant, k , are estimated. For the first-stage release kinetics, the exponent constant is in a range of 0.5-0.6, indicating a typical Fickian diffusion mode, suggesting diffusion rate is dominating the drug release over relaxation rate in the ferrosponges. However, the exponent constants are apparently decreased to a range of 0.28-0.36 at the second stage of the profile, indicating the diffusion at the second stage being heavily retarded and it turned out to be more pronounced under magnetic field, having the lowest n value. It is suggestive of an enhanced retardation for drug molecules to diffuse through the ferrosponges under magnetic field. The reduction in pore size and a corresponding shift in pore size distribution to smaller pore region under magnetic field of the magnetic particulate network of the ferrosponge, Fig. 4.10-(c), provide evidence of a diffusion barrier for drug movement in the magnetized ferrosponges. Similar release kinetic parameters can be found for the ferrosponges of different compositions, and the constants are listed in Table 4.3. The rate constant, k , for all the ferrosponges at both release stages has apparently lower k value in the presence of magnetic field, than those without the

field. This change in release kinetic is believed to be a change in the distribution of the nanoparticles when an MF is applied.

The first-stage release profile (kinetically similar to that observed for the ferrosponge under no MF) appeared to be less magnetically controllable because it corresponds to the drug release from macroporosity of the magnetic particle networks which is corresponding to a released amount of 19%. The re-alignment of the magnetic nanoparticles, (or nano-magnets) within the ferrosponges has little effect on blocking drug diffusion from those macroporosity. Nevertheless, the drug is highly regulated from mesoporosity of the ferrosponges, as a result of aggregation of those nano-magnets in the ferrosponges. The diffusion path was highly confined, resulting in a much slower diffusion of the drug molecules from the ferrosponge. A lower value of the rate constants, i.e., k_1 and k_2 , indicating a lower frequency of molecular activity, prevailed in the magnetized ferrosponges than those without magnetization for both stages of release profile provides direct evidence of the magnetically-induced inhibition effect on molecular diffusion.

Table 4.3 k and n values of ferrosponges under the modes of magnetic on (MF on) and off (MF off)

		5G-1F	5G-3F	5G-5F	15G-1F	15G-3F	15G-5F
k1	MF off	0.037	0.033	0.027	0.020	0.018	0.019
	MF on	0.030	0.020	0.010	0.014	0.012	0.011
k2	MF off	0.066	0.055	0.050	0.036	0.023	0.023
	MF on	0.057	0.053	0.046	0.032	0.019	0.019
n1	MF off	0.460	0.475	0.491	0.548	0.563	0.577
	MF on	0.470	0.527	0.615	0.618	0.595	0.590
n2	MF off	0.341	0.362	0.360	0.423	0.506	0.516
	MF on	0.334	0.314	0.284	0.377	0.483	0.497

The mechanism of drug release profiles from the ferrosponges can then be elucidated as schematically illustrated in Fig. 4.13-(d). The walls between the macropores in the magnetic particle network of the ferrosponge possess large amounts of mesopores, in which drug release is solely dominated by molecular

diffusion through the mesopores to environment. By magnetizing the iron oxide nanoparticles in the walls, the mesopore size decreased considerably, which restricted more effectively the diffusion of the drug molecules. Consequently, the drug release rates decreased immediately while applying an external magnetic field.

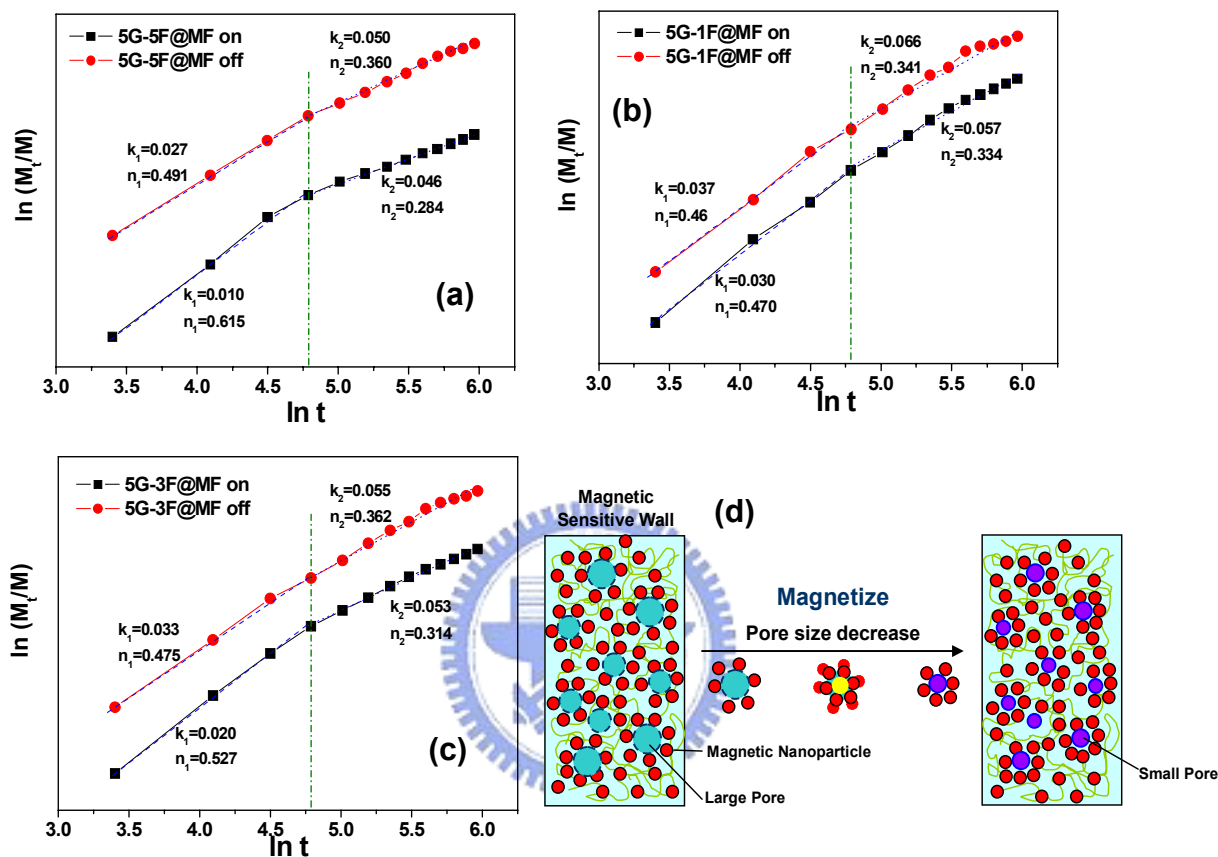


Fig. 4.13 A plot of $\ln(M_t/M)$ versus $\ln(t)$ of (a)5G-5F, (b)5G-1F and (c)5G-3F showed a two-step relationship for calculating the values of k and n , and the corresponding schematic drawing of the shrinkage of the mesopores in the ferrosponges (d) while a magnetic field was applying

4.3.8 Magnetic-sensitive behavior of ferrosponges

The preliminary result demonstrated that the ferrosponges possessed magnetic-sensitive behaviors under an MF. The “Magnetic Sensitive Behavior (%)” was defined as the difference in the amount of cumulative drug release under “MF off” minus that under “MF on”. The higher value of the “Behavior” indicates the higher sensitivity of the ferrosponge to a given strength of magnetic field in terms of drug

release. Fig. 4.14 shows the magnetic-sensitive behaviors for the ferrosponges of 5G and 15G compositions. The magnetic-sensitive behavior showed about 4-5 times more pronounced for the 5G compositions than that for the 15G series. It is possible that ferrosponge with 5G compositions possess a better elastic property and at the same time, a stronger interparticle attraction to regulate the relaxation of the gelatin molecules than those of 15G compositions, resulting in the sharply enhanced magnetic-sensitive behaviors. More plausibly, according to a recent study on the concentration effect of the nano-magnets on magnetization of a PVA-based ferrogels [Liu, 2006], it is believed that under the same relative concentration of the nano-magnets, the ferrosponges with higher relative concentration of the gelatin showed lower magnetization, and is evidenced in Fig. 4.15, where the saturation magnetization is increased linearly with increasing nano-magnet concentration and decreased with increasing gelatin concentration. On this base, it realizes that the nano-magnet concentration in the ferrosponges causes a significant variation in magnetic-sensitive behavior. Fig. 4.15 further supports a stronger interparticle attraction force and less rigidity (i.e., the molecular relaxation of the gelatin chains being less restricted) of the 5G ferrosponges. Furthermore, although 5G-1F and 15G-3F possessed the same gelatin-to- Fe_3O_4 ratio (i.e., $G/F=3/1$), 5G-1F exhibited more than twice the magnetic sensitive behaviors to that of the 15G-5F composition, because in 5G-1F, the magnetic nanoparticles binding on the looser polymer structure could be migrated easily.

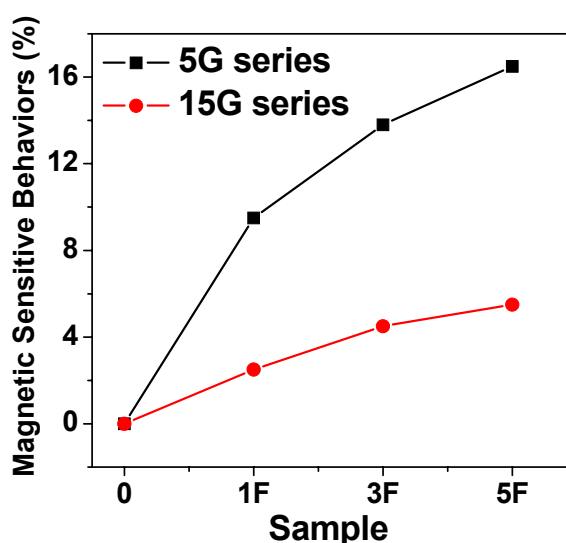


Fig. 4.14 Comparison of the magnetic-sensitive behaviors of the ferrosponges for both 5G and 15G series compositions

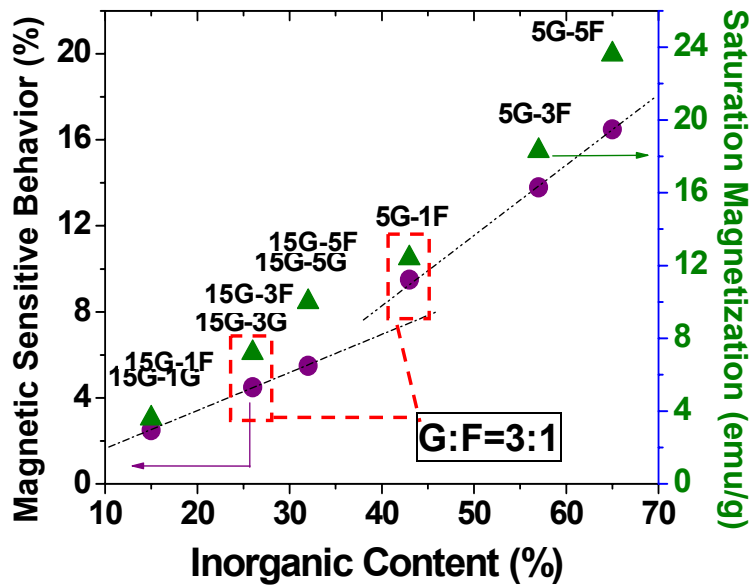


Fig. 4.15 Inorganic/organic ratios of ferrosponges related to the magnetic sensitive behaviors (%) and saturation magnetization (Ms)

Upon a consecutive on-off operation of the magnetic field to the ferrosponges, an alternative change in drug release can be identified, as shown in Fig. 4.16. The cumulative drug-release amount decreased with applied magnetic field and increased again while the MF was turned off. This tunable release rate further substantiates the re-arrangement of the magnetic nanoparticles and this further indicates a potential use of this novel ferrosponges for drug delivery applications. With increasing concentration of the nano-magnets, i.e., from 1F to 5F composition, the ability for the ferrosponges to reaching a considerable drug release rate is increased significantly when the ferrosponges to reach a consecutive MF on-off operation. This suggests that the ferrosponges gain sufficient elasticity with the incorporation of critical amount of the nano-magnets, which can be elucidated in the ferrosponge with 5G-5F composition. This also indicates a considerable improvement of the anti-fatigue property of the ferrosponges, compared to neat gelatin matrix, further encouraging the use of the ferrosponges for drug delivery application.

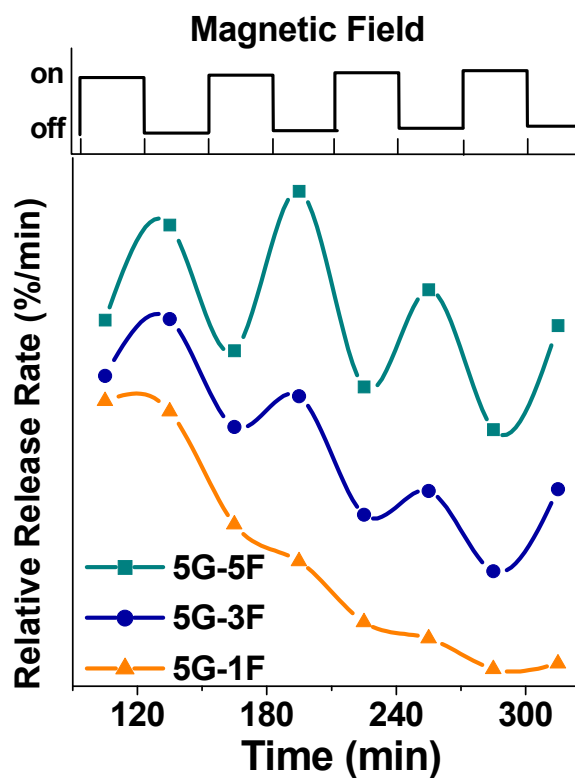


Fig. 4.16 Relative drug release rates of the ferrosponges under repeated on-off MF operations, showing a fast degradation in the release rate with less MNP concentration, but much improved release behavior with respect to cyclic operation when MNP is increased and seems to be optimized in 5G-5F composition, i.e., indicating an improved anti-fatigue property

Chapter 5

Non-Biodegradable Ferrogel (PVA): Effect of particle size and switching duration time

5.1 Introduction

Stimuli-response polymers represent one class of actuators that have the unique ability to change swelling behaviors, permeability and elasticity in a reversible manner. Owing to these useful properties, stimuli-response polymers have numerous applications, particularly in medicine, pharmaceuticals, drug-delivery, biosensors, enzyme and cell immobilization [Qiu, 2001; Miyata, 2002]. More recently, increasing interest has been devoted to the exploration of dual-responsive polymers, such as pH/thermo [Kim, 2002], thermal/magnetic [Furukawa, 2003; Deng, 2003; Pich, 2004], pH/ electric field [Fernandes, 2003], pH/magnetic [Chatterjee, 1999] sensitive hydrogels, which exhibit considerable sensitivity to external stimuli and can be used in extended fields.

Many kinds of such gels have been developed and studied with regard to their applications to several biomedical and industrial fields such as controlled drug delivery systems and muscle-like soft linear actuators. Saslawski et al. reported the gelatin microsphere that was cross-linked by polyethylenimine for the pulsed delivery of insulin by oscillating magnetic field [Saslawski, 1988]. The release rate of insulin from the alginate sphere with strontium ferrite microparticles (1 μm) dispersed can be much enhanced compared with that in the absence of magnetic field. Zrínyi et al. reported that the magnetically-sensitive hydrogels can undergo quick, controllable changes in shape by introducing magnetic particles into the chemically cross-linked PVA that can be used as a new type of actuator to mimic muscular contraction [Mitsumata, 1999; Zrínyi, 1998 & 2000]. Furthermore, the magnetic-sensitive gels, or "ferrogels", are typical representative of smart materials for mechanical actuators and have been the subjects of many studies in recent years [Hernández, 2004; Chatterlee, 2003].

Recently, it was reported that the polyelectrolyte microcapsules embedded with Co/Au nanoparticles could increase its permeability to macromolecules like

FITC-labeled dextran by alternating current (AC) magnetic switch [Lu, 2005]. However, the iron oxide nanoparticles have received wider attentions in diagnostic clinical practice as magnetic resonance imaging enhancers and currently in clinical phase IV, are the most successful application of nanotechnologies in medicine [Weissleder, 1995; Brigger, 2002]. So far, to our best knowledge, little investigation has been addressed on controlled delivery of therapeutic drugs under direct current (DC) magnetic field through the controlled deformation of the ferrogel based on iron oxide nanoparticles upon a simple “on” and “off” switch mode.

Furthermore, this magnetic-sensitive polymer is even superior to that traditional stimuli response polymer, such as pH or thermal sensitive polymer, because magnetic stimulation is an action-at-distance force (non-contact force) which is easier to adapting to biomedical devices. PVA hydrogel was used because it displays amphoteric characteristics and can be applied in aqueous environment as well as in organic solvent for the encapsulation of amphoteric drugs [Hatakeyema, 2005]. Moreover, PVA can be used as dispersing agents to uniformly disperse the Fe₃O₄ particles. In this study, we reported a magnetic-field-sensitive PVA-based ferrogel that can be used for controlled release of therapeutic drug by external magnetic stimulation. The responsivity and characteristics of the PVA-based ferrogel are systematically investigated in terms of iron oxide particles and swelling behaviors. Furthermore, a mechanism of drug release via the on-off operation is also proposed.

5.2 Ferrogel preparation

The intermolecular interactions like hydrogen bond-bridges or polymer microcrystals are responsible for the formation of the three-dimensional network structure. A so-called freezing-thawing technique was used to prepare the ferrogel [Hatakeyema, 2005]. First, 5wt% polyvinyl alcohol (PVA, Fluka, M.W.: 72,000, degree of hydrolysis: 97.5-99.5 mol%) was dissolved in 10 ml dimethylsulfoxide (DMSO) at 80°C under stirring for 6 h, and then mixed with 17 wt% of magnetic particles at 60°C under ultrasonication for 6 h to ensure that the magnetic particles can be well dispersed. Three kinds of magnetic particles were used in this study: (1) larger magnetic particle (LM), diameter ca. 150-500 nm, Aldrich; (2) middle magnetic particle

(MM), diameter ca. 40-60 nm, Alfa Aesar; (3) smaller magnetic particle (SM), diameter ca. 5-10 nm, fabricated by *in-situ* co-precipitation process [Mak, 2005]. The resulting solution was then poured into plastic dish and kept frozen at -20°C for 16 h. Subsequently, the gels were thawed at 25 °C for 5 h. This cyclic process including freezing and thawing was repeated for 5 times. Finally, prior to the release test, the ferrogels were washed five times and then immersed in the water for 24hr to completely remove DMSO. The physical gels prepared by this method were stored at 4°C until they were measured. The swelling ratio of the ferrogel [Yang, 2003] is defined as:

$$\text{Swelling Ratio (SR) S\%} = \frac{W_t - W_{\text{dry}}}{W_{\text{dry}}} \quad (5.1)$$

where W_{dry} and W_t are the weight of the dry ferrogel and the ferrogel at time t under magnetic-field (MF, 400 Oe) switching, respectively. The free liquid on the surface of the swollen ferrogel was padded dry with filter papers before weighing.

5.3 Phisycal crosslinking (freezing and thawing process) of ferrogel

The PVA ferrogel was fabricated by phisycal crosslinking method (freezing and thawing process) due to the hydroxyl groups of PVA molecules participated in hydrogen bonding. As show in Fig. 2.10, the number of crosslinking points and the cell walls of PVA hydrogels increases and become thicker with increasing freezing and thawing cycles. An in-situ experiemnt observed by DSC was used to evaluate the PVA crosslinking condition with freezing and thawing cycles. DSC measurement is based on the fabrication process of ferrogel. The control parameter in the DSC is (1) cooling from 25°C to -20°C (cooling rate: 1°C/min from); (2) kept frozen at -20°C for 16 hr; (3) heating -20°C to 25°C (heating rate: 1°C/min); (4) kept thawed at 25 °C for 5 h. This cyclic process including freezing and thawing was repeated for 6 times. The result in Fig.5.1(a) & (b) show that crystal point (T_c) of PVA increased with the cycles of freezing and thawing increased (-5.3~1.1°C, cycle 1~6, c1~c6), indicated that the the number of crosslinking points increased to induce a solid network. Furthermore, the area of crystallization (peak area) increased with the cycles increase. It also demonstrated that the higher crystallization of PVA and the strongrt network would be found in the higher cycles of freezing and thawing process, but it seems to be

“saturation” when the cycles arrives 5-6 times, implying just slightly T_c and area of crystallization increase (PVA crystallization and crosslinking have been stable) Therefore, five times of the freezing and thawing process would be used in this study.

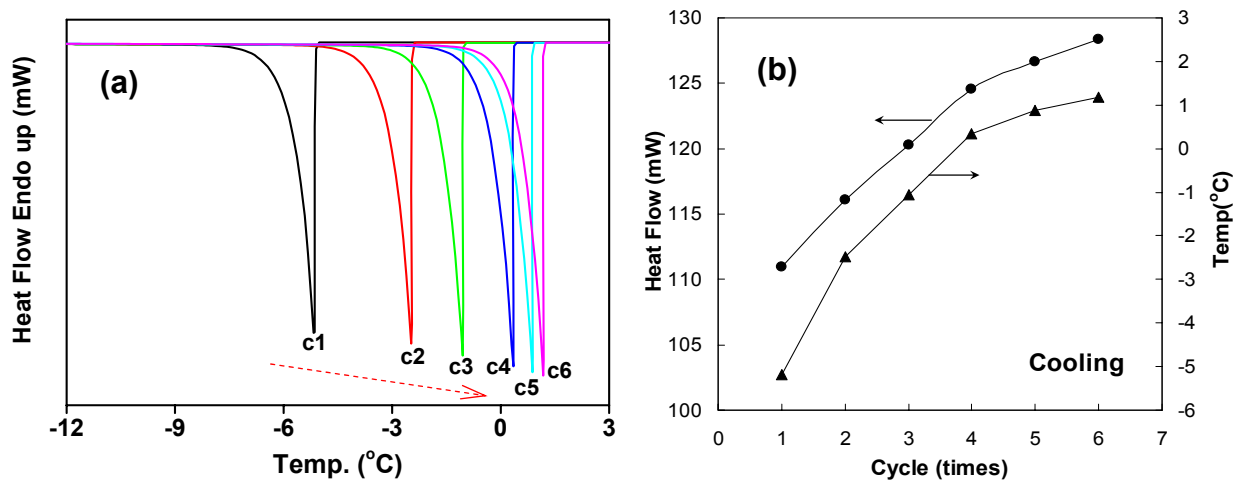


Fig. 5.1 DSC analysis of PVA physical crosslinking by freezing and thawing cycles: (a) cooling curve; (b) heat flow and temperature change with different cycles

5.4 Characterization of magnetic-sensitive ferrogels

Fig. 5.2-(a) illustrates the photographs of magnetic-sensitive PVA-based (PVA5-LM17) ferrogels, where PVA5-LM17 represents the synthesis of the ferrogels with PVA concentration of 5 wt% and larger-sized magnetic particles (LM) of 17 wt% in this work. Moreover, it is observed that the magnetic-sensitive hydrogel exhibits excellent flexibility and elasticity. Furthermore, it was observed that the Fe_3O_4 nanoparticles were uniformly distributed in the PVA ferrogels as shown in cross-sectional SEM image as no magnetic field was applied. However, as the magnetic field (MF) was developed, a volume change in response to the on-off magnetization was observed for the PVA ferrogel. This phenomenon seems to reveal that the magnetic Fe_3O_4 nanoparticles are attracted between adjacent neighbors under magnetic field. Consequently, it implies that the reduced distance between the magnetic Fe_3O_4 nanoparticles as a result of attraction force induced by a given MF can be used to develop a close configuration of the ferrogel for controlled drug release.

The swelling ratio of the ferrogel is decreased (from 3.81 to 3.33) while MF is

switching “on” which is due to its contracting pores, but it is increased (from 3.33 to 3.72) while MF was turned off as shown in Fig 5.2-(b). Hence, the decreased swelling ratio of the ferrogel in an MF switching “on” mode may be used to explain the slow diffusion of drug. Furthermore, the calculated swelling rate is also shown in Fig 5.2-(b). A transition of the swelling rate was clearly observed in response to the on-off magnetization. While MF switching from “off” to “on” mode, the swelling rate decreased, on the contrary, it increased. The magnetically sensitive swelling behaviors indicated that the ferrogel prepared in this investigation has an excellent magnetic-sensitive property.

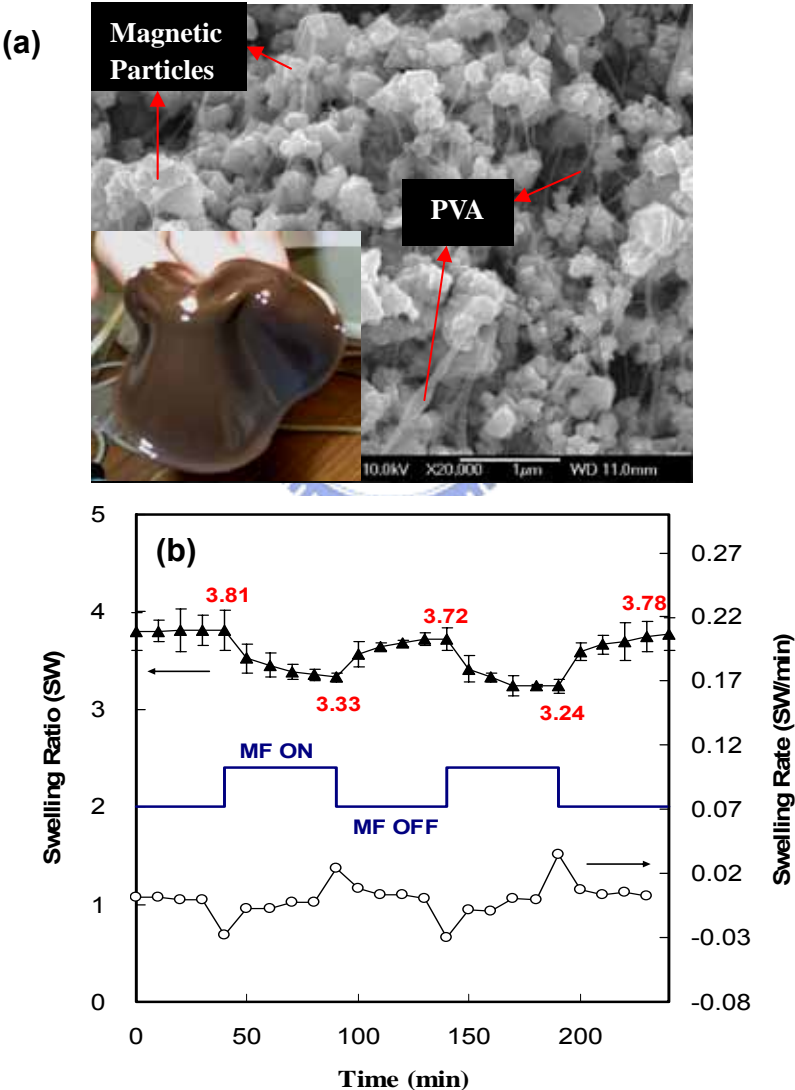


Fig. 5.2 (a) Cross-sectional SEM image of magnetic particles disperse in PVA hydrogels and OM photos of PVA5-LM17 ferrogels; (b) Swelling ratio and swelling rate of PVA5-LM17 ferrogel in the magnetic fields switching “on”-“off” mode

Table 5.1 Permeability coefficient of the ferrogels in “on” or “off” mode of a given magnetic field

Ferrogel	SDT ^a	MF ON ^b	MF OFF ^d	Magnetic Behaviors ^e	Max. drug Bursting ^f
		drug amount/min (P) ^c	drug amount/min (P) ^c		
PVA5-LM17	20	1.42±0.05 (109)	3.53±0.08 (303)	2.11 (194)	8.39±0.23
	10	0.97±0.03 (83)	5.24±0.15 (449)	4.27 (366)	18.56±0.56
	5	0.46±0.02 (40)	6.71±0.31 (586)	6.25 (546)	11.95±0.43
PVA5-MM17	5	0.92±0.05 (77)	3.10±0.34 (261)	2.18 (184)	3.81±0.13
PVA5-SM17	5	0.86±0.03 (74)	4.73±0.25 (406)	3.86 (332)	5.08±0.18
Pure PVA5	5	1.09±0.03 (107)	1.08±0.08 (105)	-0.01 (-2)	--

^a SDT means switching duration time of the magnetic field.

^b Average drug permeation amount ($\mu\text{g}/\text{min}$) and permeability coefficient ($10^{-6} \text{ cm}^2/\text{min}$) at magnetic fields (MF) switching "on" (n=3)

^c Permeability coefficient (P) calculated by Eq.(2) (n=3)

^d Average drug permeation amount ($\mu\text{g}/\text{min}$) and permeability coefficient ($10^{-6} \text{ cm}^2/\text{min}$) at MF switching "off" (n=3)

^e Average drug permeation amount ($\mu\text{g}/\text{min}$) and permeability coefficient ($10^{-6} \text{ cm}^2/\text{min}$) at MF OFF –^cAverage drug permeation amount ($\mu\text{g}/\text{min}$) and permeability coefficient ($10^{-6} \text{ cm}^2/\text{min}$) at MF ON. (n=3)

^f Average maximum drug bursting amounts ($\mu\text{g}/\text{min}$) of the drug bursting at the moment of switching MF from “on” to “off” mode. (n=3)

The magnetic-sensitive behaviors in the ferrogels can be further expressed by the difference in the permeated drug amount between the MF “off” mode and “on” mode, as shown in Table 5.1. In addition, the calculated permeability coefficient and maximum amount of drug busting were also included. It was observed that the permeability coefficient of the pure PVA5 hydrogel was determined to be $105 \times 10^{-6} \text{ cm}^2/\text{min}$, which is lower than that of PVA5-LM17 ferrogel, i.e., $586 \times 10^{-6} \text{ cm}^2/\text{min}$ while

the MF is “off”. However, when MF switching to “on” mode, the permeability coefficient of the ferrogel decreased sharply ($40 \times 10^{-6} \text{ cm}^2/\text{min}$) but that of the pure PVA hydrogels remains almost unchanged ($107 \times 10^{-6} \text{ cm}^2/\text{min}$). This is essentially due to smaller pore size as a result of agglomeration of the nano-magnetic particles in the ferrogel. Furthermore, in Table 5.1, it is further indicated that the magnetic-sensitive behavior of the ferrogel ($546 \times 10^{-6} \text{ cm}^2/\text{min}$) is much superior to that of the pure PVA gel ($-2 \times 10^{-6} \text{ cm}^2/\text{min}$). Therefore, with an applied magnetic field, considerable differences in magnetic-sensitive permeability coefficient were detected in the ferrogels, as compared to that in pure PVA hydrogel.

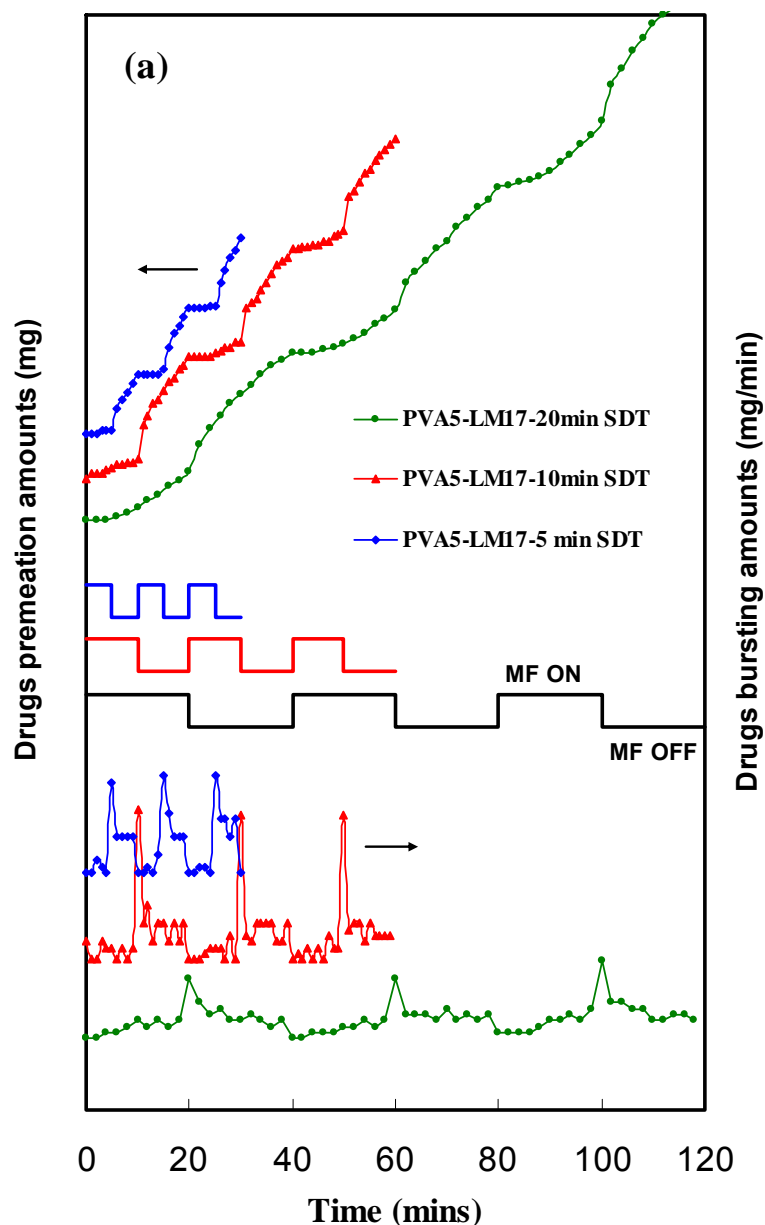
5.5 Effects of switching duration time (SDT)

In Fig. 5.3-(a), it was found that the quantity and the release profile of the model drug from the ferrogels are strongly affected by the time duration between each on-to-off stage, and here we defined it as switching duration time (SDT) of the magnetic field. For a 5-min-period SDT, the drug release profiles demonstrate that the best “close” configuration, wherein the drug was effectively locked in the ferrogel and no sign of drug release can be detected for the SDT of 5-minute period.

However, with increasing SDT to 10 and 20 minutes, the “close” configuration of the ferrogel becomes less pronounced as time elapsed, wherein sign of drug release, can be clearly detected, as illustrated in Fig. 5.3-(a) and Table 5.1. In the case of 20-min SDT, an effective “close” configuration of the ferrogel that can effectively stop drug release can be kept up for 8-10 minutes; however, drug released, although in a relatively slow rate, from the ferrogel after the “effective” time period. Such an effective SDT can be repetitively observed without considerably changed for a number of repetitive on-off operations. Furthermore, irrespective of the SDT, a normal diffusion release profile can be detected right after the given MF switching from “on” to “off”.

Since the “close” configuration of the ferrogel is an indication of particle agglomeration of the magnetic particles within the PVA matrix, on this base, a considerable reduction of the pore size and an increased tortuosity of the pore channels across the ferrogel membrane can be expected. Both factors will effectively hinder or block the diffusion of the drug solution from the other side (i.e.,

drug-containing donor side) of the ferrogel. The effective SDT of the ferrogels prepared in this study suggests an existing of an effective “closure” configuration of the ferrogel which seems to compromise with the diffusion potential of the drug solution from one compartment to the other. It is believed that such an effective “close” configuration may be explained as a result of “fatigue” of the agglomerated magnetic particles under a given MF. The fatigue behavior can be possibly due to the relaxation of the polymer gel to relieve the stress that is induced by strain in the gel network when the magnetic particles move in response to the magnetic field. This process may be faster in the presence of smaller particles, which provides explanation on the rapid increase of permeability compared to the ferrogels with larger particle.



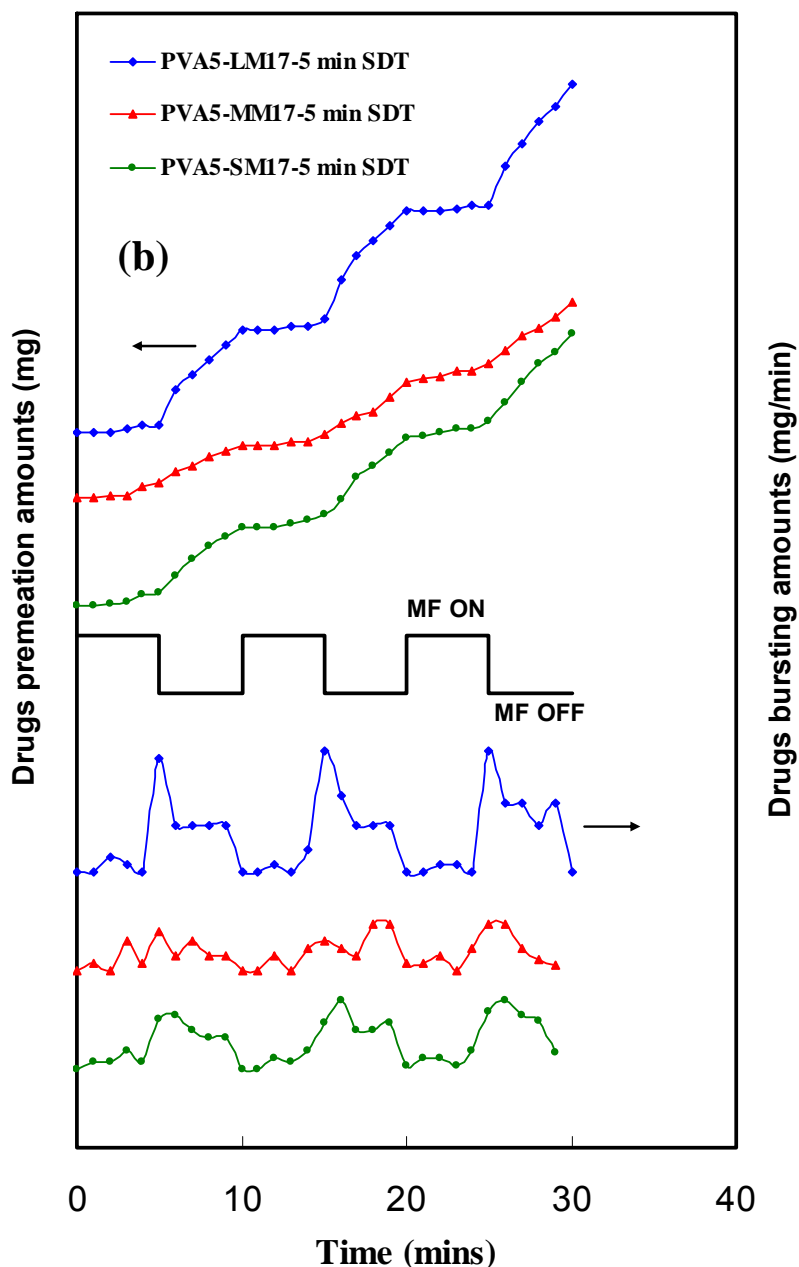


Fig. 5.3 Rapid permeation properties and “close” configuration of the ferrogels dependent on (a) different switching duration time (SDT) and (b) various particle size of Fe_3O_4 of the ferrogels in the continuous switching “on-off” mode for a given magnetic fields; the drug permeation amount on switching “on-off” mode, and corresponding differential curve are shown in each figure in order to show the maximum drug bursting

5.6 Effects of Fe₃O₄ particle size

The influence of Fe₃O₄ particle size on the effective “close” configuration is illustrated in Fig. 5.3-(b) and Table 5.1, where larger particles (LM) show effectively longer SDT. The results show the average permeability coefficient ($40 \times 10^{-6} \text{ cm}^2/\text{min}$) of PVA5-LM17 ferrogel at MF switching “on” in 5-min-SDT is much lower than that (77×10^{-6} and $74 \times 10^{-6} \text{ cm}^2/\text{min}$) of PVA5-MM17 and PVA5-SM17 ferrogels. Moreover, the magnetic-sensitive behavior and average maximum drug bursting amount of the PVA5-LM17 ferrogel is much better than those of the PVA5-MM17 and PVA5-SM17 ferrogels.

In another comparative investigation, the effect of particle size on the magnetization using a vibrating sample magnetometer (VSM, Toei VSM-5, USA) is demonstrated in Fig. 5.4. Ferrogels with larger Fe₃O₄ particle (PVA5-LM17) encapsulated ferrogel displays a hysteresis loop with a larger saturation magnetization (Ms) of 15.28 emu/g, compared to those ferrogels with middle and smaller Fe₃O₄ nanoparticles (12.39 emu/g for PVA5-MM17 and 10.84 emu/g for PVA5-SM17), indicating that a strong magnetic field can be induced in the ferrogel. However, the PVA5-MM17 ferrogel presents broader hysteresis loop and larger coercive force (Hc) than that of PVA5-LM17 (and PVA5-SM17 ferrogels), indicating that it is more difficult to reorient and move the magnetic particles in the ferrogel under magnetic fields. It is known that the hysteresis loss area and Hc are strongly dependent on the particle size and domain characteristics of magnetic particles. The PVA5-MM17 shows larger Hc because its particle size (60 nm) is near the critical size of single domain which was estimated about 100 nm for Fe₃O₄ particle [Klabunde, 2001]. Therefore, on this basis, the single-domain MM particles exhibit a greater hysteresis loss area and Hc (353.53 Oe) than the multi-domain LM particles (Hc: 159.63 Oe) in a given magnetic field; hence, the magnetic-sensitive behavior and “close” configuration of PVA5-LM17 ferrogel are superior to those of PVA5-MM17 ferrogel, as shown in Fig. 5.3-(b) and Table 5.1. On the other hand, although the SM particles display a super-paramagnetic behavior with the lowest hysteresis loss area and Hc (17.55 Oe), the Ms of PVA5-SM17 is lower than that of PVA5-LM17 and the fine nanoparticles tend to aggregate together; hence, the observed

magnetic-sensitive behavior and “close” configuration of PVA5-SM17 ferrogel are still less pronounced than that in the PVA5-LM17 ferrogel. The “magnetic-sensitive effects” in those ferrogels are in the order of PVA5-LM17> PVA5-SM17> PVA5-MM17 that is dependent on higher M_s and lower H_c , as illustrated in Fig. 5.3-(b) and Table 5.1. If the above argument is true, then, we believe that an “effective SDT” of the ferrogels from short duration period to long duration period can be well-designed with different drug release profiles.

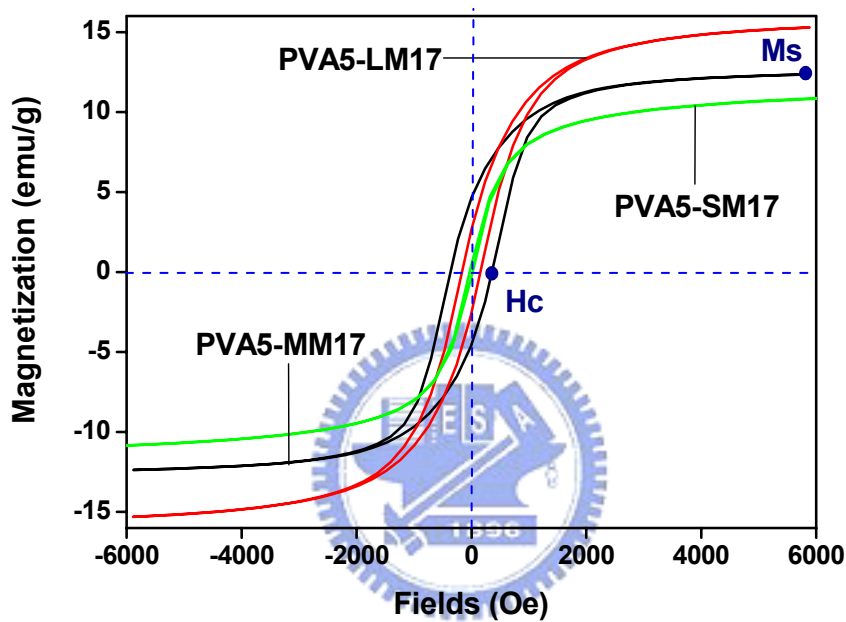


Fig. 5.4 Hysteresis loop analysis of the ferrogels incorporated with various particle sizes of Fe_3O_4

5.7 Mechanism of magnetic-sensitive drug release behavior

The possible mechanism of the drug release profile from the ferrogel is schematically illustrated in Fig. 5.5. In the beginning when there is no magnetic force (MF), the magnetic (fields) moments existing in the ferrogel are randomly oriented. The ferrogel is subjected to zero magnetization and the drug release profile displays a normal diffusion mode. While applying MF, the magnetic moments of the particles tend to align with the magnetic fields and produce a bulk magnetic moment. This induces the Fe_3O_4 particles within the ferrogel to aggregate together instantly, leading to a rapid decrease in the porosity of the ferrogel, where the ferrogel was

characterized as a “close” configuration. In other words, while the imposed field induces magnetic dipoles, mutual particle interactions occur if the particles are so closely packed that the local field can influence their neighbors. The particles attract with each other when aligned in an end-to-end configuration and thus a “pearl-chain structure” was developed [Zrínyi, 2000] due to the attractive forces that reduced the pore size of the ferrogel. Therefore, the drugs are restrictedly confined in the network of the ferrogel, causing a rapid and significant reduction in the diffusion of the drug through the ferrogel.

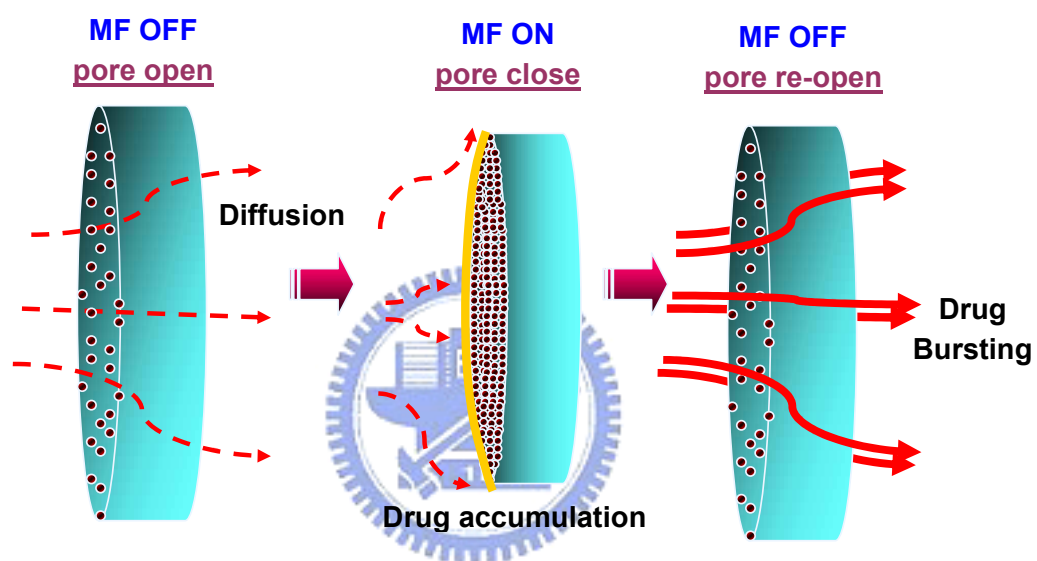


Fig. 5.5 Mechanism of “close” configuration of the ferrogels due to the aggregation of Fe_3O_4 nanoparticles under “on” magnetic fields causes the porosity of the ferrogels to decrease

While turning off the field, the pores in the membrane re-open instantly, which correspondingly results in a rapid re-filling of the drug-containing solution into the membrane from the donor side of the membrane and from the other side of the membrane, drug solution as both residual amount and later re-filled was released instantly at the moment of pore re-opening, resulting in a burst-like profile; however, the release turned back to normal diffusion profile shortly after the burst. A similar behavior is observed on polyethylenimine cross-linked alginate spheres under oscillating magnetic field [Saslawski, 1988]. By comparing with the three SDTs in PVA5-LM17 ferrogel, a maximum amount of the drug bursting ($18.56 \mu\text{g}/\text{min}$) from the

PVA5-LM17 ferrogel was observed for the SDT of 10 minutes. That is why the PVA5-LM17 ferrogel in 10-min-SDT displays more suitable switching duration time and close configuration compared to that in 5-min-SDT and 20-min-SDT, respectively.

In short, current preliminary investigation suggests a controlled release model together with a pre-determined released amount of the drug can be finely tuned through the use of this type of ferrogel, either as membrane or bulk structural configuration, via internally or externally magnetically triggered operations. By repeating the “on-off” operation of a given magnetic field, a controllable re-filling and a subsequent release of drug from the ferrogel can be programmably designed and a further detailed investigation on the effect of particle size and microstructural variation of the ferrogels on the drug release profile is underway and will be reported shortly.

5.8 Particle size effect in the AC magnetic field (HFMF)

By the way, the drug delivery behavior on the particle size effect of magnetic nanoparticle of ferrogel by the AC magnetic field was investigated in the Fig. 5.6. The model drug (vitamin B₁₂) was loading inside the PVA ferrogel. The result shows PVA5-MM17 ferrogel display the strongest magnetic-sensitive behavior for drug release (hyperthermia effect) in the AC magnetic field because H_c of PVA5-MM17 is the highest. The temperature arises 70°C (from 20 to 90°C), 50°C (20 to 70°C), and 20°C (20 to 40°C) in the PVA5-MM17, PVA-LM17, and PVA5-SM17 ferrogel, respectively. In contrast, PVA5-SM17 ferrogel displays lower hyperthermia effect due to its superparamagnetic behavior (lower H_c). In addition, the stronger hyperthermia effect would induce the higher drug bursting, which is attributed to the vibration of magnetic particle to enlarge the pore size of PVA ferrogel. Thus, PVA5-MM17 ferrogel would exhibit the highest drug bursting, whereas the PVA5-SM17 is lowest, which is in order: PVA5-MM17 (40-60 nm)>PVA5-LM17 (150-500nm)>PVA-SM17 (5-10nm), as related to the area of hysteresis curve in the Fig. 5.4. However, the phenomenon is totally different from the magnetic-sensitive behavior in the DC magnetic field, which is in order: PVA5-LM17>PVA5-SM17>PVA5-MM17. Therefore, H_c and M_s in the ferrogel would play an important role to judge the magnetic response behavior in the different magnetic field (DC and AC magnetic field)

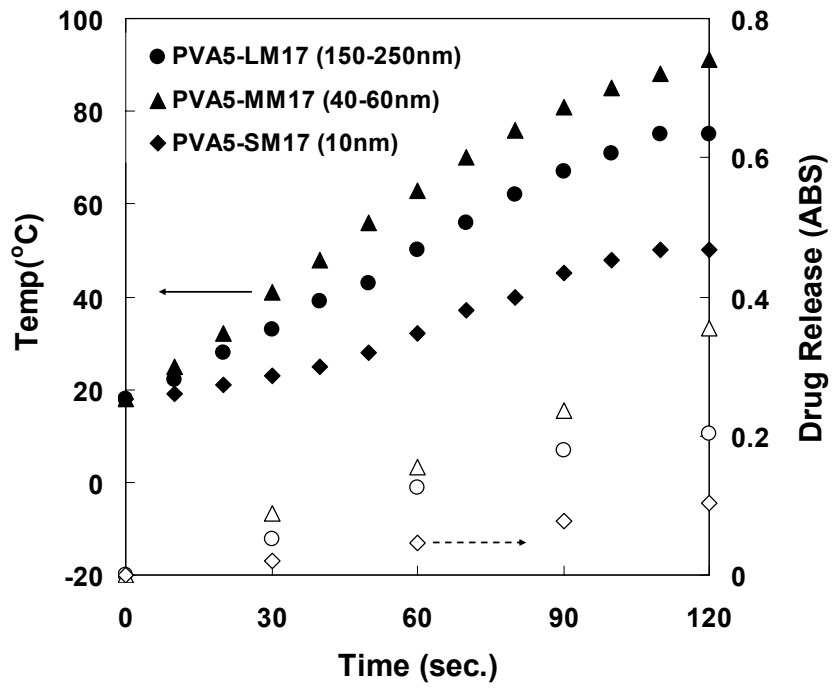
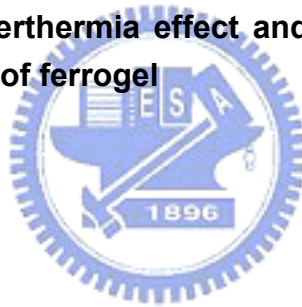


Fig. 5.6 Comparison of hyperthermia effect and drug release behavior in the various particle size of ferrogel



Chapter 6

Non-Biodegradable Ferrogel (PVA): Effect of Fe₃O₄ and PVA

6.1 Introduction

Certain polymer gels represent one class of actuators that have the unique ability to change elastic and swelling properties in a reversible manner. Volumetric phase transition in response to an infinitesimal change of external stimuli, such as pH, temperature, electric and magnetic field (MF) in various hydrogels has been observed [Xulu, 2000; Kim, 2002; Deng, 2003; Csetneki, 2006; Fernandes, 2003; Kim, 1999; Haraguchi, 2002; Mohr, 2006; Muniz, 2001; Park, 1998]. In order to accelerate the response of an adaptive hydrogel to stimuli, a magnetic-sensitive hydrogel (ferrogel) has been developed. A ferrogel is a physical (or chemical) cross-linked polymer network containing magnetic particles. Magnetic-field sensitive gels are unique materials in that they are mechanically soft and highly elastic and at the same time they exhibit a strong magnetic response.

The principle of shape deformation and motility of ferrogels in response to drug release is based on their unique magnetic-elastic behavior. Gel motions are driven and controlled by MF and the final shape is determined by a balance of magnetic and elastic interaction [Szabó, 2000]. Recently, some magnetic-stimuli in response to drug delivery have been applied in clinical therapy. For example, the polyelectrolyte microcapsules embedded with Co/Au nanoparticles could increase its permeability (P) to macromolecules like FITC-labeled dextran by alternating current (AC) magnetic switch [Lu, 2005]. Saslawski et al. reported the gelatin microsphere that was cross-linked by polyethylenimine for the pulsed delivery of insulin by oscillating MF [Saslawski, 1988]. However, little investigation has been reported on controlled permeation of drugs under the direct current (DC) MF through the controlled deformation of ferrogels upon a simple “on” and “off” switch mode. In our previous work, the bursting and magnetic-sensitive behaviors of PVA-based ferrogels were investigated with various particle sizes of Fe₃O₄ and switching duration time of magnetic fields [Liu, 2006]. From our previous experimental observation, it was found

that permeation rate of Vitamin B₁₂, as a model molecule, decreased with the increased intensity of direct current (DC) magnetic field. This induces the Fe₃O₄ particles within the ferrogel to aggregate together instantly, leading to a rapid decrease in the porosity of the ferrogel, where the ferrogel was characterized as a “closure” configuration [Liu, 2006], as shown in Fig. 6.1

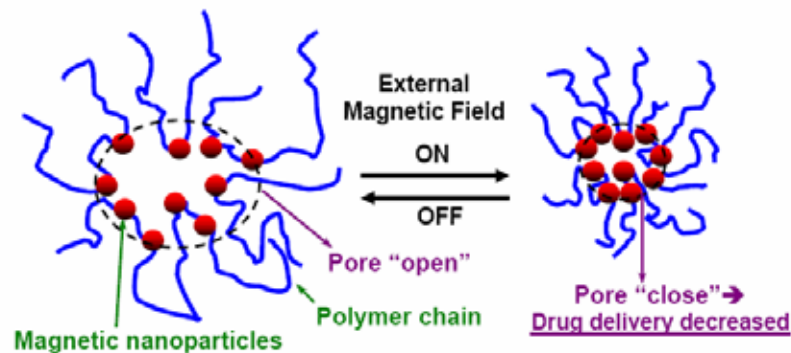


Fig. 6.1 Diagram of the mechanism of “closure” configuration of ferrogels

In other words, while the imposed field induces magnetic dipoles, mutual particle interactions occur if the particles are so closely packed that the local field can influence their neighbors. The particles attract with each other when aligned in an end-to-end configuration and thus a “pearl-chain structure” was developed (see Fig. 6.2) [Zrínyi, 2000] due to the attractive forces that reduced the pore size of the ferrogel. From the optical microscopic (OM) images, it was revealed that a simulated test that 1 w/v% magnetic particles were randomly distributed in the 10 w/v% PVA solution (dissolved in the DMSO at 80°C beforehand) in the absence of MF. However, the magnetic particles attract with each other to line up in an order form in the present of MF, as observed by SEM in Fig. 6.3.

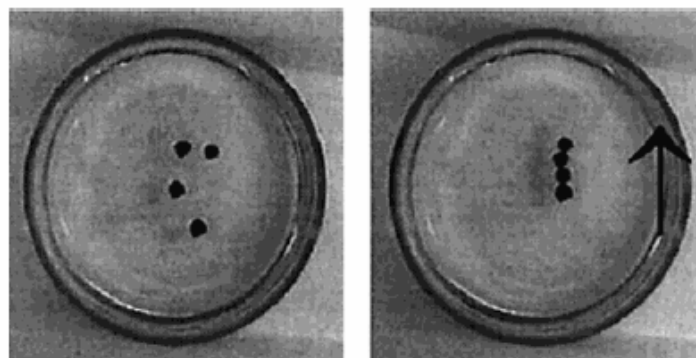


Fig. 6.2 Pearl-chain structure was developed with the magnetic field

Therefore, the drugs are restrictedly confined in the network of the ferrogels, causing a rapid and significant reduction in the diffusion of the drug from the ferrogel, due to the attractive forces that reduced the pore size of the ferrogel. While turning off the field, the pores in the ferrogel re-open instantly, the drug release turned back to normal diffusion profile.

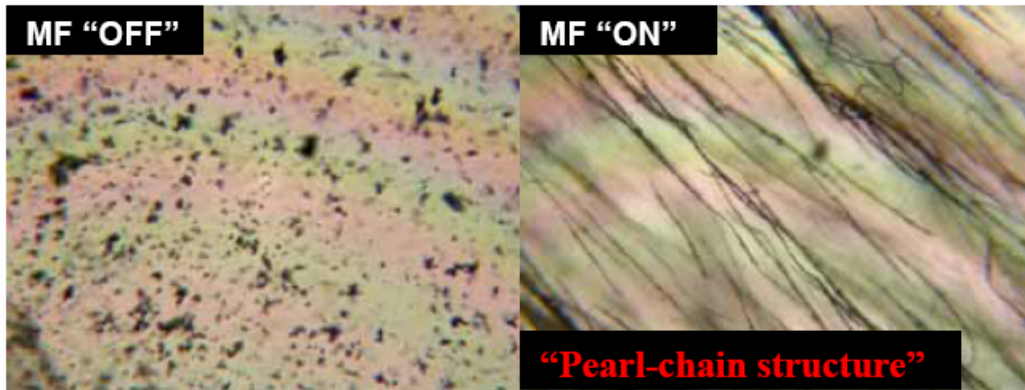


Fig. 6.3 SEM image of pearl-chain structure

The above-mentioned phenomenon indicates that the optimal magnetic-sensitive behavior of the ferrogel was not only dependent on the particle size of Fe_3O_4 but also on the constituting components, i.e., Fe_3O_4 and PVA. Therefore, the influence of the respective constituting components of the ferrogels on magnetic-sensitive behavior and partition coefficient (H) will be systematically investigated in this work. These magnetic-sensitive behaviors will be further correlated with theoretical calculation of both space restriction and magnetization. According to the proposed model, an optimal scenario from both experimental findings and calculations would be deduced to fabricate a ferrogel with controlled smart configuration.

6.2 Ferrogel preparation


A freezing-thawing technique was used to prepare the ferrogel [Hatakeyema, 2005]. In our experience, the physical-cross-linked ferrogel by a freezing-thawing technique was used in the present study because it presents more elastic and soft properties than that fabricated by chemical-cross-linking. First, various weight/volume (w/v)% of polyvinyl alcohol (PVA, Fluka, M.W.: 72,000, degree of hydrolysis: 97.5-99.5 mol%) was dissolved in 10 ml dimethylsulfoxide (DMSO) at 80°C under stirring for 6 h, and

then mixed with various (w/v)% of magnetic particles at 60°C under ultrasonication for 6 hr to ensure that the magnetic particles (diameter ca. 150-500 nm, Aldrich) can be well dispersed, as shown in Table 6.1. The resulting solution was then poured into plastic dish and kept frozen at -20°C for 16 h. Subsequently, the gels were thawed at 25 °C for 5 hr. This cyclic process including freezing and thawing was repeated for 5 times. Finally, prior to the release test, the ferrogels were washed five times and then immersed in the water for 24hr to completely remove DMSO.

6.3 Role of iron oxide content

According to our pervious study [Liu, 2006], it was found that the larger magnetic particles exhibited better magnetic-sensitive behaviors. Therefore, magnetic particles with size between 150 to 500 nm were employed in the present investigation. Table 6.1 gives a series of resulting average P values of the ferrogels with a number of Fe₃O₄ concentrations at a given amount of PVA concentration.

Table 6.1 Average permeability coefficient (P) of the ferrogels at a given magnetic field



Ferrogels	PVA	Fe ₃ O ₄	P _{ON} ^b	P _{OFF} ^c	P _{OFF-ON} ^d
Pure PVA10	10	--	54±3	54±5	0
PVA10-MP3.75	10	3.75	123±6	172±9	49
PVA10-MP8.5	10	8.5	86±9	170±5	84
PVA10-MP17	10	17	54±9	161±12	107
PVA10-MP25.5	10	25.5	43±11	154±5	111
PVA10-MP34	10	34	31±5	141±7	110
PVA10-MP51	10	51	40±8	131±9	91
PVA10-MP68	10	68	45±6	117±5	72

^a (w/v)% means the weight/volume percentage (weight of PVA or Fe₃O₄ particles / volume of DMSO (v), ex. 1g of PVA and 10 ml of DMSO is 10 (w/v)% of the column of PVA (w/v)%.

^b Average permeability coefficient (10⁻⁶ cm²/min) at magnetic fields switching "on" (MF ON) (n=3)

^c Average permeability coefficient (10⁻⁶ cm²/min) at magnetic fields switching "off" (MF OFF) (n=3)

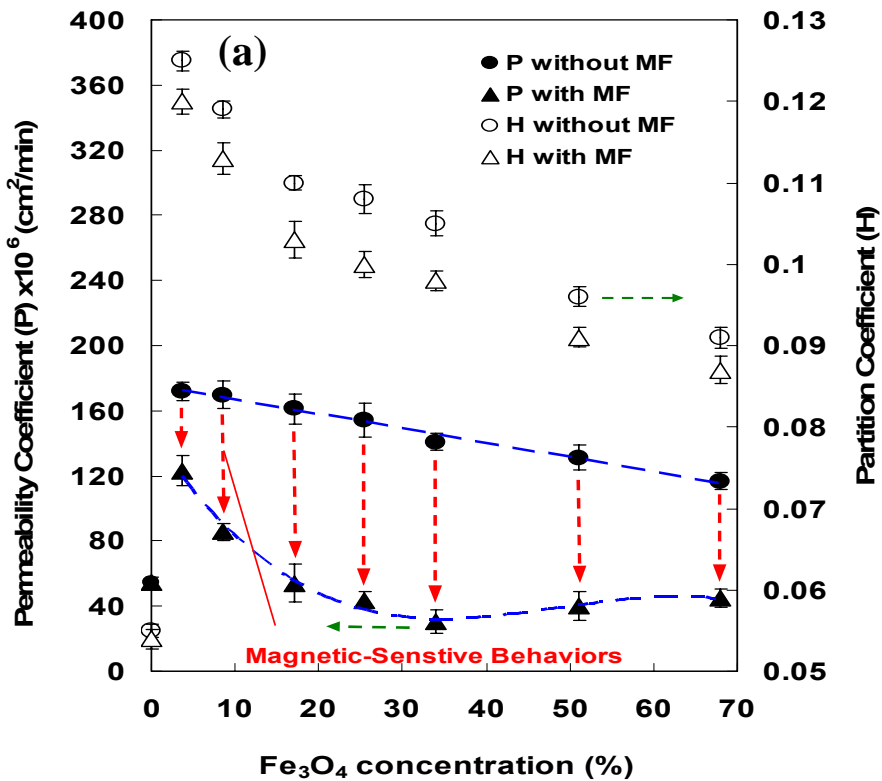
^d Magnetic sensitive behaviors: average permeability coefficient (10⁻⁶ cm²/min) at MF OFF–Average permeability coefficient (10⁻⁶ cm²/min) at MF ON. (n=3)

The influence of Fe_3O_4 concentration is then constructed into Fig.6.4-(a) with respect to a corresponding change of the P value upon on-off operation of the MF. As shown in Fig. 6.4-(a), as the Fe_3O_4 nanoparticles were added into the PVA, the P value was much increased compared to that of pure PVA. It was found that the P value in the ferrogel membrane with only 3.75 w/v% Fe_3O_4 is more than 3 times permeable to vitamin B_{12} than that of pure PVA in the absence of MF. However, with the increase of Fe_3O_4 addition, the P value decreased linearly and slowly with Fe_3O_4 concentration in the absence of magnetic fields (P_{OFF}).

In contrast, the drug permeation in the presence of magnetic fields (P_{ON}) decreased rapidly with Fe_3O_4 up to 34%, then, increased slightly with further increase to 68%. A plethora of Fe_3O_4 (51% and 68%) added in the PVA hydrogel caused a phase separation of PVA to form broken pores; P_{ON} thus increased slightly in the later half. It was believed that there exists a relationship between the P and H value of the drug inside the membrane (see Eq. (3.5), where $P=DH$). As illustrated in Fig. 6.4-(a), when a smaller amount of 3.75 w/v% Fe_3O_4 particles was added into PVA (ex. PVA10-MP3.75), it caused a considerable increase (2.3 times) in the H value (0.125) compared to that (0.055) in the pure PVA hydrogel. It is then suggested that the addition of iron oxide nanoparticles in the membrane may induce higher porosity to promote the ability of drug absorption of the ferrogel. However, it was observed that the H value decreased with increasing Fe_3O_4 contents. Especially in the presence of MF, the decrease in the H value becomes more remarkable compared to that in the absence of MF. The decreased H value in the presence of MF is probably related to the shrunk volume of ferrogels induced by Fe_3O_4 nanoparticles aggregation to further decrease the pore size and porosity. From above-mentioned results, it can be inferred that the magnetic-sensitive behaviors, i.e., the difference in the P value between MF “on” and “off” modes were primarily affected by the change of H and D value, especially D value (for the concentration of 34%, $\Delta P_{\text{OFF-ON}}/P_{\text{OFF}} = 110/141 = 0.78$, whereas $\Delta H_{\text{OFF-ON}}/H_{\text{OFF}} = 0.01/0.11 = 0.09$). The influence of Fe_3O_4 concentration value on the corresponding change of D value is then constructed into Fig.6.4-(b) upon on-off operation of the MF (D_{ON} and D_{OFF}). It could be found that the D curves show similar trend to the P. The D value decreased slightly with Fe_3O_4 concentration

in the D_{ON} , but decreased rapidly with Fe_3O_4 up to 34%, then, increased slightly with further increase to 68% in the D_{OFF} . A plateau of magnetic sensitive behavior ($D_{without MF} - D_{with MF}$) was found in the range of 17 and 34% Fe_3O_4 . It means the drug inner the ferrogel was obstructed more strongly in this range, rather than the others, ex. 8-17% and 34-68%. The vale of D would be used to determine how the interaction between neighboring Fe_3O_4 to hinder the drug diffusion was. Therefore, the diffusion coefficient (D) will play a rather important role to evaluate the behavior of drug inner the ferrogel.

In addition, as shown in a magnetic-sensitive behavior map of Fig. 6.4-(c), it showed an increase with Fe_3O_4 until 17%, indicating the region of increasing sensitivity (Region A). Subsequently, a plateau profile is reached while Fe_3O_4 is lying between 17 and 34%, indicating the magnetic-sensitive behavior reaching a saturation region (Region B). However, the magnetic-sensitive behaviors decreased with further addition of Fe_3O_4 up to 68% (Region C), indicating a decreased sensitivity to a given magnetic stimulation. These results indicated that the best magnetic-sensitive behaviors occur for the 10% PVA-ferrogels with 17-34% Fe_3O_4 concentration. As the P value, the value of D also displayed the similar curves, as shown in Fig. 6.4-(c).



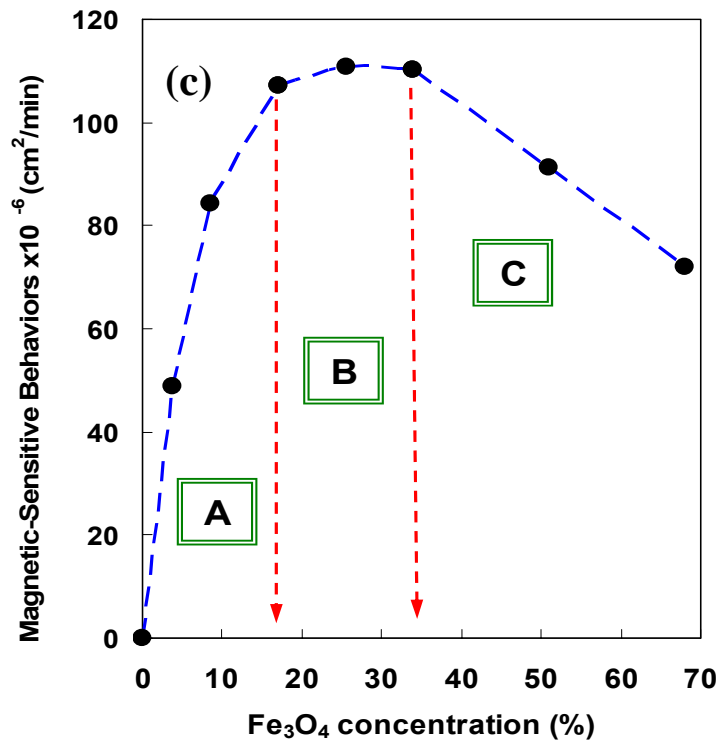
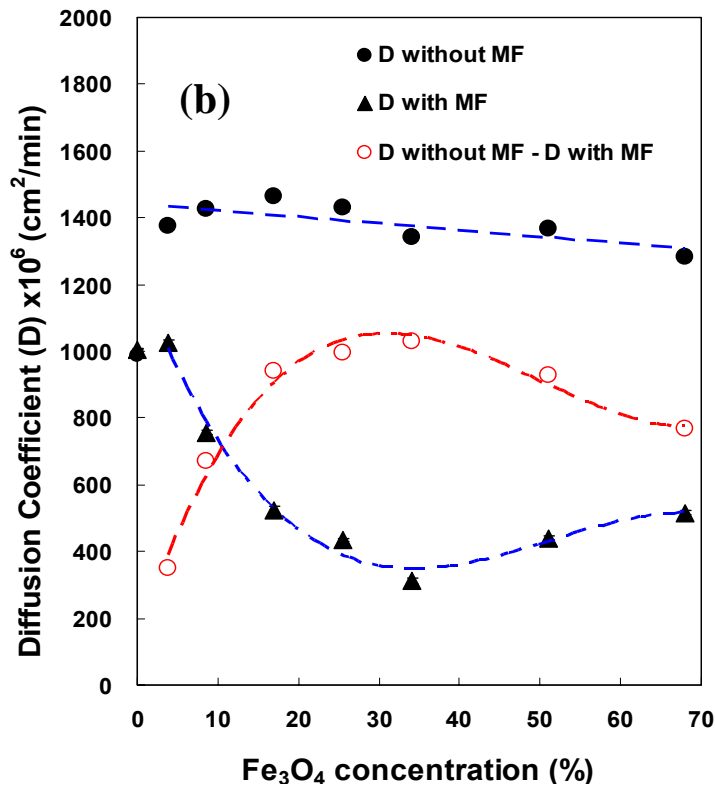


Fig. 6.4 (a) Both permeability coefficient (P) and partition coefficient (H) of ferrogels in “on” or “off” mode of a given magnetic field; (b) Diffusion coefficient (D) of ferrogels in “on” or “off” mode of a given magnetic field.; (c) Magnetic-sensitive behaviors of ferrogels with different Fe_3O_4 concentration; Region A: Region of Increasing “Sensitivity”; Region B: Saturation Region; Region C: Region of Decreasing “Sensitivity”

6.4 Effects of space restriction

The reason for such a dependence of Fe₃O₄ concentration on the evolution of the magnetic-sensitive map may be accountable for as a result of space restriction and magnetization. In Fig. 6.5-(a), where a model with a fixed volume of the unit cell is adapted for schematically illustrating the spatial arrangement of the magnetic particles (presumed to be uniformly distributed) in the ferrogels (namely PVA10-MP17, PVA10-MP34 and PVA10-MP68). Here, the SEM cross-sectional image of the PVA10-MP17, PVA10-MP34, and PVA10-MP68 ferrogels, Fig. 6.5-(b), in corresponding to model in Fig. 6.5-(a) shows that the magnetic particles are well-dispersed in the PVA hydrogel, and it seems to be intertwined with Fe₃O₄ particles. The volume fraction, $V_f(Fe_3O_4)$ of Fe₃O₄ particles in the ferrogel and the number of Fe₃O₄ particles for unit volume of the ferrogel ($No.(Fe_3O_4)$) in the unit cell can be calculated as follows:

$$V_f(Fe_3O_4) = \frac{W_{Fe_3O_4} / \rho_{Fe_3O_4}}{V_{ferrogel}} \times 100\% \text{ (v/v\%)} \quad (6.1)$$

$$No.(Fe_3O_4) = \frac{V_f(Fe_3O_4)}{4/3\pi r^3} \text{ (no. Fe}_3\text{O}_4\text{/per unit cell)} \quad (6.2)$$

where $\rho_{Fe_3O_4}$ is the density of Fe₃O₄ particles (5.2 g/cm³); $W_{Fe_3O_4}$ means the total addition weight of the Fe₃O₄ particles in the ferrogel. Therefore, $W_{Fe_3O_4} / \rho_{Fe_3O_4} = V_{Fe_3O_4}$ represents the total volume of Fe₃O₄ in the ferrogel. $4/3\pi r^3$ indicates the volume of a Fe₃O₄ particle if the particle is assumed to be spherical. The total number of the Fe₃O₄ particles is $V_{Fe_3O_4} / 4/3\pi r^3$ where r is the radius of the iron oxide particle and is assumed to have an average diameter of 250 nm, i.e., r = 125 nm. For the PVA10-MP17 ferrogel, there are 17.1 Fe₃O₄ particles in the unit cell (1 μm³), 33.3 Fe₃O₄ particles in the PVA10-MP34 ferrogel, and 58.7 Fe₃O₄ particles in the PVA10-BM68 ferrogel, which are schematically shown in the Fig. 6.5-(a). In order to conveniently and clearly express the relative number of the Fe₃O₄ particles in a basic unit cell, a model unit cell with a volume of 600 nm³ was used, as displayed in Fig. 6.5-(a), and there are ca. 3.69 Fe₃O₄ particles in the given volume of the model cell for PVA10-MP17 ferrogel, 7.19 and 12.69 Fe₃O₄ particles for PVA10-MP34 and PVA10-MP68 ferrogels,

respectively. Furthermore, $V_{Ferrogel}$ represents the bulk volume of the ferrogel determined by the length, width, and thickness of various ferrogels.

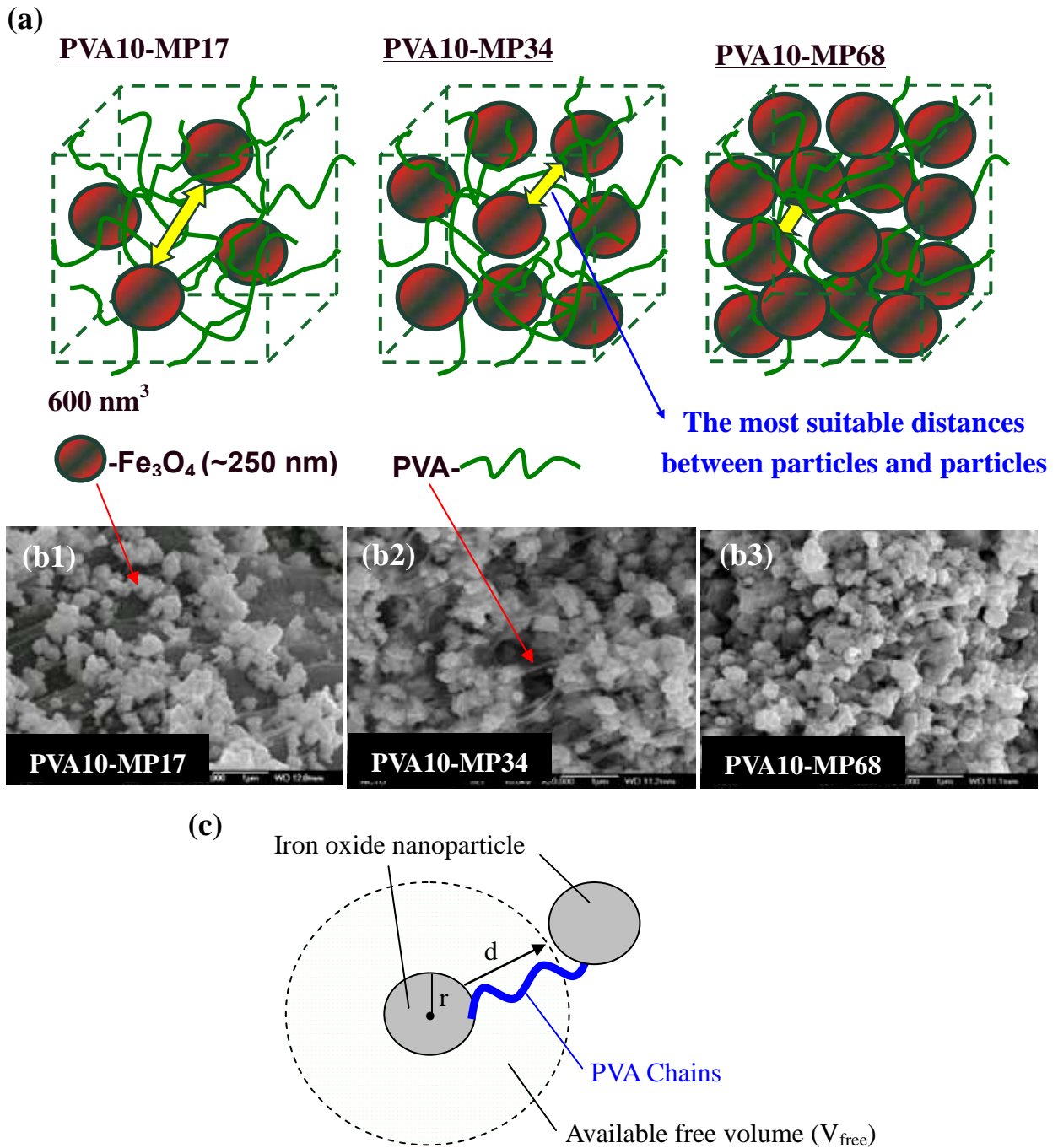
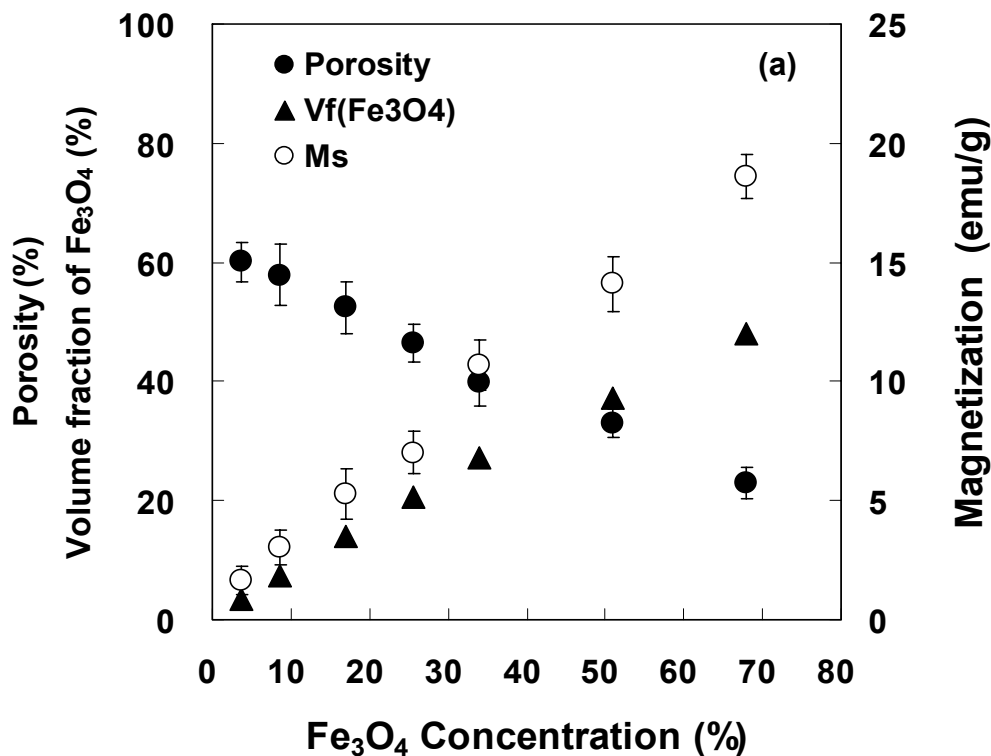


Fig. 6.5 (a) Models of the unit cell (600nm^2) of PVA-based ferrogels which Fe_3O_4 particles distributed; (b) SEM cross-section image of PVA10-MP34 ferrogel. (c) Schematic drawing of the relationship of surface-to-surface distance between two neighboring particles (d) and available free volume (V_{free})

In addition, the average porosity (%) of these ferrogels can be measured by a pycnometer and calculated by Eqs. (3.7)-(3.9), where the porosity in the ferrogel decreased with increasing Fe_3O_4 , as illustrated in Fig. 6.6-(a). This indicates that increase in the concentration of Fe_3O_4 caused a reduction of porosity, and the lower porosity will slower the permeation rate of the model drug in the absence of MF, i.e., MF "OFF". Moreover, it was found that the porosity of the ferrogel decreases linearly with the volume fraction occupied by iron oxide. The variation of those two parameters can be fitted by following equation:

$$\text{Porosity}(\%) + V_f(Fe_3O_4) \text{ (v/v\%)} + x = 100\%$$

where $x = 33.6 (+/- 1.8) \%$ may be interpreted as the volume fraction of organic matrix (i.e. PVA, and DMSO)



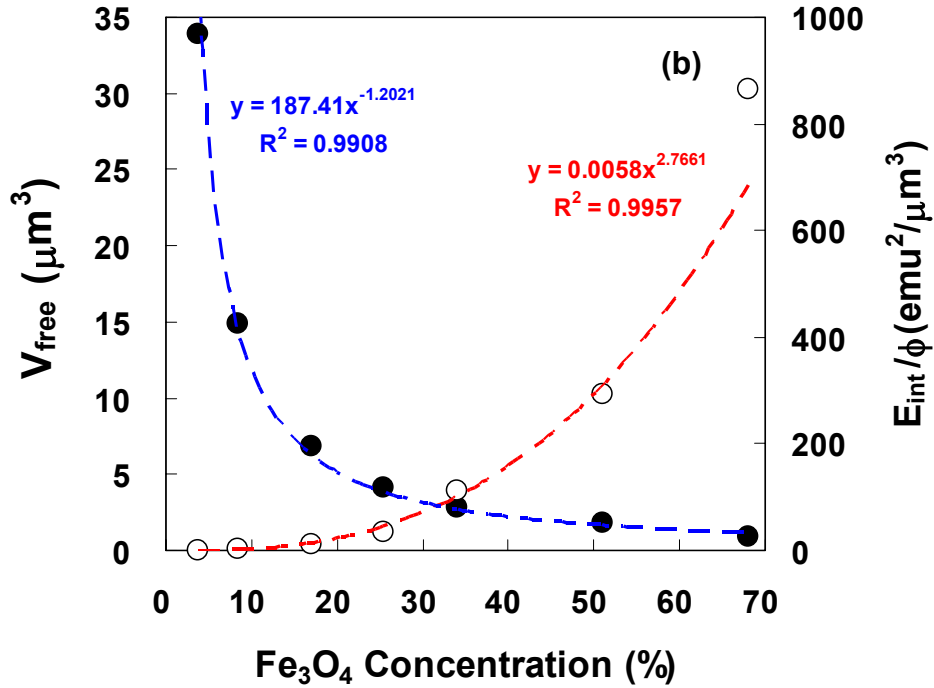


Fig. 6.6 Comparison of (a) porosity (%), volume fraction of Fe_3O_4 particles ($V_f(Fe_3O_4)$) and magnetization (Ms); (b) both available free volume (V_{free}) and interaction energy (E_{int}) of ferrogels dependence of various Fe_3O_4 concentrations

Although greater amount of Fe_3O_4 particles can increase the magnetization of the ferrogel, the space available for the Fe_3O_4 particles to freely move (defined as available free volume (V_{free})) will correspondingly decrease. While the available free volume for the Fe_3O_4 particles is too small, it will inhibit the movement of the Fe_3O_4 particles in the unit cell, thus, the magnetic-sensitive behavior will decrease even though those particles exhibited high magnetization (Ms).

The available free volume of each magnetic particle can be calculated by Eq. (6.3):

$$\text{Available free volume } (V_{free}) = \frac{\text{Porosity}(\%) \times V_{ferrogel}}{\text{No.}(Fe_3O_4)} \quad (6.3)$$

As given in Fig. 6.6-(b), V_{free} is decreased in a power-law-dependent manner with increasing Fe_3O_4 concentration. V_{free} in the PVA10-MP3.75 ferrogel ($33.88 \mu m^3$) is about 30 times higher than that in the PVA10-MP68 ferrogel ($0.95 \mu m^3$), calculated by Eq. (6.3).

6.5 Effects of magnetization

In regard to the magnetization of the Fe₃O₄ in the ferrogels, the interaction energy (E_{int}) between two particles with identical moment magnetization (M_s) can be given as follows [Chatterjee, 2002; Dai, 2000]:

$$E_{int} \propto \frac{M_s^2 (3 \cos \psi_1 \cos \psi_2 - \cos \alpha)}{\delta^3} \quad (6.4)$$

where δ (μm) is the center-to-center distance between two neighboring particles, which is calculated by $(d + 2r)$; r is the average radius of Fe₃O₄ particles (ca. 125 nm); d is the surface-to-surface distance between two neighboring particles; ψ_1 and ψ_2 are the angles between δ and two moments, respectively; α is the angle between the two moments. However, d is hardly precisely measured. Therefore, a rough measurement was performed by SEM as observed in Fig.2-(b). For example, the average d value in the PVA10-MP34 ferrogel was about 1 μm that is approximately the same order of magnitude to that (0.75 μm) calculated from the following presumed model (see Fig. 2-(c) and Eq. (10)). From the schematic drawing, it can be found that V_{free} is equal to $\frac{4\pi}{3} [(d+r)^3 - r^3]$.

Therefore,

$$d = \left(\frac{3}{4\pi} V_{free} + r^3 \right)^{1/3} - r \quad (6.5)$$

Therefore, the average distance (d) between particles will be used in this work to evaluate the E_{int} . The M_s of various ferrogels was measured by a vibrating sample magnetometer (VSM, Toei VSM-5, USA). The M_s increased with the Fe₃O₄ addition, as illustrated by the magnetization curves in Fig. 6.7 Further, $(3 \cos \psi_1 \cos \psi_2 - \cos \alpha)$ and other interrelated factors were hypothesized as constant (ϕ). Hence, to combine Eq.(9) with Eq.(10), the interaction energy (E_{int}) can be well characterized using Eq.(6.6)

$$E_{int} = \frac{M_s^2}{(d + 2r)^3} \phi \quad (6.6)$$

The E_{int} -Fe₃O₄ concentration correlation, shown in Fig. 6.6-(b), shows that the interaction energy is increased, followed by a power-law dependence, with increasing Fe₃O₄ concentration. The interaction energy in the PVA10-MP68 ferrogel (865.68 $\text{emu}^2/\mu\text{m}^3 \times \phi$) is about 3150 times higher than that in the PVA10-MP3.75 ferrogel (0.27

$\text{emu}^2/\mu\text{m}^3 \times \phi$), as shown in Fig. 6.6-(b).

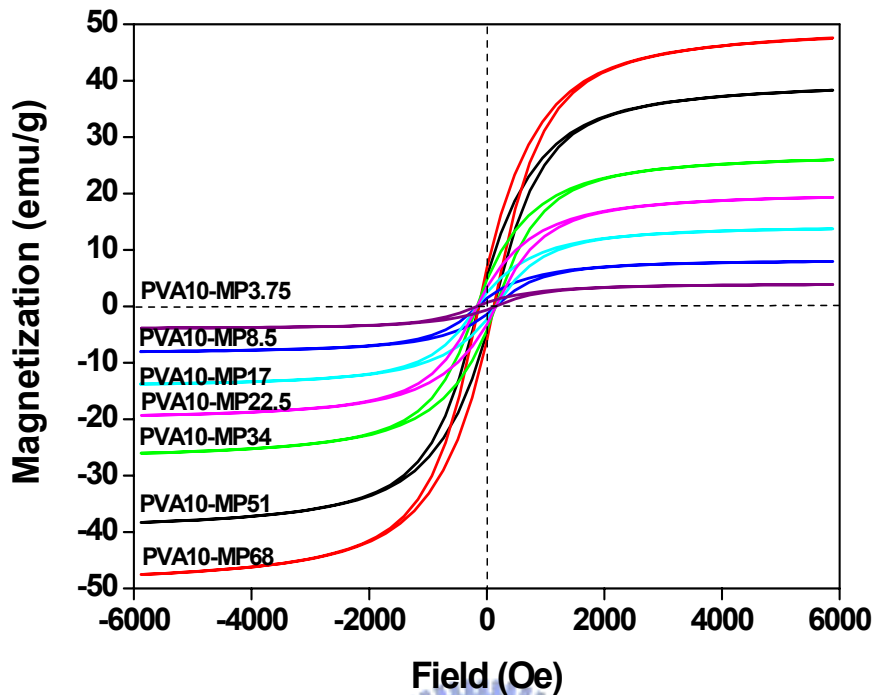


Fig. 6.7 Hysteresis loop analysis of the ferrogels incorporated with various Fe_3O_4 additions measured by VSM

Based on these calculations, it is clearly demonstrated that the lower Fe_3O_4 concentration leaves larger V_{free} but poorer interaction energy between the particles in the ferrogels, and vice versa, for the ferrogels with higher Fe_3O_4 concentration. Therefore, the “optimal” magnetic-sensitive behavior is virtually interplaying between the V_{free} and the interaction energy in the ferrogels. The concentration of the Fe_3O_4 for the optimal balance between the two factors can be obtained from the intersection of two power-law-dependent curves in Fig.6.6-(b), where an amount of between 30-34% of the Fe_3O_4 was derived. This concentration range is exactly located within the saturation region of the magnetic sensitivity map (Region B) shown in Fig. 6.4-(c). It can be anticipated that the ferrogels with Fe_3O_4 concentration in the range of 30-34% offers the best spatial configuration of the particles in the unit cell model facilitating both V_{free} and magnetization. By translating to what experimentally observed, the PVA10-MP34 ferrogel does display the optimal “opening-&-closure” configuration with respect to “on-off” MF operation and also illustrated the best magnetic-sensitive

behavior, as evidenced in Fig.6.4-(a). In other words, the magnetic particles distributed in the PVA10-BM34 ferrogel presents the best spatial configuration for optimizing both V_{free} and magnetization among the other compositions.

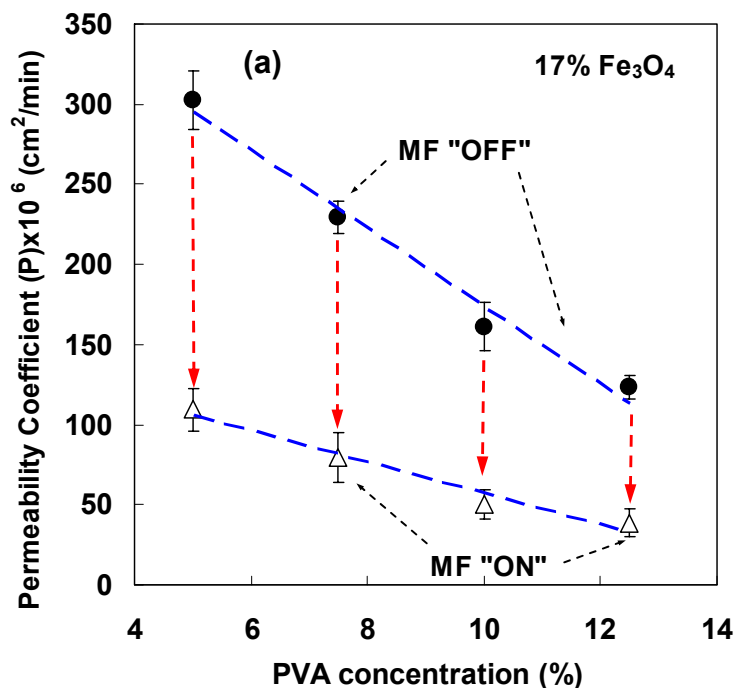
6.6 Role of PVA content

Since the “closure” and “opening” configurations of the ferrogels are dependent solely on the operating mechanism of both magnetic particles and the polymeric phase, i.e., PVA, under the action (ON mode) and removal (OFF mode) of the magnetic field. The polymeric phase is virtually a passive phase that intimately associated with the movement of magnetizing or de-magnetizing Fe_3O_4 nanoparticles in the ferrogel. However, PVA addition reduced the porosity and formed more rigid ferrogels and thus, the drug-permeation rate, corresponding to P value, will surely reduce under on-off operation of the magnetic field. Thus, the change in the concentration of the polymeric phase in the ferrogels will affect its ability to effectively enclose and release an active ingredient from the ferrogels under a fixed amount of Fe_3O_4 concentration in a given strength of magnetic field. To elucidate the influence of the PVA on the magnetic-sensitive behavior in the ferrogels, PVA concentrations of 5%, 7.5%, 10%, and 12.5% were selected for the ferrogels with 17% and 34% Fe_3O_4 nanoparticles (hereinafter termed 17% and 34% Fe_3O_4 ferrogels), which has been shown in Fig.6.4-(b) to exhibit stable and excellent magnetic-sensitive behavior (Region B).

Figures 6.8-(a) & (b) show the variation of P value of the ferrogels before (i.e., MF”OFF”, P_{OFF}) and after (MF”ON”, P_{ON}) an MF operation. For 17% Fe_3O_4 ferrogel, that the value of P_{OFF} decreased sharply with increasing PVA concentration [see Fig. 6.8-(a)], but P_{ON} decreased slowly with PVA concentration. In addition, the change in the P value with respect to the PVA concentration for 34% Fe_3O_4 ferrogels exhibits similar trend before (MF”OFF”), and after (MF”ON”) magnetization. However, compared with 17% Fe_3O_4 ferrogels, P_{ON} of 34% Fe_3O_4 ferrogels decreased slightly (followed by a power-law dependence) with the increased PVA concentration, in Fig. 6.8-(b). It displays a “saturation” region while increasing PVA over the range of 10-12.5%, implying the best “closure” configuration in this system is lying between 10

and 12.5% PVA content. According to these findings, it can be found that the magnetic sensitivity is decreased considerably and linearly with increasing PVA concentration for the 17% Fe₃O₄ ferrogels but decreased relatively slowly for the 34% Fe₃O₄ ferrogels as shown in Fig.6.8-(c), indicating that the magnetic sensitive behavior of the ferrogels is proportionally decreased by the addition of PVA. However, the effect of PVA appears to be less pronounced in the 34% Fe₃O₄ ferrogel, since its magnetic behavior does not display remarkable fluctuation or change with increasing PVA as compared to that with 17% Fe₃O₄ ferrogel.

The above-mentioned results can be further explained in terms of the effect of space restriction and magnetization, as illustrated in Fig. 6.8 for 17% and 34% Fe₃O₄ ferrogels, respectively. PVA addition in both ferrogels (i.e., 17% and 34% Fe₃O₄) leads to a reduction in both V_{free} (calculated using Eq. (6.3)) and the interaction energy (E_{int}). Consequently, P value under MF "OFF" is decreased sharply. In the meantime, it also reveals a reduction in the permeation rate of the drug from the ferrogels with increasing PVA under MF "ON" operation due to lower porosity, and these have been experimentally supported in Fig.6.8-(a) and 6.8-(b). It is evidenced that increasing PVA not only reduces V_{free} but also weakens E_{int} of the magnetic particles in the ferrogels. Therefore, both V_{free} and E_{int} are decreased linearly with PVA concentration.



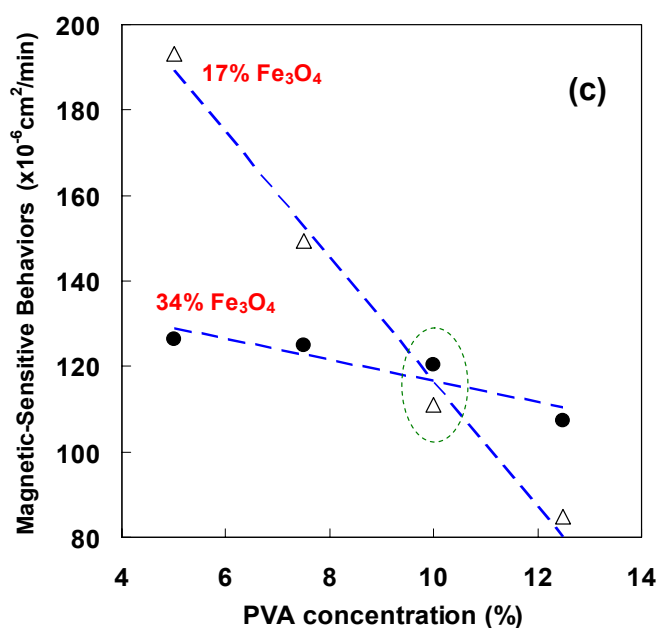
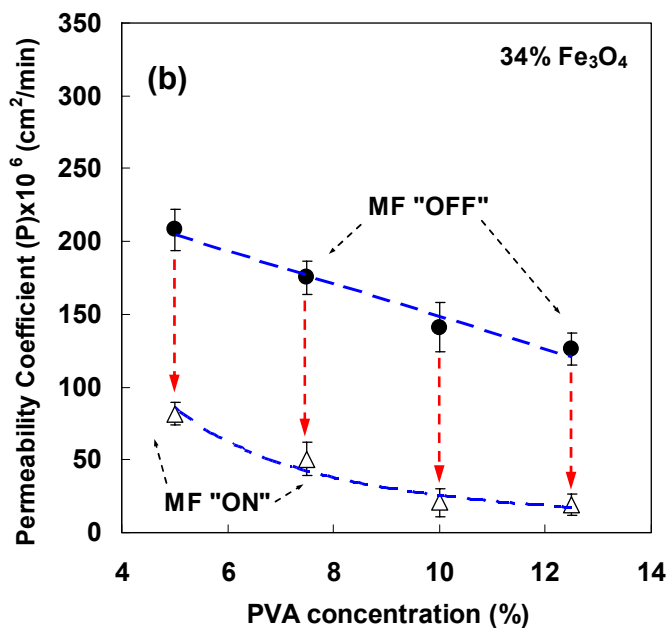


Fig. 6.8 Permeability coefficient of various PVA addition in “on” or “off” mode of a given magnetic field with (a) 17% Fe₃O₄ contents and (b) 34% Fe₃O₄ contents; (c) Comparison of magnetic sensitive behaviors between 17% and 34% Fe₃O₄ contents

In addition, 17wt% series ferrogel exhibited better magnetic sensitivity in the lower concentration region of PVA (ex. 5wt% PVA) compared to 34wt% series ferrogel, because the V_{free} of 17wt% ($7.3 \mu\text{m}^3$) is larger than that of 34wt% ($3.1 \mu\text{m}^3$),

as shown in Fig. 6.9. It means that iron oxide is easier to move in the 17wt% series ferrogel than that in the 34wt% series. However, the interaction energy (E_{int}) of 17wt% series ferrogel ($15.6 \text{ emu}^2/\mu\text{m}^3\phi$) is much smaller than that of 34wt% series ($224.8 \text{ emu}^2/\mu\text{m}^3\phi$). Therefore, E_{int} value in the 17wt% series might be not large enough for magnetic sensitivity with higher PVA addition, which is the reason that the magnetic sensitivity decreased so sharply in the 17wt% series. In contrast, 34wt% series ferrogel displays smaller V_{free} but higher E_{int} , which means they exhibit a higher E_{int} but limited V_{free} . That is why the magnetic sensitive of 34wt% series is higher than 17wt% series (higher E_{int} and lower V_{free}), although both factors of 17wt% and 34wt% series were decreased with increasing PVA.

Moreover, as compared to Fig. 6.6-(b) with an increase of Fe_3O_4 , E_{int} increased but V_{free} decreased, it is clear to realize that both the Fe_3O_4 and PVA constituents play different roles for drug permeation behavior and magnetic sensitive behavior of the resulting ferrogels. Accordingly, the resulting ferrogels can be manipulated externally and magnetically with a precise control of the opening and closure of pore configuration within the network structure of the ferrogels.

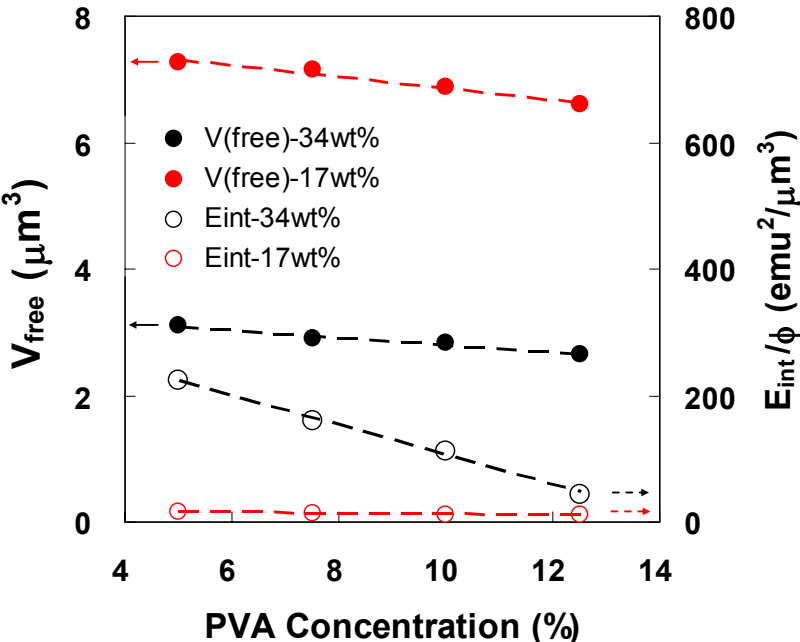


Fig. 6.9 Correlation of both available free volume (V_{free}) and interaction energy (E_{int}) in the ferrogels between 17% Fe_3O_4 and 34% Fe_3O_4 contents

6.7 Melting temperature (T_m) of PVA ferrogel

For further comparison, by taking PVA10-MP17 and PVA10-MP34 ferrogels in the Fig. 6.8-(c) as example, the selection is based on the magnetic-sensitive behavior map of “saturation” region, illustrated in Fig.6.4-(c) because they have similar magnetic-sensitive behavior. It can be observed that PVA10-MP34 ferrogels exhibit better “close” configuration than PVA10-MP17 ferrogels due to the lower porosity and more elastic properties and rigid body as evidenced by a comparison of melting temperature (T_m) in the PVA10-MP17 and PVA10-MP34 ferrogel by DSC (Diamond, Perkin-Elmer), as illustrated in Fig. 6.10. The value of T_m increases with the increase the concentration of Fe_3O_4 particles (pure PVA10 ($219.2^\circ C$) < PVA10-MP17 ($223.9^\circ C$) < PVA10-MP34 ($225.8^\circ C$)) which is probably related to the interaction of Fe_3O_4 and PVA.

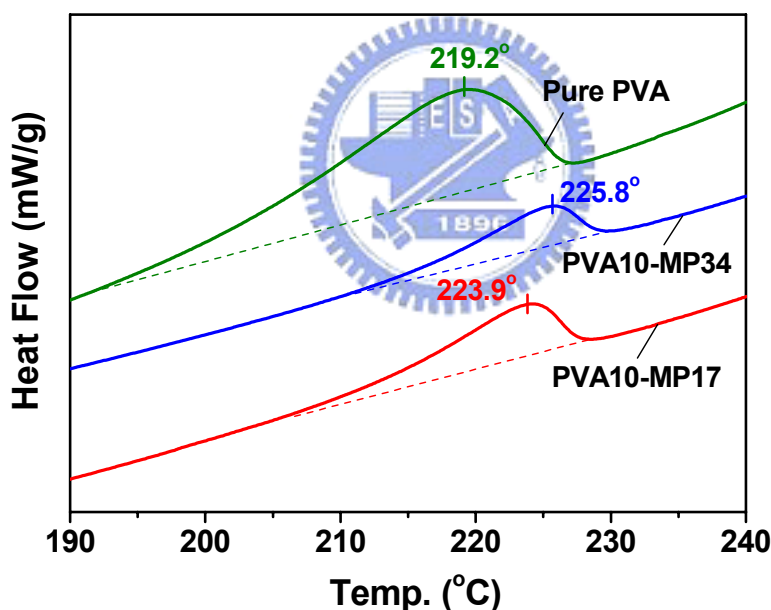


Fig. 6.10 Comparison of melting temperature (T_m) in the pure PVA10, PVA10-MP17 and PVA10-MP34 ferrogel by DSC

6.8 Other applications (Arrangement nanoparticles in the ferrogel)

The main purpose of the present work was to establish the effect of various direct of magnetic fields on the drug diffusion behavior. We have prepared PVA networks loaded with randomly and vertically, parallelly distributed iron oxide nanoparticles,

modulated by random and uniform magnetic field (vertical and parallel direction), as illustrated in Fig. 6.11. Fig. 6.11-(a) represents that the arrangement of iron oxide nanoparticles of ferrogel is parallel to the direction of magnetic field; whereas that is “vertical” to the drug diffusion direction, and Fig. 6.11-(b) illustrates that the arrangement of iron oxide nanoparticles of ferrogel is vertical to the direction of magnetic field; whereas that is “parallel” to the drug diffusion direction. In addition, the drug diffusion behavior was described in Fig. 6.12. The result shows that the drug diffusion rate would change with different the arrangement of iron oxide nanoparticles, implying the parallel direction exhibits the highest rate of drug diffusion whereas the vertical direction is lowest. It demonstrated that the drug might be restricted and thus difficult to pass through in the vertical ferrogel, but it is freely flowing in the parallel ferrogel. Therefore, it was anticipated to control the arrangement of iron oxide nanoparticles in the ferrogel could modulate the drug diffusion rate. It would be useful for the application in the dialysis membrane by magnetic field controlling.

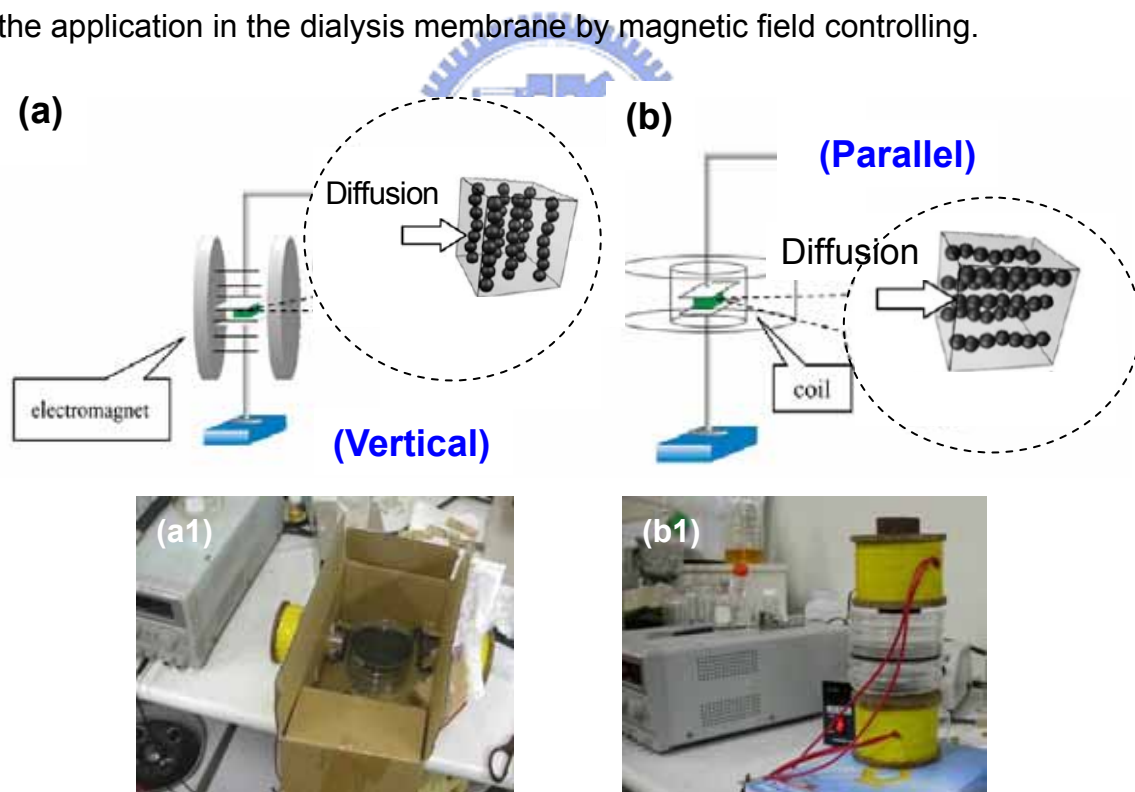


Fig. 6.11 Schematic representation of the experimental set-up for ferrogel preparation under uniform magnetic field: (a) & (a1) drug diffusion direction is vertical to the arrangement of iron oxide nanoparticle; (b) & (b1) drug diffusion direction is parallel to the the arrangement of iron oxide nanoparticle [Varga, 2006]

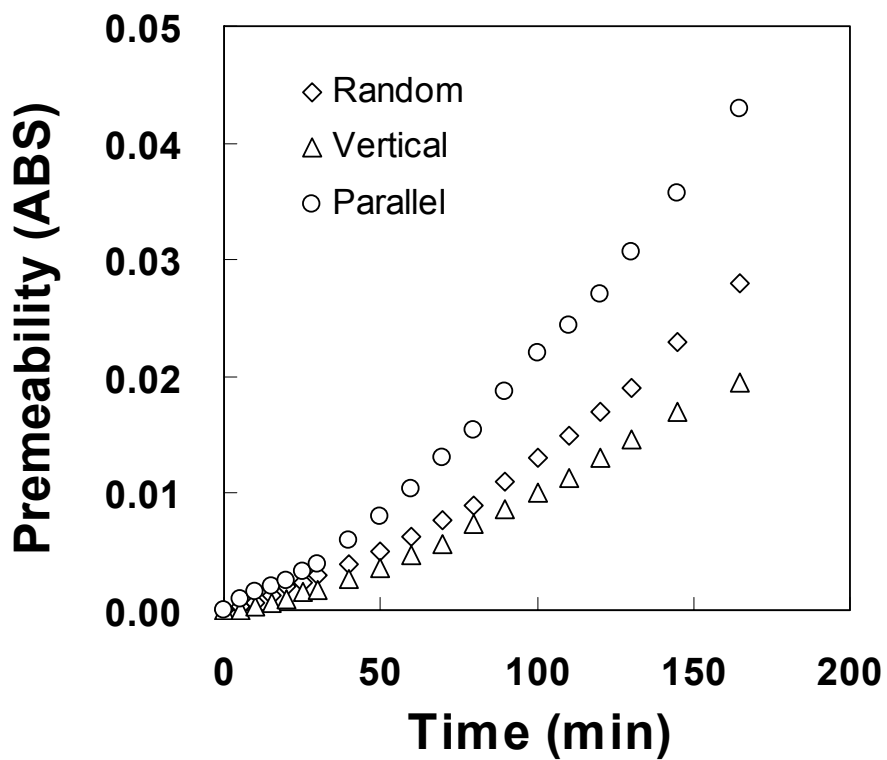


Fig. 6.12 Drug diffusion behavior in the various ferrogel; random, vertical and parallel means the arrangement of iron oxide nanoparticle is random, vertical and parallel to the drug diffusion direction, respectively

Chapter 7

Thermo-sensitive Ferrofluids

7.1. Introduction

Recently, ferrofluids are widely employed in the fields of biology and biomedicine such as enzyme and protein immobilization, genes, radiopharmaceuticals, magnetic resonance imaging (MRI), diagnostics, immunoassays, RNA and DNA purification, separation, and targeting drug delivery devices [Mak, 2005; Kim, 2002]. In order to develop functional nano-sized magnetite particles, a stable dispersion of the magnetic nanoparticles in organic or aqueous media are critically required an effective surface modification with organic compounds or polymers as dispersing agents. A delicate balance of hydrophilicity/ hydrophobicity in the polymer structure is responsible for exhibiting a lower critical solution temperature (LCST) phenomenon or critical micellization temperature (CMT). A series of tri-block copolymers composed of poly (ethylene oxide)-poly (propylene oxide)-poly (ethylene oxide) (Pluronic) are a kind of temperature-sensitive polymers, and they also demonstrate reversible solution transition behaviors in aqueous solution [Bromberg, 2003 & 2004]. Consequently, the novel thermo-sensitive ferrofluids that combine Pluronic-based-polymers (Pluronic F127) with magnetite nanoparticles could lead to a temperature responsive drug carrier system, because the magnetite would provide a source of heat in the alternating magnetic field by hyperthermia [Park, 2005].

7.2 Fabrication of thermo-sensitive ferrofluids

The stable thermo-sensitive ferrofluids was synthesized using the method of *in-situ* co-precipitation of Fe(II) and Fe(III) salts in the presence of Pluronic F127 (F127, Sigma). In this process, 0.05g of F127, 1.35g of $\text{FeCl}_3 \cdot 6\text{H}_2\text{O}$ (5mmol, Riedel-deHaën), and 0.498g of $\text{FeCl}_2 \cdot 4\text{H}_2\text{O}$ (2.5mmole, Fluka) were dissolved in 50 ml of water with vigorous stirring at 60°C. Then, the ammonia solution (33%, Riedel-deHaën) was quickly added to the reactor and stirred until pH arrives 10, followed by hydrothermal treatment at 80°C for 30 min. After washed five times, filtrated, and freezing-dried, core (magnet)-shell (F127) nano-magnetic-particles (NMPs) were successfully prepared. Finally, the 1g of core-shell NMPs were

dispersed in the 10 ml of 40% (w/v) F127 aqueous solution (pure F127-fluids, dissolved at 4°C beforehand) by sonication at 4°C for 6 hr. The well-dispersed thermo-sensitive ferrofluids were fabricated. Besides, Fe₃O₄ NMPs (diameter ca. 5-10 nm) fabricated by *in-situ* co-precipitation process would be used for reference [Mak, 2005].

7.3 Characterization of thermo-sensitive ferrofluids

TEM photos (JEOL-2000FX) in Figure 7.1-(a) show the core-shell structure of magnet-F127 NMPs. According to the TEM photos, the average thickness of F127 layers was found to be 1-2 nm, and the magnet diameter was about 5-7 nm.

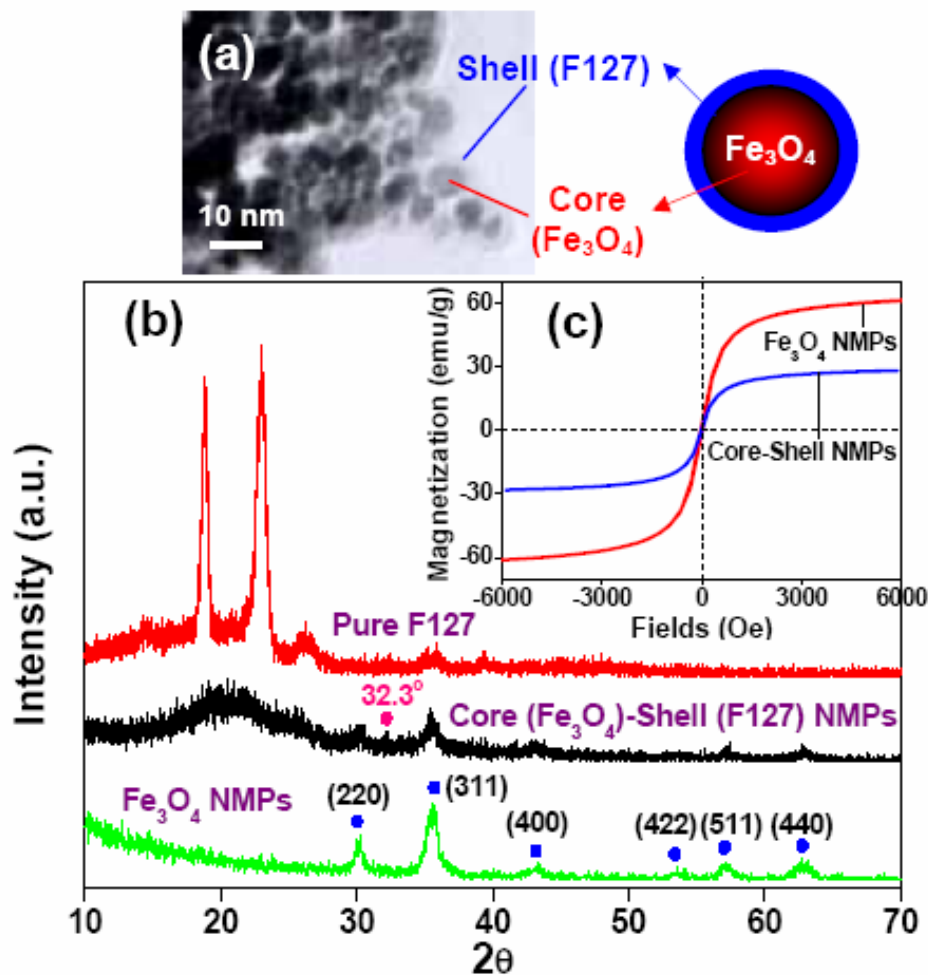


Fig. 7.1 (a) TEM photo of core-shell NMPs; (b)XRD pattern of core-shell NMPs.; (c) Magnetization curve of core-shell NMPs using VSM

Moreover, it was found in the XRD (Rigaku) pattern [Fig. 7.1-(b)] that six

diffraction peaks at $2\theta = 30.1^\circ, 35.6^\circ, 43.3^\circ, 53.5^\circ, 57.2^\circ, 62.9^\circ$ are the characteristic peak of standard Fe_3O_4 crystal. Hence, the resulting magnet NMPs can be defined as Fe_3O_4 NMPs. An additional diffraction peak at ca. $2\theta = 32.3^\circ$ was detected in the NMPs, which is a characteristic peak of standard Fe_2O_3 crystal, indicating a small amount of Fe_2O_3 was associated with the core-shell NMPs but the superparamagnetic behavior of the core-shell NMPs was not affected. Furthermore, the pure F127 showed two characteristic peaks at $2\theta = 18.8^\circ$, and 23.1° , indicating that the F127 displays high degree of crystallization. However, the core-shell NMPs exhibits a broad diffraction pattern peaked at 21° , which is believed due to a too thin layer of F127 to be more difficult to crystalize or subjected to a much slower crystallization of the F127 lattices. In addition, Figure 7.1-(c) shows that Fe_3O_4 NMPs display a magnetization (M_s) (60.9 emu/g), which is higher than core-shell NMPs i.e., M_s (28.4 emu/g), measured using the vibrating sample magnetometer (VSM, Toei VSM-5). An incorporation of the F127 may cause damages in some domains of Fe_3O_4 resulting in a decreased M_s . From these results, it can be confirmed that F127 is truly existed around Fe_3O_4 nanoparticles.

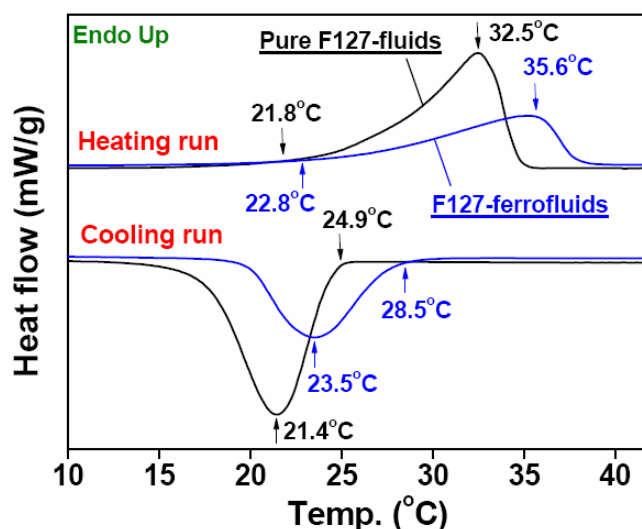


Fig. 7.2 DSC heating and cooling scans of pure F127-fluids and F127-ferrofluids

Figure 7.2 shows the DSC (Perkin Elmer, Diamond DSC) spectra with heating and cooling thermograms ($5^\circ\text{C}/\text{min}$) for both pure F127-fluids and F127-ferrofluids with a process of the gellation and liquefaction, respectively. An endothermic peak of pure F127-fluids and F127-ferrofluids in the heating run was detected which is due to

the aggregation transition (gel formation) of these two fluids in aqueous suspension. Such aggregation is caused by the temperature sensitivity of the PPO segments of the Pluronic that being anchored to the gel network. Much like the un-cross-linked Pluronic, polymers can form intra- and intermolecular micelle-like aggregates due to the hydrophobic interaction [Bromberg, Langmuir, 2004]. The gellation started at 21.8°C and maximized at 32.5°C for pure F127-fluids, and it commenced at 22.8°C and maximized at 35.6°C for F127-ferrofluids. It is more difficult to identify where CMT point is with so broad peak. In this case, the exothermic peak in the cooling run, i.e., melting thermospectrum, can be used to identify the CMT, due to its sharper peak. The liquefaction started at 24.9°C and maximized at 21.4°C for pure F127-fluids, but commenced at 28.5°C and maximized at 23.5°C for F127-ferrofluids. Therefore, CMT of the pure F127-fluids can be defined in the range of 21-25°C, which is similar to literature data [Bromberg, 2003]. However, it is lower than the CMT of F127-ferrofluids in the range of 23-28°C. The reason that CMT point shift was that core-shell NMPs might play a role of cross-linked point, and hence increased CMT point. Similar results can be found in PNIPAAm /clay systems [Haraguchi, 2002].

The thermo response behavior of ferrofluid by temperature increase was illustrated in Fig. 7.3. It was found that the ferrofluid (liquid state, Fig. 7.3-(a)&(b)) transferred rapidly to ferrogel (gel state, Fig. 7.3-(c)&(d)) while the temperature from 4 to 30°C for 5min. It demonstrated that the thermo sensitive ferrofluids could transfer to ferrogel very rapidly.



Fig. 7.3 Series image of thermo response behavior of ferrofluids: (a)&(b) liquid state (ferrofluids); (c)&(d) gel state (ferrogel)

In addition, a model drug can be dispersed homogenously in F127-ferrofluids below CMT, and then encapsulated into F127-ferrogel above CMT, and higher drug uptake was obtained. Moreover, it could be anticipated that the temperature increased of F127-ferrofluids modulated by hyperthermia of magnetic nanoparticles in external alternating magnetic fields [Park, 2005] can transform to F127-ferrogels. The further investigation is now in progress in our group



Chapter 8

Thermal and Magnetic Nano Ferrospheres

8.1 Introduction

Drug carriers that are responsive to external stimuli, such as temperature, pH, light, mechanical signal, electric field, and magnetic fields have received great attention in recent years [Kim, 2002; Zhang, 2004; Chiu, 2005; Lu, 2005; Qiu, 2001; Etrych, 2001; Chen, 2004; Murdan, 2003; Mamada, 1990]. A wide variety of materials, such as carbon nanotubes, dendrimers, biodegradable nanoparticles (PLGA or PLA), lipid vesicles (micelles), and gold or magnetic nanoparticles have been employed as matrix materials to deliver drugs. Among them, magnetic nanoparticles (MNPs) provide more interesting opportunities since they can be effectively activated in a controllable manner through a non-contact stimulus [Kohler, 2006], as compared with other materials. Although gold nanoparticles also displayed a similar inductive heating ability by infrared light stimulus, the manipulation and heating ability of magnetic nanoparticles were superior to those of the gold nanoparticles. The ability of magnets to convert magnetic energy into heat by the hysteresis effect has been known for a long period of time [Kim, 2005]; for instance, the ability has been used as antenna material for inductive heating in anti-tumor therapy, but the efficiency has not been as good as desired without combining inductive heating with drug delivery. In order to enhance the tumor-inhibition ability, the combination of the heat transfer and drug release in nanoparticles will be more interesting. In our previous work, we developed magnetic hydrogels (ferrogels) [Liu, 2006 & 2008; Hu, 2007] and magnetically sensitive nanospheres for controlled drug release by a high-frequency magnetic field (HFMF) [Hu, 2007 & 2008]. However, the silica seems to be a thermally insensitive material, and it was believed that the nanostructure did not change with temperature increases. In order to accelerate the rate of drug release, a thermo-sensitive polymer was used in this system because it exhibited a huge volume change when the temperature was increased [Choi, 2006].

A number of polymeric materials are known to exhibit a discontinuous change of properties when subjected to a temperature change [Choi, 2006; Schmidt, 2007;

Coughlan, 2004; Bhattacharya, 2007; Li, 2006; Bae, 2007; Desai, 2001]. Some of these systems, e.g. thermo-reversible gels, have been based on the existence of a lower critical solution temperature (LCST), or critical micellization temperature (CMT), and have usually been applied as intelligent drug carriers [17-23]. Poly(N-isopropylacrylamide) (PNIPAAm), poly(ethylene glycol)-poly(lactic acid)-poly(ethylene glycol) triblocks (PEG-PLA-PEG), and poly(ethylene oxide)-poly(propylene oxide)-poly(ethylene oxide) (PEO-PPO-PEO) triblocks have been among the most important reverse thermal gelation-displaying polymers. These triblocks, especially *Ploxamer 407*, also known by the trade name Pluronic® F127 (PEO100-PPO65-PEO100), have been investigated for wound covering and controlled drug delivery. Furthermore, Pluronic® series copolymer has excellent biocompatibility and is one of the very few synthetic polymers approved by the US Food and Drug Administration (FDA) for use as a food additive and pharmaceutical ingredient [Bae, 2007; Desai, 2001]. Pluronic® series copolymer is also a potential candidate for biomedical applications.

In the present work, a dual-functional nanoparticle was developed by integrating a nanomagnetic core with a shell layer of thermo-sensitive hydrogel to encapsulate an anti-cancer agent. Inductive heat was generated in the presence of HFMF. When heated, the thermo-sensitive polymer collapsed around the iron oxide nanoparticles, inducing an accelerative drug release. In recent years, some researchers [Zhang, 2007; Chen, 2007; Deng, 2005; Detlef, 2006] have reported that dual-functional drug carriers included magnetic/thermal sensitivity, but few reports emphasized the controlled drug release using HFMF. In addition, raising the temperature of the drug carriers from the surrounding heat source has been insufficient; a better alternative would be to supply the heat source by the drug carrier, e.g., the inductive heating effect induced by HFMF to a magnet core. This type of drug carrier can have great potential for disease treatment.

Moreover, the use of high-frequency magnetic stimulus can also achieve an “instantaneous” burst release of drug by the rapid heating to induce an instant shrinkage of the F127 hydrogel. Choi et al. [Choi, 2006] reported that Pluronic/Heparin nanocapsules exhibit a 1000-fold thermally reversible volume transition when the

temperature changes from 25 to 37°C. The violent volume-shrinkage would induce a rapid drug release. Therefore, the combination of magnetic and thermal properties would be a very interesting alternative for tumor therapy. Here, we developed a novel Pluronic®/iron oxide magnetic nanoparticle formulated by an in-situ co-precipitation process and evaluated it as a drug carrier. The proposed synthesis process of F127-MNPs is depicted in Fig.8.1-(a) and is characterized by transmission electron microscopy (TEM), X-ray diffraction (XRD), Raman spectroscopy, X-ray photoelectron spectroscopy (XPS), spectrofluorophotometry (PL), and dynamic light scattering (DLS). Thereby, we demonstrated an approach to form water-dispersible and magnetic/thermo-responsive nanoparticles formulated with F127 and iron oxide nanoparticles, which can be applied to the biomedical devices, such as drug carriers.



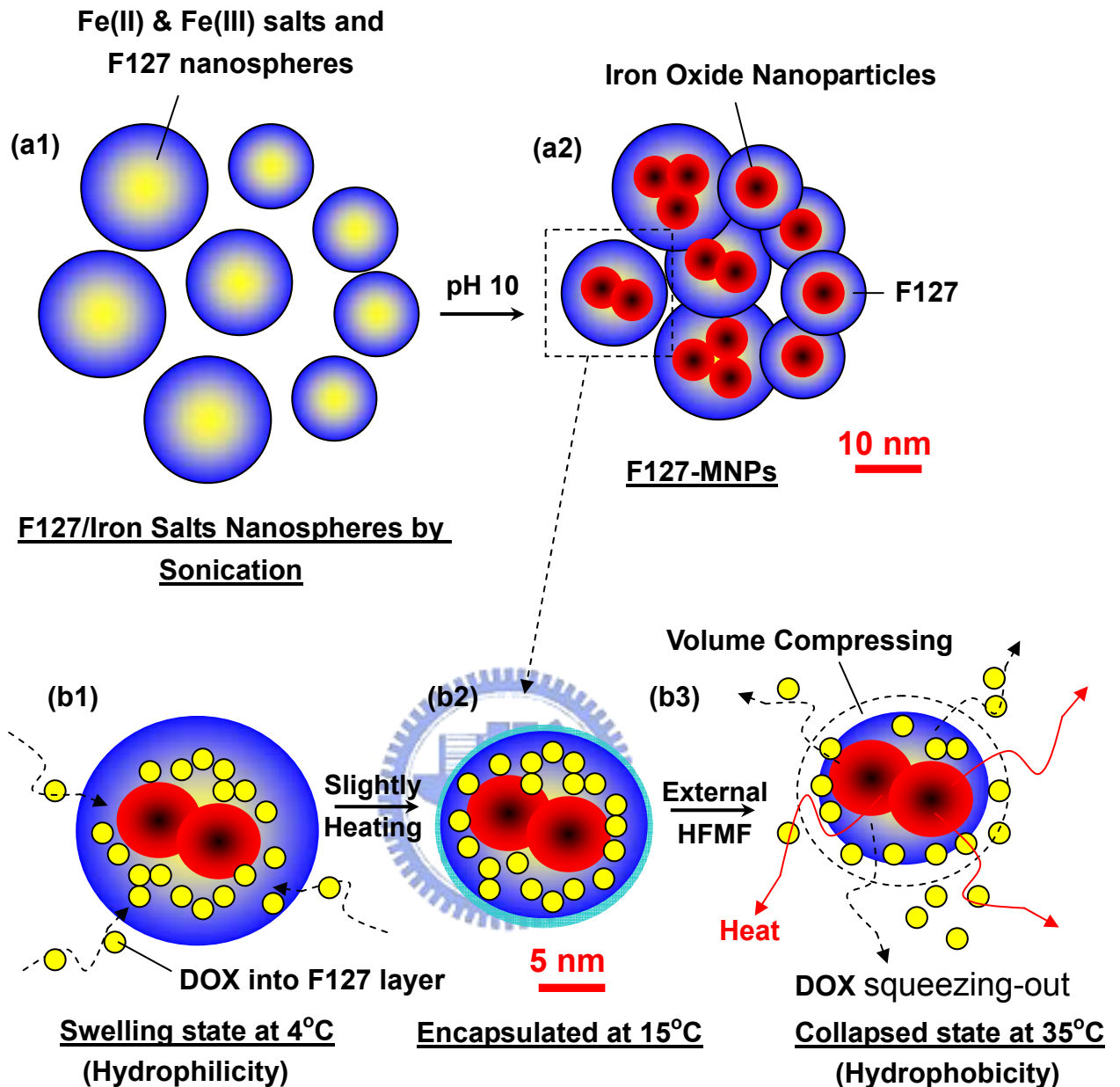


Fig. 8.1 Diagram showing the proposed synthesis process of F127-MNPs: (a1) F127/iron salts nanosphere formation by sonication; (a2) F127-MNPs formation after adding ammonia solution to $\text{pH} = 10$; Proposed mechanism for drug encapsulation and delivery process of F127-MNPs by HFMF: (b1) Drug diffuses into the nanospheres at lower temperature (4°C , swelling state); (b2) Slight volume shrinkage and drug encapsulated in the nanospheres after slight heating to 15°C ; (b3) Sharp volume shrinkage with accelerative drug release under HFMF treatment

8.2 Fabrication of Pluronic® F127 ferrosphere

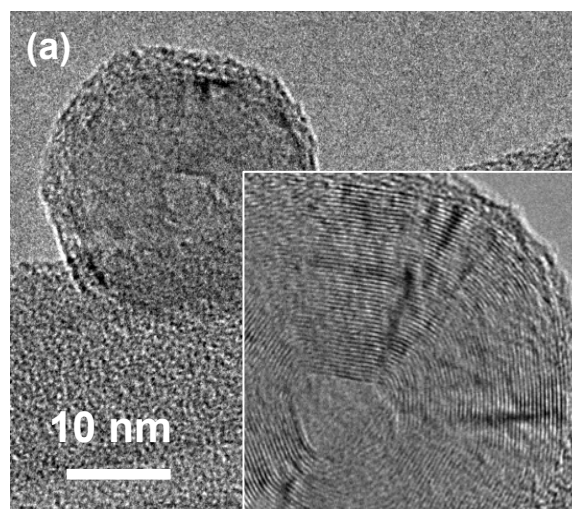
Nanospheres of Pluronic® F127 (F127) and magnetic nanoparticles (F127-MNPs) were synthesized using an in-situ co-precipitation of Fe(II) and Fe(III) salts in the presence of Pluronic® F127 (F127, Sigma). In this process, the optimum ratio of iron oxide precursor and F127 hydrogel was described. 0.05 g of F127, 5 mmol of $\text{FeCl}_3 \cdot 6\text{H}_2\text{O}$ (Riedel-deHaën), and 2.5 mmole of $\text{FeCl}_2 \cdot 4\text{H}_2\text{O}$ (Fluka) were dissolved in 50 ml of water while being vigorously stirred at 60° C. The dissolved solution was sonicated by a horn-type ultrasonic homogenizer (VC-500 watts, Cole-Parmer Instruments, USA) operating at a constant frequency of 20 kHz for 10 min. Then, Pluronic® F127/iron oxide salt nanospheres were prepared, as shown in Fig. 8.1-(a1) (where pure F127 nanospheres (appropriate size: 10-30 nm) were made in a similar process with sonication). Later, the pH was adjusted to 10 by adding ammonia solution (33%) to the reactor while stirring. This was followed by heating to 60°C, where it remained for 30 min. After washing five times with phosphate buffered saline (PBS, pH 7.4), subsequent filtering by Acrodisc® syringe filters (Aldrich, diameter 25 mm, pore size 0.2 μm), and vacuum-drying, F127-MNPs were then successfully prepared, as shown in Fig. 8.1-(a2).

Doxorubicin (DOX, MW: 580, Sigma, USA), a well-known anti-cancer drug, was used as a model molecule. DOX was employed because of its amphoteric characteristics; it can dissolve in an aqueous environment (ca. 10 mg/ml) or in an organic solvent (high solubility in methanol and chloroform). For incorporation in the F127-MNPs, 2 ml of an aqueous solution of DOX (2 mg/ml) was added drop by drop to 3 ml of an aqueous dispersion of F127-MNPs (100 mg of particles in the 3 ml PBS solution) while stirring. Stirring was continued overnight at 4°C to allow the drug to disperse into the F127-MNPs (see Fig. 8.1-(b1)). Because the F127-MNPs exhibit swelling at lower temperatures (4°C), DOX easily diffused into the ferrospheres. Then, DOX was well encapsulated under 15°C (the collapsing state was at a higher

temperature, which formed the protecting-like layer (skin layer) and prevented drug escape), as shown in Fig. 8.1-(b2). Then, drug-loaded ferrospheres were separated from the un-entrapped drug using a magnet. F127-MNPs were washed three times by being re-suspended in distilled water and separated, as described above, using the magnetic field. The resultant samples were dialyzed by a dialysis membrane with an MW cutoff at 14,000 and stored at 4°C before the nanospheres were used.

8.3 Morphology and Characterization of F127-MNPs

Morphology of F127-shell MNPs was examined by TEM (JEM-2010, JEOL, Japan). Figure 8.2-(a) shows the TEM images of pure F127 nanospheres, displaying a ring-like structure, which was a phenomenon due to the block-copolymer (Pluronic® F127) self-assembly. After the precursors of Fe(II) and Fe(III) salts and the ammonia solution were added, the iron oxide nanoparticles started to form by co-precipitation. Figure 8.2-(b) shows that well-distributed F127-MNPs have a spherical geometry of 10-20 nm in diameter. Moreover, under high resolution TEM [Fig. 8.2-(b1)], the iron oxide nanoparticles were encapsulated in the interior region of F127 nanospheres, and it was a crystalline structure [in the insert, Fig. 8.2-(b2)]. In addition, the selected area diffraction pattern of the F127-shell MNPs showed five planes, namely, [220], [311], [400], [511], and [440], indicating the presence of iron oxide nanoparticles, as well as an amorphous phase, e.g., cloudy ring (see Fig. 8.2-(b3)). This again suggests that the iron oxide nanoparticles were encapsulated by F127 hydrogel.



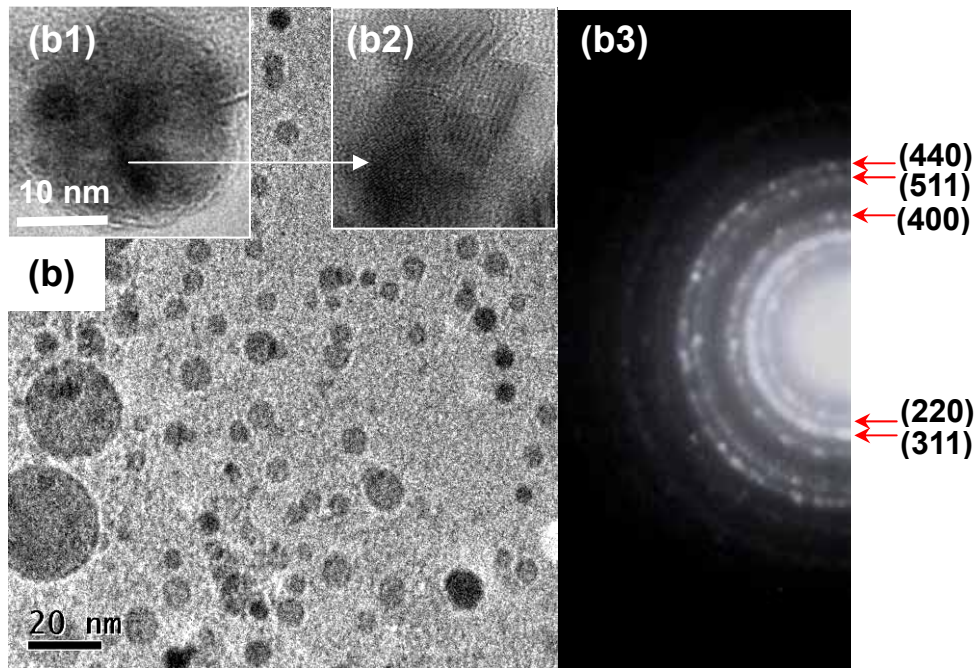


Fig. 8.2 TEM image of the morphology of (a) Pure F127 nanospheres; (b) Distribution of F127-MNPs; (b1) TEM image of F127-MNPs nanospheres (iron oxide nanoparticles were encapsulated in the F127 nanospheres); (b2) High resolution TEM image showing crystalline condition of iron oxide in the F127 nanosphere; (c) Diffraction pattern of F127-MNPs

Figure 8.3 shows the results of the XRD (M18XHF, Mac Science, Japan) of the F127 nanospheres and F127-MNPs. In Fig. 8.3-(a), six diffraction peaks at $2\theta = 30.1^\circ$, 35.6° , 43.3° , 53.5° , 57.2° , and 62.9° were the characteristic peaks of the crystal plane, which was the same as JCPDS 85-1436 [Long, 2004], suggesting the nanoparticles were Fe_3O_4 . Furthermore, the XRD spectrum of pure F127 nanospheres showed two characteristic peaks at $2\theta = 18.8^\circ$ and 23.1° , representing a high degree of ring-like crystallization of the F127, which was in good agreement with the results of the TEM image [Fig. 8.2-(a)]. In addition, F127-MNPs not only exhibited six characteristic peaks of Fe_3O_4 but also showed a broad diffraction pattern, which peaked at 21° . The diffraction pattern was assumed to be due to the presence of iron oxide that deferred the ring-like crystallographic structure of the F127 phase. These results were similar to those of the diffraction pattern of the TEM (cloudy ring), indicating that both phases were intimately contacted.

Raman spectra are potentially more useful than diffraction techniques to track

subtle structural differences between the vibration frequencies of F127 and Fe₃O₄ MNPs. Figure 8.3-(b) shows that, although F127 hydrogel were surrounded with iron oxide nanoparticles, a significant difference between these phases can be recognized from the Raman spectra. Both 665 and 704 cm⁻¹ bands, assigned to the characteristic band of Fe₃O₄ [Long, 2004] were attributed to the vibrational modes. These consisted of the stretching mode of oxygen atoms along Fe-O bonds (metal oxide bond), and four characteristic peaks at 492, 537, 603, and 709 cm⁻¹ were assigned to F127 nanospheres. Furthermore, from the sample of F127-MNPs, six peaks, including the peaks from both F127 and Fe₃O₄ MNPs, were observed where the two peaks of 492 and 537 cm⁻¹ were almost combined to form a broad peak. This suggests that there was some interaction between metal oxide and the -OH group in the F127 when the iron oxide nanoparticles were formed inside the F127 hydrogel.

In addition, the change in chemical-binding energy in F127-MNPs was investigated in the XPS (ESCALAB 250, Thermo VG Scientific, West Sussex, UK), equipped with Mg K α at 1253.6 eV at the anode. As illustrated in Fig. 8.3-(c), the binding energy of O1s was detected from 526.0 to 538.0 eV, and the peak of iron oxide was at 530.0 eV. This peak represented the metal oxide, which was reasonably consistent with peak reported in the literature, i.e., 528-531 eV. Also, the -OH group peak of pure F127 nanospheres was found in the 532.8 eV, which was similar to the report of Anderson et al. [Anderson, 2001], showing a highly ordered arrangement of ring-like crystallization of the F127 nanospheres. However, after incorporation into the iron oxide nanoparticles (F127-MNPs), the peak at 532.8 eV shifted to a lower energy, 532.4 eV, indicating that the ring-like crystallization of the F127 nanospheres had been deteriorated to an amorphous-like structure due to the presence of iron oxide nanoparticles. In the meantime, the peak of the metal oxide in the F127-MNPs shifted to a higher energy, i.e., from 530.0 to 530.3 eV, suggesting that some interactions occurred between the metal oxide and the -OH group in the F127 hydrogel when the iron oxide was formed inside the F127 hydrogel. Although the actual mechanism for the shift of the binding energy of metal oxide was unclear at present, it is believed that iron ions can be encapsulated by the F127 hydrogel. This hydrogel promoted a self-assembly of the iron oxide salt to form crystal structure while increasing solution

pH upon synthesis, and it thus accompanies some ion-ion interaction to change the binding energy of metal oxide [Hu, 2007].

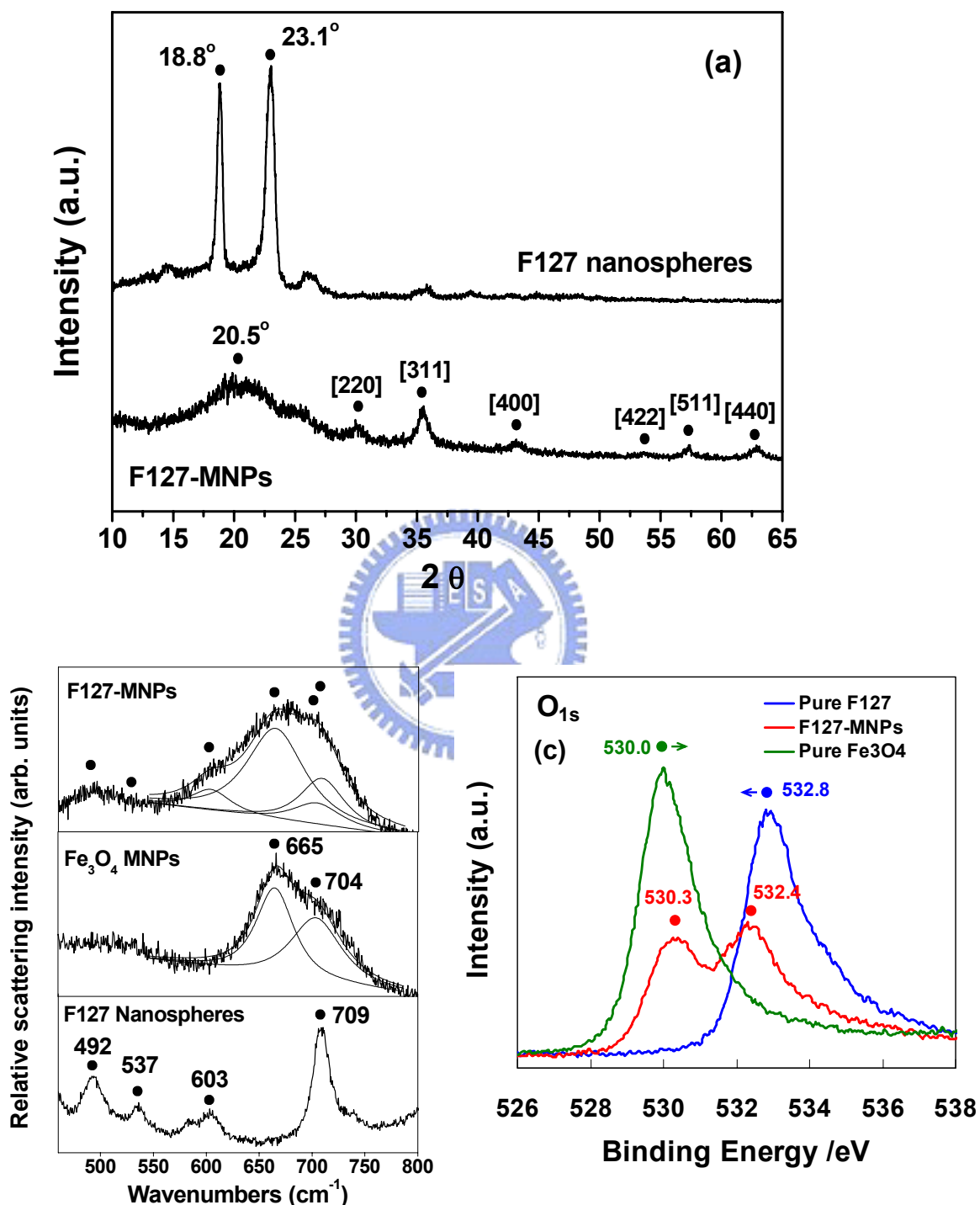


Fig. 8.3 Characterization analysis of F127 and F127-MNP nanospheres: (a) X-ray diffraction, (b) Raman spectra, and (c) XPS spectra

8.4 Hydrophilic/Hydrophobic properties

Pyrene is poorly soluble in a polar environment, but it strongly emits radiation when it is self-aggregated or forms microdomains (i.e., microaggregates) in an aqueous solution. The intensity ratio (I_{372}/I_{385}) of the first peak (372 nm) and the third peak (385 nm) of the fluorescence emission spectrum for pyrene has been shown to be sensitive to the polarity of the microenvironment [Bromberg, 1999 & 2003]. The reason was that increasing the polarity of the medium induces an increase in the intensity of the first peak, I_{372} , corresponding to the forbidden transition, while the intensity of the third peak, I_{385} , corresponding to the allowed transition, remains unchanged. The ratio was higher in a polar medium; for example, in water, $I_{372}/I_{385} = 2.0$, while, in hexane, $I_{372}/I_{385} = 0.6$. Therefore, the critical micellization temperature (CMT), which is the threshold temperature of self-aggregate formation by intra- and/or intermolecular association, could be determined from the change of the I_{372}/I_{385} ratio of pyrene in the presence of polymeric amphiphiles. Figure 8.4 shows that the I_{372}/I_{385} ratio in the aqueous suspension of the F127-MNPs varies with temperature between the transition temperatures of 20 and 25°C, which was the CMT of the F127-MNPs. The I_{372}/I_{385} ratio was higher in water below the CMT, indicating a strongly polar environment. However, above the CMT, the I_{372}/I_{385} ratio dropped to a lower level as the pyrene partition changed to a more hydrophobic environment as micellar aggregation began to form. These results were comparable with the CMT of pure F127 (23°C) in the literature [Bae, 2007; Desai, 2001], which meant that the F127-MNPs will be more hydrophobic above 25°C.

Another approach was based on the change of particle size of the F127-MNPs, with respect to temperatures, to indicate the hydrophilicity of the nanoparticles. As shown in Fig. 8.4, the particle size of the F127-MNPs was 40.1 nm at 4°C and 37.8 nm at 15°C, but it sharply decreased to 19.3 nm at 25°C and 16.2 nm at 35°C, as measured by a dynamic light scattering instrument (DLS, zetasizer-3000HS, Malvern, UK). The particles exhibited a 2- and 2.3-fold diameter transition from 15°C to 25°C and 35°C, respectively. That was roughly equal to a 10-fold volume transition from 15°C to 35°C. The 10-fold volume shrinkage of the F127-MNPs was enough to pump the drug out.

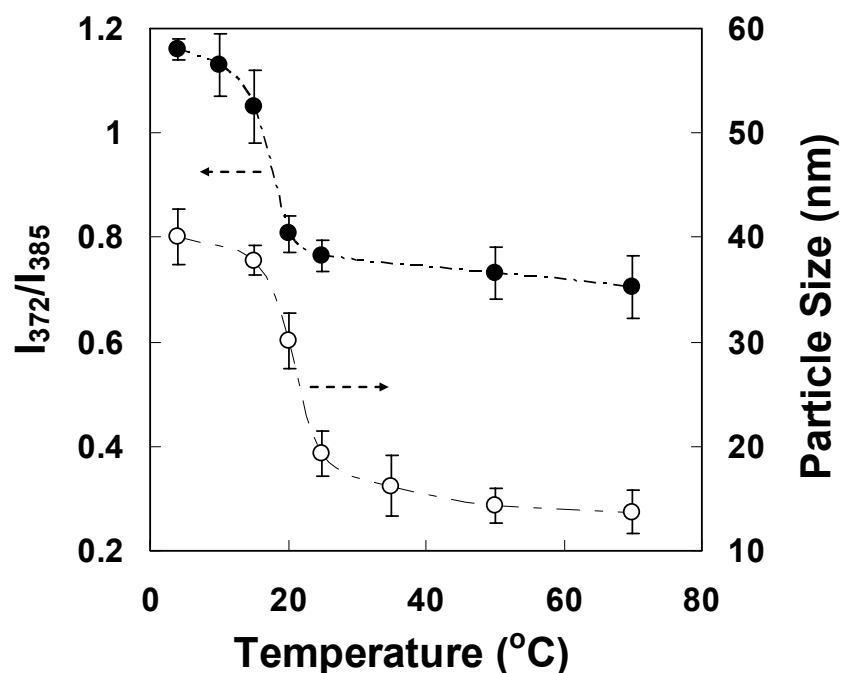


Fig. 8.4 Hydrophilic/Hydrophobic test of F127-MNPs with various temperatures: Solid circle curve indicates CMT test by PL (left axis), whereas particle size test by DLS (right axis) is indicated by open circle curve

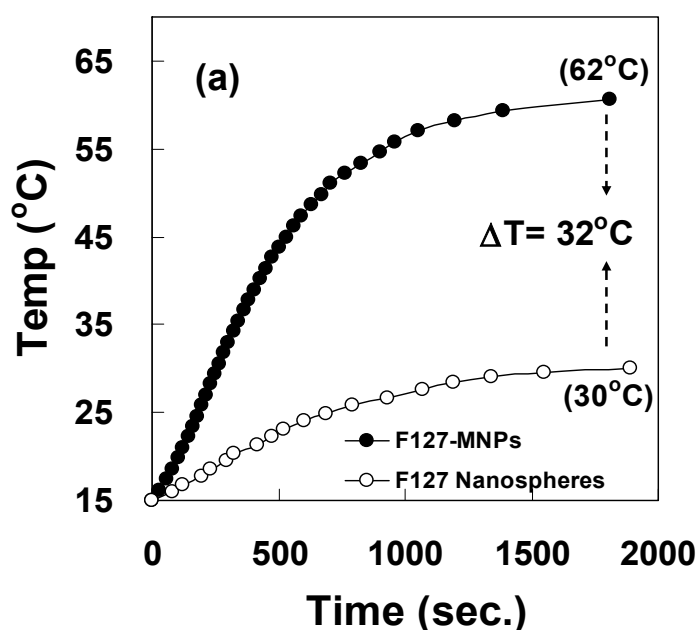
8.5 Drug delivery test by HFMF

Figure 8.5-(a) shows the results of inductive heating of the F127 MNPs, where the temperature was measured by an ethanol thermometer in an aqueous F127-MNPs suspension. Inductive heating is thermal energy induced from the hysteresis loss of ferrites and dependent on the type of remagnetization process in the high-frequency magnetic field (HFMF) [Kim, 2005]. The results showed that, under the selected field parameters (50-100 kHz and 15 kW), sufficient energy deposition was achieved, and the temperature was substantially increased in the solution within a short period of time. As expected, the temperature increased considerably (62°C) for the F127-MNPs suspension (0.2 g samples in 10 ml of PBS in the tube) and was approximately 2.0 times higher than that of the pure F127 nanospheres (30°C), indicating that this temperature difference (62°C-30°C, $\Delta T=32^\circ\text{C}$) was solely attributed to the inductive heating effect of the iron oxide in the presence of HFMF.

Figure 8.5-(b) shows the relationship between the temperature change and drug release behavior of the F127-MNPs. In the absence of the magnetic field, the drug

(DOX) displayed a stable release at a rate of $0.23 \mu\text{g ml}^{-1}\text{hr}^{-1}$. However, while reaching 35°C under magnetic stimulus, the drug release rate increased sharply from 0.23 to $7.94 \mu\text{g ml}^{-1}\text{hr}^{-1}$ during the first 5-min period (S-T1) and then reduced to $2.23 \mu\text{g ml}^{-1}\text{hr}^{-1}$ after a further 25-min stimulus (S-T2). The increased release rate when the temperature increased from 15°C to 35°C (above CMT) may be attributed to the volume shrinkage of the F127 shell layer. Similar reports have also been addressed in the literature [Chung, 1999]. For instance, Chung et al. indicated that the poly(N-isopropylacrylamide) and poly(butyl-methacrylate) polymeric micelles showed reversible structural changes allowing drug release upon heating/cooling fluctuations with a the lower critical solution temperature (LCST). These micelles released drug upon heating above the LCST, and the release was accelerated by a volume-shrinkage mechanism, like a pumping effect. The effect was eliminated upon cooling below the LCST.

Furthermore, upon magnetic manipulation, the drug also showed a two-stage release behavior. DOX exhibited a burst-like release for the first 5 min at a rate of ca. $38.77 \mu\text{g ml}^{-1}\text{hr}^{-1}$ (S-H1) and then stabilized to ca. $1.84 \mu\text{g ml}^{-1}\text{hr}^{-1}$ (S-H2) for the following 25 min of operation. The rate of burst release in the first 5-min period with HFMF was 4.9 times higher than that at 35°C in the water bath. The plausible reason was due not only to the volume shrinkage at higher temperature but also to the change in the pore structure of the nanospheres under HFMF.



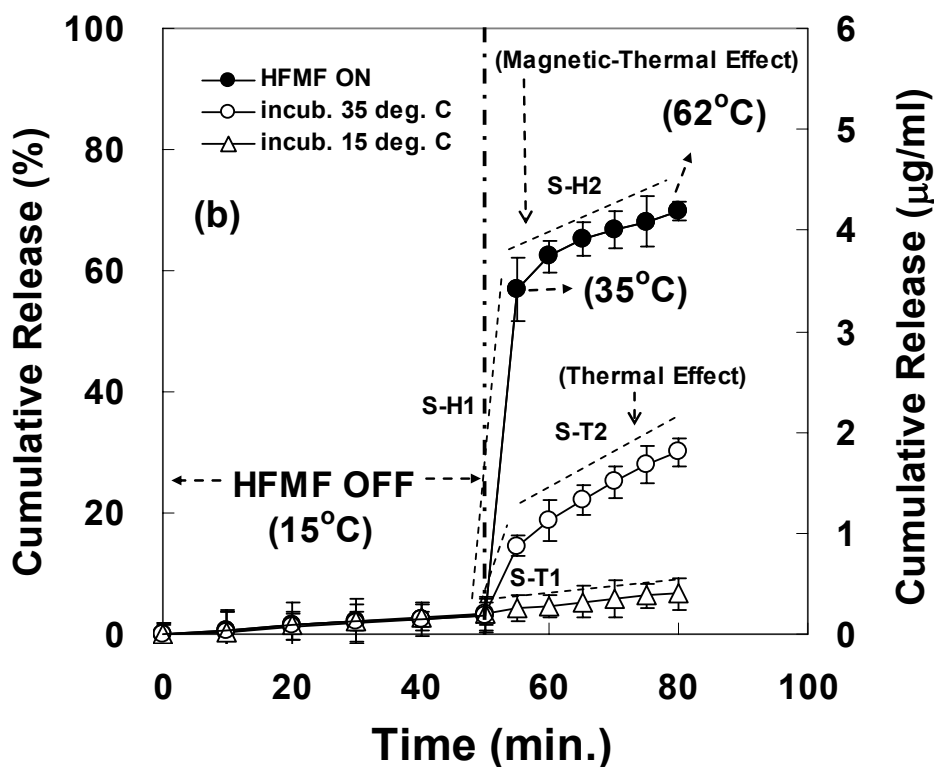


Fig. 8.5 (a) Inductive heating experiments under HFMF treatment; solid circle curve and open circle curve indicate F127-MNPs and F127 nanospheres, respectively; temperature increased to 62°C for the F127-MNPs under HFMF treatment for 60 min, but, for F127 nanospheres, it reached only 30°C; (b) Drug delivery test of F127-MNPs. Solid circle curve indicates that the samples were first incubated at 15°C (water bath) for 50 min and then exposed to HFMF (magnetic-thermal effect). Open circle curve indicates that, after incubated at 15°C for 50 min, the samples were incubated at 35°C in a water bath (thermal effect, without HFMF), but open triangle means the samples have been incubated at 15°C in a water bath (50 + 30 min)

Lu et al. group [Lu, 2005] reported on ferromagnetic cobalt nanoparticles coated with gold shells (Co@Au nanoparticles) embedded into polyelectrolyte capsules. They demonstrated that such magnetic capsules resulted in an increase of wall permeability due to magnetostatic interaction between nanoparticles under oscillating MF. Moreover, a similar mechanism of pore size enlargement under HFMF was also verified by BET analysis in our previous work [Hu, 2007 & 2008].

The average pore diameter of the F127-MNPs was determined to be 7.2 and 11.6 nm without and with 10 min of exposure to the HFMF, respectively, as shown in Fig.

8.6. The pore size after HFMF treatment was approximately twice that without HFMF treatment, and the pore was enlarged and even broken with HFMF treatment. This indicates that the nanostructure of the F127-MNPs can be manipulated with the HFMF and that the corresponding pore enlargement will induce a rapid drug release, i.e., a burst-like drug release pattern.

The insert TEM image of Fig. 8.6 depicts the collapsed and cracked F127-MNPs. This suggests that the instantaneous drug release under HFMF was due not only to the volume shrinkage but also to the pore rupture of the structure. The collapsed situation was caused by a temperature increase due to generated heat, but the pore rupture might be induced by the violent magnetic vibration of nanoparticles under HFMF. Therefore, HFMF-induced energy can cause the vibration of iron oxide and enlarge pores increasing the permeability of the F127 hydrogel. Also, the heat energy was conveyed to shrink the F127 hydrogel to pump the drug out. As a result, an instantaneous drug release was achieved using the F127-MNPs by combining the thermal and dynamic energy (vibration of iron oxide nanoparticles) to pump the drug out. Both factors (heat and enlarged pore size) will increase the permeability of the F127, and thus causing the rapid release of the DOX from the F127-MNPs.

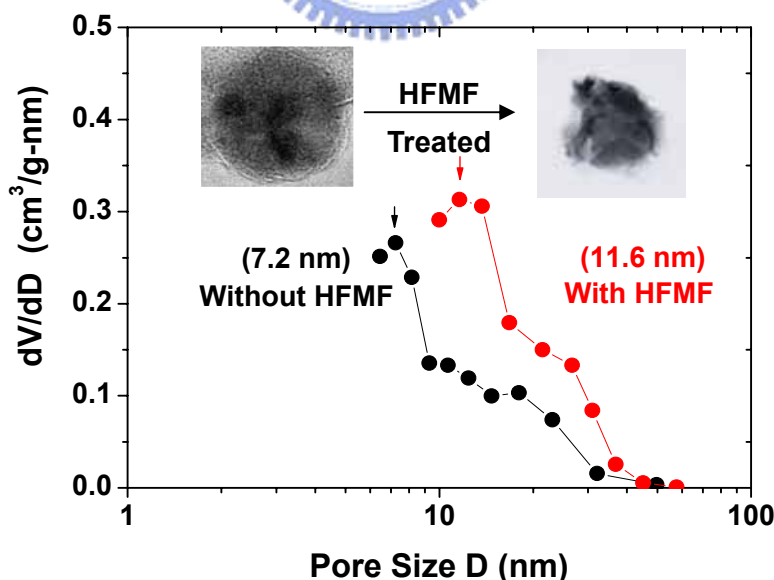


Fig. 8.6 BET analysis on pore size change and TEM images of F127-MNPs with and without HFMF. One sample is without HFMF treatment (left side), and the other one is “after” the magnetic filed treatment (right side) in the TEM images

8.6 Cytotoxicity test

The cytotoxicity of F127-MNPs was evaluated by the proliferation of smooth muscle cell (SMCs), as shown in Fig. 8.7. The result shows that F127-MNPs displays almost non-cytotoxicity compared as control (no F127-MNPs), implying F127-MNPs is belong to biocompatible drug carriers. In addition, it exhibits slightly cytotoxicity when the drug (DOX) loading into the F127-MNPs. It was presumed that a little drug leaked outside by natural diffusion. However, the samples after treated with HFMF exhibited huge cytotoxicity, which means most of cells were killed by bursting drug. Similar results were shown in the optical microscope observation, as illustrated in Fig. 8.8. SMCs grow very well in the both of F127-MNPs without (Fig. 8.8-(a)) and with (Fig. 8.8-(b)) drug loading in the absence of HFMF; whereas most of SMCs died in the samples with drug in the presence of HFMF. Thus, it could be anticipated that F127-MNPs would be used to kill tumor cells by HFMF treatment.

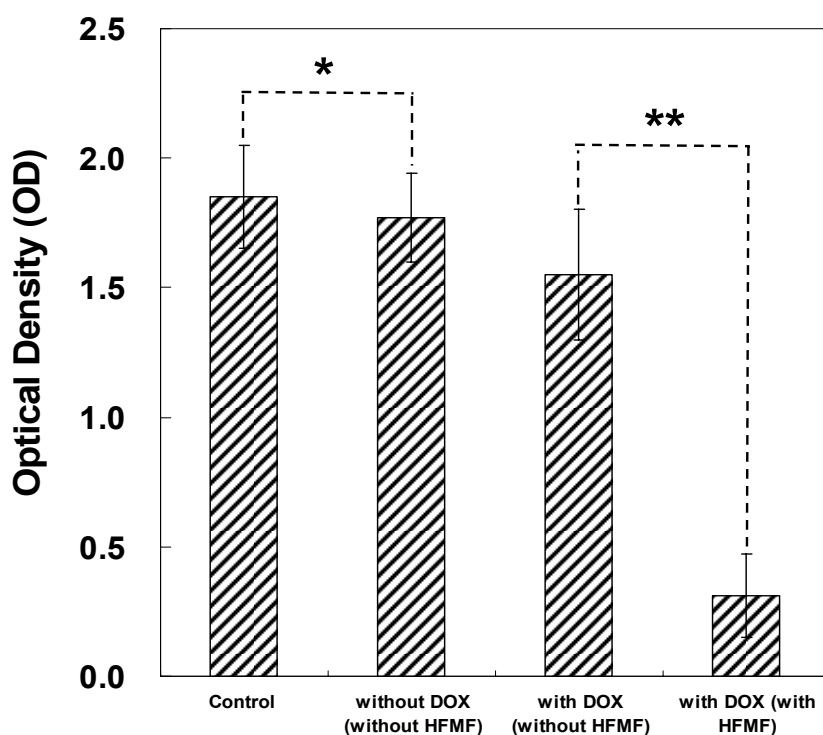


Fig. 8.7 Comparison of SMCs proliferation on the F127-MNPs loading drug (DOX) with and without HFMF by MTT assay. The star means they display insignificant difference, while the double star means that they display significant difference (n=5)

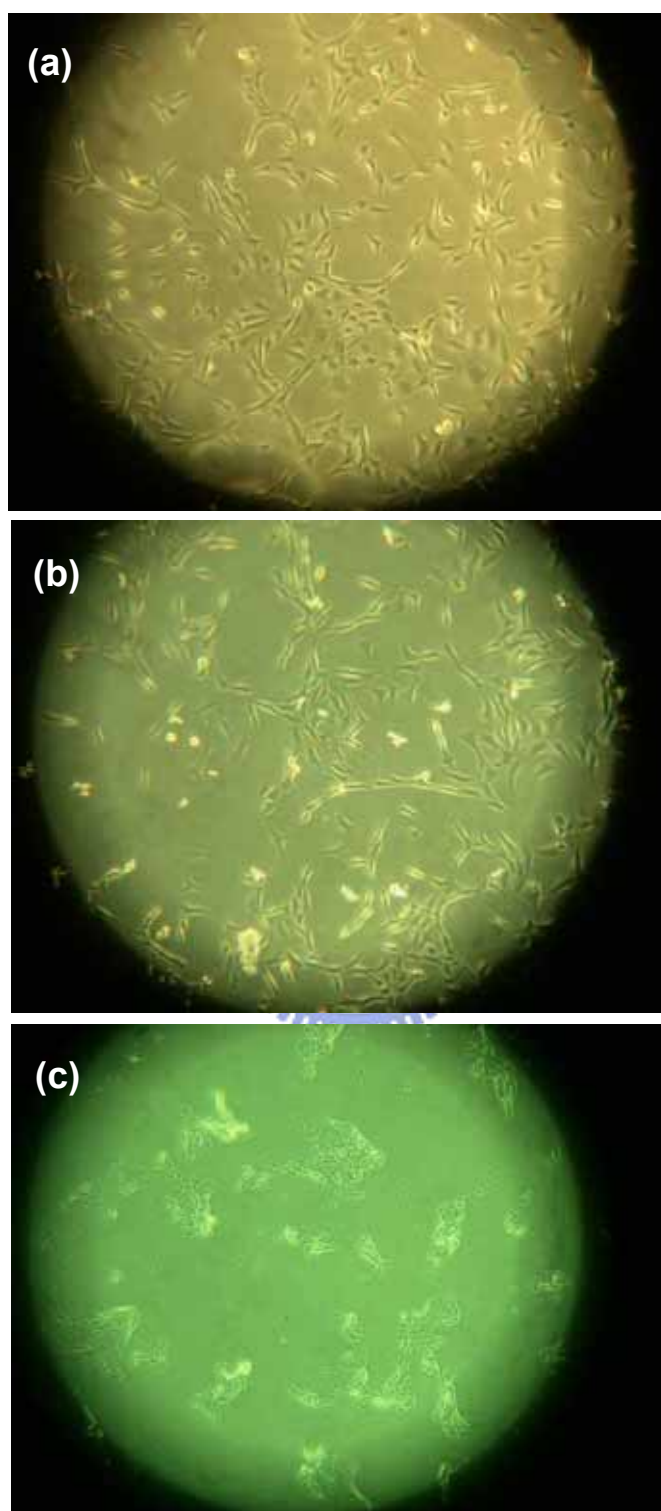


Fig. 8.8 Proliferation of smooth muscle cell for 72 hr incubation in the F127-MNPs (a) without drug in the absence of HFMF; (b) with drug in the absence of HFMF; (c) with drug in the presence of HFMF

Chapter 9

Thermal and Magnetic Nano Ferrocapsules

9.1 Introduction

Intelligent or pulsatile drug delivery carriers are attractive for release of therapeutics, which can be self-regulated, pre-programmed [Stubbe, 2004; Grayson, 2003] depending on presence of specific drug and biomolecule, or can be externally actuated by applying various stimuli from outside environment, such as temperature, pH, light, mechanical signal, electric field, and magnetic fields. Among them, thermally sensitive drug delivery carriers that can be remotely actuated are attractive for therapeutic and patient management [Satarkar, 2008]. One possible approach is to use a composite carrier made of a thermally sensitive polymer micelle with a temperature-dependent drug release profile in conjunction with a magnetic core, so that the core can be self-heated in response to an external magnetic stimulus to trigger the release of drug contained within the micelle. It has been known that application of high frequency magnetic field (HFMF) to iron oxide nanoparticles generates heat due to Neel and Brownian relaxations [Schmidt, 2007; Vaishnava, 2007]. The idea is a natural extension of two concepts, magnetic heating for tumor treatment (i.e., hyperthermia) or drug release and thermally induced volume/hydrophobicity transition in polymers or hydrogels. However, composite magnetic nanoparticles that combine favorable biocompatibility, a fast actuation and a high on-off ratio of drug release operating at about the physiological temperature will require a careful design of material constituents and their self assembly. Here we undertake such a study using poly(ethylene-oxide)-poly(propylene-oxide) (PEO-PPO) block copolymers, crosslinking ligands and polymers, iron oxide nanoparticles and a model drug vitamin B₁₂ [Bae, 2007; Desai, 2001].

In particular, the idea of using external magnetic fields to achieve drug release from polymer composites was first reported by Kost et al. who demonstrated insulin release from a magnetic composite of ethylene vinyl acetate under a low frequency magnetic field [Kost, 1987]. Recently, Paoli et al. reported enhancement in dextran release from a magnetic nanocomposites of collagen under a field [Paoli, 2006].

The latter study as well as our previous work on magnetic ferrogels used iron oxide as the magnetic particles [Lu, 2005; Derfus, 2007]. On thermally sensitive polymers, Choi et al. [Choi, 2006] reported pluronic/heparin nanocapsules that exhibited 1000-fold thermally reversible volume transition when the temperature was raised from 25 to 37°C. The latter study built on the well known properties of PEO-PPO-PEO triblock polymers (commercially known as Pluronic®) that manifest a range of critical micellization temperature (CMT) for volume/hydrophobicity transition, but the volume change of the capsules were further enhanced by introducing cross-linking to the outer shell.

Since both PEO-PPO and iron oxide have excellent biocompatibility, we have chosen them as the basic constituents in the present study. Our nanoparticle thus contains a magnetic core of iron oxide immersed in water and vitamin B-12, a thermally responsive polymer hydrogel with a core-shell structure, and a cross-linked outer shell that serves to fine tune the CMT, the volume change and the drug release characteristics. The hypothesized self-assembly process is depicted in Scheme 1, to be further explained in the next section. The preparation procedure of the nanoparticles and the experimental evidence in support of these Schemes, from transmission electron microscopy (TEM), X-ray diffraction (XRD), dynamic light scattering (DLS) and transport measurements, are described below.

9.2 Fabrication of Pluronic® ferrocapsules

9.2.1 Synthesis of Activated PEO-PPO-PEO Polymers (F127 and F68) [Choi, 2006]

We used two commercial PEO-PPO-PEO thermosensitive polymers, Pluronic® F127 and F68, (Sigma, USA) as the material to form a core-shell nanocapsule in this study. F127 has a (EO)100(PO)65(EO)100 block structure with an EO/PO ratio of 3.08, and F68 has a (EO)76(PO)29(EO)76 block structure with an EO/PO ratio of 5.24. The polymer (20 g of F127 or F68) was dissolved in 60 ml of methylene chloride (Fisher Scientific, USA). In a dropwise manner this solution was added to a stirred solution of 60 ml methylene chloride containing 2 g of 4-nitrophenyl chloroformate (NPC). The activation reaction proceeded with gentle stirring for 5 h at room

temperature under a nitrogen atmosphere. The activated polymer (F127-NPC or F68-NPC) was precipitated, washed five times in ice-cold diethyl ether, then dried under vacuum. To determine the activation density, a known amount of F127-NPC or F68-NPC was treated with 0.2 N NaOH at 25°C for 2 h. The chemical reaction represents in Scheme 9.1-(a)

9.2.2 Fabrication of Activated PEO-PPO-PEO Nanocapsules [Choi, 2006]

Single-layer nanocapsules containing one layer of activated PEO-PPO-PEO were synthesized using a single-emulsification (SE)/solvent-evaporation method. An oil phase (methylene chloride solution, 1 ml) containing various amount of F127-NPC or F68-NPC (0.05-1.5 g) was added dropwise to 10 ml of a water phase (phosphate buffered solution, PBS) at pH 7.4. The mixture was sonicated for 10 min using a horn-type ultrasonic homogenizer (Virsonic, VirTis, USA) operating at 20 kHz to obtain oil-in-water micelles, F127-SE or F68-SE.

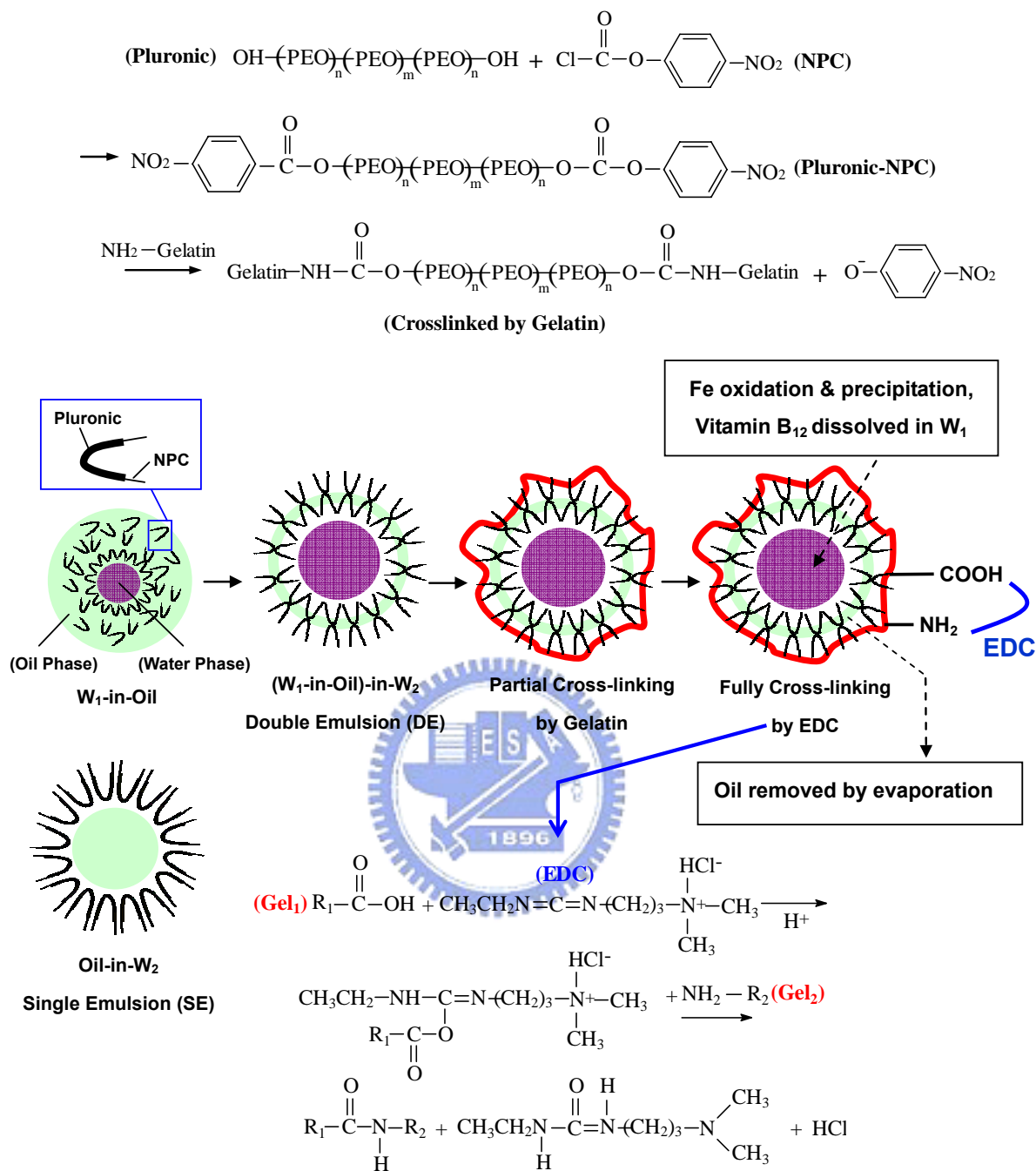
Double-layer nanocapsules containing two layers of PEO-PPO-PEO were synthesized using a double-emulsification (DE)/solvent-evaporation method. The first water phase W_1 (PBS, 0.1 ml) was added dropwise to an oil phase (methylene chloride solution, 1 ml) containing various amount of F127-NPC or F68-NPC (0.05-1.5 g). The mixture was sonicated for 10 min to obtain water (W_1)-in-oil micelles. Next, the micelle solution was added dropwise to a second water phase W_2 (PBS, 10 ml). The mixture was again sonicated for 10 min to obtain W_1 -in-oil-in- W_2 micelles. The sample was called F127-DE or F68-DE (or F127-NPC-DE and F68-NPC-DE to emphasize that the outer shell is activated F127-NPC or F68-NPC.) These emulsion solutions were then dialyzed (dialysis membrane with the Mw cutoff 14,000) and the product stored at 4°C until further use.

9.2.3 Fabrication of Double-layer Cross-linked Pluronic®/Gelatin Nanocapsules

A schematic of the nanocapsules with a cross-linked shell is depicted in Scheme 9.1-(b). Essentially, the F127-DE or F6-DE with NPC is cross-linked with a hydrolyzed amino-acid-polymer (gelatin, Sigma, USA). To introduce gelatin to these double-layer micelles, we modified the second step in their preparation and added gelatin of

various amounts (1-10 mg/ml) to the W_2 phase (PBS) prior to the addition of the W_1 -in-oil micelles. The emulsion of the resultant W_1 -in-oil-in- W_2 micelles was immediately transferred to a water bath at 4°C and held for 24 h to cross-link gelatin. After that, the emulsion solution was stirred at 30°C to remove residual methylene chloride until the solution became clear. In addition, the gelatin can be fully cross-linked with the (dropwise) addition of 1ml of 0.1M 1-ethyl-3-(3-dimethylaminopropyl) carbodiimide (EDC, Sigma) to the above solution, held at 4°C for 24 hr. These emulsion solutions were also dialyzed and the product stored at 4°C until further use. The product after the first-step cross-linking will be referred to as F127-Ge or F68-Ge, and the product after the second-step cross-linking will be referred to as F127-EDC or F68-EDC.

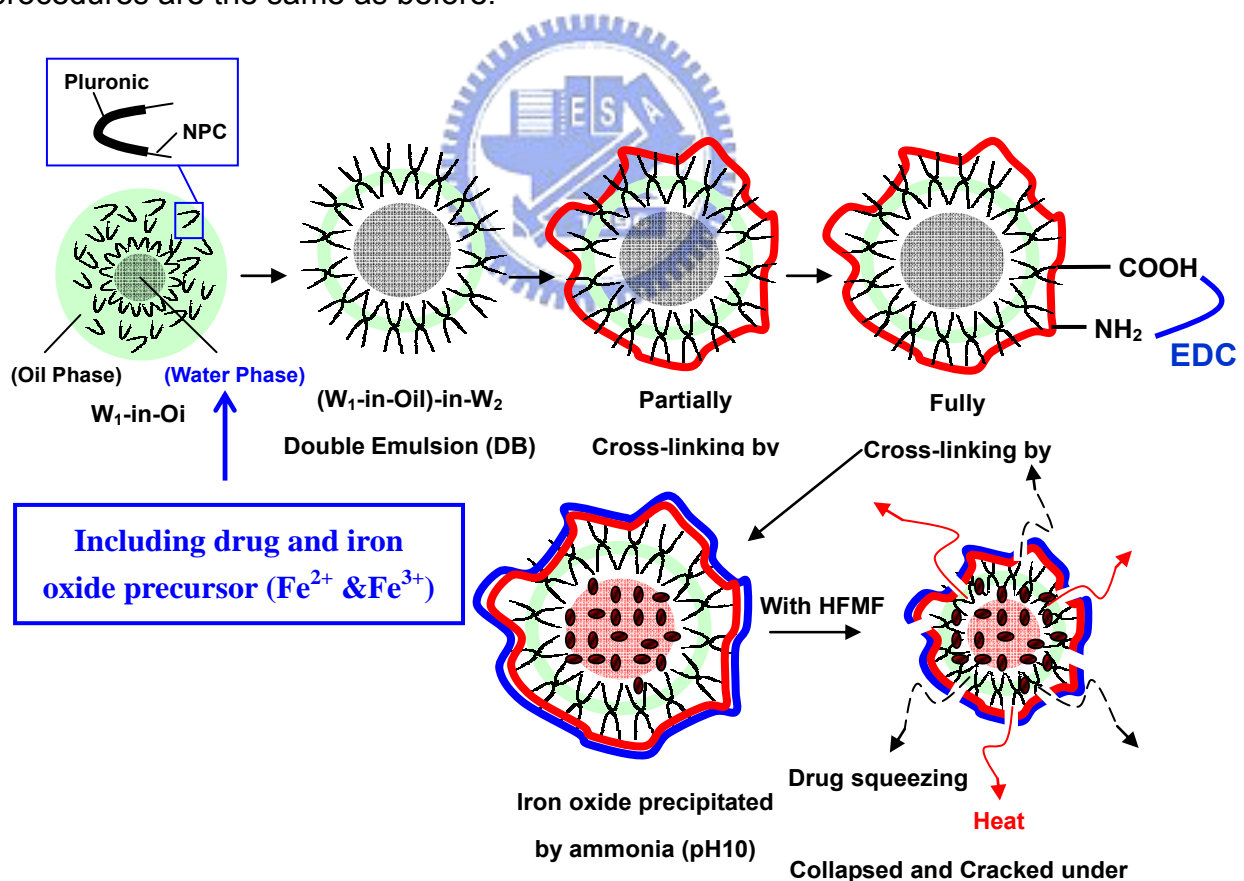




Scheme 9.1 (a) Chemical reaction of activated Pluronic® by NPC; (b) Fabrication of ferrocapsules by single/double emulsion and crosslinked by gelatin and EDC

9.2.4 Encapsulated Drug and Iron Oxide Nanoparticles into Nanocapsules

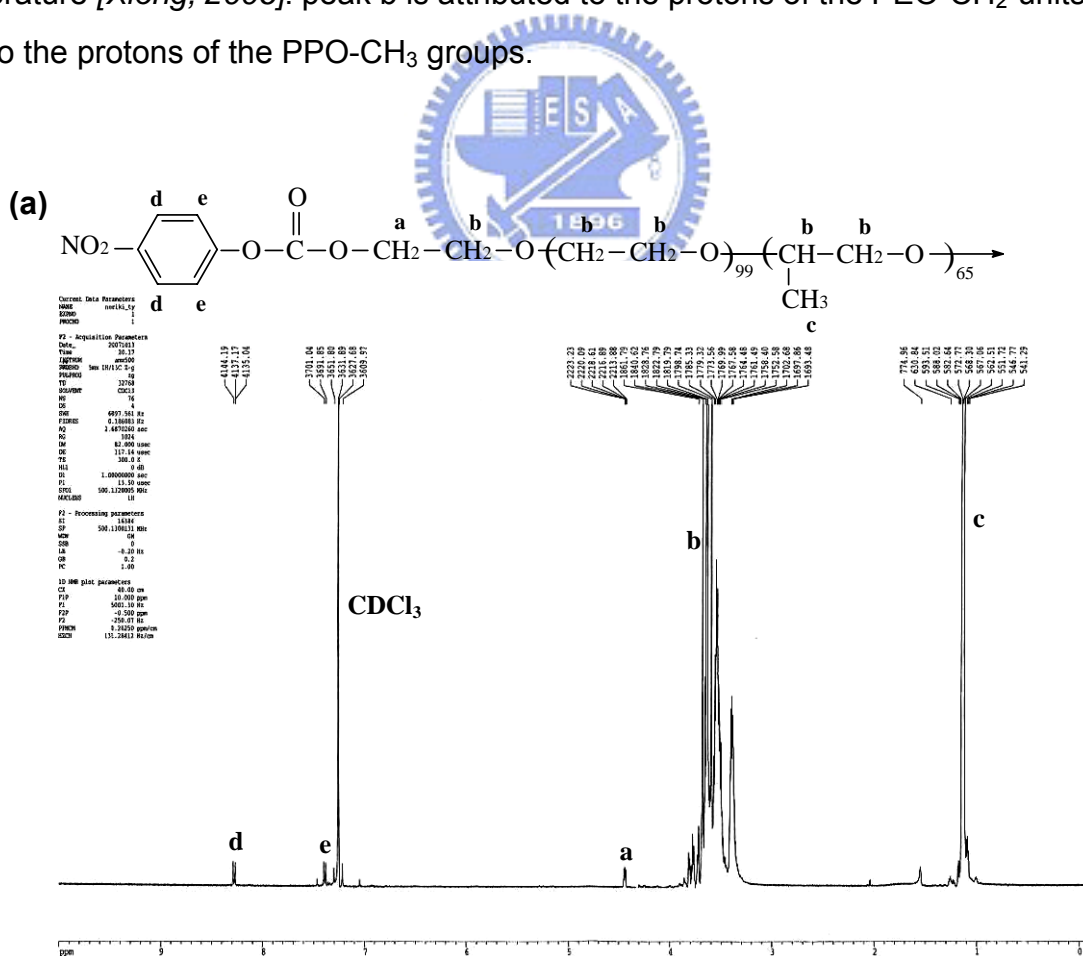
The above procedure was modified to incorporate a model drug vitamin B₁₂ (Sigma, USA), a cobalamin, into the W₁ phase, then using this phase to prepare the double-layer nanocapsules as before, followed by cross-linking. The concentration used was 10 mg/ml vitamin B₁₂ in 0.1 ml PBS. To incorporate iron oxide, we used in-situ co-precipitation of Fe(II) and Fe(III) salts. Briefly, 0.1 ml of 1.08 g/ml of FeCl₃.6H₂O (Riedel-deHaën) and 0.4 g/ml FeCl₂.4H₂O (Fluka), together with vitamin B₁₂ (10 mg/ml) were mixed into the PBS solution to form the W₁ phase, then using this phase to prepare the double-layer nanocapsules as before. After the cross-linking steps, the pH of the mixture solution was adjusted to 10 by adding ammonia solution (33%) under stirring, followed by heat treatment at 60°C for 30 min to precipitate iron oxide particles. This product will be referred to as F68-IO. Other washing and storage procedures are the same as before.



Scheme 9.2 Process of encapsulated drug and iron oxide into the ferrocapsules and mechanism of drug bursting by HFMF (AC magnetic field)

9.3 Structure of NPC-Activated F127 and F68

¹H NMR spectra are shown in Fig. 9.1 for F127-NPC (Fig. 9.1-(a)) and F68-NPC (Fig. 9.1-(b)) in deuterated chloroform (CDCl₃) solution. The activated polymer differs from the unactivated one in that the terminal alcohols on PEO-PPO-PEO are converted into nitrophenyl groups in a chloroformate environment. Evidence for this in the spectrum is labeled as peak d, e and a, where peak d represents the chemical shifts (δ) of protons in the ortho (o)-position (near the -NO₂ side) in the nitrophenyl (NO₂Ph) group, peak e is attributed to the protons in the meta (m)-position (near the -COO side) in the nitrophenyl group, and peak a is associated to -NO₂Ph-OCOO-CH₂ which identified NPC's attachment to the -OH group of PEO. Other peaks are assignable to the solvent CDCl₃ (7.26 ppm) and the PEO-PPO-PEO backbone (peak b and c) similar to the spectra of unactivated polymer reported in the literature [Xiong, 2006]: peak b is attributed to the protons of the PEO-CH₂-units; peak c to the protons of the PPO-CH₃ groups.



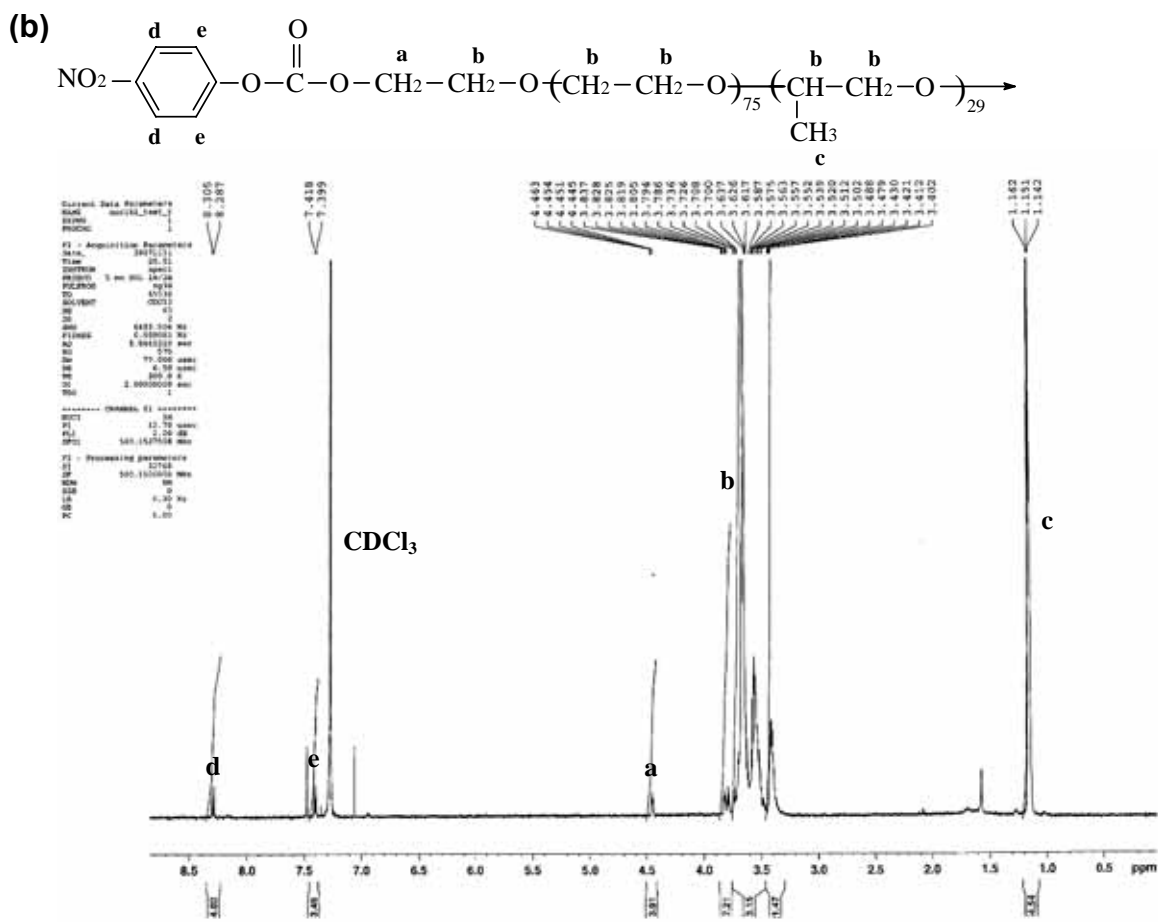


Fig. 9.1 $^1\text{H NMR}$ spectra of activated Pluronic® (a) F128 and (b) F68 by NPC

9.4 Size of Nanocapsules

The size of double-layer F127-NPC and F68-NPC nanocapsules at 25°C are shown in Fig. 9.2. Since these nanocapsules (F127-NPC-DE in Fig. 9.2-(a) and F68-NPC-DE in Fig. 9.2-(b)) are in the form of double-emulsion ($W_1\text{-in-oil-in-}W_2$), we also compare them with single emulsion (oil-in- W_2) nanocapsules (F127-NPC-SE and F68-NPC-SE in Fig. 9.2) and $W_1\text{-in-oil}$ nanocapsules (F127-NPC- $W_1\text{-in-oil}$ and F68-NPC- $W_1\text{-in-oil}$, see insets of Fig. 9.2-(a) and -(b)). For both polymers, the size of the nanocapsules decreases with the addition of the polymer, but the size is always smaller in the F127-series than in the F68-series, and it decreases in the order of $\text{DE} > \text{SE} > W_1\text{-in-oil}$. Moreover, in the case of the DE and SE series, a constant size is reached at around 0.1 g/ml (change unit in Fig. 9.2) of polymer. This critical concentration was used in the further experiment.

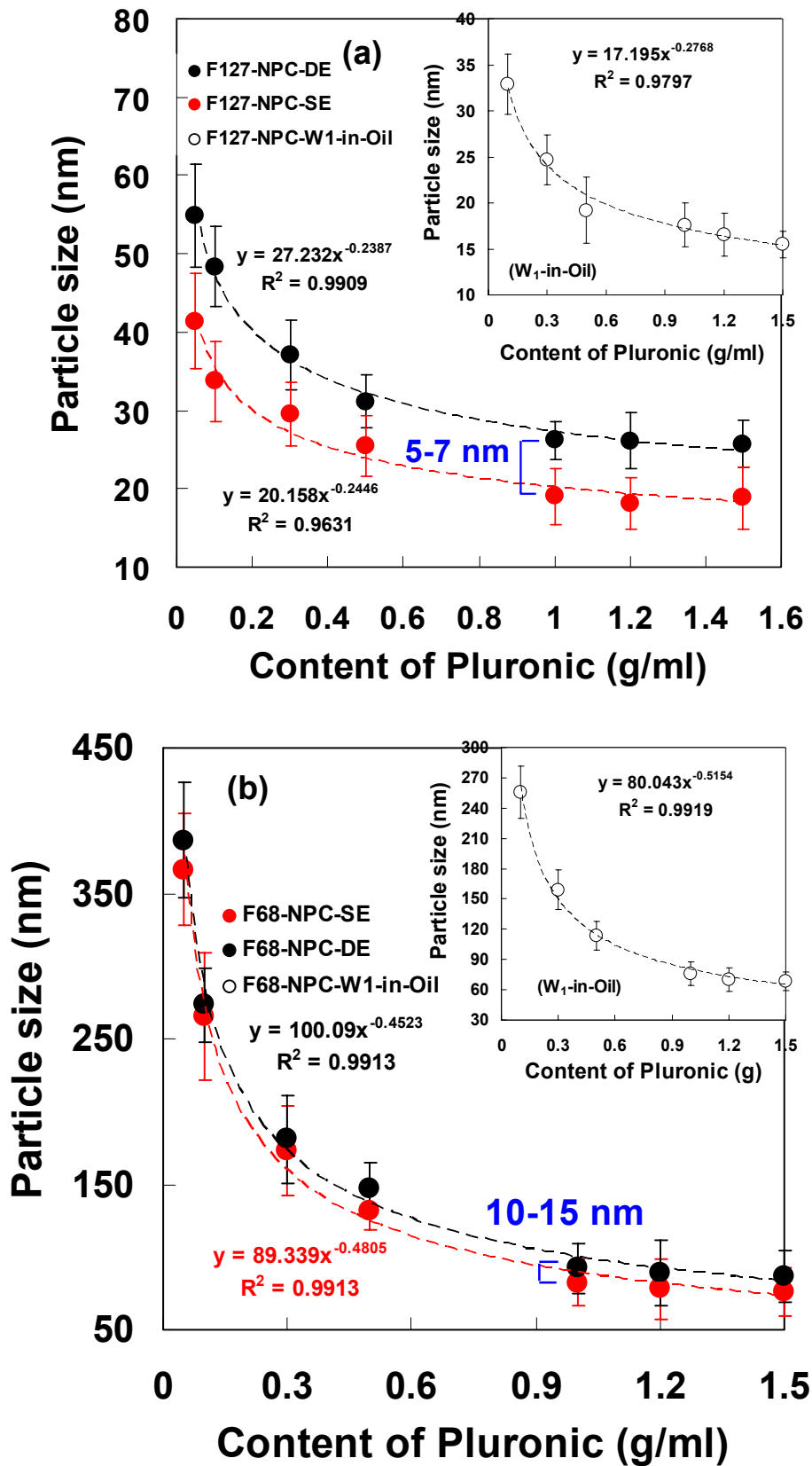


Fig. 9.2 Relationship of particle size and content of Pluronic® (a) F127-NPC; (b) F68-NPC) in the single emulsion, double emulsion, and W1-in-oil process

9.5 Cross-linked Nanocapsules

The size of double-layer nanocapsules F127-NPC-DE was measured after the addition and cross-linking of gelatin, as shown in Fig. 9.3. With the addition of 1 mg/ml gelatin in the W_2 PBS solution, there is a small size increase from a peak value of 28.4 nm to 35.6 nm. Later, we will show that this is mostly due to a small increase of the CMT (from 21.9°C to 22.8°C, see Table 9.1) and not the thickness of gelatin. It is also clear in Fig. 3 that at a much higher concentration of gelatin, the size distribution broadens and a secondary peak at a much larger size develops, indicating some agglomeration of cross-linking between different nanocapsules. Therefore, the concentration of 1 mg/ml gelatin in the W_2 PBS solution was used in the further experiment. Very similar results were found for F68-NPC-DE after gelatin addition and cross-linking as summarized in Table 9.1.

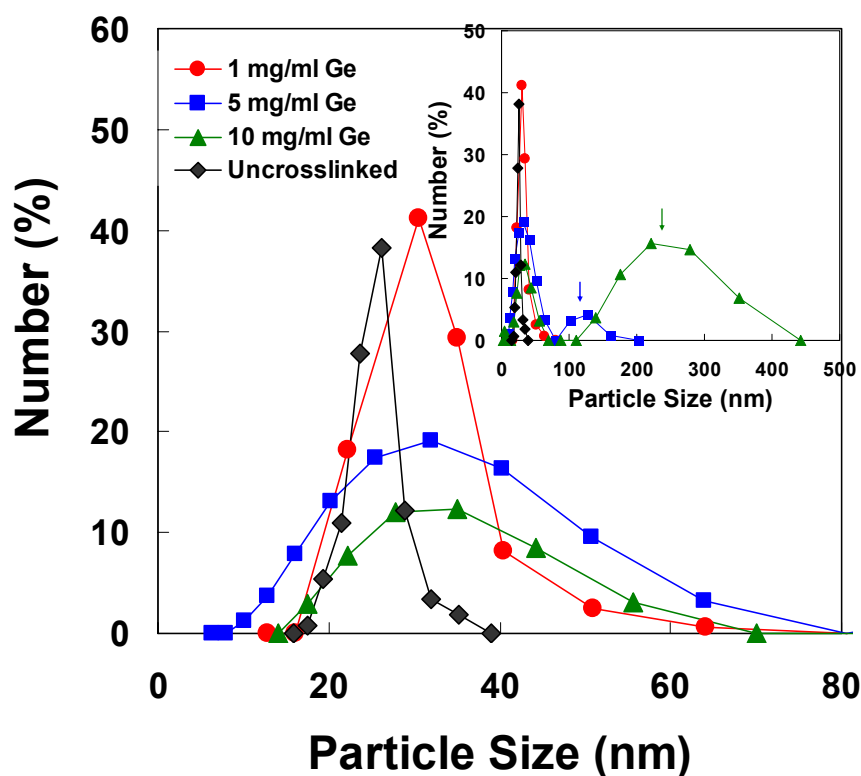


Fig. 9.3 Relationship of particle size distribution and gelatin concentration measured by DLS

In addition, the size of nanocapsules after the second cross-linking step using EDC was measured but a size decrease (from 35.6 nm to 30.5 nm) was found as

shown in Table 9.1 (d_{RT}). A similar trend was found for F68 nanocapsules. Since the change in CMT due to EDC is relatively small, the small shrinkage is largely attributed to a more compact structure after $-NH_2$ and $-COOH$ cross-linking.

Table 9.1 Characterization of F127 and F68-series micelles in the content of 1g/ml Pluronic®

Samples	F127/F68	F127/F68-NPC	F127/F68-Ge	F127/F68-EDC	F68-EDC-IO
CMT(°C)	25.8/43.2	21.9/39.3	22.8/40.1	22.4/39.6	40.5
d_{max} (nm)^a	115.7/143.1	78.2/86.4	91.4/105.3	82.1/97.0	113.1
d_{RT} (nm)^b	60.8/135.2	28.4/85.3	35.6/101.5	30.5/94.2	108.3
d_{min}(nm)^c	23.6/ 22.1	27.3/22.0	27.3/23.8	25.1/23.6	43.1
Size Ratio^d	4.9/6.5	--	3.3/4.4	3.2/4.1	2.6
DR Ratio-1^e	--/12.1	--	-/39.4	-/45.5	57.3
DR Ratio-2^f	--/5.9	--	-/11.6	-/14.3	17.2
DR Ratio-3^g	--/3.5	--	-/6.8	-/8.2	9.5

^a Maximum particle in diameter measured at 10°C for F127-series and 20°C for F68-series

^b Particle size in diameter measured at room temperature (25°C)

^c Minimum particle in diameter measured at 40°C for F127-series and 50°C for F68-series

^d Ratio of size change from 10°C to 40°C for F127-series, from 20°C to 50°C for F68-series

^e Ratio of Drug cumulative release (%) change from 4°C to 45°C for 6 hrs

^f Ratio of Drug cumulative release (%) change from 25°C to 45°C for 6 hrs

^g Ratio of Drug cumulative release (%) change from 37°C to 45°C for 6 hrs

The morphology of F68-NPC-DE revealed by TEM is exhibited in Fig. 9.4. A freshly formed nanocapsule after double emulsion is shown in Fig. 9.4-(a) which has a spherical geometry. It would be found the small activated Pluronic® particle (ca. 3nm) is self-assembly to the geometry of sphere structure (ca. 100 nm), indicating the evidence which the nanocapsule was fabricated originally from a small activated Pluronic® particle. After washing 5 times and dialysis, the nanocapsule has the size (Fig. 9.4-(b)) of about 100 nm, which is very close to the peak value according to DLS (see Table 9.1). After gelatin and EDC cross-linking the size is again similar but a higher electron density has developed on the skin (Fig. 9.4-(c)).

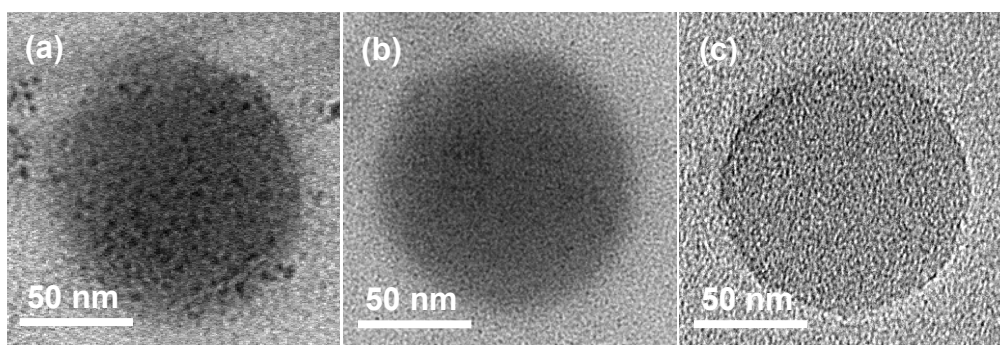


Fig. 9.4 TEM images of formation of 1 g/ml activated Pluronic® F68 nanocapsules: Pluronic® particle is self-assembly to the geometry of sphere structure (a) without washing and (b) after washing; (c) nanosphere was crosslinked by gelatin and EDC

9.6 Nano Ferrocapsules Formation

After the precursors of Fe(II) and Fe(III) salts were incorporated and ammonia solution were added, the iron oxide nanoparticles (IO) start to form by co-precipitation. The X-Ray Diffraction (XRD) was used to examine and it showed five planes of Fe_3O_4 phase, namely [220], [311], [400], [422] and [511] on the activated Pluronic®-F68, indicating the presence of iron oxide nanocrystals, as shown in Fig. 9.5. In particular, extra peak was observed at $2\theta=32.8^\circ$, which became stronger and shaper with the Pluronic® F68-NPC content increasing, indicating some interaction between Pluronic® F68-NPC and iron oxide nanoparticle; on the contrary, the peak in the main plane [311] of Fe_3O_4 phase was broader with the Pluronic® F68-NPC content increasing, implying the particle size of nanocapsules and iron oxide nanoparticle would decrease with increasing Pluronic® content. The further work is in the process to modulate the different particle size of iron oxide nanoparticles by various Pluronic® content addition (as a tank of producing iron oxide nanoparticles) and would reported in the future. Moreover, extra peak at $2\theta=32.8^\circ$ tentatively assigned to iron carbonyl ($\text{C}_9\text{Fe}_2\text{O}_9$), confirmed by JCPDS 21-1141. These results suggest that the iron oxide nanocrystals were structurally encapsulated by F68-NPC.

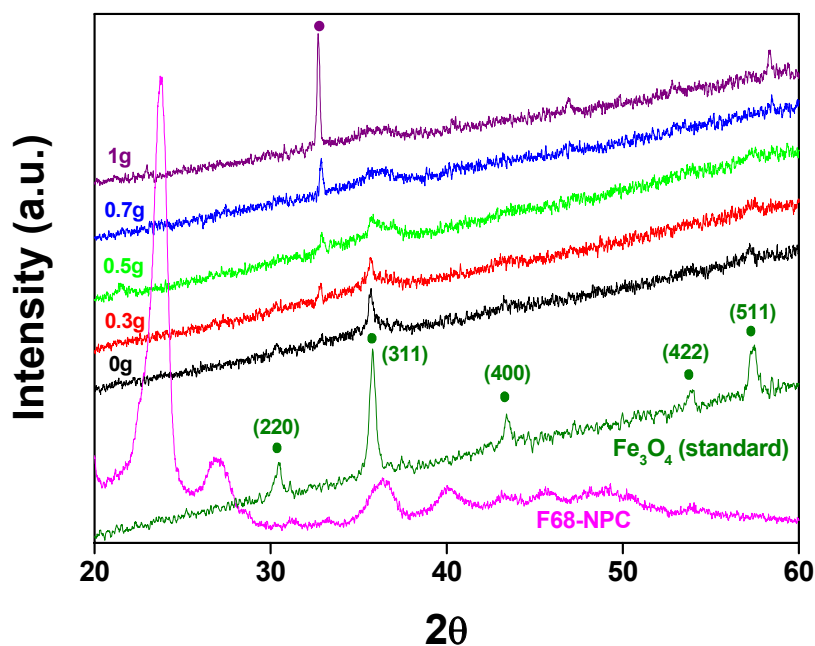


Fig. 9.5 Crystallization change with the Pluronic® concentration increase measured by XRD

Furthermore, Figure 9.6-(a) shows TEM images of fully cross-linked 1g/ml of Pluronic®-F68 nanocapsules by gelatin and EDC and encapsulated the iron oxide nanoparticles (nano ferrocapsules), displaying a spherical geometry of ca. 100 nm in diameter at 25°C. Furthermore, the iron oxide nanoparticles was observed in the slight crystallizing structure in the diameter of 5-8 nm, as illustrated in Fig. 9.6-(a1). It also been proved by diffraction pattern of TEM (see Fig.9.6-(a2)), indicating the presence of iron oxide nanocrystals. Moreover, It could be found clearly the skin layer was formed after gelatin and EDC cross-linking, as shown in Fig. 9.6-(a3). The dense skin layer can avoid and the iron oxide nanoparticles escaping and decrease the drug release rate at lower temperature.

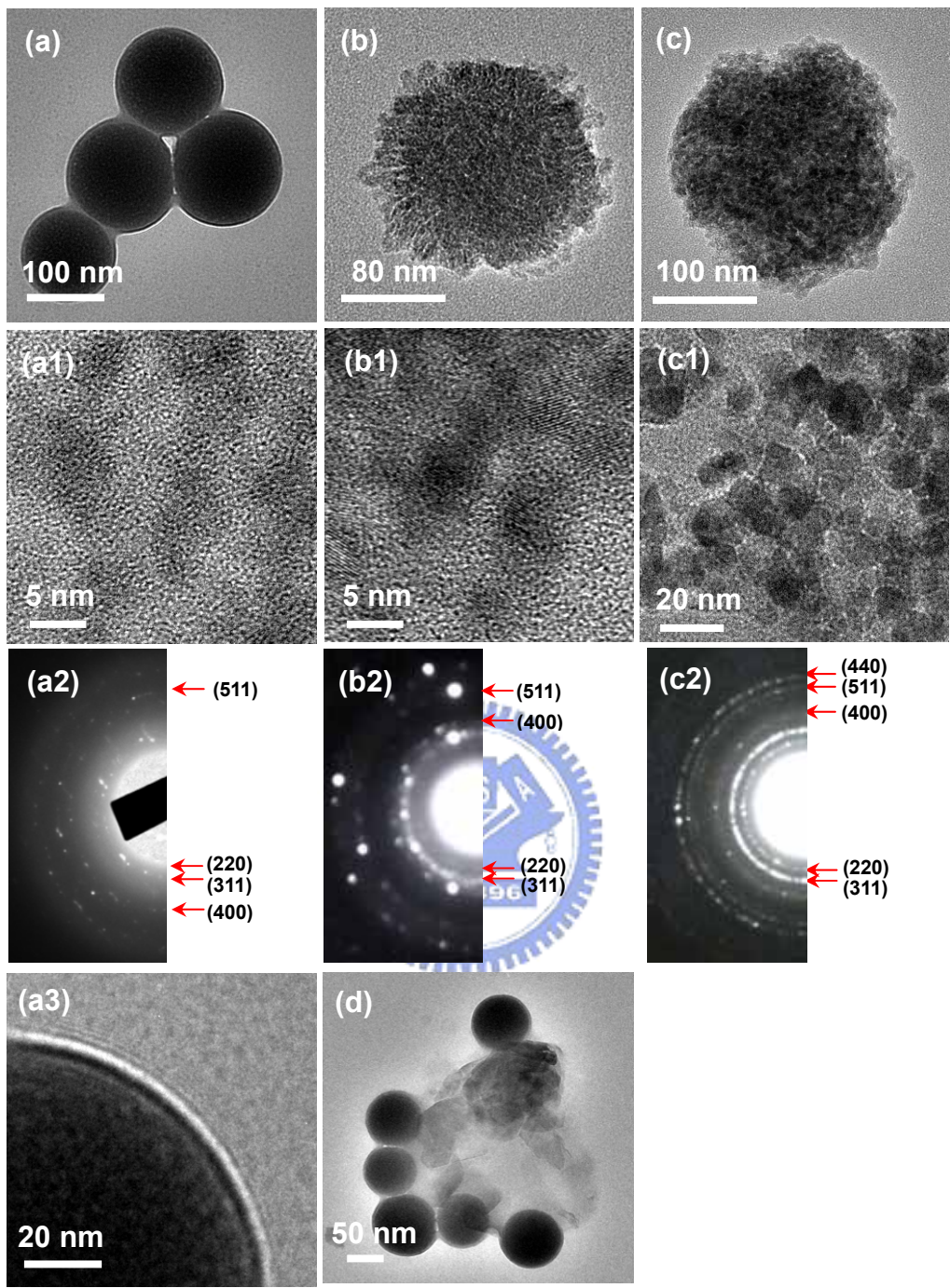


Fig. 9.6 TEM images of (a) 1 g/ml, (b) 0.5 g/ml and (c) 0.3 g/ml of Pluronic® F68-NPC nano ferrocapsules; (a1) 1 g/ml, (b1) 0.5 g/ml and (c1) 0.3 g/ml of iron carbonyl nanoparticles loading in the nanocapsules; (a2) 1 g/ml, (b2) 0.5 g/ml and (c2) 0.3 g/ml of TEM diffraction pattern of ferrocapsules; (a3) Skin layer in the ferrocapsule; (d) ferrocapsules have been disintegrated after HFMF treatment

However, 0.5 g/ml of Pluronic®-F68 ferrocapsules show a spherical-like geometry of ca.150 nm (see Fig.9.6-(b)) in diameter at 25°C, and the iron oxide nanoparticles was observed in the stronger crystallizing structure in the diameter of 8-10nm, as shown in Fig. 9.6-(b1) & (b2). Furthermore, when the concentration of F68-NPC arrives 0.3 g/ml, the structure of ferrocapsule became irregular geometry of ca. 200nm (see Fig.9.6-(c)) in diameter at 25°C, and the size of iron oxide nanoparticle grew up to ca. 15nm, displaying very strong crystallization, as shown in Fig. 9.6-(c1)&(c2). Thus, it provided important evidence that controlling the concentration of Pluronic® to fabricate different size micelles (as a tank to incubate the iron oxide nanoparticles) and thus could dominate the size of iron oxide nanoparticles. In addition, the irregular geometry of ferrocapsules in the 0.3 g/ml Pluronic® addition is attributed to the rare concentration of Pluronic® to make the micelles unstable. Hence, 1 g/ml of Pluronic® F68-NPC addition was used in this study.

9.7 Thermo sensitive behavior

Our nanocapsules exhibit a thermal sensitive behavior similar to that of the PEO-PPO-PEO polymer showing shrinkage above the CMT signifying a hydrophilic/hydrophobic transition. However, the detail of this transition in terms of CMT and volume change is altered by the chemical modification (e.g., NPC, gelatin cross-linking). This was determined by following the DLS peak size as a function of temperature. This transition is manifested by a large volume shrinkage as evident in Fig. 9.7. To analyze the data, we define the CMT as the inflection point in Fig. 9.7, and the size ratio as d_{max}/d_{min} , in which d_{max} is the maximum particle diameter below the CMT at the lowest measurement temperature and d_{min} is the minimum particle diameter above the CMT at the highest measurement temperature. It is clear that the larger size of F68 series nanocapsules is mainly due to a much higher CMT (43.2°C) than that of F127 (25.8°C). (This largely reflects a higher EO/PO ratio in F68, which is 5.24, compared to that of F127, which is 3.08.) In addition, there is a slight decrease (about 4°C) of CMT for activated polymers, presumably because of a hydrophilicity decrease due to NPC. In contrast, there is a slight increase (about 1°C) in CMT in gelatin-cross-linked nanocapsules, and an even minor decrease (about 0.5°C) in CMT

when EDC was added to further cross-linking. These small changes in CMT summarized in Table 9.1 are consistent with the size data at 25°C shown there.

The size ratios of various nanocapsules show a significant decrease as the nanocapsules are cross-linked, although the difference is small when additional cross-linking due to EDC was performed (Table 9.1). Since F68 series always has a higher ratio, it was used in the further experiment to encapsulate iron oxide and vitamin B₁₂. However, although a size ratio of 4.1 (corresponding to a volume ratio of about 67) was observed in F68-EDC after cross-linking, the IO-containing F68 nanocapsule (F68-EDC-IO in Table 9.1) has a considerably smaller ratio of 2.6 corresponding to a volume ratio of 18. From Fig. 9.7, it is clear that the IO addition causes both a decrease of d_{max} and an increase of d_{min}, so both the hydrophilic “swollen” state and the hydrophobic “shrunk” state appear to be sterically constrained from reaching their respective fully relaxed sizes.

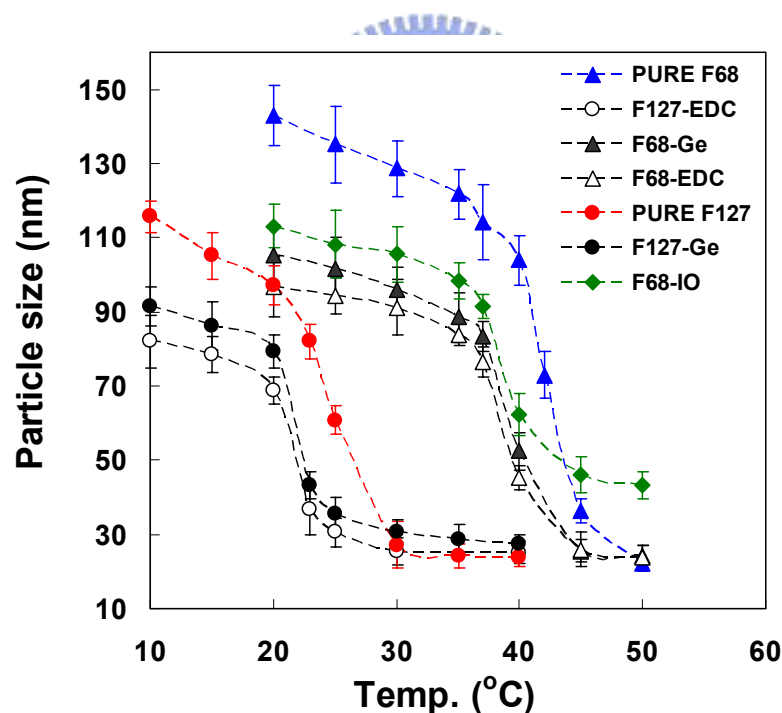


Fig. 9.7 CMT measurement and particle size change with temperature change by DLS

9.8 Drug release behavior

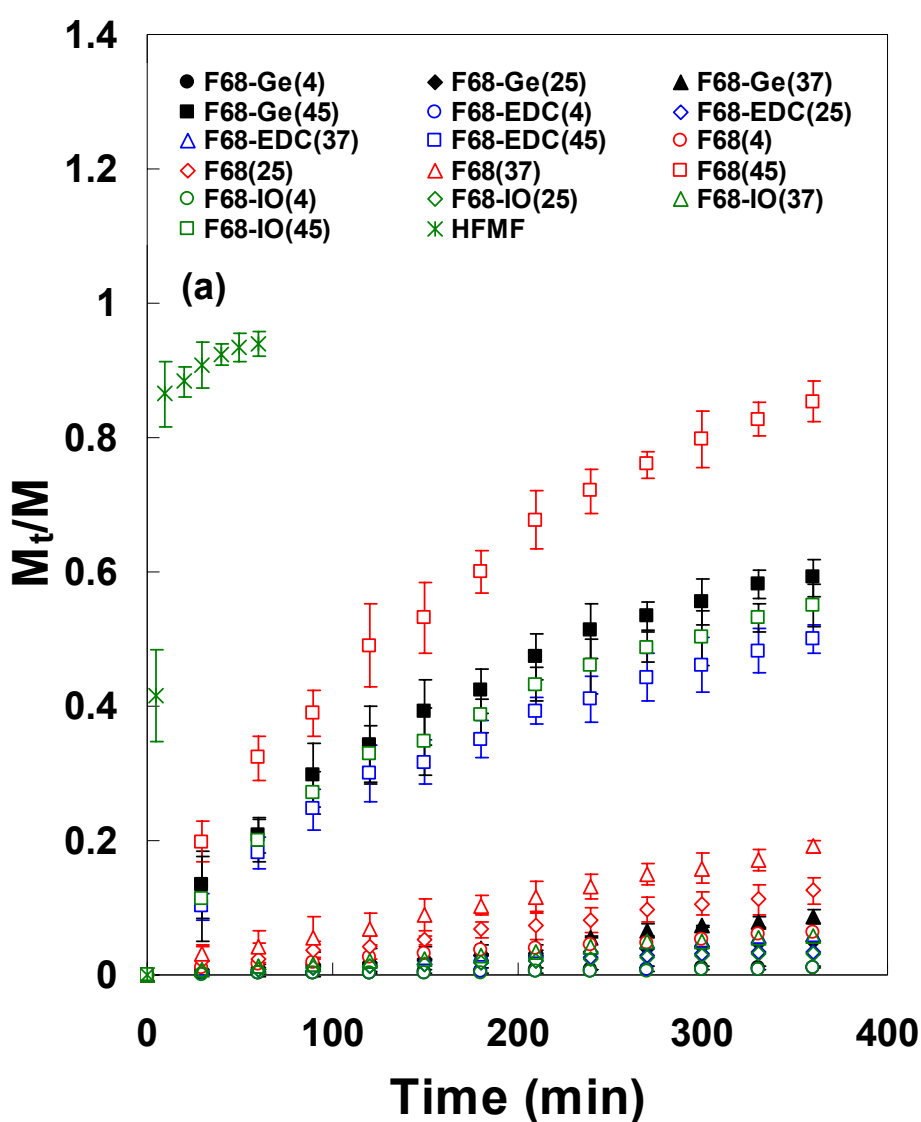
9.8.1 Nanocapsules

Figure 9.8-(a) shows the cumulative released pattern of vitamin B₁₂ from the F68-series nanocapsules. These sample exhibited thermal-sensitive behaviors, indicating a very slow release at 4°C, but the amount of drug releasing gradually increased with temperature increasing. In particular, the rate of drug release in the sample at 45°C (above CMT of F68-EDC) would increase greatly. The ratio of drug release change from 4 to 45°C (DR ratio-1) in Table 9.1 is attributed to the volume shrinking and is about 12.1, 39.4, and 45.5 in the pure F68, F68-Ge, and F68-EDC, respectively. The reason could be that the fully cross-linked by EDC (F68-EDC) exhibits denser porosities, and hence causes the drug released rate decreased, displaying a near zero-order release. Although the drug burst release of F68-EDC would decrease slightly at 45°C, the drug would be difficult to release under lower temperature; hence, DR ratio-1 would be raised (from 39.4 in F68-Ge to 45.5 in F68-EDC). Similarly, the DR ratio-2 (from 25 to 45°C) and DR ratio-3 (from 37 to 45°C) display the similar trend, which were in the order: pure F68 (5.9 and 3.5) > F68-Ge (11.6 and 6.8) > F68-EDC (14.3 and 8.2) in DR ratio-2 and DR ratio-3, respectively. All of results exhibited the fully cross-linked by EDC (F68-EDC) would display the higher DR ratio and could avoid the drug release at lower temperatures, implying it's easy to store at 4°C.

Furthermore, the parameters n were calculated from Eq. (3.2) & (3.3) are listed in Table 9.2 and Fig. 9.8-(b). Some researchers distinguished three classes of diffusional release mechanism from various swellable controlled release systems [Lin, 2005; Ritger, 1987]. The first is Fickian diffusion ($n=0.5$), in which the rate of diffusion is much smaller than the rate of relaxation. In this case, the system is controlled by diffusion (diffusion control). The second is Case II transport ($n=1.0$), where the diffusion process is much faster than the relaxation process. The controlling step is the velocity of an advancing front, which forms the boundary between swollen gel and glassy core. Hence, the system is controlled by relaxation (swelling control). The third class is anomalous (non-Fickian) transport ($n=0.5-1.0$), which describes those cases where the diffusion and relaxation rates are comparable.

The results show that all transport in these nanocapsules is non-Fickian diffusion, with both diffusion- and relaxation controlled systems. The n values of pure F68,

F68-Ge, and F68-EDC were 0.762, 0.773 and 0.776 at 37°C, respectively; however, the n values decreased greatly to 0.588, 0.603 and 0.616 when the temperature increased to 45°C. It was demonstrated that mechanism of drug release transferred from swelling control to diffusion control when the temperature is from low to high, illustrating that the volume shrinkage of nanocapsules from swelling to deswelling state. Moreover, the n value of pure F68, F68-Ge, and F68-EDC were in the range of 0.762 and 0.808 with lower temperature (4°C and 25°C), and the n value decrease slightly with the temperature increasing.



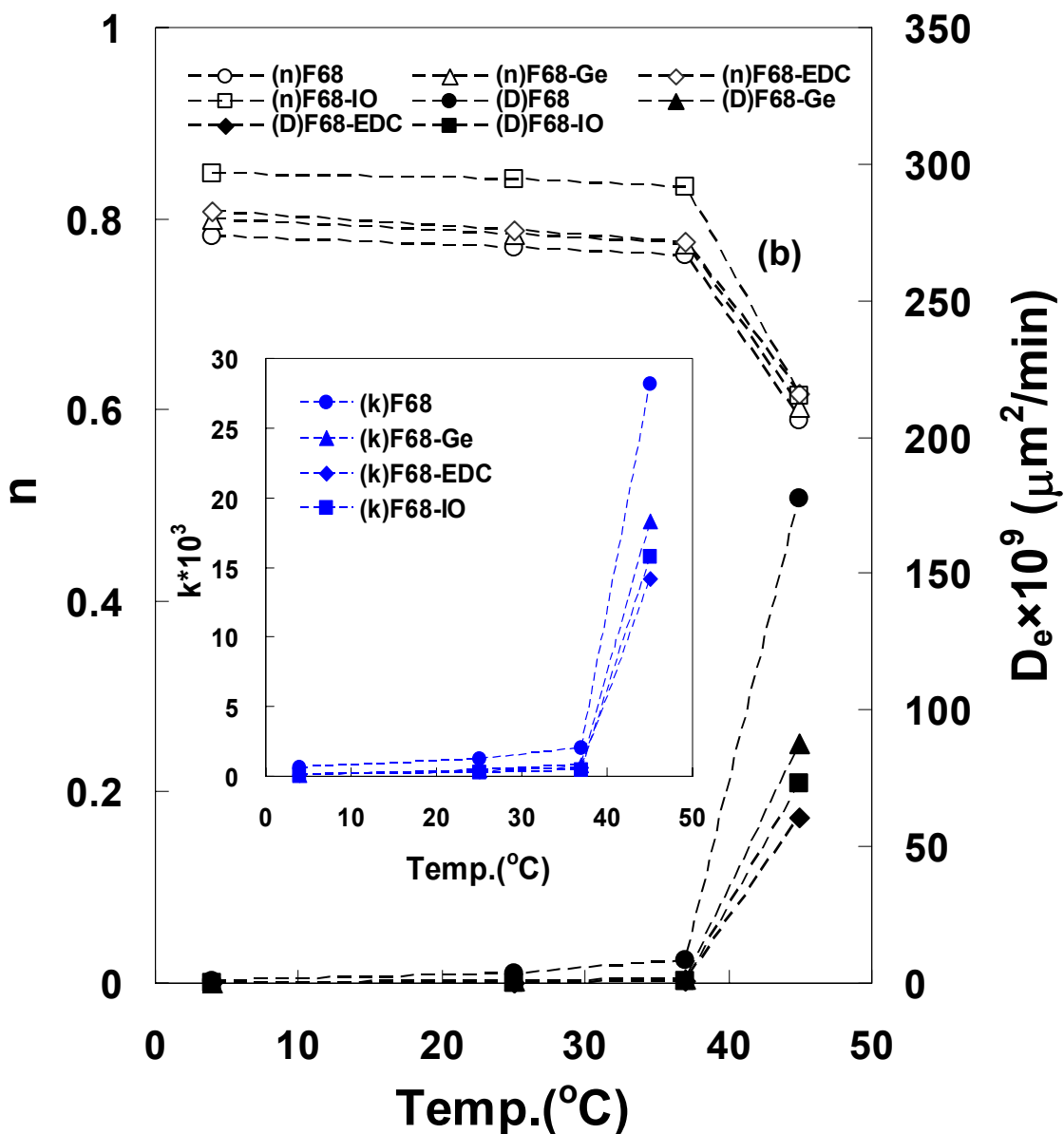


Fig. 9.8 (a) Drug release behavior of nanocapsules and ferrocapsule under thermal and HFMF modulation; (b) calculation of the parameters of drug delivery (n , k and D_e)

Although all of n values are belong to anomalous (non-Fickian) transport, it could be observed that the mechanism of drug release transferred from swelling control to diffusional control when the temperature is from low to high. The reason is the volume compression when the temperature is above CMT, leading to the nanocapsules collapse (water deswelling) and drug release at a faster rate). In this case, the rate of

relaxation is much higher than the rate of diffusion, which means the mechanism of drug release prefer to swelling control; therefore, the n value would be decreased when the temperature increased.

Table 9.2 Calculation of the parameters of drug delivery (n, k and D_e) in the Pure 68, F68-Ge, F68-EDC and F68-EDC-IO

Sample	Temp. (°C)	n	$k \times 10^3$	$D_e \times 10^9$ ($\mu\text{m}^2 \text{min}^{-1}$)
Pure F68	4	0.781	0.62	0.96
	25	0.77	1.22	3.63
	37	0.762	2.00	8.49
	45	0.588	28.15	177.12
F68-Ge	4	0.799	0.10	0.03
	25	0.783	0.47	0.62
	37	0.773	0.79	1.73
	45	0.603	18.26	87.57
F68-EDC	4	0.808	0.07	0.02
	25	0.787	0.33	0.31
	37	0.776	0.59	0.91
	45	0.616	14.18	60.67
F68-EDC-IO	4	0.846	0.05	0.02
	25	0.84	0.24	0.25
	37	0.833	0.41	0.85
	45	0.615	15.71	73.02

In addition, the values of k calculated from Eq. (3.2) & (3.3) in these nanocapsules were in the order: Pure F68 > F68-Ge > F68-EDC with various temperatures (4, 25, 37 and 45°C), and the k value would increase with the temperature raising in the range of 0.05×10^{-3} and 28.15×10^{-3} , as shown in Table 2.

Table 9.2 and Fig. 9.8-(b) lists the effective diffusion coefficients (D_e) calculated from Eq. (3.4). A plot of M_t/M_∞ versus $t_{1/2}$ showed a linear relationship for $M_t/M_\infty < 0.6$. The value of D_e in HA/HEP PEC coating substrates were in the order: pure F68 > F68-Ge > F68-EDC with various temperature, as shown in Table 9.2. The value of D_e would increase slightly with temperature rising below CMT, but increase greatly above CMT. This result is similar with the above cumulative released (%) and the values of k. Among these drugs released parameters, F68-EDC exhibited the lowest drug released rate due to their denser structure below CMT, which means the drug would

be avoid losing when it was stored at refrigerator and pass through the body. Thus, it could be anticipated that F68-EDC nanocapsules would be used to control the drug released rate for clinical therapy application.

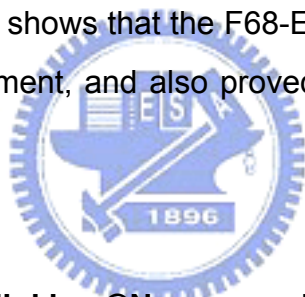
9.8.2 Nano ferrocapsules

Figure 9.8-(a) illustrated the cumulative released pattern of the nanocapsule after encapsulated iron oxide nanoparticles (F68-EDC-IO). F68-EDC-IO also exhibited thermal-sensitive behaviors, indicating a very slow release at 4°C (lower than F68-EDC nanocapsules), but the amount of drug releasing increased rapidly at 45°C (higher than F68-EDC nanocapsules), implying the DR ratio-1 (57.3 times) is higher than F68-EDC nanocapsules, which means the thermo response behavior is better than those without iron oxide nanoparticles. The reason is that the iron oxide occupied some spaces in the nanocapsules to cause the steric barriers and hence the drug is more difficult to release at 4°C, and the diameter of F68-EDC-IO (113.1 nm) is higher than F68-EDC (97.0 nm) at 4°C, implying the drug release would decrease in the expanding nanocapsule. However, the rapid drug release accompanying the volume shrinkage (diameter shrinking: 2.6 times) was found when the temperature rise to 45°C. Although the diameter shrinkage of F68-EDC-IO is just 2.6 times (lower than F68-EDC nanocapsules), the free volume (the space to fill drug) of F68-EDC-IO (with iron oxide nanoparticles occupied) might be lower than F68-EDC, to induce the rapider drug release when the volume shrinking at 45°C.

In addition, the three parameters (n , k D_e) of nano ferrocapsule also were listed in Table 9.2 and Fig. 9.8-(b). The results show that they display similar situations with Pure F68, F68-Ge and F68 at the nature drug delivery. Briefly, all of the value of n in the F68-EDC-IO is anomalous (non-Fickian) diffusion, but mechanism of drug release is inclined to swelling control below CMT and diffusion control above CMT, indicating that the volume shrinkage of nanocapsules from hydrophilic to hydrophobic state. Furthermore, both of k and D_e would increase gently with the temperature increase below CMT, but increase rapidly above CMT.

Figure 9.8-(a) also shows the results of drug release behavior with inductive heating (also called hyperthermia) on the nano ferrocapsules (F68-EDC-IO) in the

presence of the high frequency magnetic field (HFMF). Hyperthermia is a thermal energy from the hysteresis loss of ferrites and is dependent on the type of the remagnetization process in the high-frequency magnetic field (HFMF) [Kim, 2005]. The results showed that under the selected field parameters (50-100 kHz and 15 kW), sufficient energy deposition was achieved and substantially increased the temperature in the solution within a short time period. As expected, it just takes 5 minutes, the temperature arrived at 45°C in the F68-EDC-IO (0.2g samples in the 10 ml PBS of the tube), and this temperature rise is attributed to the hyperthermia effect of the iron oxide. About 40% drug burst in the first 5-min period with HFMF, which was 20 times rate higher than that at 45°C in the water bath, and about 85% drug burst in the 10-min period (ca. 55°C) and then stabilized for the following 60 min of operation. The plausible reason is not only due to the volume shrinkage at higher temperature but also the change in the pore structure of the nanospheres under HFMF. The result in the TEM image (Fig. 9.6-(d)) shows that the F68-EDC-IO nanocapsules have been disintegrated after HFMF treatment, and also proved the nanocapsule was a hollow structure.



9.9 Overall Discussion

9.9.1 Pluronic®/Gelatin Cross-linking @Nanocapsules

The idea to fabricate the activated pluronic® nanocapsules is original from the literature [Choi, 2006]. Choi et al. group reported the thermally reversible Pluronic®/Heparin nanocapsules exhibiting 1000-fold volume transition. The amazing thousands-fold volume change is sufficient to be used in the development of controlled drug release. Thus, the idea of Pluronic® activated by NPC and then cross-linked by biomolecules would be used in our studies. However, some processes would be modified in order to fabricate the optimum drug carriers. First, we used the process of double emulsion (DE) instead of single emulsion (SE) in the literature, because the drug uptake in the DE is much higher than that in the SE. Moreover, the stabilization of the process of DE is better than that of SE, and it can fabricate the thicker and denser shell layer if the process of DE was used. Second, gelatin was used instead of heparin, Poly(ethylenimine), hyaluronic acid, different backbone

lengths of diamine compounds, because gelatin (nature protein) is full of carboxyl and amino group, which means it is easy to crosslink by themselves or convenient to conjugate others molecules you wanted. Third, Pluronic® F68 was selected to compare with Pluronic® F127. The chemical structure is very similar (see Fig. 9.1-(a) & (b)) between F68 and F127, but CMT display huge difference ($\Delta=18^{\circ}\text{C}$, Table 9.1) due to different ratio of poly(ethylene oxide) and poly(propylene oxide) (PEO/PPO ratio) in the block copolymer (F127: 3.08 and F68: 5.24). It was well-known PEO is more hydrophilic polymer; in contrast, PPO is belong to hydrophobic polymer, which means the higher PEO/PPO ratio the more hydrophilic properties were. Thus, F68 displayed the more hydrophilic properties and hence the CMT of F68 is higher than that of F127. The higher CMT (ca. 40°C) in the F68 is better to be used *in vivo*, because the body temperature is about 37°C . It would be better CMT is higher than body temperature, because the huge volume change would happen after heating. Finally, we planed to encapsulate the iron oxide nanoparticles into the inner of nanocapsules, implying the nanocapsules would display dual functional (thermal and magnetic) response behavior. The advantage to use iron oxide nanoparticles is it can produce the heat by itself (do not need to depend surround heat) under a high frequency magnetic field (HFMF) to induce the volume shrinking. It would be discussed in the next section (9.9.2).

The comparison of activated Pluronic® nanocapsules was summarized in Figure 9.9-(a). It shows the plot of the particle size changed with various Pluronic® F127 and F68 concentrations. The results show the multiple cores of F68-NPC nanocapsules were found in the large micelles (ca. 300 nm in Fig. 9.9-(b)) under dilute concentration and single core were found in the small micelles under high concentration (ca. 100 nm in Fig. 9.9-(c)) at room temperature (25°C), implying the amount of Pluronic® addition would modulate the particle size. The single core nanocapsule (Pluronic® addition: 1g/ml) would be used in the further experiment in the present study. Besides, it also was found the ratio of size change in the F127-NPC nanocapsules was smaller than that in the F68-NPC nanocapsules. The reason is that CMT of F127-NPC nanocapsules (ca. 21.9°C) is very close to the room temperature (25°C), but CMT of F68-NPC (ca. 39.3°C) is 15°C higher than room temperature; hence, the solubilization

and hydrophilicity in the F68-NPC nanocapsules were better than those in the F127-NPC nanocapsules at 25°C to induce the particle size in the F68-NPC was twice as big as that in the F127-NPC at 1g Pluronic® addition, as shown in Fig. 9.9-(c) & (d).

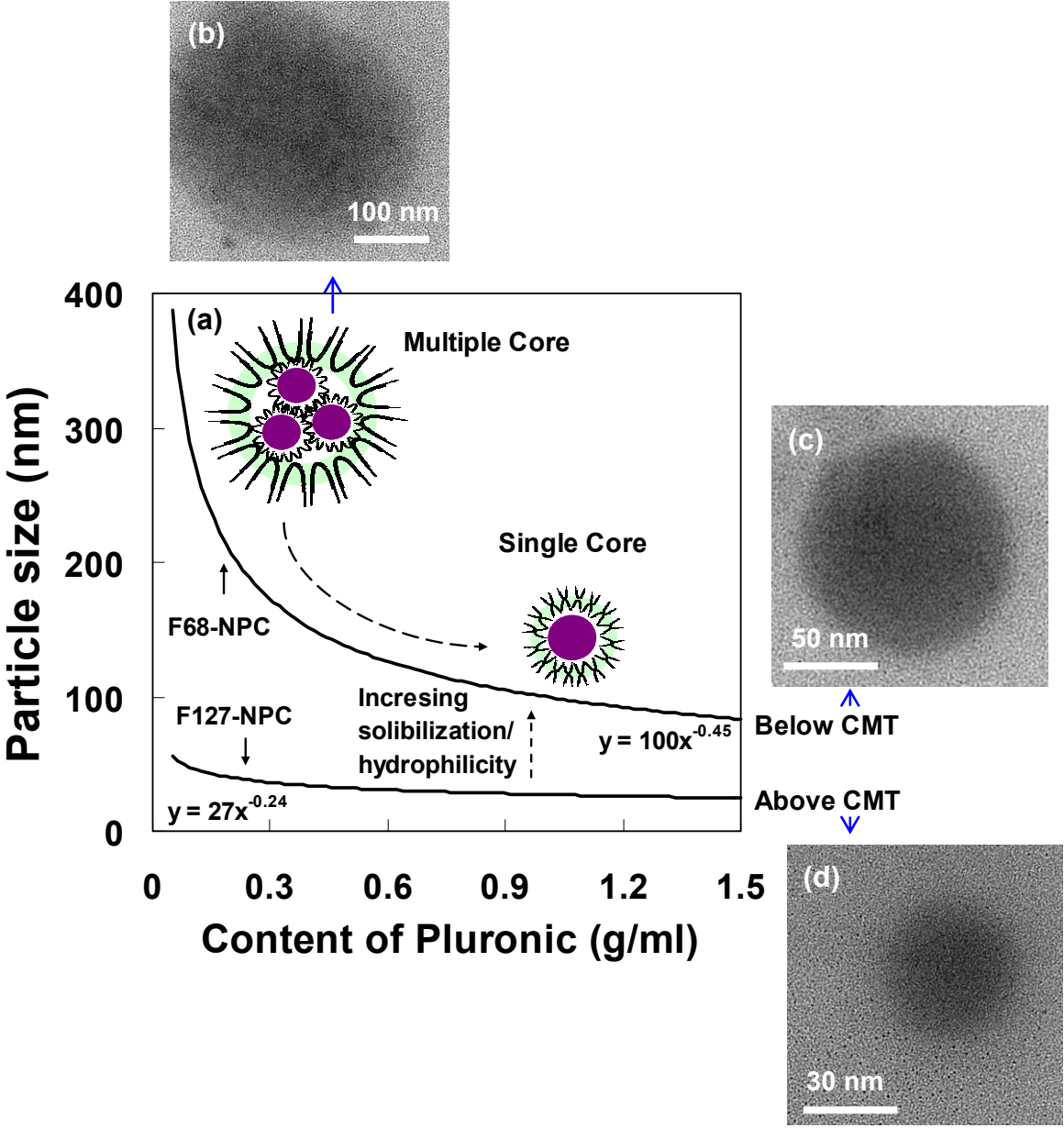


Fig. 9.9 (a) Diagram of comparison of particle size change in the activated Pluronic® F127 and F68 nanocapsules; TEM images of F68-NPC (b) multiple core under dilute concentration (c) single core under high concentration; (d) F127-NPC single core nanocapsules

9.9.2 Pluronic®/Gelatin Nano Ferrocapsules

The iron oxide nanoparticles were formed in the inner of nanocapsules by in-situ precipitated process and the particle size of iron oxide would change with distinct Pluronic® concentrations, as shown in Fig. 9.5 (XRD analysis) and Fig. 9.6 (TEM observation). It could be found the peak in the main plane [311] of Fe_3O_4 phase was broader with the Pluronic® F68-NPC concentration increasing, which proved the size of iron oxide nanoparticles would be changed when the different concentration of Pluronic® was added. It demonstrated this is a feasible method to use Pluronic® nanocapsules as a tank to fabricate different size or shape of iron oxide nanoparticles by in-situ precipitated method. The advantage of this method is focus on the rapid and convenient process and the particle could be well-dispersed when it was formed, compared as the iron oxide nanoparticles directly encapsulated into the nanocapsules (easy to aggregate and difficult to encapsulate).

9.9.3 Thermo sensitive behavior

The thermo sensitive behavior in the F127 and F68 series nanocapsules were listed in Table 9.1 and Fig. 9.7. It shows the CMT of F68-series nanocapsules (above body temperature) is not only much higher than that of F127-series (below body temperature), but also the ratio of size change of F68-series (4.1 times) is greater than that of F127-series (3.2 time). The results shows F68-series nanocapsules are more suitable in the application of thermo response drug carriers. In particular, it still displayed the thermo response behavior when the iron oxide was precipitated and well-dispersed into the inner of nanocapsules, indicating the precipitation of iron oxide nanoparticles would not affect the chemical behavior of Pluronic® (CMT between F68-EDC and F68-EDC-IO were almost the same), but physical behavior would display some change (steric barriers) which the ratio of size change would decrease. However, we assumed that the true ratio of size might not decrease after the occupied volume of iron oxide nanoparticles (5-10 vol%) was deducted.

The main advantage of using Pluronic® F68 is the CMT (43.2°C) is above body temperature, even though it was modified by NPC (39.3°C), gelatin (40.1°C) and EDC (39.6°C). These CMT of Pluronic® F68 is more suitable to be used in the body than

the Pluronic® F127 and some traditional thermo-sensitive polymer, ex. Poly (N-isopropylacrylamide) (PNIAAm, CMT: 30-35°C). Another advantage of Pluronic® F68 is more hydrophilic than Pluronic® F127 and hence the ratio of size change in Pluronic® F68-series (4.1-6.5 times) is higher than that in Pluronic® F127-series (3.2-4.9 times). The ratio of size change in Pluronic® F68-series is still lower than Pluronic® F127/heparin nanocapsules in the literature [Choi, 2006], which exhibits 10-times fold in the diameter, but the stabilization and drug uptake of Pluronic® F68-series are much better than Pluronic® F127/heparin nanocapsules. The reason is that Pluronic® F127/heparin nanocapsules just used single emulsion (SE). We presumed the stabilization in the single layer is not excellent even though cross-linked by heparin. Moreover, it is just partially cross-linking by using heparin in the Pluronic® F127/heparin nanocapsules, which is another unstable factor. In our works, we used double emulsion and make second step cross-linking (fully cross-linking) by EDC to strength the shell layer. Although the ratio of size change exhibit some decrease, the increasing stabilization is good for storage to avoid the drug release.

9.9.4 Drug release behavior

Figure 9.8-(a) shows the relationship between the temperature change and drug release behavior of F68-series nanocapsules as well as drug release by HFMF in the F68-EDC-IO nanocapsules. Briefly, all of F68-series nanocapsules display stable release in the range of 4 and 37°C and the drug release rate would increase gradually with temperature rising (4-37°C), but the rate of release accelerates rapidly when the temperature arrive 45°C (above CMT). The increase of release rate may be attributed to the volume-shrinkage of nanocapsules. Similar report has also revealed in the literature [Chung, 1999] For instance, Chung et al. indicated that the poly(N-isopropylacrylamide) and poly(butyl-methacrylate) polymeric micelles showed reversible structural changes allowing drug release upon heating /cooling fluctuations through the lower critical solution temperature (LCST). These micelles released drug upon heating above the LCST and was accelerated by volume-shrinkage, like a pumping effect, and the effect was eliminated by just cooling below the LCST.

In particular, we are interested in drug release rate at 4°C, because it would be

storage temperature. From the results, the drug release rate of F68-EDC-IO is lowest and in the order: F68-EDC-IO < F68-EDC < F68-Gel < Pure F68. The reason is that the shell layer would be dense after gelatin and EDC cross-linking to reduce the rate of drug release. In other words, the drug is difficult to escape after the shell layer was cross-linked. Moreover, similar to literature, presence of iron oxide particles (Sample F68-EDC-IO) would induce a slight reduction in release rate in the absence of HFMF [Satarkar, 2008]. This is hypothesized to result from hindered diffusion of drug due to the physical presence of the nanoparticles in the network and also potentially from affinity interactions between the drug and the nanoparticles. In the other hand, it was also possible the particle size is slight larger than others at 4°C to induce the lower drug delivery.

In addition, the sample F68-EDC-IO exposed to HFMF would release drug much faster (ca. 20 times) as compared to the sample placed at 45°C water bath. Similar with the literature [Satarkar, 2008], placing the sample in 45°C water bath induces a skin layer to form (surface collapses first), leading to slower diffusion of water out of gel, and hence slower drug release. This effect of collapse is significantly different than the squeezing effect of the uniform heating due to the applied HFMF. Here, the surface starts collapsing first and hence it completely hinders transport of drug from core of the disc to the outside [Kaneko, 1995]. In contrast, the uniform heating in nano ferrocapsules by HFMF is significantly faster process since it internally heats hydrogel as opposed to raising temperature of the surrounding solution. Since the HFMF did not heat water or the polymers, it had negligible effect on swelling properties of control hydrogels. This also implies that the HFMF will induce minimal heating in tissues when used for implant type of applications.

Furthermore, upon magnetic manipulation, the drug showed a two-stage release behavior, the drug exhibits squeezing release for first 10 minutes, and then stabilized release for the following 60 min of operation. The rate of squeezing release in the first 5-min period (ca. 45°C measured in water bath) with HFMF was 20 times higher than that at 45°C in the water bath without HFMF. The plausible reason is not only due to the volume shrinkage at higher temperature but also the change in the pore structure of the nanospheres under HFMF. Lu et al. group [Lu, 2005] reported ferromagnetic

cobalt nanoparticles coated with gold shells (Co@Au nanoparticles) were embedded into polyelectrolyte capsules. They demonstrated that such magnetic capsules resulted in an increase of their wall permeability due to magnetostatic interaction between nanoparticles under oscillating MF. Moreover, similar mechanism of pore size enlargement under HFMF was also verified by BET analysis in our previous work [Hu, 2007 & 2008]. The average pore diameter of F68-EDC-IO nanocapsules were determined by BET to be 6.2 and 12.8 nm without and with exposing 10 min to the HFMF, respectively,. The pore size after HFMF treatment was about twice of that without HFMF treated, and the pore was enlarged and even broken with HFMF treatment.

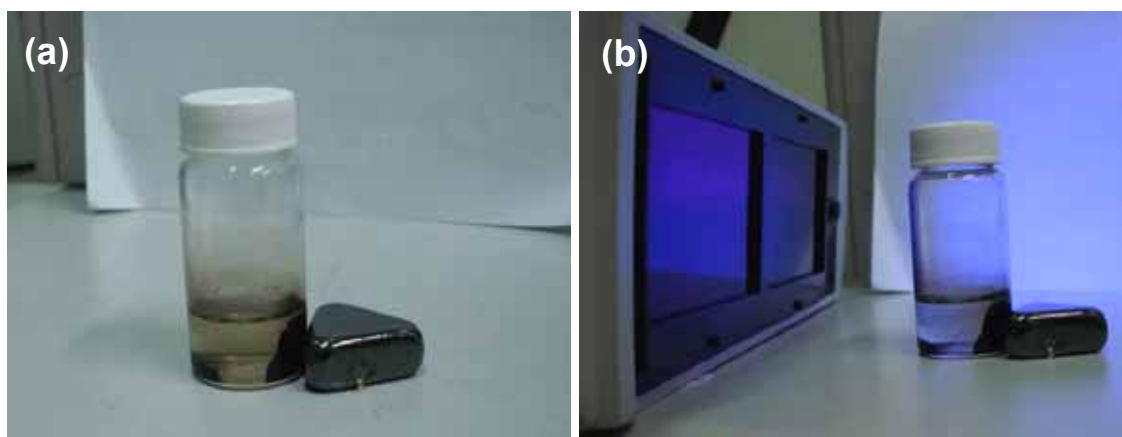
The insert TEM image of Fig. 9.6-(d) depicts the collapsed and cracked F68-EDC-IO nanocapsules. This suggests that the instantaneous drug delivery under HFMF is due not only to the volume shrinkage but also the pore fracture (or pore expansion). The collapsed situation was caused by temperature rising but the pore expansion (or fracture) might be induced by magnetic vibration of nanoparticle under HFMF. The changes in the porosities evidenced that a non-contact HFMF can transfer a kinetic energy into the F68-EDC-IO nanocapsules, and when the magnetic nanoparticles received the energy, the inner structures of the nanocapsules deformed and subsequently produced or enlarged those pores in the magnetic nanospheres. Therefore, the HFMF-induced energy can induce the vibration of iron oxide to enlarge those pores to increase the permeability of the F68-EDC-IO nanocapsules, and also convey the heat energy to shrink the volume of F68-EDC-IO nanocapsules to pump the drug out. Pluronic F68 is thermo-response materials, and it is believed that the nanostructure is changed by increasing temperature. It would achieve the instantaneous drug release using the F68-EDC-IO nanocapsules by combining the heat and dynamic energy to squeeze the drug out. Both factors (heat and enlarging pore size) will increase the permeability of the nano ferrocapsules, and hence cause the rapid and high amount drug-delivery

Chapter 10

Application

10.1 Fluorescence dye release in the ferrocapsules

To demonstrate the release behavior of the fluorescence dye (as model molecule encapsulated in the center) from the ferrocapsules under HFMF, two cuvettes were infused with fluorescence-loaded ferrocapsules dispersed in the aqueous solution. The ferrocapsules encapsulated fluorescence dye (yello-green color) showed no signal of release from the ferrocapsules under UV light detection after 24 hours (Fig.10.1-(a)&(b)), suggesting that the dye molecules were enclosed in the ferrocapsules and effectively inhibited from diffusion to surrounding solution for a time period of 24 hours, where such a time period is far over the time duration required for a metabolic operation in healthy body. However, while applying a high frequency magnetic field (HFMF, 50 kHz and a power output of 15W) to the cuvette for 5 minutes (Fig. 10.1-(c)&(d)), fluorescence dye molecule was detected in the queous solution, indicating the molecules were released rapidly from the ferrocapsules under magnetic stimulus, indicating that the ferrocapsules are highly sensitive to HFMF stimulus and show outstanding remotely controlled release behavior.



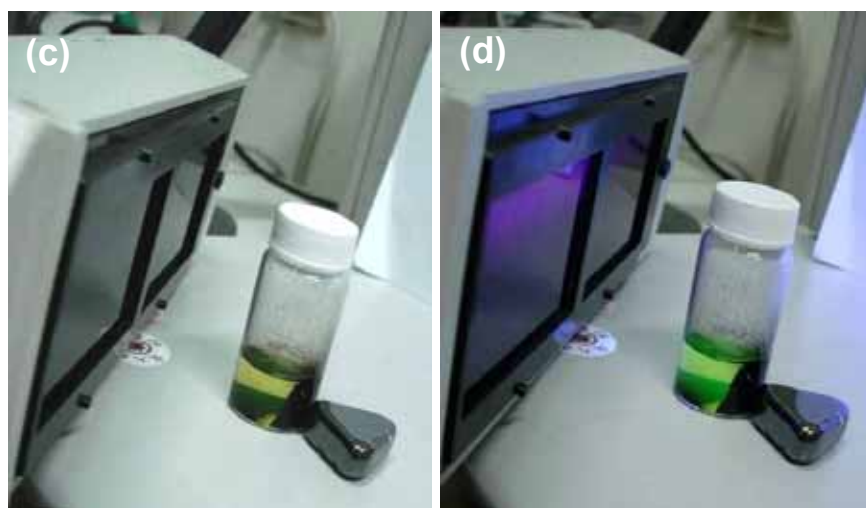


Fig. 10.1 Fluorescence dye release behavior from the ferrocapsules: (a) without HFMF and UV light; (b) without HFMF and with UV light; (c) with HFMF without UV light; (d) with HFMF and UV light

In addition, 1g of these F68-NPC ferrocapsules loading fluorescence dye were dispersed in the 10 ml of 40% (w/v) F127-NPC aqueous solution (F127-NPC-fluids, dissolved at 4°C beforehand) by sonication at 4°C for 6 hr to form F127-NPC ferrofluids. Later, the Si substrate were silanized with aminotrimethoxysilane (ATMS, NH₂-silane, Aldrich) by soaking and sonicating in a 1 wt% toluene solution of ATMS for 1h. After rinsing with toluene and ethanol, and finally sonicating in ethanol for 5 min, they were dried in air. The purpose to use ATMS was it could be as a crosslinking agent between Si substrate and polymer. F127-NPC ferrofluids was spinned coating on the silanized Si substrate and repeated 5 times (5-layer coating, ca. 50 μm), as shown in insert SEM image in Fig. 10.2. NO₂-Ph group of F127-NPC would be conjucted with NH₂ group of ATMS to immobilize on the Si substrate. The coating substrate was immersed in the 10% (w/v) gelatin aqueous solution for incubated 24 h, and then immersed in the 1.5% (w/v) EDC solution for another 24 hr, in order to fully crosslink the F127-NPC layer, which is a protection layer to avoid the ferrocapsule to escape. In addition, F127-NPC layer would transfer to ferrogels from ferrofluids when the temperature above to 23°C (CMT of F127-NPC) to from stable network. The

scheme of the coating process was depicted in the Fig. 10.2.

The resulting samples would release the fluorescence dye under HFMF treatment for 5 min, but it would not work in the absence of HFMF, as shown in Fig. 10.3. Fig. 10.3-(a)&(b) depicted that no signal (yellow-green color) before and after UV light exposed without external HFMF. However, the signal was detected in the Fig. 10.3-(d), it exhibited that yellow-green color when UV light exposed, implying the dye was bursted in the presence of HFMF. According to this simple trial, we believed that it could be applied in the biomedical device, such as biochip and intelligent drug delivery system, by magnetic field modulation in the future.



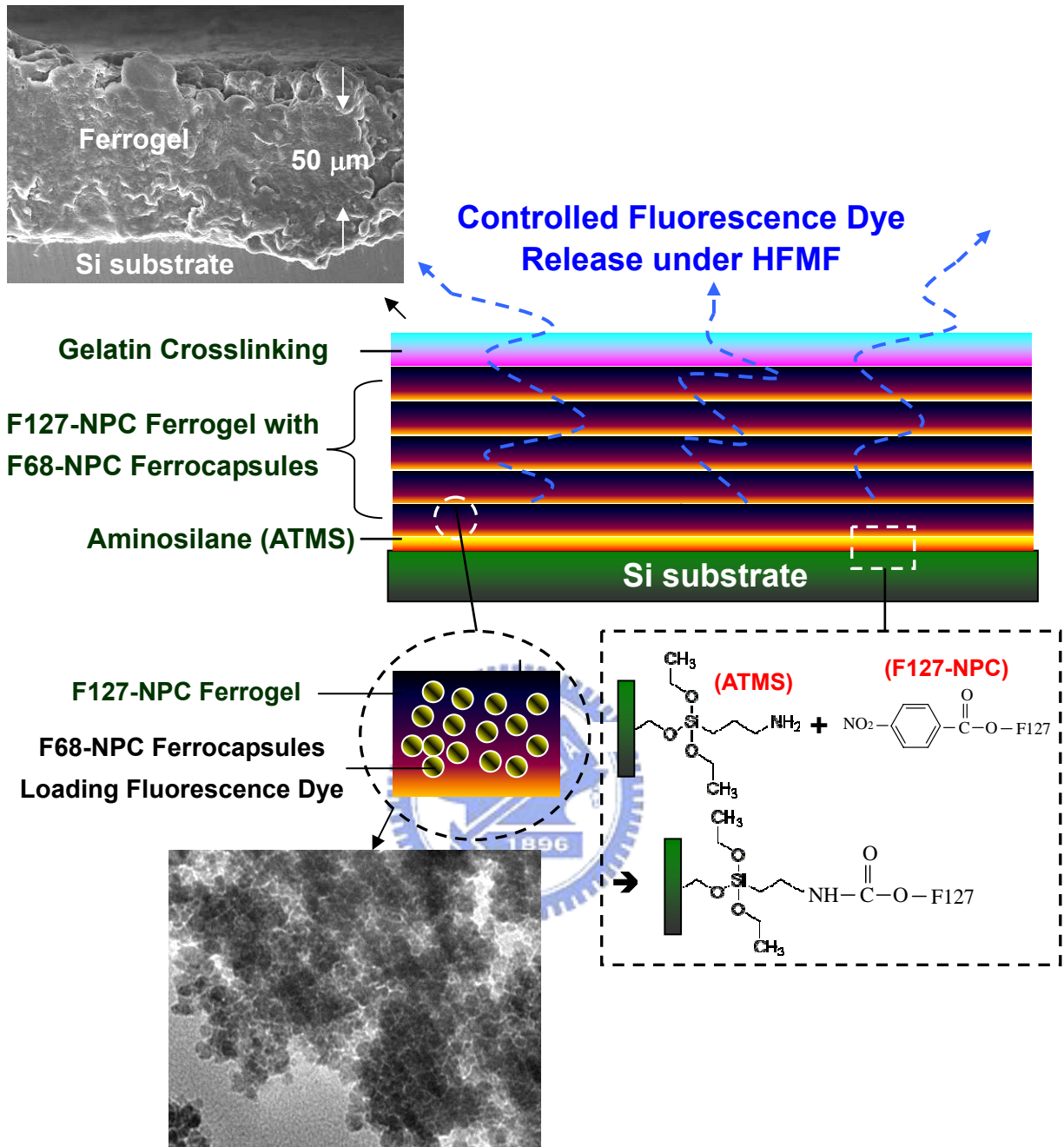


Fig. 10.2 Scheme of the coating process and chemical reaction of F127-NPC ferrofluids loading F68-NPC ferrocapsules on the Si substrate

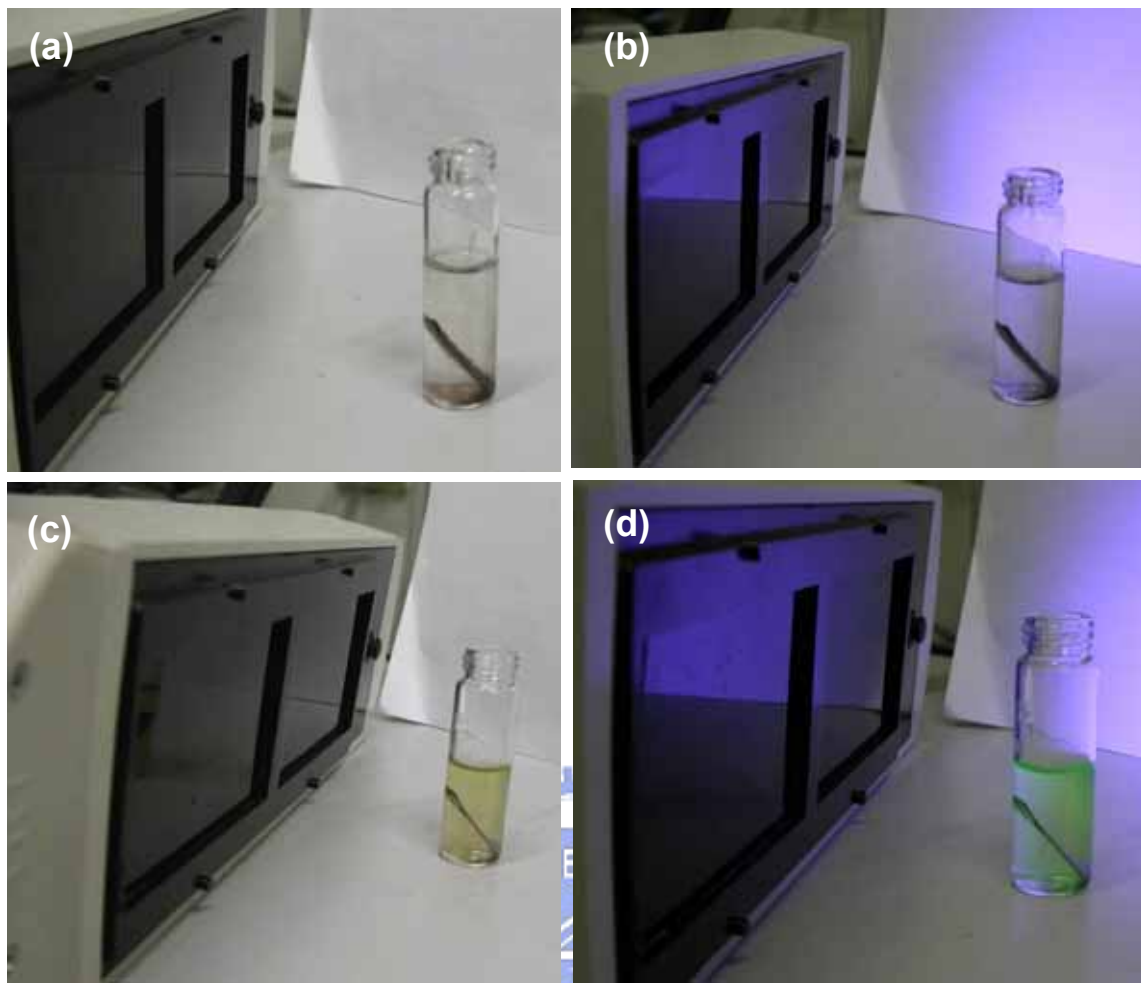


Fig. 10.3 Fluorescence dye release behavior from the Si substrate coating with ferrogel (a) without HFMF and UV light ; (b) without HFMF and with UV light ; (c) with HFMF without UV light ; (d)with HFMF and UV light

Chapter 11

Conclusion

11.1 Biodegradable Ferrogel (Gelatin)

1. It could be anticipated that this smart magnetic hydrogels in drugs carriers to control the drugs release rate under a MF controlling.
2. Softer ferrogels cause the more obvious magnetic sensitive properties of drugs release in MF switching “on” is demonstrated.
3. Nano-ferrosponges with tunable magnetic sensitive behavior were successfully prepared by an in-situ synthesis of magnetic nanoparticles in the presence of gelatin.
4. Nanopores with size ranging from 2 to 100 nm in diameter can be synthesized within the magnetic nanoparticulate network .The nanopores are then manipulated with a reduced size by externally controlled magnetic field, which allows the resulting ferrosponges suitable for control release of active agents.
5. Release kinetics of a model drug, i.e., vitamin B₁₂, also showed a series of tunable kinetic parameters under magnetization, and this finding allows a slow release of drug molecules achievable for practical uses.
6. Ferrosponge with optimal 5G-5F composition was evaluated, where an optimal “magnetic sensitive behavior” was detected as a result of its stronger Ms and looser polymeric structure.
7. Ferrosponge with 5G-5F composition also illustrated a considerably improved anti-fatigue property under repeated on-off MF operations for a consecutive drug release control.

11.2 Non-Biodegradable Ferrogel (PVA)

1. A PVA ferrogel with magnetic-sensitive properties has been successfully prepared by mixing PVA hydrogels and Fe₃O₄ magnetic particles through freezing-thawing cycle.
2. The best “magnetic-sensitive effects” in the DC magnetic field are observed in

PVA5-LM17 ferrogel due to its stronger M_s and smaller H_c . The order in the DC is PVA5-LM17 (150-500nm)>PVA5-SM17 (5-10nm)>PVA5-MM17 (40-60 nm).

3. The phenomenon is totally different from the magnetic-sensitive behavior in the AC magnetic field. PVA5-MM17 ferrogel would exhibit the highest drug bursting in the AC magnetic field, whereas the PVA5-SM17 is lowest, which is in order: PVA5-MM17>PVA5-LM17 >PVA-SM17, as related to the area of hysteresis curve.
4. H_c and M_s in the ferrogel would play an important role to judge the magnetic response behavior in the different magnetic field (DC and AC magnetic field)
5. Amount of drug release can be controlled by fine-tuning of the switching duration time (SDT) through an externally controllable on-off operation of the given magnetic field.
6. It was found that the amounts of the drug released from the ferrogel can be controlled by changing the duration time between each on-off operation of the magnetic field. This observation suggests that the controlled release of drug with adjustable amount can be properly designed for practical needs.
7. Effect of the Fe_3O_4 and matrix PVA on the magnetic-sensitive behavior of ferrogels also was systematically investigated. Magnetic sensitive behavior map in terms of Fe_3O_4 concentration was constructed and the behavior reached a "saturation" region in the range of 17-34% Fe_3O_4 . Below or above that region, a reduction in the magnetic sensitive behavior was observed
8. Both the concentration dependence of the magnetic sensitive behavior with respect to PVA and Fe_3O_4 can be explainable in terms of a space restriction model (translated into available free volume) and magnetization (translated into the interaction energy).
9. These two factors impose opposite effect to the resulting magnetic sensitive behavior, and accordingly, an optimal combination of both available free volume and interaction energy can be found for the ferrogels with a composition of 17-34% Fe_3O_4 and 10-12.5% PVA.
10. It is anticipated that the ferrogels with an optimal mixture of PVA and Fe_3O_4 displays a magnetic-sensitive behavior that permits the ferrogels technologically

applicable as a microdevice for delivery of therapeutic drugs in a highly controllable manner.

11. This novel ferrogel that displays a magnetic-sensitive behavior can be used as a microdevice with simple and precise control of mechanical movement of the ferrogels for controlled delivery of therapeutic drugs.

11.3 Thermal sensitive Ferrogel (Pluronic®)

1. Novel thermo-sensitive ferrofluids were successfully synthesized with core-shell MNPs and F127-fluids, and can be modulated by temperature changes to form ferrogels.
2. By its thermo-triggered operations and higher drug uptake properties, it is potential that this typed F127-ferrofluids can be applied as a biomedicine application, such as drug carriers.
3. The dual-functional (magnetic/thermal) drug carriers were successfully fabricated by in-situ and self-assembly process, and the core-shell structure was examined by TEM, XRD, Raman spectra and XPS. Furthermore, the thermal sensitivity of F127-shell MNPs also was measured by controlled-temperature UV-Vis spectra, PL, and DLS.
4. The unique feature of our novel drug carriers is that it is possible to load amphoteric drug (or a combination of drug) that can partition into the F127 shell surrounding iron oxide nanoparticles.
5. The actuating mechanism of this-type drug carrier is used the hyperthermia to arise temperature. When the arising temperature is higher than CMT or LCST, the drugs can be burst from the dual-functional drug carriers by the volume compressed.
6. By an external oscillating MF, the heat source can be produced to induce the instantaneous drug delivery by sharply volume transition (10-fold) from 15°C to 35°C, which is approximately 5 times higher at first 5-min than that just by incubation at 35°C water bath.
7. This bursting drug delivery is very important to tumor and some emergency

therapy. In addition, the F127-shell MNPs can produce heat by hyperthermia, which not only provides thermal response on the F127 shell, but also kills the tumor cell when the temperature rises above 40°C.

8. Therefore, the dual functional magnetic drug carriers offer a promising technology for “switchable” drug release in the biomedical studies by using an external magnetic field.
9. However, it would be better if CMT of F127-MNPs can be raised to 40°C, because it is more suitable and potential for human body, which means it will release drug at 40°C but stop at 37°C.
10. It is in the progress in our group to synthesize the Pluronic series by covalently bonding with hydrophilic compounds in order to achieve the higher CMT. In other words, it is also possible to functionalize our F127-shell MNPs with ligand or antibodies to further enhance their potential, including as agents (ex. quantum dots) for magnetic imaging or tracking.
11. The single and double layer of activated Pluronic® nanocapsules (F127-NPC and F68-NPC) were prepared by single and double multistep/solvent evaporation method, respectively, and then cross-linked by gelatin and EDC (two-step cross-linking).
12. The dual-functional (magnetic/thermal) drug carriers (F68-EDC-IO) were successfully fabricated by in-situ precipitate and self-assembly processes, and the characterization was examined by TEM and XRD analysis. The iron oxide nanoparticle encapsulated into the nanocapsules was tentatively assigned to iron carbonyl ($C_9Fe_2O_9$) and displays nanocrystal characterization.
13. Controlling the concentration of Pluronic® could fabricate different size micelles (as a tank to incubate the iron oxide nanoparticles) and thus could dominate the size of iron oxide nanoparticles (The lower concentration Pluronic® F68-NPC, the larger particle size and stronger crystallization of iron oxide nanoparticle are).
14. All of nanocapsules exhibited thermo response behavior (CMT of F127-series: 22-26°C; CMT of F68-series: 39-43°C), and CMT measured by DLS would obviously decrease after activated by NPC and slightly increase after gelatin

cross-linking. Moreover, CMT was almost no obvious change after EDC cross-linked and iron oxide nanoparticles encapsulated. F68-series nanocapsules were more suitable and potential to use in the body, because the CMT is above body temperature

15. For the natural drug release, all of nanocapsules display stable release in the range of 4 and 37°C and the drug release rate would increase gradually with temperature rising (4-37°C), but the rate of release accelerates fast at 45°C (above CMT). The increase of release rate may be attributed to the volume-shrinkage of nanocapsules.
16. By an external oscillating MF, the heat source can be produced to induce the instantaneous drug delivery by sharply volume transition (ca. 10-fold) from 20°C to 45°C, accompanying the enlarged and cracked pore by magnetic vibration of iron oxide nanoparticle, which is approximately 20 times higher at first 10-min operation than that just by incubation at 45°C water bath. This squeezing drug delivery is very important to apply in tumor and some emergency therapy.
17. Heat can produce by hyperthermia in the sample F68-EDC-IO nanocapsules, which not only provides thermal response on the Pluronic® shell, but also kills the tumor cell when the temperature rises above 40°C. Therefore, the dual functional magnetic drug carriers offer a promising technology for “switchable” drug release in the biomedical studies by using an external magnetic field. The novel “smart” biomaterials promise numerous potential applications in externally actuated drug delivery systems for release of drug molecules, such as tumor and epilepsy therap.
18. In summary, the dual-responsive (magnetic/thermal) materials can be anticipated for a much promising drug-delivery systems and can enhance the practicability of thermo-sensitive hydrogels.
19. The magnetic nanoparticles still provides some advantages, such as grafted probe-protein onto magnetic nanoparticles for “target” drug delivery systems and using magnetic resonance image (MRI) techniques for cell-tracking, as well as the magnetic materials can be “recycle” used and separating cells by magnet catching. Therefore, according to combine these techniques with thermo-sensitive

ferrogel, it is easy to find the region of disease, and delivers drug in the accuracy region by magnetic fields controlled (hyperthermia).



References

- Adriane, K. Huang, J.; Ding, G.; Chen, J.; Liu, Y., *J. Drug Targeting* 14 (2006) 243-253
- Ahn, J.S.; Choi, H.K.; Chun, M.K.; Ryu, J.M.; Jung, J.H.; Kim, Y.U.; Cho, C.S., *Biomaterials* 23 (2002) 1411
- An, X.; Su, Z., Zeng, H., *J. Chem. Technol. Biotechnol.* 78 (2003) 596-600
- Anderson, D.; Nguyen, T.; Lai, P.K.; Amiji, M., *J. Appl. Polym. Sci.* 80 (2001) 1274-1284
- Bae, K.H.; Choi, S.H.; Park, S.Y.; Lee, Y.; Park, T.G., *Langmuir* 22 (2006) 6380-6384
- Bae, K.H.; Lee, Y.; Park, T.G., *Biomacromolecules* 8 (2007) 650-656
- Bhattacharya, S.; Eckert, F.; Boyko, V.; Pich A., *Small* 3 (2007) 650-657
- Breimer, D.D., *J. Control. Release* 62 (1999) 3-6
- Brigger, I.; Dubernet, C.; Couvreur, P., *Adv. Drug Del. Rev.* 54 (2002) 631-651
- Bromberg, L.; Barr D.P., *Macromolecules* 32 (1999) 3649-3657
- Bromberg, L.; Temchenko, M.; Alakhov, V.; Hatton, T.A., *Int. J. Pharm.* 282 (2004) 45-60
- Bromberg, L.; Temchenko, M.; Hatton, T. A., *Langmuir* 19 (2003) 8675-8648
- Bromberg, L.; Temchenko, M.; Moeser, G. D.; Hatton, T. A., *Langmuir* 20 (2004) 5683
- Chatterjee, J.; Haik, Y.; Chen, C. J., *J. Appl. Polym. Sci.* 74 (1999) 1752-1761
- Chatterjee, J.; Haik, Y.; Chen, C.J., *J. Magn. Mater.* 246 (2002) 382-391
- Chatterlee, J.; Haik, Y.; Chen, C., *J. Colloid. Polym. Sci.* 281 (2003) 892-896
- Chen, G.; Ushida, T.; Tateishi, T., *Key Eng. Mater.* 192-1 (2000) 7 53
- Chen, J.; Yang, L.; Liu, Y.; Ding, G.; Pei, Y.; Li, J.; Hua, G.; Huang, J., *Macromol. Symp.* 225 (2005) 71-80
- Chen, K.S.; Ku, Y.A.; Lee, C.H.; Lin, H.R.; Lin F.H.; Chen T.M., *Mat. Sci. Eng. C-Bio. S.* 25 (2005) 472-478
- Chen, S.; Li, Y.; Guo, C.; Wang, J.; Ma, J.; Liang, X.; Yang, L.R.; Liu, H.Z., *Langmuir* 23 (2007) 12669-12676
- Chen, S.C.; Wu, Y.C.; Mi, F.L.; Lin, Y.H. ; Yu, L.C. ; Sung, H.W., *J. Control. Release* 96 (2004) 285-300
- Chiu, G.N.C.; Abraham, S.A.; Ickenstein, L.M.; Ng, R.; Karlsson, G.; Edwards, K.; Wasan, E.K.; Bally, M.B., *J. Control. Release* 104 (2005) 271-288

Choi, S.H.; Lee, J.H.; Choi, S.M.; Park T.G., *Langmuir* 22 (2006) 1758-1762

Chu, L.Y.; Li, Y.; Zhu, J.H.; Wang, H.D.; Liang, Y.J., *J. Control. Release* 97 (2004) 43-53

Chung J.E.; Yokoyama M., Yamato M., Aoyagi T., Sakurai Y., Okan T., *J. Control. Release* 62 (1999) 115-127

Claude, A.; Hoarau, C.; Leroux, J.C., *Biomacromolecules* 5 (2004) 2082-2087

Cortesi, R.; Nastruzzi, C.; Davis, S.S., *Biomaterials* 19 (1998) 1641

Coughlan, D.C.; Quilty, F.P.; Corrigan, O.I., *J. Control. Release* 98 (2004) 97-114

Crescenzi, V.; Francescangeli, A.; Taglienti, A., *Biomacromolecules* 3 (2002) 1384-1391

Csetneki, I.; Filipcsei, G.; Zrínyi, M., *Macromolecules* 39 (2006) 1939-1942

Dai, J.; Wang, J.Q.; Sangregorio, C.; Fang, J.; Carpenter, E.; Tang, J., *J. Appl. Phys.* 87 (2000) 7397-7399

de Faria, D.L.A.; Silva, S.V.; de Oliveria, M.T., *J. Raman Spectrosc.* 28 (1997) 873-878

De Paoli, V. M.; De Paoli Lacerda, S. H.; Spinu, L.; Ingber, B.; Rosenzweig, Z.; Rosenzweig, N. *Langmuir* 22 (2006) 5894-5899

Deng, Y.; Wang, C.; Shen, X.; Yang, W.; Jin, L.; Gao, H.; Fu, S., *Chem. Eur. J.* 11 (2005) 6006- 6013

Deng, Y.; Yang, W.; Wang, C.; Fu, S., *Adv. Mater.* 15 (2003) 1729-1732

Derfus, A.M.; Maltzahn, G.V.; Harris, T.J.; Duza, T.; Vecchio, K.S.; Ruoslahti, E.; Bhatia, S.N., *Adv. Mater.* 19 (2007) 3932-3936

Desai, P.R.; Jain, N.J.; Sharma, R.K.; Bahadur, P., *Colloid. Surface A* 178 (2001) 57-69

Detlef, M.S.; Thomas, S.R., *J. Magn. Magn. Mater.* 302 (2006) 267-271

Ding, G.; Adriane, K.; Chen, X.; Chen, J.; Liu, Y., *Int. J. Pharm.* 328 (2007) 78-85

Dziubla, T.D.; Torjman, M.C.; Joseph, J.I.; Murphy-Tatum, M.; Lowman, A.M., *Biomaterials* 22 (2001) 2893-2899

Edelman, E.R.; Kost, J.; Bobeck, H.; Langer, R., *J. Biomed. Mater. Res.* 19 (1985) 67-83

Eeckman, F.; Moës, A.J.; Amighi, K., *Int. J. Pharm.* 273 (2004)109-119

Elaïssari, A.; Bourrel, V., *J Magn. Magn. Mater.*, 225 (2001) 151-155

Etrych, T.; Jelínková, M.; Říhová, B.; Ulbrich, K., *J. Control. Release* 73 (2001) 89-102

Fernandes, R.; Wu, L. Q.; Chen, T.; Yi, H.; Rubloff, G. W.; Ghodssi, R.; Bentley, W. E.; Payne, G. F., *Langmuir* 19 (2003) 4058-4062

Francois, N.J.; Allo, S.; Jacobo, S.E.; Daraio, M.E., *Inc. J. Appl. Polym. Sci.* 105 (2007) 647-655

Fricker, J.; Writer, F., *Drug. Deliv. Today* 6 (2001) 387-389

Furukawa, H.; Shimojyo, R.; Ohnishi, N.; Fukuda, H., *Appl. Microbiol. biotechnol.* 62 (2003) 478-483

Gaponik, N.; Radtchenko, I.L.; Sukhorukov, G.B.; Rogach, A.L., *Langmuir* 20 (2004) 1449-1452

Giri, S.; Trewyn, B.G.; Stellmaker, M.P.; Lin, V.SY., *Angew. Chem. Int. Ed.* 44 (2005) 5038-5044

Grayson, A.C.R.; Choi, I.S.; Tyler, B.M.; Wang, P.P.; Brem, H.; Cima, M.J.; Langer, R., *Nature Mater.* 2 (2003) 767-772

Grinberg, N.; Dubovik, A.; Grinberg, V.; Kuznetsov, D.; Makhaeva, E.; Frosberg, A.; Tanaka, T., *Macromolecules* 32 (1999) 1471-1475

Guo, L.; Colby, R.H., *J. Rheol.* 45 (2001) 1223

Gupta, A.K.; Gupta, M., *Biomaterials* 26 (2005) 3995-4021

Gutowska, A.; Bark, J.S.; Kwon, I.C.; Bae, Y.H.; Cha, Y.; Kim, S.W., *J. Control. Release* 48 (1997) 141-148

Habeck, M., *Cancer drug delivery is hot stuff*, *DDT*, 6 (2001) 754 (News)

Haraguchi, K.; Takehisa, T.; Fan, S., *Macromolecules* 35 (2002) 10162-10171

Hassan, C. ; Peppas, N., *Macromolecules* 33 (2000) 2472

Hatakeyema, T.; Uno, J.; Yamada, C.; Kishi, A.; Hatakeyama, H. *Thermochimica Acta* 431 (2005) 144-148

Hernández, R.; Sarafian, A.; López, D.; Mijangos, C., *Polymer* 46 (2004) 5543-5549

Hsieh, D.S.T; Langer, R.; Folkman, J., *PANS* 78 (1981) 1863-1867

Hu, F.X.; Neoh, K.G.; Kang, E.T., *Biomaterials* 27 (2006) 5725-5733

Hu, S.H.; Liu, T.Y.; Huang, H.Y.; Liu D.M.; Chen, S.Y., *Langmuir* 24 (2008) 239-244

Hu, S.H.; Liu, T.Y.; Liu, D.M.; Chen, S.Y., *J. Control. Release* 121 (2007) 181-189

Hu, S.H.; Liu, T.Y.; Liu, D.M.; Chen, S.Y., *Macromolecules* 40 (2007) 6786-6788

Jain, T.K.; Morales, M.A.; Sahoo, S.K.; Leslie-Pelecky, D.L.; Labhasetwar, V., *Molecular Pharmaceutics* 2 (2005) 194-205

Jeong, B.; Kim, S.; Bae, Y., *Adv. Drug Delivery Rev.* 54 (2002) 37

Jun, Y.W.; Huh, Y.M.; Choi, J.S.; Lee, J.H.; Song, H.T.; Kim, S.J.; Yoon, S.; Kim, K.S.; Shin, J.S.; Suh, J.S.; Cheon, J., *J. Am. Chem. Soc* 127 (2005) 5732-5733

Kaiser, A.; Gelbrich, T.; Schmidt, A.M., *J. Phys.: Condens. Matter* 18 (2006) S2563–S2580

Kaneko, Y.; Yoshida, R.; Sakai, K.; Sakurai, Y.; Okano, T., *J. Membrane Sci.* 101 (1995) 13-22

Kang, H.W.; Tabata, Y.; Ikada, Y., *Biomaterials* 20 (1999) 1339}1344

Kim, D.H.; Lee, S.H.; Kim, K.N.; Kim, K.M.; Shim, I.B.; Lee, Y.K. *J. Magn. Magn. Mater.* 293 (2005) 320-327

Kim, J. Y.; Lee, S. B.; Kim, S. J. Lee, Y. M., *Polymer* 43 (2002) 7549-7558

Kim, M.R.; Park, T.G., *J. Control. Release* 104 (2002) 69-77

Kim, S.Y.; Lee, Y.M., *J. Appl. Polym. Sci.* 74 (1999) 1752-1761

Klabunde, K.J., *Nanoscale materials in chemistry*, New York: Wiley-Interscience, (2001) pp.169-221

Kohler, N.; Sun, C.; Fichtenholtz, A.; Gunn, J.; Fang, C.; Zhang, M., *Small* 2 (2006) 785-792

Kost, J.; Noecker, R.; Kunica, E.; Langer, R., *J. Biomed. Mater. Res.* 19 (1985) 935-940

Kost, J.; Wolfrum, J.; Langer, R., *J. Biomed. Mater. Res.* 21 (1987) 1367-1373

Leach J. B., Schmidt C.E., *Biomaterials* 26 (2005) 125

Lee, C.; Grodzinsky, A.; Spector, M., *Biomaterials* 22 (2001) 3145

Lee, C.; Grodzinsky, A.; Spector, M., *Tissue Eng.* 9 (2003) 27

Lee, K.Y.; Mooney, D.J.; *Chem. Rev.* 101 (2001) 1869

Lee, K.Y.; Peters, M.C.; Mooney, D.J., *Adv. Mater.*13 (2001) 837-839

Li, L.; Chen, D.; Zhang, Y.; Deng, Z., Ren, X.; Meng, X.; Tang, F.; Ren, J.; Zhang, L. *Nanotechnology* 18 (2007) 405102

Li, Y.Y.; Zhang, X.Z.; Kim, G.C.; Cheng, H.; Cheng, S.X.; Zhuo, R.X., *Small* 2 (2006) 917-923

Lin, C.L.; Lee, C.F.; Chiu, W.Y., *J. Colloid. Interf. Sci.* 291 (2005) 411-420

Lin, W.C.; Yu D.G.; Yang, M.C., *Colloids Surf. B* 44 (2005) 143

Liu, T.Y.; Hu, S.H.; Liu, K.H.; Liu, D.M.; Chen, S.Y., *J. Magn. Magn. Mater.* 304 (2006) e397-e399

Liu, T.Y.; Chen S.Y.; Li, J.H.; Liu, D.M., *J. Control. Release* 112 (2006) 88-95

Liu, T.Y.; Hu, S.H.; Liu, K.H.; Liu, D.M.; Chen, S.Y., *J. Control. Release* 126 (2008) 228-236

Liu, T.Y.; Hu, S.H.; Liu, T.Y.; Liu, D.M.; Chen, S.Y., *Langmuir* 22 (2006) 5974-5978

Long, J.W.; Logan, M.S.; Rhodes, C.P.; Carpenter, E.E.; Stroud, R.M.; Rolison, D.R., *J. Am. Chem. Soc.* 126 (2004) 16879-16889

Lu, H.; Nutt, S., *Macromolecules* 36 (2003) 4010-4016

Lu, Z. M.; Prouty, D.; Guo, Z.; Golub, V.O.; Kumar, C.S.S.R.; Lvov, Y. M., *Langmuir* 21 (2005) 2042-2050

Mak, S.Y.; Chen, D.H. *Macromol. Rapid Commun.* 26 (2005) 1567-1571

Mamada, A.; Tanaka, T.; Kungwachakun, D.; Irie, M., *Macromolecules* 23 (1990) 1517-1519

Mandal, T.K.; Bostanian, L.A. ; Graves, R.A.; Chapman, S.R., *Pharm. Res.* 19 (2002) 1713

Martens, P.J.; Bryant, S.J.; Anseth, K.S., *Biomacromolecules* 4 (2003) 283

Matsuoka, F.; Shinkai, M.; Honda, H.; Kubo, T.; Sugita, T.; Kobayashi, T., *BioMagnetic Research and Technology* 2 (2004) 1-6

Mitsumata, T.; Ikeda, K.; Gong, J. P.; Osada, Y.; Szabó, D.; Zrínyi, M., *J. Appl. Phys.* 85 (1999) 8451-8455

Miyajima, M.; Koshika, A.; Okada, J.; Ikeda, M., *J. Control. Release* 60 (1999) 199-209

Miyata, T.; Uragami, T.; Nakamae, K., *Adv. Drug Deliver. Rev.* 54 (2002) 79-98

Mohr, R.; Kratz, K.; Weigel, T.; Lucka-Gabor, M.; Moneke, M.; Lendlein, A., *PNAS* 103 (2006) 3540-3545

Müller-Schultheis, D.; Schmitz-Rodeb, T., *J. Magn. Magn. Mater.*, 302 (2006) 267-271

Muniz, E.C.; Geuskens, G., *Macromolecules* 34 (2001) 4480-4484

Murdan, S., *J. Control. Release* 92 (2003) 1-17

Neuberger, T.; Dchöpf, B.; Hofmann, H.; Hofmann, M.; Rechenberg, B.V., *J. Magn. Magn. Mater.* 293 (2005) 483-496

Nuttelman, C.; Mortisen, D.; Henry, S.; Anseth, K., *J. Biomed. Mater. Res.* 57 (2001) 217

Pankhurst, Q.A.; Connolly, J.; Jones, S. K.; Dobson, J.; *J. Phys. D: Appl. Phys.* 36 (2003)167

Paoli, V.M.D.; Lacerda, S.H.D.P.; Spinu, L.; Ingber, B.; Rosenzweig, Z.; Rosenzweig, N., *Langmuir* 22 (2006) 5894-5899

Park, J.H.; Im, K.H.; Lee, S.H.; Kim, D.H.; Lee, D.Y.; Lee, Y.K.; Kim, K.M.; Kim, K.N., *J. Magn. Magn. Mater.* 293 (2005) 328-333

Park, T.G.; Choi, H.K., *Macromol. Rapid Commun.* 19 (1998) 167-172.

Payne, G.F., *Langmuir* 19 (2003) 4058-4062

Peppas, N.A.; Bures, P.; Leobandung, W.; Ichikawa, H., *Eur. J. Pharm. Biopharm.* 50 (2000) 27

Peppas, N.A.; Hilt, J.Z.; Khademhosseini, A.; Langer, R., *Adv. Mater.* 18 (2006) 1345-1360

Peppas, N.A.; Langer, R. *AIChE J.* 50 (2004) 536

Peppas, N.A.; Wood, K.M.; Blanchette, J.O., *Expert. Opin. Biol. Ther.* 4 (2004) 881

Pich, A.; Bhattacharya, S.; Lu, Y.; Boyko, V.; Adler, H.J. P., *Langmuir* 20 (2004) 10706-10711

Qiu, Y.; Park, K. *Adv. Drug Deliver. Rev.* 53 (2001) 321-339

Ritger, P.L.; Peppas, N.A., *J. Control. Release* 5 (1987) 37

Rosengart, A.J.; Kaminski, M. D.; Chen, H.; Caviness, P.L.,; Ebner, A.D; Ritter, J.A., *J Magn. Magn. Mater.* 293 (2005) 633

Rotariu, O.; Strachan, N.J.C., *J Magn. Magn. Mater.* 293 (2005) 639

Sasaki, S.; Kawasaki, H.; Maeda, H., *Macromolecules* 30 (1997)1847-1848

Saslowski, O.; Weingarten, C.; Benoit, J.P.; Couvreur, P., *Life Science* 42 (1988) 1521-1528

Satarkar, N.S.; Hilt, J.Z., *Acta Biomaterialia* 4 (2008) 11-16

Schmidt, A.M., *Colloid. Polym. Sci.* 285 (2007) 953-966

Schmidt, A.M., *J. Magn. Magn. Mater.*, 289 (2005) 5-8

Schoof, H.; Apel, J.; Heschel, I.; Rau, G., *J. Biomed. Mater. Res.* 58 (2001) 352

Seo, S.B.; Yang, J.; Hyung, W.; Cho, E.J.; Lee, T.I.; Song, Y.J.; Yoon, H.G.; Suh, J.S.; Huh, Y.M.; S. Haam, *Nanotechnology* 18 (2007) 475105

Sershen, S.; West, J., *Adv. Drug Delivery Rev.* 54 (2002) 1225-1235

Sershen, S.; West, J., *Adv. Drug Delivery Rev.* 55 (2003) 439

Sershen, S.R.; Westcott, S.L.; West, J.L.; N.J. Halas, *Appl. Phys. B* 73 (2001) 379-381

Shaheen, S.M.; Yamaura, K., *J. Controlled Release* 81 (2002) 367

Singha, D.K.; Raya, A.R., *J. Membrane Sci.* 155 (1999) 107-112.

Storrie, H.; Mooney, D.J., *Adv. Drug Del. Rev.* 58 (2006) 500-514.

Stringer, J.L.; Peppas, N.A., *J. Controlled Release* 42 (1996) 195

Stubbe, B.G.; Smedt, S.C.D.; Demeester, J., *Pharm. Res.* 21 (2004) 1732-1740.

Sutani, K.; Kaetsu, I.; Uchida, K., *Radiat. Phys. Chem.* 61 (2001) 49-54.

Szabó, D.; Czakó-Nagy, I.; Zrínyi, M.; Vértws, A., *J. Colloid Interf. Sci.* 221 (2000) 166-172

Szabó, D.; Szeghy, G.; Zrínyi, M., *Macromolecules* 31 (1998) 6541-6548

Tanaka, T.; Matsukawa, S.; Kuroso, H.; Ando, I., *Polymer* 39 (1998) 4703-4706

Tannenbaum, R.; Zubris, M.; Goldberg, E.P.; Reich, S.; Dan, N., *Macromolecules* 38 (2005) 4254-4259

Uhrich K.E.; Cannizzaro, S.M.; Langer, R.S.; Shakesheff, K.M., *Chem. Rev.* 99 (1999) 3181-3198

Vaishnava, P.P.; Tackett, R.; Dixit, A.; Sudakar, C.; Naik, R.; Lawes, G., *J. Appl. Phys.* 102 (2007) 063914

Varga, Z.; Filipcsei, G.; Zrínyi, M., *Polymer* 47(2006) 227-233

Veiseh, O.; Sun, C.; Gunn, J.; Kohler, N.; Gabikian, P.; Lee, D.; Bhattarai, N.; Ellenbogen, R.; Sze, R.; Hallahan, A.; Olson, J.; Zhang, M., *Nano letters* 5 (2005)1003-1008

Wakamatsu, H.; Yamamoto, K.; Nakao, A.; Aoyagi, T., *J. Magn. Magn. Mater.*, 302 (2006) 327-333

Wan, W.K.; Campbell, G.; Zhang, Z.F.; Hui, A.J.; Boughner, D.R., *J. Biomed. Mater. Res.* 63 (2002) 854

Weissleder, R.; Bogdanov A.; Neuwelt, E.A.; Papisov, M., *Adv. Drug. Deliv. Rev.* 16 (1995) 321-334

Xiong, X.Y.; Tam, K.C.; Gan, L. H., *J. Appl. Polym. Sci.* 100 (2006) 4163-4172

Xulu P.M.; Filipcsei, G.; Zrínyi, M., *Macromolecules* 33 (2000) 1716-1719

Yang, J.; Lee, H.; Hyung, W.; Park, S.B.; Haam, S., *J. Microencapsulation* 23 (2006) 203-212

Yang, J.; Park, S.B; Yoon, H.G.; Huh, Y.M.; Haam, S., *Int. J. Pharm.* 324 (2006) 185-190

Yang, M.C.; Liu, T.Y., *J. Membrane Sci.* 226 (2003) 119-130

Zhang, J.L., Srivastava, R.S.; Misra, R.D.K., *Langmuir* 23 (2007) 6342-6351

Zhang, X.Z.; Wu, D.Q., Chu, C.C., *Biomaterials* 25 (2004) 3793-3805

Zhang, X.Z.; Yang, Y.Y.; Chung, T.S.; Ma, K.X., *Langmuir* 17 (2001) 6094-6099

Zhao, A.; Yao, P.; Kang, C.; Yuan, X.; Chang, J.; Pu, P., *J. Magn. Magn. Mater.*, 295 (2005) 37-43

Zhou, J.; Wu, W.; Caruntu, D.; Yu, M.H.; Martin, A.; Chen, J.F., O'Connor, C.J.; Zhou, W.L., *J. Phys. Chem. C* 111 (2007) 17473-17477

Zrínyi, M. *Colloid. Polym. Sci.* 278 (2000) 98-103

Zrínyi, M.; Szabó, D.; Kilian, H. G. *Polym. Gels and Networks* 6 (1998) 441-454



Appendix 1: Magnetic Variables and Units [Klabunde, 2001]

The magnetic field strength (or intensity) is usually represented by H . H will be reserved for fields that result solely from free currents, such as an electric current flowing in a wire. The magnetic moment per unit volume of a magnetic material is measured by M , the magnetization (or polarization). M results from the two atomic motions: the orbital and spin motion of the electron, mentioned above. These are often viewed macroscopically as equivalent or effective currents. Finally, the general case of a field due to both free and equivalent currents is described by the magnetic induction, B . These three quantities are tied together in the field equation

$$B = H + 4\pi M \quad [\text{cgs}] \quad [\text{A1}]$$

Thus B can result from a combination of H and M . For example, an electromagnet made by winding coils of copper wire around an iron rod and then passing a current through the wire has an H from this current, an M from atomic motion of the electrons in the iron, and a total B that is the sum of these two as described by Eq. (A1)

The units of H , M , and B are fundamentally all the same, as implied by Eq. (A1), and depend on the system of units being used. There are number of unit conventions, each with advantages and disadvantages. There are currently three systems of units that see widespread use. Historically, workers in magnetic materials have used the cgs (centimeter, gram, second) or Gaussian system. More recently attempts have been made to change over to the SI system (in mechanics SI implies mks-meter, kilogram, second). There are two SI system, the Kennelly and the Sommerfeld conventions, the latter slowly gaining acceptance in the magnetism community. Table A1 gives the units for the important magnetic quantities.

Conversion factors are:

$$1 \text{ oersted (Oe)} = (1000/4\pi) \text{ A m}^{-1}$$

$$1 \text{ gauss (G)} = 10^{-4} \text{ tesla (T)}$$

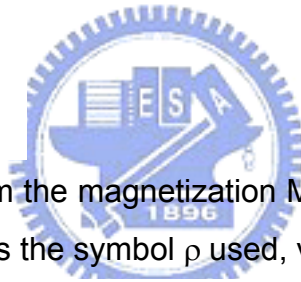
$$1 \text{ emu cm}^{-3} = 1000 \text{ A m}^{-1}$$

Table A1 Magnetic units. A is ampere, cm is centimeter, m is meter, emu is electro magnetic unit, B is magnetic induction, H is magnetic field strength, M is magnetization of a substance per unit volume, $\mu_0 = 4\pi \times 10^{-7}$ newton/ampere² is the permeability of free space. In the SI-Kennelly convention the magnetization is I, the intensity of the magnetization

Quantity	cgs (emu)	SI (Sommerfeld)	SI (Kennelly)
<i>B</i>	gauss	tesla	tesla
<i>H</i>	oersted	A m ⁻¹	A m ⁻¹
<i>M</i>	emu cm ⁻³	A m ⁻¹	–
<i>I</i>	–	–	tesla
Field equation	$B = H + 4\pi M$	$B = \mu_0(H + M)$	$B = \mu_0 H + I$
Energy	$E = -\mu \cdot H$	$E = -\mu_0 \mu \cdot H$	$E = -\mu \cdot H$

With the information in Table A1 one can show:

$$\begin{aligned}
 1 \text{ emu} &= 1 \text{ erg Oe}^{-1} \\
 &= 1 (\text{erg cm}^3)^{1/2} \\
 1 \text{ Oe} &= 1 (\text{erg cm}^{-3})^{1/2}
 \end{aligned}$$



Also note that in the cgs system the magnetization *M* can also be written per gram of substance. Then one often finds the symbol ρ used, viz.

$$\sigma = M/\rho \quad (\text{emu g}^{-1}) \quad \text{[A2]}$$

where ρ is the mass density.

Examples of magnetic field are those of the earth, for which $B \cong 0.8\text{G} = 8 \times 10^{-5}\text{T}$, or near a pole of a common permanent magnet where $B \sim 1000\text{G}$, etc. Beware, however, because usage of magnetic units is often not careful and units get mixed.

Appendix 2: (News) Smart magnetic hydrogels for drug release



[Subscribe | RSS 2.0](#) | [Link To Us](#) | [Contact Us](#)

[Home](#) | [Database](#) | [News](#) | [Resources](#) | [Community](#) | [Nanowerk](#) | [Nanomaterials Introduction](#)

[Periodicals](#) | [Books](#) | [Research Labs & Associations](#) | [Reports](#) | [Patents/IP](#) | [Encyclopaedia](#)



Nanowerk > Spotlight >

May 18, 2006

Smart magnetic hydrogels for drug release

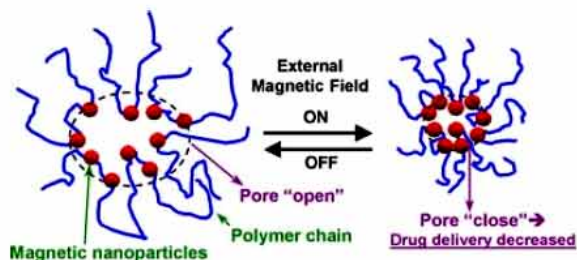
(*Nanowerk Spotlight*) Smart magnetic hydrogels were investigated by researchers in Taiwan for the development of a new magnetically induced drug delivery system. By applying magnetic fields, they were able to switch the the drug release profile of the hydrogels between "on" and "off" mode.

The research was carried out by Professor [San-Yuan Chen](#) and his group at the [Department of Materials Science and Engineering](#) at National Chiao Tung University in Taiwan.

So far, there has been little advance in the field of ferrogel specifically for drug delivery applications although magnetic materials have been widely used in the field of biotechnology in bio-separation, artificial muscles and drug carriers. The Taiwanese researchers' recent work demonstrates a good example for ferrogel applications, and going further, a controlled drug delivery and release mechanism that can be externally manipulated.

Their work primarily explores the physical mechanism of the mechanical movement of the ferrogel (magnetic hydrogel) upon the introduction of magnetic particles of different size and different inorganic/organic concentrations.

The sensitivity of the resulting ferrogel upon a given magnetic field can be enhanced by manipulating from nanoscale to microscale. Furthermore, this magnetic-sensitive ferrogel is even superior to traditional stimuli response polymer, such as pH or thermal sensitive polymer, because magnetic stimulation is an action-at-distance force (non-contact force) that is easier to adapt to biomedical devices.



Mechanism of magnetic-sensitive behaviors
(Source: San-Yuan Chen, National Chiao Tung University)

Most Recent
Smart magnetic hydrogels for drug release
Posted: May 18th, 2006

New insights into the nanostructures and mechanical properties of single nanofibers
Posted: May 17th, 2006

New techniques for fabricating carbon nanotube field emission displays
Posted: May 16th, 2006

Controlled drug delivery systems in neurodegenerative diseases
Posted: May 15th, 2006

Tailoring boron nanowire junctions
Posted: May 12th, 2006

High-pressure nano-structuring of materials
Posted: May 11th, 2006

Lithographically defined self-assembled nanoparticle films
Posted: May 10th, 2006

[...more articles](#)

Chen's recent paper, titled "[Preparation and characterization of smart magnetic hydrogels and its use for drug release](#)" is currently posted as corrected proof on the *Journal of Magnetism and Magnetic Materials*' website. A paper titled "Magnetic-sensitive behavior of intelligent ferrogels for controlled release of drug" will be published in an upcoming issue of *Langmuir*.

Chen explains to Nanowerk the specific problem that his team's work has overcome: "In conventional drug delivery systems the drug is continuously released from the drug carrier, once it is administrated into patient's body, even when there is no need any more. This could raise potential toxicity issues."

"However, for the ferrogel prepared in our current work," Chen says "the release of the drug can be held or ceased altogether when the patient's body does not require any further dose; and the drug can be released again if and when needed via an externally-triggered magnetic field. As a result, an efficient and effective drug therapy can be administered at the right time with the right dosage."

Chen sees biologically triggered, magnetically-induced drug delivery systems as an important contribution to future biotech developments. "This work is one of the fundamental achievements in our research team" he says.

By Michael Berger, Copyright 2006 Nanowerk LLC. All rights reserved.

[Privacy Statement](#) | [Terms](#) | [Contact Us](#) | [Nanowerk Home](#) | [Top of Page](#)

The contents of this site are copyright © 2005-2006, Nanowerk LLC. All Rights Reserved

Appendix 3: Controlled Pulsatile Drug Release from a Ferrogel by a High-Frequency Magnetic Field

6786

Macromolecules 2007, 40, 6786–6788

Controlled Pulsatile Drug Release from a Ferrogel by a High-Frequency Magnetic Field

Shang-Hsiu Hu, Ting-Yu Liu, Dean-Mo Liu,* and San-Yuan Chen*

Department of Materials Sciences and Engineering, National Chiao Tung University, Hsinchu, Taiwan, 300, ROC

Received March 30, 2007

Revised Manuscript Received July 31, 2007

Stimuli-responsive controlled release drug from polymeric devices has been received great attention, as it provides advantages such as better delivery efficiency and site-specific therapy over the conventional routes of drug delivery. By making use of these advantages, a number of studies have been successfully proposed to integrate active drug molecules and host materials, to manipulate drug release desirably. Many previous studies have been reported in response to specific stimuli, such as temperature,^{1–3} pH,^{4,5} electric field,^{6,7} mechanical signal,⁸ and ultrasound.⁹ A very recent achievement of a protein-containing hydrogel, reported by Ehrick et al.,¹⁰ addressed the stimuli-sensitive hydrogel that can be triggered as a result of the conformational change of the embedded calmodulin protein interacting to bioactive agents. Such a transfer from sensing actuation to mechanical action is novel, but it may be hard for it to reach high accuracy and sensitivity in therapeutic dosing as a burst-controlled drug delivery system. The use of a magnetic field to modulate drug release from polymeric matrices was previously developed.^{11–13} Saslawski et al. reported the alginate microspheres for pulsed release of insulin by an oscillating magnetic field.¹⁴ The release rate of insulin from alginate–strontium ferrite microspheres was enhanced in the absence of a magnetic field. Recently, a polyelectrolyte microcapsule embedded with Co/Au used external magnetic fields of 100–300 Hz and 1200 Oe to increase its permeability to macromolecules.¹⁵ In previous studies, a ferrogel with direct current (dc) magnetic-sensitive properties has been characterized and the amount of drug released from the ferrogel was effectively restricted while applying an external dc magnetic field.^{16,17} So far, little investigation has been addressed on the controlled drug release under high-frequency magnetic fields (HFMF). A real-time burst release of drug needs a fast-responsive drug release system to “inject” a precise dose of drug when the body needs it and to “stop” or “slow” the release right after the injection; however, it is hard to easily achieve this with traditional stimuli-responsive hydrogels. A controllable pulsatile-type drug delivery device with repeatable dosing ability in therapeutically effective precision is clinically desirable. Therefore, in this communication, a high-frequency magnetic field (HFMF) triggered pulsatile drug delivery ferrogel with a mechanically reliable and flexible hybrid structure composed of gelatin and magnetic nanoparticles (nanomagnets) of 10–250 nm in diameter is reported. Furthermore, under cyclic exposures to the high-frequency magnetic stimuli, a highly controllable and repeatable burst release with desirable precision from the ferrogels is achieved.

* Corresponding authors. Telephone: +886-3-5731818. Fax: +886-3-5725490; E-mail: (S.-Y.C.) sanyuanchen@mail.nctu.edu.tw; (D.-M.L.) deanmo_liu@yahoo.ca.

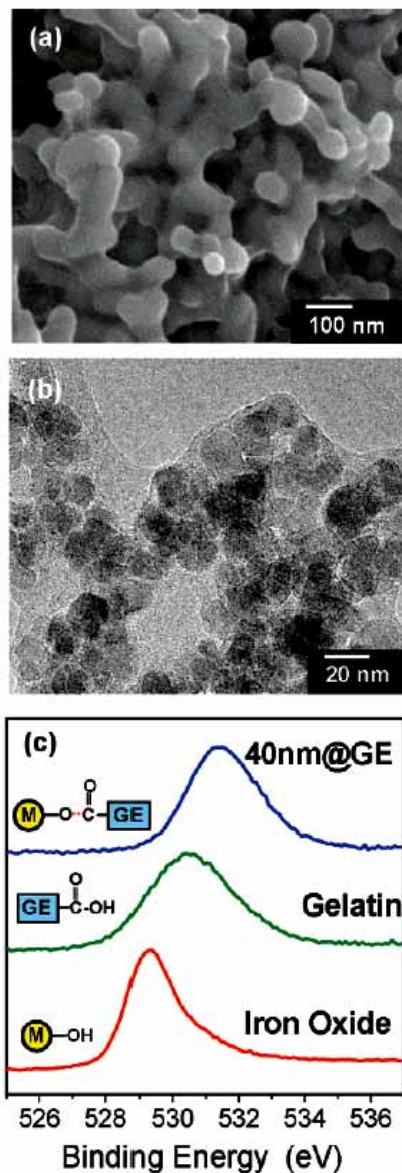


Figure 1. (a) SEM, (b) TEM, and (c) XPS analyses of ferrogels composed of iron oxide nanoparticles and a gelatin matrix.

Figure 1a illustrates the SEM images of one of the ferrogels shaping in cylindrical geometry, namely 40nm@GE ferrogel, where 40nm@GE represents the ferrogels with gelatin cross-linked with genipin, reinforced by 2 wt % chitosan, and 3% Fe₃O₄ magnetic nanoparticles (nanomagnets) of average 40 nm in diameter. Chitosan provides several functions in the final hybrid structure, such as (1) matrix for drug encapsulation, (2) materials to provide deformation motion, and (3) binder to link the nanoparticles. As shown, the iron nanoparticles were embedded into the polymer matrix and the nanomagnets displayed a uniform spherical size and dispersed well in the ferrogel. TEM image, i.e., Figure 1b, exhibits that the gelatin

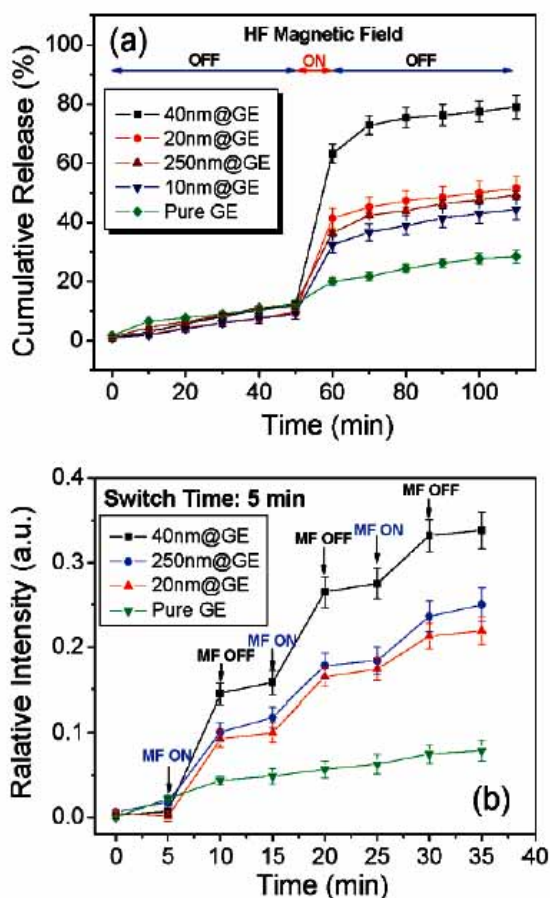


Figure 2. (a) Drug release behaviors of the ferrogels under a 10 min exposure of high-frequency magnetic field (HFMF) and (b) the on-off switch operations of high-frequency magnetic field (HFMF) manipulating the cumulative drug release of the ferrogels with different sizes of the nanoparticles.

was intimately attached to the surface of the nanoparticles, and the nanoparticle particles also percolated as a continuous phase, indicating the resulting ferrogels are virtually an interpenetrating network composites. This also suggests that the physical or thermal interactions between these two closely contact, interpenetrating phases can be easily triggered and accessible from

one phase to the other at a nanometric level. This also ensures fast-responsive properties of the ferrogels that can be achieved as disclosed in the forthcoming analysis.

The nanomagnets were essentially chemically bounded with the gelatin matrix to form the ferrogel, which further evidenced from XPS analysis, in Figure 1c. The binding energy of O_{1s} is detected from 527.0 to 537.0 eV, and the peak of iron oxide was at 529.3 eV, which is reasonably consistent with literature report, i.e., 528–531 eV. A peak at 530.4 eV for the gelatin indicates its carboxylic acid group; however, a shifting to higher energy region (531.4 eV) when the iron oxide particles were incorporated, implying that the carboxylic acid was chemically bonds or immobilized, onto the nanomagnet surface. The higher binding energy is believed to be a result of esterification between hydroxide moiety on the surface of the MNPs and carboxylic acid group of gelatin, forming a $COO-Fe$ bonding, indicating an excellent chemical affinity between both participating phases and a mechanically strong solid network of the ferrogels is achieved.

Upon magnetic manipulation, the drug (vitamin B_{12}) released from the ferrogels was demonstrated in Figure 2a. The ferrogels with different particle sizes of the nanomagnets showed different release rates even though they possessed the same concentration of the nanomagnets. In comparison, pure polymer gelatin showed faster drug release rate than that of the ferrogels, indicating the nanoparticles are acting as physical barriers to inhibiting the diffusion of the drug molecules. After the initial time period (50 min) of slow release, the high-frequency magnetic field (HFMF) was applied to the ferrogels for 10 min, and then was removed. The amount of drug release from the 40nm@GE ferrogel burst to a level as high as about 63%, compared to 12% during the first 50-min release in the absence of the HFMF. The finding strongly indicates that the applied HFMF accelerated considerably the drug release from the ferrogels of 40nm@GE composition by as large as 5 times. More specifically, the amounts of drug release from the ferrogels with different particle size were increased in the order of 40nm@GE > 20nm@GE > 250nm@GE > 10nm@GE > pure gelatin under the same magnetic stimulus. However, the release profiles after the 10-min burst, restored almost completely right after removal of the high-frequency magnetic stimulus, and behaved almost exactly the same as those at the initial 50-min period. A real-time, fast-responsive drug delivery ferrogels can be achieved and the faster responsivity of the ferrogels with respect to the HFMF stimulus offers greater potential for an in-time drug release device for medical applications.

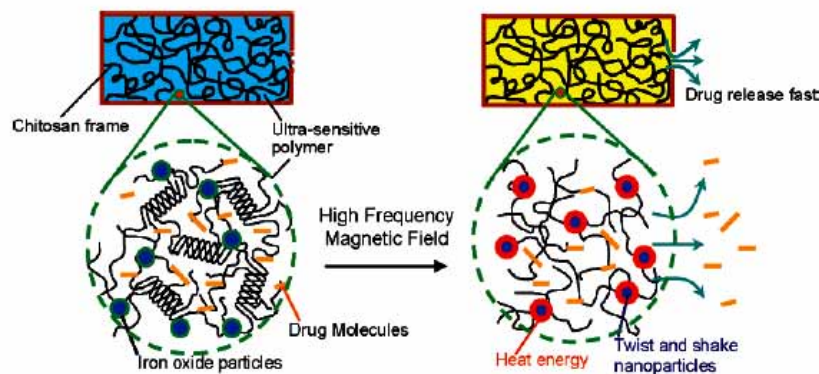


Figure 3. Schematic drawing of structures of ferrogel which exhibited a triple-helix structure to restrict the drug molecules to release. While applying the high-frequency magnetic field (HFMF), the magnetic nanoparticles provides the heat energy to release the structures and twist and shake the polymer molecular chains to effectively accelerate drug release rate.

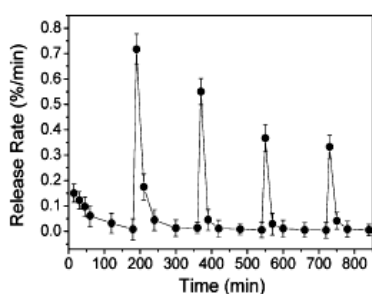


Figure 4. Cyclic drug release rates of 40nm@GE ferrogels under a 5-min period of HFMF stimuli and a long 180 min switching duration, where a longer switching time period ensures the drug to reach a kinetically favorable distribution in the ferrogel for a subsequent burst release.

Upon tripled on-off operations of the HFMF to the ferrogels, Figure 2b shows that reproducible slow-to-burst release profiles while consecutively applying the magnetic stimulus at a 5-min switching time period and the release profile restored immediately when the stimulus was removed. The findings imply two important characteristics underlying the drug release pattern of the high-frequency-induced ferrogels: first, under a short time "on-off" exposure of the magnetic stimulus, the ferrogels followed exactly the signals switching from burst to slow release of the drug instantly, and second, the amounts of drug bursting from the ferrogels maintained accurate dosing under cyclic on-off operations of the HFMF. The latter suggests the ferrogels prepared deformed elastically and showed potential antifatigue behavior, while the former indicates a fast-acting response of the ferrogels that can be technically achieved with desirable stimuli-sensitive control of drug delivery through the incorporation of 40 nm nanomagnets (average diameter).

The bursting release of the drug from the ferrogels is indicative of a mixture of mechanical actions imposed by the ferrogels, which may include (1) an "open" configuration of the network structure and (2) an elastic deformation (i.e., contractile deformation) of the ferrogels, while being subject instantly to the HFMF stimulus. Under HFMF, the nanomagnets were activated kinetically and possibly thermally (for larger nanoparticles), and they transformed the structural or molecular configuration of the ferrogels upon microstructural deformation (shrinking) of the gelatin matrix. Gelatin is considered to be a thermosensitive polymer since its conformation is a coil in the warm water (> 40 °C) but turns into a gel structure involving triple-helix sequences on cooling.^{18,19} Among the ferrogels prepared, magnetization evaluation (see Supporting Information, Figure S1) showed 40nm@GE composition exhibiting the broadest hysteresis loop compared to the others, indicating more energy can be generated instantly under the high-frequency magnetic stimulus. In other words, the 40nm@GE ferrogel was effectively thermally activated, where a rapid change in molecular conformation of the gelatin matrix from denser to looser configuration, as schematically illustrated in Figure 3, is expected in the ferrogels by a high-frequency magnetically induced thermal variation near the nanoenvironment surrounding the nanomagnets.

For a long HFMF switching duration, i.e., 180 min, Figure 4 illustrates a series of bursts started after a first 3-h slow release,

under a 5-min duration of HFMF stimuli, where a gradual reduction in the burst release rate was detected with time. Even though the longer switching time period of the high-frequency magnetic stimulus ensures a kinetically favorable drug migration, the insufficient drug amount in the ferrogel can hardly sustain the same burst release rate. However, a relatively slow to near-zero release rate was detected immediately after removal of the HFMF and kept relatively constant during the time duration, i.e., 180 min, between each stimulus. The same scenario of burst and slow release profiles repeated accurately for a time period of 840 min of drug release operation proved that the ferrogels exhibited an excellent elastic deformation property. This allows consecutive operation for a continuously controlled burst release of a drug into a patient's body to maintain a therapeutically effective dose in the body for a longer period of time to efficiently treat the disease locally or systemically. One clinically important advantage of this high-frequency-modulated fast-acting drug delivery ferrogel over other existing drug delivery devices is that it can potentially meet immediate urgent physiological needs and, with dosing, compatibly match chronological changes in patients' bodies.

Supporting Information Available: Text giving experimental details and effect of magnetic particle size with a figure showing the latter. This material is available free of charge via the Internet at <http://pubs.acs.org>.

References and Notes

- Zhang, X. Z.; Wu, D. Q.; Chu, C. C. *Biomaterials* **2004**, *25*, 3793–3805.
- Eeckman, F.; Moës, A. J.; Amighi, K. *Int. J. Pharm.* **2004**, *273*, 109–119.
- Hu, Z.; Xia, X. *Adv. Mater.* **2004**, *16*, 305–309.
- Chen, S. C.; Wu, Y. C.; Mi, F. L.; Lin, Y. H.; Yu, L. C.; Sung, H. W. *J. Controlled Release* **2004**, *96*, 285–300.
- Das, M.; Mardiyani, S.; Chan, W. C. W.; Kumacheva, E. *Adv. Mater.* **2006**, *18*, 80–83.
- Murdan, S. J. *J. Controlled Release* **2003**, *92*, 1–17.
- Abidian, M. R.; Kim, D. H.; Martin, D. C. *Adv. Mater.* **2006**, *18*, 405–409.
- Lee, K. Y.; Peters, M. C.; Mooney, D. J. *Adv. Mater.* **2001**, *13*, 837–839.
- Kim, H. J.; Matsuda, H.; Zhou, H. I.; Honma, A. *Adv. Mater.* **2006**, *18*, 3083–3088.
- Eheick, J. D.; Deo, S. K.; Browning, T. W.; Bachas, L. G.; Madou, M. J.; Daumert, S. *Nat. Mater.* **2005**, *4*, 298–302.
- Kost, J.; Wolfrum, J.; Langer, R. *J. Biomed. Mater. Res.* **1987**, *21*, 1367–1373.
- Edelman, E. R.; Kost, J.; Bobeck, H.; Langer, R. *J. Biomed. Mater. Res.* **1985**, *19*, 67–83.
- Kost, J.; Noecker, R.; Kumica, E.; Langer, R. *J. Biomed. Mater. Res.* **1985**, *19*, 935–940.
- Saslowski, O.; Weingarten, C.; Benoit, J. P.; Couvreur, P. *Life Sci.* **1988**, *42*, 1521–1528.
- Lu, Z.; Prouty, M. D.; Guo, Z.; Golub, V. O.; Kumar, C. S. S. R.; Lvov, Y. M. *Langmuir* **2005**, *21*, 2042–2050.
- Liu, T. Y.; Hu, S. H.; Liu, T. Y.; Liu, D. M.; Chen, S. Y. *Langmuir* **2006**, *22*, 5974–5978.
- Liu, T. Y.; Hu, S. H.; Liu, K. H.; Liu, D. M.; Chen, S. Y. *J. Magn. Mater.* **2006**, *304*, e397–e399.
- Crescenzi, V.; Francescangeli, A.; Taglienti, A. *Biomacromolecules* **2002**, *3*, 1384–1391.
- Bulcke, A. I. V. D.; Bogdanov, B.; Rooze, N. D.; Schacht, E. H.; Cornelissen, M.; Berghmans, H. *Biomacromolecules* **2000**, *1*, 31–38.

MA0707584

Appendix 4: Magnetic Nanoparticles as recycling anticoagulants



Copyright © 2007 American Scientific Publishers
All rights reserved
Printed in the United States of America

*Journal of Biomedical
Nanotechnology 3 (2007)
353-359*

Core–Shell Magnetic Nanoparticles of Heparin Conjugate as Recycling Anticoagulants

Ting-Yu Liu, Li-Ying Huang, Shang-Hsiu Hu, San-Yuan Chen*, and Ming-Chien Yang

¹Department of Materials Sciences and Engineering, National Chiao Tung University, Hsinchu, Taiwan, 300, ROC

²Department of Polymer Engineering, National Taiwan University of Science and Technology, Taipei, Taiwan, 106, ROC

Polyvinyl alcohol-shell magnetic nanoparticles (PVA-shell MNPs, PMNPs) were successfully prepared by *in-situ* co-precipitation process. Heparin (HEP) was then covalently conjugated on the PMNPs by using aminotrimethoxysilane (ATMS) and 4,4-diphenyl methane diisocyanate (HMDI) as molecular coupling agent (spacer). The morphology of the core–shell PMNPs was examined using transmission electron microscope (TEM), X-ray diffraction (XRD), and Raman spectrometry to demonstrate the core–shell structure, as well as X-ray photoelectron spectroscopy (XPS) to provide direct evidence that the heparin molecules were immobilized on the surface of the core–shell PMNPs. Anticoagulant activity was evaluated with several parameters including activated partial thrombin time (APTT), prothrombin time (PT), fibrinogen time (FT), and thrombin time (TT). The results show that longer spacer would give better anticoagulant activity since lower steric hindrance can induce higher heparin grafting density. It might be anticipated that PMNPs of heparin conjugate can be used as anticoagulants instead of traditional free heparin, owing to its recycling characteristics by magnetic fields.

Keywords: Core–Shell, Magnetic Nanoparticles, Anticoagulants, Heparin.

1. INTRODUCTION

Recently, the use of magnetic nanoparticles (MNPs) of iron oxide is mainly focused on biomedical applications because they show rather low toxicity than other magnetic materials, such as radiopharmaceuticals, magnetic resonance imaging (MRI), diagnostics, immunoassays, purification, separation, reproducible properties, hyperthermia, and controlled drug release.^{1–10} For these applications, well-dispersed magnetic nanoparticles are needed. Up to now, several polymers have been used as coating agents to improve colloidal stability of MNPs by adsorption or covalent binding, namely bovine serum albumin (BSA), starch, poly(ethylene glycol) (PEG), Pluronic, poly(acrylic acid) (PAA), and poly(vinyl alcohol) (PVA).^{1,2,4,10–14} However, the stabilization of MNPs thus prepared was longwinded and complicated processes. Therefore, the *in-situ* process to fabricate core (magnet)-shell (PVA) MNPs is more convenient and simpler than those traditional methods. PVA-shell was selected because it displays amphoteric characteristics and can be applied in aqueous environment and in organic solvent for the encapsulation of amphoteric drugs, as well as used as dispersing agents to uniformly disperse the Fe₃O₄ particles.¹⁵

In addition, surfaces grafted with biomolecules are important for modern biotechnology and life science. The functions and modification of the surface of MNPs with various biocompatible and biodegradable materials using various organic or inorganic substrates have been widely examined in biomedical fields.^{1,2,5,6,10–14,16–19} Dextran-, albumin-, and transferring-coated MNPs have been tested *in vitro* using human dermal fibroblasts cells, as well as MNPs conjugated with antibodies, enzymes, and proteins, have been tested to specific targeted cells as drug delivery systems.^{12,19} Moreover, heparin immobilized on magnetic-microspheres for anticoagulation and avoiding thrombosis has been reported.¹³

Heparin, an anticoagulant and a highly sulfated, anionic polysaccharide composed of repeating disaccharides of 1,4-linked glucosamine and uronic acid residues, can prevent the thrombus formation by interacting with antithrombin III (AT-III) after contacting blood.^{20–21} When someone needs to transfuse blood, both of them (blood and heparin) will be injected to human body at the same time. However, a great amount of heparin will cause an allergic reaction in the human body. So, it was aimed to design a recycling anticoagulant by combining iron oxide and heparin to prevent heparin from getting into body. In this condition, the heparin could be removed before injected into blood because the PMNPs of heparin conjugate can be collected

*Author to whom correspondence should be addressed.

by magnetic field. Therefore, the new developed PMNPs of heparin conjugate can be used as recycling anticoagulants instead of traditional free heparin.

However, the immobilization process is usually quite complicated and strongly dependent on special coupling agents. Organosilanes are bifunctional molecules with the general formula $X-(CH_2)_n-SiR_n(OR)_{3-n}$, where X represents the headgroup functionality, $(CH_2)_n$ a flexible spacer, and $Si(OR)_n$ the anchor groups by which (after hydrolysis of the alkoxy group) they can attach to free Si-OH surface groups.²²⁻²³ Alkoxysilanes with a variety of X functionalities are commercially available. Therefore, aminotrimethoxysilane (ATMS), an aminosilane, was used in this study. The fabrication process of PVA shell MNPs (PMNPs) was aiming to immobilize heparin onto PMNPs by ATMS and HMDI with different spacers through *in-situ* co-precipitation of Fe(II) and Fe(III) salts in the presence of PVA. The morphologies were characterized by transmission electron microscope (TEM), X-ray photoelectron spectroscopy (XPS), X-ray diffraction (XRD), and Raman spectrometry. Interactions between blood and modified core-shell MNPs were examined in terms of the blood coagulation times to evaluate the effect of grafting density of heparin and the spacer length on the blood-MNPs interaction.

2. EXPERIMENTAL DETAILS

2.1. Preparation of Modified PVA-Shell Magnetic Nanoparticles (PMNPs)

Figure 1 depicts the process of surface modified PMNPs. The stable PVA-shell magnetic nanoparticles (PMNPs) were synthesized using the method of *in-situ* co-precipitation of Fe(II) and Fe(III) salts in the presence of PVA (Fluka, M.W.: 72,000, degree of hydrolysis: 97.5–99.5 mol%). In this process, 0.05 g of PVA, 1.35 g of $FeCl_3 \cdot 6H_2O$ (5 mmol, Riedel-deHaën), and 0.498 g of $FeCl_2 \cdot 4H_2O$ (2.5 mmole, Fluka) were dissolved in 50 ml of water under vigorous stirring at 60 °C. Then, ammonia solution (33%, Riedel-deHaën) was quickly added to the reactor and stirred until pH arrives 10, followed by hydrothermal treatment at 80 °C for 30 min. After washed five times, filtered, and freezing-dried, PMNPs were successfully prepared. Besides, bare Fe_3O_4 MNPs fabricated via the co-precipitation process were used as the reference materials.²

The PMNPs (or Fe_3O_4 MNPs) then were silanized with aminotrimethoxysilane (ATMS, NH_2 -silane, Aldrich) by soaking and sonicating in a 1 wt% toluene solution of ATMS for 1 h.²⁴ After rinsing with toluene and ethanol, and finally sonicating in ethanol for 5 min, they were freezing-dried. These samples were denoted as PMNPs-ATMS. PMNPs-ATMS were soaked and sonicating in 10 ml of 10 vol% HMDI for 1 h to cause the conjugation between $-NH_2$ of ATMS and $-NCO$ of HMDI (denoted

as PMNPs-HMDI). After rinsing with toluene, ethanol and doubly distilled water, PMNPs-HMDI were placed in the aqueous solution of 2000 IU/ml HEP for 1 h in order to bind $-OH$ functional groups of HEP to the $-NCO$ groups of HMDI. These samples were washed 3 times with phosphate buffer saline (PBS) and doubly-distilled water. The resulting samples were freezing-dried at -50 °C using a freeze-dryer for 24 h. The resulting samples were designated as PMNPs-ATMS-HEP (long spacer). The preparation of PMNPs-HEP (without ATMS, short spacer) is similar to that of PMNPs-ATMS-HEP, except skipping the process of ATMS conjugation. Thus HEP was immobilized onto PMNPs by reacting the $-NCO$ group of HMDI to the $-OH$ groups of both PMNPs and HEP.

2.2. Surface Characterization Analysis

The surface density of amino groups of ATMS and heparin immobilized density were determined by dyeing with C.I. Acid Orange 7 (Tokyo Kaseo Kogyo Co., Ltd., Japan) and toluidine blue O (TB, Sigma, USA), respectively.²⁵⁻²⁷ The absorbance of the dye uptaken was measured using a spectrophotometer (Ultraspec 1100 pro, Biochrom Ltd., Cambridge, UK).

The morphology of PMNPs was examined using field-emission scanning electron microscope (FESEM, JEOL-6500, JEOL, Japan) and transmission electron microscope (TEM, JEOL-2000FX, JEOL, Japan). The crystal structure was determined using X-ray diffraction (XRD) (Siemens-D5000, Germany) with $CuK\alpha$ radiation. The functional groups on the modified-PMNPs were analyzed using Raman Spectrum (Horiba Jobin Yvon, USA; He/Ne Laser: 632.8 nm) and X-ray photoelectron spectroscopy (XPS) (Escalab 250, Thermo VG Scientific, West Sussex, UK) equipped with $Mg K\alpha$ at 1253.6 eV at the anode. A survey scan for O_{1s} , Si_{2p} , N_{1s} and S_{2p} were taken. The relative amount of the magnetic nanoparticles associated with the PVA shell was determined using thermogravimetric analysis (TGA) (Perkin Elmer). Samples were dried in a vacuum oven for 48 hours and analyzed in the platinum plate at a heating rate of 10 °C/min under nitrogen atmosphere.

2.3. Blood Coagulation Time²⁴⁻²⁶

Platelet-poor plasma (PPP) was provided from the Blood Center in Taiwan. 0.1 g of modified-PMNPs was added to 1.5 ml of PPP and was incubated at 37 °C for 60, 180, 360, and 540 min. The coagulation times, including activated partial thrombin time (APTT), prothrombin time (PT), thrombin time (TT), and fibrinogen time (FT) were determined using an automated blood coagulation analyzer (CA-50, Sysmex Corp., Kobe, Japan). The negative control was measured against the glass tube without the test sample. The blood coagulation cascade included intrinsic pathway, extrinsic pathway, and common pathway. Among

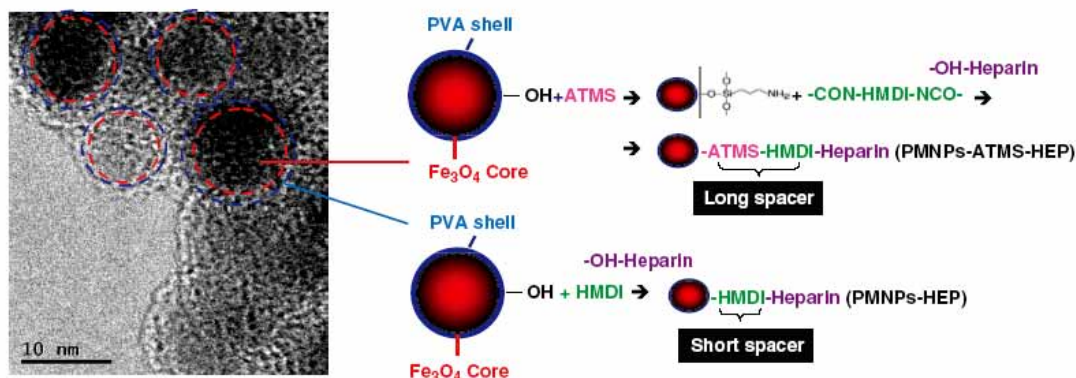


Fig. 1. TEM photos and a diagram process of surface-modified PMNPs by ATMS, HMDI, and HEP.

those coagulation times, the APTT relates mainly to the intrinsic and common pathway, PT relates mainly to the extrinsic and common pathway, and FT and TT are used as a measure for the time of the fibrinogen transferring to fibrin.

3. RESULTS AND DISCUSSION

3.1. Morphology

Figure 1 shows the TEM photo of the core-shell structure of PMNPs. According to the TEM observation, the average thickness of PVA layers was found to be ~ 2 nm, and the magnet diameter was about 5–10 nm. Furthermore, six diffraction peaks at $2\theta = 30.1^\circ, 35.6^\circ, 43.3^\circ, 53.5^\circ, 57.2^\circ, 62.9^\circ$ in the XRD pattern (see Fig. 2) are the characteristic peaks of standard Fe_3O_4 crystal [according to Fe_3O_4 (JCPDS 85-1436)].²⁸ Hence, the resulting magnet MNPs can be confirmed as Fe_3O_4 MNPs. In addition, the XRD

spectrum of pure PVA showed a broad peak in the range of $15\text{--}27^\circ$ (maximum: 17.9°), indicating that PVA displays the semi-crystallization. The core-shell MNPs also exhibited a diffraction pattern peaked at 18.0° and the six characteristic peaks of Fe_3O_4 crystal, thus indicating that PVA indeed existed in the Fe_3O_4 MNPs.

The diameter of magnet can be calculated according to Debye-Scherrer equation. (2):

$$D = \frac{0.9\lambda}{\beta \cos\theta} \quad (1)$$

where D is the average crystallite size (\AA), λ is the wavelength of X-rays ($\text{CuK}\alpha := 1.5418 \text{ \AA}$), θ is the Bragg diffraction angle, and β is the full width at half maximum (FWHM). By using Eq. (1) and FWHM of the diffraction peak at $2\theta = 35.6^\circ$, the crystallite size of PMNPs was estimated about 10.6 nm (FWHM: 0.78°), which was smaller than the size of the magnet (14.1 nm, FWHM: 0.59°) synthesized in the absence of PVA, shown as the insert in Figure 2. The spectrum of PMNPs in Figure 3 exhibited five peaks by curve-fitting which correspond to that of PVA and Fe_3O_4 MNPs phase. Three peaks ($489.7, 601.8, 707.9 \text{ cm}^{-1}$) can be identified from the Raman spectra of the PVA phase. In addition, other two peaks (664.2 and 704.5 cm^{-1}) are characteristics of bare Fe_3O_4 MNPs, belonging to the vibration frequencies of Fe_3O_4 . From these results, it can be confirmed that PVA truly existed around Fe_3O_4 nanoparticles.

This result suggests that the presence of PVA can reduce the particle size of Fe_3O_4 because PVA can not only promote the nucleation but also inhibit the growth of the Fe_3O_4 particles.² The contents of PVA-layer also can be examined by TGA. As shown in Figure 4, the difference of weight loss (%) between Fe_3O_4 MNPs and PVA-shell MNPs could reach 6.6 wt% measured by TGA. The difference suggests that about 7 wt% PVA encapsulated the core of iron oxide (ca. 93 wt%). These weight fractions can be converted to the volume fractions, indicating that 24 vol% PVA shell encapsulated 76 vol% iron oxide (the

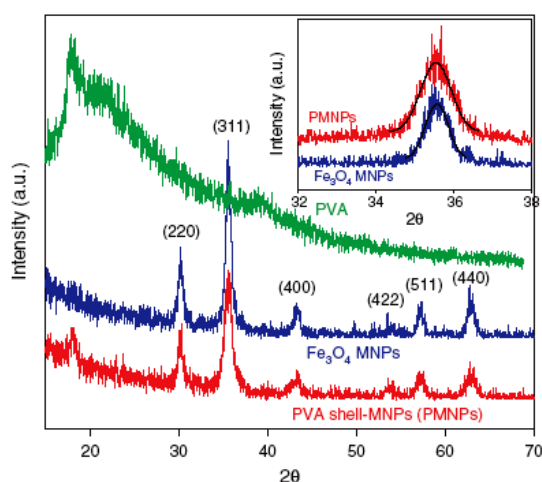


Fig. 2. XRD patterns of Fe_3O_4 MNPs, PVA and PMNPs.

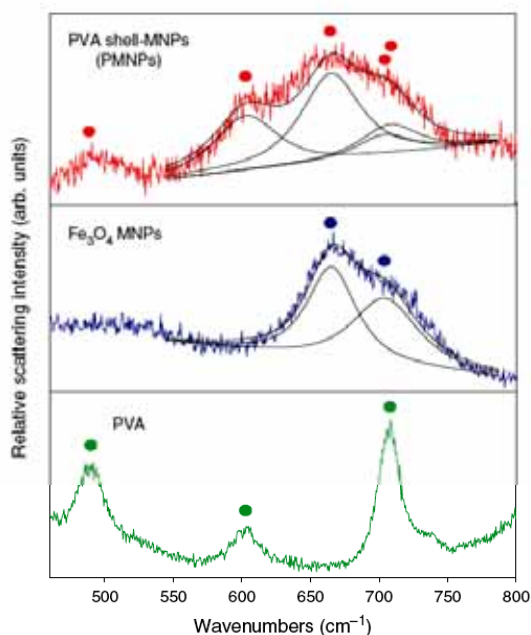


Fig. 3. Raman spectra of Fe_3O_4 MNPs, PVA and PMNPs.

densities of PVA and iron oxide were 1.27 and 5.2 g/cm^3 , respectively). Figure 5 shows that bare Fe_3O_4 MNPs display a magnetization (M_s) (60.9 emu/g), which is higher than those of PMNPs (52.4 emu/g), PMNPs-ATMS (50.2 emu/g) and PMNPs-ATMS-HEP (45.8 emu/g), measured using the vibrating sample magnetometer (VSM, Toei VSM-5). An incorporation of PVA, ATMS and HEP may cause damages in some domains of Fe_3O_4 , resulting in a lower M_s . From these results, it can be confirmed that PVA and HEP were indeed conjugated around Fe_3O_4 nanoparticles.

3.2. Surface Characterization

Figure 6 compares the XPS spectra of PMNPs, PMNPs-ATMS, and PMNPs-ATMS-HEP. The XPS analysis shows

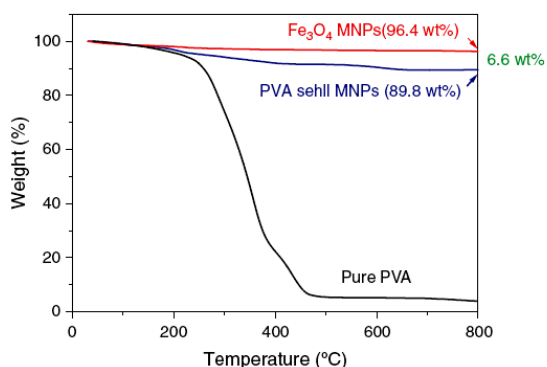


Fig. 4. TGA curves of PVA and modified-PMNPs.

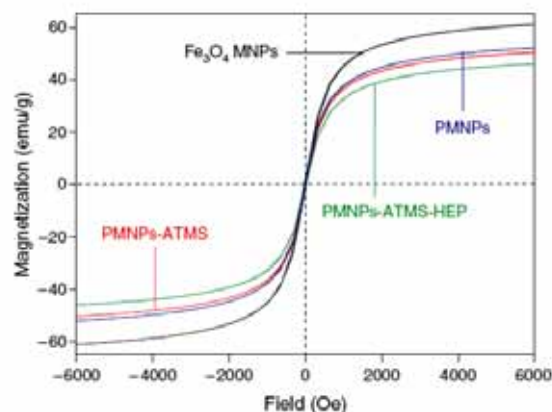


Fig. 5. Hysteresis loop of PVA and modified-PMNPs.

that the surface was mainly composed of O, Si, N, and S atoms. Figure 6(a) shows the O_{1s} spectra of PMNPs, PMNPs-ATMS and PMNPs-ATMS-HEP. The peaks at 530.1 and 531.1 eV represented the metal oxide and the $-\text{OH}$ group of PVA, respectively. After conjugating ATMS, an additional peak was found at 532.0 eV, attributing to the silane functional group. Moreover, two extra peaks were observed in the spectra of PMNPs-HEP, representing the $-\text{NCO}$ group (531.3 eV) of HMDI and the $-\text{COOH}$ group (532.5 eV) of heparin in the core-shell MNPs.

Figure 6(b) shows the XPS data of Si_{2p} in PMNPs, PMNPs-ATMS, and PMNPs-ATMS-HEP. The Si peak at 101.6 eV was found in the spectra of PMNPs-ATMS and PMNPs-ATMS-HEP, implying that ATMS was immobilized onto PMNPs. Moreover, the NH_2 peak (399.4 eV) was observed in the N_{1s} scan spectrum of PMNPs-ATMS, also indicating that ATMS was immobilized onto PMNPs, as shown in Figure 6(c). However, the NH_2 peak was shifted from 399.4 eV to 399.9 eV when heparin-OH was conjugated with ATMS- NH_2 by the NCO group of HMDI, implying the formation of urea bond ($-\text{NHCONH}$) and urethane ($-\text{OCONH}$), respectively. Furthermore, on comparing the spectra of PMNPs, PMNPs-ATMS and PMNPs-ATMS-HEP, it was found that only the spectrum of PMNPs-ATMS-HEP exhibited the S_{2p} peak of HEP (binding energy 168.6 eV), as shown in Figure 6(d). These results indicate that ATMS, HMDI and HEP are indeed conjugated onto PMNPs.

3.3. Grafting Density Assay

As listed in Table I, the grafting density of the amino group on PMNPs-ATMS attained 67.5 nmol/cm^2 by C.I. Acid Orange 7 dye assay, which is higher than that of MNPs-ATMS (25.1 nmol/cm^2). This can be attributed to the fact that PMNPs have more $-\text{OH}$ groups from PVA to connect with ATMS than that in the MNPs which only have metal oxide. Higher grafting density of ATMS would lead to

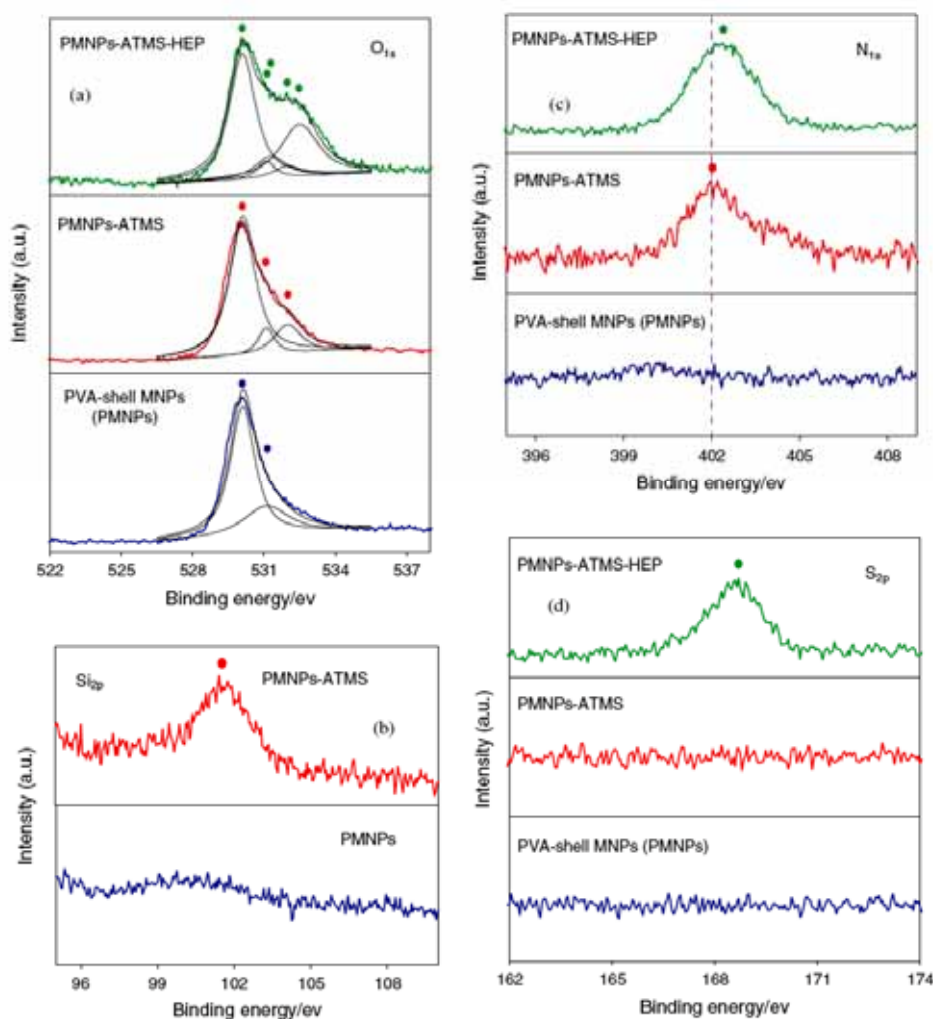


Fig. 6. XPS survey scan spectra of (a) O_{1s} scan spectra, (b) Si_{2p} scan spectra, (c) N_{1s} scan spectra, and (d) S_{2p} scan spectra.

higher grafted density of HEP. Therefore, the grafting density of HEP for PMNPs-ATMS-HEP was about 1.5 times of that for MNPs-ATMS-HEP. Moreover, the PMNPs with

Table I. Surface grafted density and anticoagulant activity of modified nanomagnetic particles during 60 min-incubation (mean \pm std).

Membrane type	Surface density	Anticoagulant activity (APTT) ^c
Fe ₃ O ₄ MNPs (MNPs)	—	38.9 \pm 1.8
MNPs-ATMS	25.12 \pm 1.6 ^a	38.7 \pm 1.7
MNPs-ATMS-HEP	2.11 \pm 0.18 ^b	358 \pm 14
PVA-shell MNPs (PMNPs)	—	40.6 \pm 1.7
PMNPs-ATMS	67.5 \pm 2.3 ^a	38.2 \pm 1.5
PMNPs-ATMS-HEP	3.15 \pm 0.37 ^b	No coagulation
PMNPs-HEP (without ATMS)	1.67 \pm 0.24 ^b	268 \pm 12

^aAmino group (nmol/g), determined with dye staining of C.I. Acid Orange 7 ($n = 6$).

^bHeparin (μ g/g), determined with dye staining of toluidine blue O ($n = 6$).

^cIncubation time of modified MNPs is 60 min.

long spacer (PMNPs-ATMS-HEP) exhibited higher grafting density than that PMNPs-HEP (with short spacer). The difference in the HEP-grafting density also would reflect on the anticoagulant activity and hemocompatibility.

3.4. Blood Coagulation

Figure 7(a) and Table I shows the effect of HEP immobilization on the APTT, PT, FT and TT of MNPs, PMNPs, PMNPs-ATMS, and PMNPs-ATMS-HEP. Immobilized heparin can activate AT III, and hence in turn prevent the formation of thrombus.²⁹ Up to now, most researchers have focused on the immobilization of heparin on the substrate in the applications of dialysis or coronary stents.²⁴⁻²⁶ To our best knowledge, fewer researchers investigated the effect of magnetic nanoparticle on heparin for recycling anticoagulants, and the role of different grafted

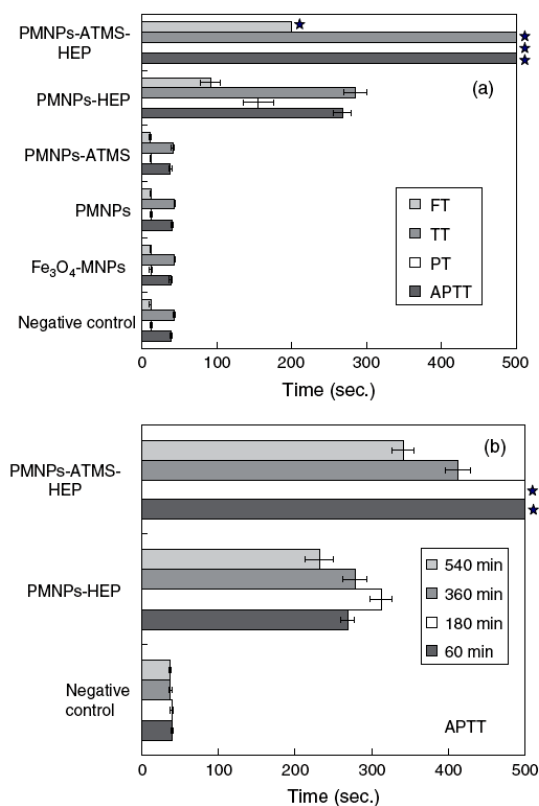


Fig. 7. (a) Blood clotting times of modified-Fe₃O₄ MNPs and PMNPs include APTT, PT, FT and TT during 60-min incubation ($n = 5$); (b) comparison of APTT between PMNPs-HEP (shorter spacer) and PMNPs-ATMS-HEP (longer spacer) during 60–540 min ($n = 5$). The star means “no coagulation” of the samples.

spacer (with and without ATMS) in the hemocompatibility. The results showed that the APTT, PT, FT, and TT of PMNPs-ATMS-HEP (long spacer) display non-coagulation that is superior to the PMNPs-HEP (short spacer). The reason is that PMNPs-ATMS-HEP exhibited higher surface density of HEP (3.15 $\mu\text{g/g}$) than PMNPs-HEP (1.67 $\mu\text{g/g}$), as shown in Table I. The clotting times of pure Fe₃O₄ MNPs, PMNPs, and PMNPs-ATMS were close to those of human plasma (the negative control), indicating that they had no anticoagulation activity. Moreover, the clotting time of MNPs-ATMS-HEP (358 s) is shorter than that of PMNPs-ATMS-HEP (no coagulation), as shown in Table I. It demonstrated that longer spacer and higher HEP-density would prolong the clotting time to attain better anticoagulation.

Figure 7(b) shows the time dependence of the activity of immobilized heparin that was evaluated by APTT after 60–540 min of incubation. From the results, no coagulation was observed for PMNPs-ATMS-HEP before 180 min, but the clotting time was reduced to 412 and 341 s after incubating for 360 and 540 min, respectively.

This suggested that the activity of immobilized HEP can maintain at least 9 h. Comparing with PMNPs-HEP, PMNPs-ATMS-HEP exhibited longer anticoagulation time and higher activity due to its higher surface density of HEP and lower steric hindrance attributing to longer spacer, as shown in Table I. The use of ATMS can increase the backbone length of heparin to promote the activity of heparin. Therefore, the magnetic nanoparticles conjugated heparin not only can display the anticoagulation but also separate from blood by magnetic field when the blood is going to be injected in to body. Especially, the longer spacer (PMNPs-ATMS-HEP) exhibited the better ability of anticoagulation and it will be further investigated *in vivo* test in the future.

4. CONCLUSION

Core (Fe₃O₄)-shell (PVA) MNPs were successfully prepared and further conjugated with HEP to provide anticoagulation. The core-shell structure was confirmed by TEM, XRD, Raman spectra, XPS, and dye assay. Moreover, the PVA shell of the PMNPs can not only improve the dispersion of the MNPs in the resulting suspension, but also provide more -OH groups for conjugating HEP. The results demonstrated that PMNPs-ATMS-HEP exhibited better hemocompatibility than MNPs-ATMS-HEP. Moreover, longer spacer (ATMS) resulted in more HEP and gave rise to higher anticoagulant activity than shorter spacer (without ATMS). Owing to the magnetic Fe₃O₄ core and the immobilization of HEP, PMNPs could be used as recyclable anticoagulants by magnetic fields to prevent heparin from getting into body to cause certain allergic reaction.

Acknowledgment: This work was financially supported by the National Science Council of the Republic of China, Taiwan under Contract No. NSC-95-2221-E-009-126.

References and Notes

1. M. Mikhaylova, D. K. Kim, N. Bobrysheva, M. Osmolowsky, V. Semenov, T. Tsakalakos, and M. Muhammed, *Langmuir* 20, 2472 (2004).
2. C. L. Lin, C. F. Lee, and W. Y. Chiu, *J. Colloid. Interf. Sci.* 291, 411 (2005).
3. R. Weissleder, A. Bogdanov, E. A. Neuwelt, and M. Papisov, *Adv. Drug Deliv. Rev.* 16, 321 (1995).
4. D. K. Kim, M. Mikhaylova, F. H. Wang, J. Kehr, B. Bjelke, Y. Zhang, T. Tsakalakos, and M. Muhammed, *Chem. Mater.* 15, 4343 (2003).
5. S. Y. Mak and D. H. Chen, *Macromol. Rapid Commun.* 26, 1567 (2005).
6. H. Furukawa, R. Shimojo, N. Ohnishi, and H. Fukuda, *Appl. Microbiol. Biotechnol.* 62, 478 (2003).
7. Z. Lu, M. D. Prouty, Z. Guo, V. O. Golub, C. S. S. R. Kumar, and Y. M. Lvov, *Langmuir* 21, 2042 (2005).

8. J. H. Park, K. H. Im, S. H. Lee, D. H. Kim, D. Y. Lee, Y. K. Lee, K. M. Kim, and K. N. Kim, *J. Magn. Magn. Mater.* 293, 328 (2005).
9. A. Jordan, R. Scholz, P. Wust, and H. Schirra, *J. Magn. Magn. Mater.* 194, 185 (1999).
10. D. K. Kim, M. Mikhaylova, Y. Zhang, and M. Muhammed, *Chem. Mater.* 15, 1617 (2003).
11. S. A. Gómez-Lopera, J. L. Arias, V. Gallardo, and Á.V. Delgado, *Langmuir* 22, 2816 (2006).
12. M. Mikhaylova, D. K. Kim, C. C. Berry, A. Zagorodni, M. Toprak, A. S. G. Curtis, and M. Muhammed, *Chem. Mater.* 16, 2344 (2004).
13. G. M. Qiu, Y. Y. Xu, B. K. Zhu, and G. L. Qiu, *Biomacromolecules* 6, 1041 (2005).
14. X. H. Li, D. H. Zhang, and J. S. Chen, *J. Am. Chem. Soc.* 128, 8382 (2006).
15. T. Hatakeyama, J. Uno, C. Yamada, A. Kishi, and H. Hatakeyama, *Thermochimica Acta* 431, 144 (2005).
16. R. Veyret, T. Delair, and A. Elaissari, *J. Magn. Magn. Mater.* 293, 171 (2005).
17. N. S. Kommareddi, M. Tata, V. T. John, G. L. McPherson, and M. F. Herman, *Chem. Mater.* 8, 801 (1996).
18. W. Chen, X. Li, G. Xue, Z. Wang, and W. Zou, *Appl. Surf. Sci.* 218, 215 (2003).
19. J. Li, X. He, Z. Wu, K. Wang, G. Shen, and R. Yu, *Anal. Chim. Acta* 481, 191 (2003).
20. G. Koromila, G. P. A. Michanetzis, Y. F. Missirlis, and S. G. Antimisiaris, *Biomaterials* 27, 2525 (2006).
21. Y. I. Chung, S. Y. Lee, and G. Tae, *Colloid. Surface A* 284–285, 480 (2006).
22. S. R. Corrie, G. A. Lawrie, and M. Trau, *Langmuir* 22, 2731 (2006).
23. I. J. Bruce and T. Sen, *Langmuir* 21, 7029 (2005).
24. L. Y. Huang and M. C. Yang, *J. Nanosci. Nanotechnol.* 6, 3163 (2006).
25. T. Y. Liu, W. C. Lin, L. Y. Huang, S. Y. Chen, and M. C. Yang, *Biomaterials* 26, 1437 (2005).
26. W. C. Lin, T. Y. Liu, and M. C. Yang, *Biomaterials* 25, 1947 (2004).
27. S. G. Hu, C. H. Joe, and M. C. Yang, *J. Appl. Polym. Sci.* 86, 2977 (2002).
28. J. W. Long, M. S. Logan, C. P. Rhodes, E. E. Carpenter, R. M. Stroud, and D. R. Rolison, *J. Am. Chem. Soc.* 126, 16879 (2004).
29. J. S. Bae, E. J. Seo, and I. K. Kang, *Biomaterials* 20, 529 (1999).

Received: 4 July 2007. Revised/Accepted: 24 August 2007.

Curriculum Vitae

Ting-Yu Liu (劉定宇)

Advisor: Prof. San-Yuan Chen

Department of Materials Science Engineering,

National Chiao Tung University

1001 Ta Hsueh Road, Hsinchu, TAIWAN 300

Email: tingyuliu@hotmail.com; tingyuliu.mse92g@nctu.edu.tw

I. B. S.: Yuan-Ze University (1997-2001), Chung-Li, Taiwan.

Major: Chemical Engineering

Prof.: Yi-Ming Sun

Research Topic: Thermo-Sensitive Behaviors of Semi-IPN Hydrogel (NIPAAm/EVAL)

II. M. S.: National Taiwan University of Science and Technology (2001-2003), Taipei, Taiwan

Major: Polymer Engineering

Prof.: Ming-Chien Yang

Specialized field: Biomedical Material-Hemodialysis (Hollow Fiber), Artificial Kidney (or Liver)

Research Topic: Permeation performance and hemocompatibility of polyacrylonitrile and poly(vinylidene fluoride) blend hemodialysis membranes immobilized with biomolecules

III. Ph.D.: National Chiao Tung University (2003-2008), Hsinchu, Taiwan

Major: Materials Science and Engineering

Prof.: San-Yuan Chen

Specialized field : (1) Ferrogel for Drug Controlled Release
(2) Thermal Response Ferrosphere

Research Topic: Study on Intelligent Magnetic Hydrogel and Nanosphere for Drug Controlled Release

IV. Visiting Student: Scholarship study in University of Pennsylvania (2007.04-2008.04), Philadelphia, USA

Major: Materials Science and Engineering

Prof.: I-Wei Chen

Research Topic: A study on processing development of intelligent drug delivery systems based on magnetic-sensitive hydrogel (ferrogel) for chronic disease therapy

Publications

Ting-Yu Liu

News:

- Smart magnetic hydrogels for drug release, *Nanowerk Spotlight News*, May 18th, 2006 (<http://nanowerk.com/spotlight/spotid=507.php>)

SCI Paper:

1. Ming-Chien Yang and **Ting-Yu Liu**, The permeation performance of Polyacrylonitrile/Polyvinylidene Fluoride blend membranes, *J. Membrane Sci.* **226** (2003) 119–130. (*Impact Factor: 2.432*)
2. Wen-Ching Lin, **Ting-Yu Liu** and Ming-Chien Yang, Hemocompatibility of polyacrylonitrile dialysis membrane immobilized with chitosan and heparin conjugate, *Biomaterials* **25** (2004) 1947–1957. (*Impact Factor: 6.262*)
3. **Ting-Yu Liu**, Wen-Ching Lin, Li-Ying Huang, San-Yuan Chen and Ming-Chien Yang, Surface characteristics and hemocompatibility of PAN/PVDF blend membranes, *Polym. Adv. Technol.* **16** (2005) 413–419. (*Impact Factor: 1.504*)
4. **Ting-Yu Liu**, Wen-Ching Lin, Li-Ying Huang, San-Yuan Chen and Ming-Chien Yang, Hemocompatibility and anaphylatoxin formation of protein-immobilizing polyacrylonitrile hemodialysis membrane, *Biomaterials* **26** (2005) 1437–1444. (*Impact Factor: 6.262*)
5. **Ting-Yu Liu**, Wen-Ching Lin, Ming-Chien Yang and San-Yuan Chen, Miscibility, thermal characterization and crystallization of poly(L-lactide) and poly(tetramethylene adipate-co-terephthalate) blend membranes, *Polymer* **46** (2005) 12586–12594. (*Impact Factor: 3.065*)
6. **Ting-Yu Liu**, Hung-Chou Liao, Chin-Ching Lin, Shang-Hsiu Hu and San-Yuan Chen, Bio-functional ZnO nanorods arrays grown on flexible substrates, *Langmuir* **22** (2006) 5804-5809. (*Impact Factor: 4.009*)
7. **Ting-Yu Liu**, Shang-Hsiu Hu, Kun-Ho Liu, Dean-Mo Liu and San-Yuan Chen, Preparation and characterization of smart magnetic hydrogels and its use for drug release, *J. Magn. Magn. Mater.* **304** (2006) e397-e399 (*Impact Factor: 1.704*)

8. **Ting-Yu Liu**, Shang- Hsiu Hu, Tse-Ying Liu, Dean-Mo Liu and San-Yuan Chen, Magnetic-sensitive behavior of intelligent ferrogels for controlled release of drug, *Langmuir* **22** (2006) 5974-5987 (*Impact Factor: 4.009*)
9. Tse-Ying Liu, **Ting-Yu Liu**, San-Yuan Chen, Shian-Chuan Chen and Dean-Mo Liu, Effect of hydroxyapatite nanoparticles on ibuprofen release from carboxymethyl-hexanoyl chitosan/o-hexanoyl chitosan hydrogel, *J. Nanosci. Nanotechnol.* **6** (2006) 2929-2935 (*Impact Factor: 1.987*)
10. **Ting-Yu Liu**, Shang-Hsiu Hu, Sheng-Hsiang Hu, Szu-Ping Tsai and San-Yuan Chen, Preparation and characterization of thermal-sensitive ferrofluids for drug delivery application, *J. Magn. Magn. Mater.* **310** (2007) 2850-2852 (*Impact Factor: 1.704*)
11. Shang-Hsiu Hu, **Ting-Yu Liu**, Chia-Hui Tsai and San-Yuan Chen, Preparation and characterization of magnetic ferroscaffolds for tissue engineering, *J. Magn. Magn. Mater.* **310** (2007) 2871-2873 (*Impact Factor: 1.704*)
12. Shang-Hsiu Hu, **Ting-Yu Liu**, Dean-Mo Liu and San-Yuan Chen, Nano-ferrosponges for controlled drug release, *J. Control. Release* **121** (2007) 181-189 (*Impact Factor: 4.756*)
13. Shang-Hsiu Hu, **Ting-Yu Liu**, Dean-Mo Liu and San-Yuan Chen, Controlled pulsatile drug release from a ferrogel by a high-frequency magnetic field", *Macromolecules*, **40** (2007) 6786-6788 (*Impact Factor: 4.411*)
14. **Ting-Yu Liu**, Li-Ying Huang, Shang- Hsiu Hu, Ming-Chien Yang and San-Yuan Chen, Core-shell magnetic nanoparticles of heparin conjugate as recycling anticoagulants, *J. Biomed. Nanotechnol.* **3** (2007) 353–359
15. Kun-Ho Liu, **Ting-Yu Liu**, San-Yuan Chen and Dean-Mo Liu, Effect of clay content on electrostimulus deformation and volume recovery behavior of a clay–chitosan hybrid composite, *Acta Biomaterialia*, **3** (2007) 919-926 (*Impact Factor: 3.113*)
16. Shang-Hsiu Hu, **Ting-Yu Liu**, Hsin-Yang Huang, Dean-Mo Liu and San-Yuan Chen, Magnetic-sensitive silica nanospheres for controlled drug release, *Langmuir* **24** (2008) 239-244 (*Impact Factor: 4.009*)
17. **Ting-Yu Liu**, Shang- Hsiu Hu, Kun-Ho Liu, Dean-Mo Liu and San-Yuan Chen, Study on controlled drug permeation of magnetic-sensitive ferrogels: Effect of Fe₃O₄ and PVA, *J. Control. Release* **126** (2008) 228-236 (*Impact Factor: 4.756*)

18. Kun-Ho Liu, **Ting-Yu Liu**, San-Yuan Chen and Dean-Mo Liu, Drug release behavior of chitosan–montmorillonite nanocomposite hydrogels following electrostimulation, *Acta Biomaterialia* **4** (2008) 1038–1045 (*Impact Factor: 3.113*)
19. Kun-Ho Liu, **Ting Yu Liu**, Dean-Mo Liu, and San-Yuan Chen, Electrical-Sensitive Nanoparticle Composed of Chitosan and TEOS for Controlled Drug Release, *J. Nanosci. Nanotechno.* (2008) *in press* (*Impact Factor: 1.987*)
20. Shang-Hsiu Hu, **Ting-Yu Liu**, Hsin-Yang Huang, Dean-Mo Liu, and San-Yuan Chen, Stimuli-Responsive Controlled Drug Release from Magnetic-Sensitive Silica Nanospheres, *J. Nanosci. Nanotechno.* (2008) *in press* (*Impact Factor: 1.987*)
21. **Ting-Yu Liu**, Shang- Hsiu Hu, Kun-Ho Liu, Dean-Mo Liu and San-Yuan Chen, Instantaneous Drug Delivery of Magnetic/Thermal Sensitive Nanospheres by a High Frequency Magnetic Field, *Langmuir* (2008) *revised* (*Impact Factor: 4.009*).

International Conferences:

1. **Ting-Yu Liu**, Hung-Chou Liao, Chin-Ching Lin, Shang-Hsiu Hu and San-Yuan Chen, Immobilization of Proteins on Arrayed ZnO Nanorods Grown on Thermoplastic Polyurethane (TPU) Flexible Substrate for Biomedical Applications, *2005 Materials Research Society (MRS) Spring Meeting (2005)* San Francisco, USA. (**Oral presentation**)
2. **Ting-Yu Liu**, Shang-Hsiu Hu, Kun-Ho Liu, Dean-Mo Liu and San-Yuan Chen, Preparation and characterization of smart magnetic hydrogels and its use for drug release, *ISAMT/SOMMA 2005 Conference (2005)* Tapei, Taiwan. (**Poster presentation**)
3. **Ting-Yu Liu**, Shang-Hsiu Hu, Kun-Ho Liu, Dean-Mo Liu and San-Yuan Chen., Self-assembled core-shell magnetic nanoparticles of heparin conjugates as recycling anticoagulants, *NIPER-NANO-2006- Nanotechnology in advanced drug delivery Conference (2006)* Chandigarh, India. (**Poster presentation**)
4. **Ting-Yu Liu**, Shang-Hsiu Hu, Sheng-Hsiang Hu, Szu-Ping Tsai, Dean-Mo Liu and San-Yuan Chen, Preparation and characterization of thermal-sensitive ferrofluids for drug delivery application, *The 17th International Conference on Magnetism (ICM) (2006)* Kyoto, Japan (**Oral presentation**)
5. Shang-Hsiu Hu, **Ting-Yu Liu**, Kun-Ho Liu, Dean-Mo Liu and San-Yuan Chen.,

Drug controlled release characteristics of intelligent magnetic- gelatin nanospheres, NIPER-NANO-2006-Nanotechnology in advanced drug delivery Conference (2006) Chandigarh, India.

6. Kun-Ho Liu, **Ting-Yu Liu**, Dean-Mo Liu and San-Yuan Chen, Ultra-fast reactive drug release system composed of electrical-sensitive chitosan and TEOS-IPN hybrid nanoparticle under applied DC electrical fields, *NIPER-NANO-2006-Nanotechnology in advanced drug delivery Conference (2006)* Chandigarh, India.
7. **Ting-Yu Liu**, Shang-Hsiu Hu, Sheng-Hsiang Hu, Szu-Ping Tsai and San-Yuan Chen, Preparation and characterization of thermal-sensitive ferrofluids for drug delivery application, *International Conference on Magnetism (2006)* Kyoto, Japan
8. Shang-Hsiu Hu, **Ting-Yu Liu**, Chia-Hui Tsai and San-Yuan Chen, Preparation and characterization of magnetic ferroscaffolds for tissue engineering, *International Conference on Magnetism (2006)* Kyoto, Japan

Domestic Conference:

1. **Ting-Yu Liu**, Shang-Hsiu Hu, Kun-Ho Liu, Dean-Mo Liu and San-Yuan Chen, Magnetic-sensitive characterization of the ferrogels and its use for drug release, 九十四年度中華民國生醫材料暨藥物釋放研討會 (2005) 新竹，清華大學。(Poster presentation)
2. Jo-Hao Li, **Ting-Yu Liu**, Tse-Ying Liu and San-Yuan Chen, 2003/11, The preparation and release properties investigation of Organic/ inorganic in-situ process of chitosan/CDHA hydrogel beads, 2003 中華民國生醫年會(2003) 台北，陽明大學。

Award:

胡尚秀，**劉定宇**，蕭繼聖，智慧型生物訊號誘導藥物釋放系統前瞻研究，2007第五屆國家新創獎學生組第二名